A Novel Flow-Modified Heat Pipe – Development and Experimental Investigation

by

GUOHUI ZHENG

Department of Mining, Metals and Materials Engineering
McGill University
Montreal, Canada
June 18, 2003

A Thesis Submitted to McGill University in Partial Fulfillment
of the Requirements of the Degree of Doctor Philosophy

Canada

Dedicated to my wife, Ying Zhao, and our son, Yixiao

ABSTRACT

Heat pipes have been investigated, developed and applied in many industrial fields since 1964. However, heat pipe technology is still a relatively new topic in high heat flux environments such as are encountered in the metallurgical and energy industries. This study focused on the development of a novel heat pipe that can be used under high heat flux conditions. The state of the technology prior to this study was that heat pipes were not suitable for high heat flux applications.

Even though numerous patents have been granted for heat pipes and related applications, most are based on the basic concepts of the conventional heat pipe as detailed in the literature. Researchers have found that there are a number of problems with these heat pipes when they are applied in high heat flux environments. Thus, it was a prime objective of this study to develop a novel heat pipe that is suitable for such high heat flux operations. In addition, some basic fundamental issues regarding the overall makeup of heat pipes were also investigated and explained.

The fundamental study showed that the film boiling phenomenon can be a serious problem when a conventional heat pipe is used under high heat flux conditions. Film boiling can make a conventional heat pipe lose its ability for sustained heat transfer with a small temperature gradient.

The flow modified heat pipe that was invented and studied eliminates film boiling in the evaporator of the heat pipe. In this kind of heat pipe, a flow-modifier element was introduced into the heat pipe chamber to improve the heat transfer of the two-phase flow. The experimental data indicated that the flow modified heat pipe was dramatically better than a conventional heat pipe under a comparable high heat flux load. This novel heat pipe successfully combined the flow modified heat pipe and the loop heat pipe and, thus, effectively overcame film boiling by collapsing the formed films. It was shown that the novel heat pipes are suitable for high heat flux and high temperature operation where conventional heat pipes will only function at a fraction of the heat load.

RESUME

Les tuyaux de chaleur ont été étudiées, développées et appliquées dans beaucoup de domaines industriels depuis 1964. Cependant, la technologie de pipe de chaleur est une matière relativement nouvelle dans les environnements élevés de flux de la chaleur comme sont produites toujours dans les industries métallurgiques et d'énergie. Cette étude s'est concentrée sur le développement d'une pipe de chaleur de roman qui peut être utilisée dans des conditions élevées de flux de la chaleur. L'état de la technologie avant cette étude était que les tuyaux de chaleur n'étaient pas appropriées aux applications élevées de flux de la chaleur.

Même bien qu'on ait accordé de nombreux brevets pour des tuyaux de chaleur et des applications reliées, plus sont basés sur les concepts de base de la pipe de chaleur conventionnelle comme détaillé dans la littérature. Les chercheurs ont constaté qu'il y a un certain nombre de problèmes avec ces tuyaux de chaleur quand ils sont appliqués dans les environnements élevés de flux de la chaleur. Ainsi, il est nécessaire de développer une pipe de chaleur de roman qui convient à de telles opérations élevées de flux de la chaleur. En outre, quelques issues fondamentales de base concernant le maquillage global des tuyaux de chaleur ont été également étudiées et expliquées.

l'étude fondamentale a prouvé que le phénomène d'ébullition de film peut être un problème sérieux quand une pipe de chaleur conventionnelle est utilisée dans des conditions élevées de flux de la chaleur. L'ébullition de film peut faire une pipe de chaleur conventionnelle perdre ses capacités pour le transfert thermique soutenu avec un petit gradient de la température.

l'écoulement a modifié la pipe de chaleur qui a été inventée et étudié systématiquement élimine le film bouillant dans le vaporisateur de la pipe de chaleur. Dans ce genre de pipe de chaleur, un élément de couler-modificateur a été présenté dans la chambre de pipe de chaleur pour améliorer le transfert thermique de l'écoulement biphasé. Les données expérimentales ont indiqué que la pipe de chaleur modifiée par écoulement était nettement meilleure qu'une pipe de chaleur conventionnelle sous une charge élevée comparable de flux de la chaleur. Cette pipe de chaleur de roman a avec succès combiné la pipe de chaleur modifiée par écoulement et la pipe de chaleur de

boucle et, ainsi, a efficacement surmonté le film bouillant en s'effondrant les films formés. Il a été montré que les tuyaux de chaleur de roman conviennent au flux élevé de la chaleur et à l'opération à hautes températures où les tuyaux de chaleur conventionnelles fonctionneront seulement à une fraction de la charge thermique.

ACKNOWLEDGEMENTS

I would like to express my sincere gratitude to my thesis supervisor, Professor Frank Mucciardi, for his guidance, encouragement and support through the whole course of this work. His kindness, and unique, scientific approach, and hard work have been of themselves an experiment that I have tried and are engraved on my mind and which I will emulate in the future.

The pleasant and friendly international environment of studying and working created by my classmates and department staff along with their knowledge and skills are deeply appreciated. I would like to thank Walter Greenland for his patience and enormous help in the fabrication of heat pipes, and to Robert Paquette for his assistance in experiments.

I would like to express my sincere gratitude to my wife, Ying Zhao, and our son, Yixiao, for their love, encouragement, and patience. I am also much indebted to my parents, parents-in-law, and friends for their understanding, and continuous support.

TABLE OF CONTENTS

LIST OF FIGURES

LIST OF TABLES

CHAPTER 1. INTRODUCTION

As environmental issues have taken on prominence, the energy industry has had to take a significant position in the protection of the environment. Chief among the factors of energy utilization is energy efficiency as it is a major factor that influences the environment. The two issues related to energy efficiency are 1) the concern about resource management, especially the possibility of exhausting fossil fuel resources and, 2) the concern about the environmental impacts of energy technologies, especially air pollution from particulates, effects on land use (such as strip-mining) and emerging concerns about radioactive contamination from nuclear power. The main resource concerns and environmental analysis tended to look towards the future by protecting the resource base for this future, as well as by addressing the concerns about long-term environmental damage.

As we enter the 21st century, we face a mountain of environmental problems wrought by technological development and increased energy consumption patterns. We humans know, both intellectually and intuitively, that we are pushing the limits of what our planet can stand. Well-publicized issues like energy crisis, global warming, atmospheric pollution, and rainforest destruction have emphasized the importance of energy resource and environmental problems and the urgent need for action. The challenge we face as we step into the 21st century is to bring our technologically intense civilization into balance with the natural cycles. It is not an easy task.

The metallurgical industry is one of the major pillars of world industry. It is also one of the largest sources of energy consumption and environmental pollution. Worldwide production of four metals — aluminum, iron, copper and zinc — total about 800 megatonnes per year. Table 1-1 [1] shows world production in 1990 of primary aluminum, steel, copper, zinc, magnesium, and titanium presented by geographical area. Metals production including ore mining, extracting, refining and finishing consume huge amounts of energy.

Table 1-2 [1] shows energy consumption. The minimum and maximum values of the total energy consumed are presented. The energy consumption varies widely, as it differs

1

in the ore concentration, the process technology route that is adopted, the availability of economical energy, and the assumed thermal efficiencies.

Table 1-1. Primary Metal Production in 1990

Region	Production (millions of tonnes)					
	Al	Steel	Cu	Zn	Mg	Ti
America	7.42	139.6	4.16	1.45	0.181	0.027
Europe	6.77	365.9	3.69	3.39	0.160	0.051
Asia	1.91	237.9	2.14	1.79	0.028	0.027
Africa	0.60	16.9	0.81	0.17	--	--
Oceania	1.50	7.4	0.25	0.30	--	--
Total	18.21	767.7	11.07	7.10	0.369	0.105

Table 1-2. Energy Consumption in the Production of Various Metals

Item	Energy Consumption (kWh [thermal] /tonne of primary metal)					
	Al	Steel	Cu	Zn	Mg	Ti
Mining	1,668	1,711	6,500	139	0	NEA*
Ore Preparation	8,507	922	10,920	1,101	NEA	NEA
Smelting	35,384	6,055	26,520	17,560	103,000	113,000
Casting & Finishing	4,937	2,452	5,970	14,920	NEA	NEA
Total Minimum	30,000	5,321	14,370	6,125	35,000	113,700
Total Maximum	75,000	11,140	49,910	20,300	123,000	127,900

*NEA = No Estimate Available

By Combining Table 1-1 and Table 1-2, Figure 1-1 is obtained, and it presents the minimum and maximum values of energy consumption for primary metals in the world. Of note copper, nickel, lead, zinc and other non-ferrous metals are extracted from ores of relatively low concentrations. Moreover, the technologies used require large volumes of energy in the form of fuel and electricity (electrolysis, sublimation etc). Though the volume of energy used for steel making is lower than for non-ferrous metals, the large

total production makes ferrous metallurgy very energy intensive too. At the same time, both ferrous and non-ferrous smelting produce large quantities of gas, liquid and solid wastes.

	Al	Steel	Cu	Zn	Mg	Ti
■ Minimum	546,300	4,084,932	159,076	43,488	12,915	386,466
□ Maximum	1,365,750	8,552,178	552,504	144,130	45,387	434,732
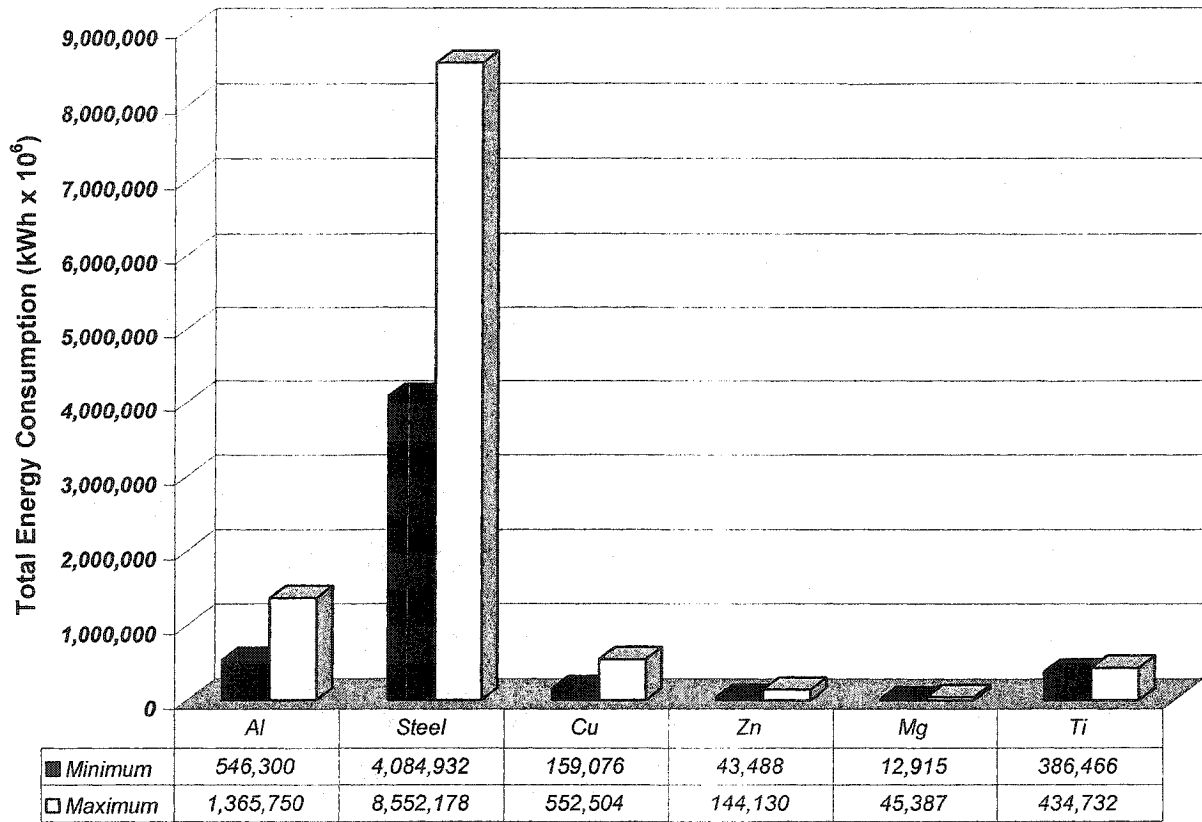
Figure 1-1. Energy Consumption of Primary Metals in 1990

Unfortunately, the energy efficiency of most metallurgical processes is low. Vladimir Stepanov and Sergey Stepanov estimated the effectiveness of energy conversion processes using energy (η_{en}) and exergy (η_{ex}). The results are presented in Table 1-3 [2] as three types of efficiencies: Real, Idealized and Relative efficiencies. The ideal analogue is a theoretical process proceeding with $\eta_{ex}=1$ and the I_{cons}^{th} E_{cons}^{th} consumed energy and exergy. It enables the real process efficiencies to be estimated as:

$$\eta_{en}^{real} = I_{cons}^{th} / I_{cons}^{real} \quad and \quad \eta_{ex}^{real} = E_{cons}^{th} / E_{cons}^{real} \tag{1}$$

The ideal analogue of an energy consuming process can be compared to the Carnot cycle in the thermal power industry. However, such a limiting degree of idealization doesn't allow a deep analysis of real processes. Therefore, the analogues with a lower degree of idealization for energy consuming processes were created. As with a real process, an idealized process also has certain energy efficiencies:

$$\eta_{en}^{id} = I_{cons}^{th} / I_{cons}^{id} \qquad and \qquad \eta_{ex}^{id} = E_{cons}^{th} / E_{cons}^{id} \qquad (2)$$

Where I_{cons}^{id} and E_{cons}^{id} energy and exergy inputs of an idealized process, respectively.

Table 1-3. Energy and Exergy Efficiencies of Some Metallurgical Production

Product, Technology	Real		Idealized		Relative	
	η_{en}	η_{ex}	η_{en}	η_{ex}	η_{en}	η_{ex}
1. Steel from concentrates, average for industry via: Open hearth furnace	0.299	0.288	0.826	0.796	0.362	0.362
Oxygen converter	0.308	0.293	0.826	0.796	0.373	0.368
2. Steel from scrap via electric arc furnace	0.664	0.648	0.826	0.796	0.804	0.814
3. Aluminum from alumina	0.421	0.378	0.870	0.818	0.484	0.462
4. Aluminum from nepheline	0.197	0.181	0.846	0.785	0.233	0.230
5. Copper (electrolytic) from a concentrate via reverberatory furnace	0.065	0.046	0.234	0.228	0.278	0.202
6. Lead from a concentrate via last furnace	0.093	0.056	0.334	0.331	0.280	0.170
7. Zinc (electrolytic) from a sulphide concentrate	0.214	0.200	0.417	0.394	0.513	0.508

In such an idealized process, chemically pure compounds are used as the raw material feeds and pure products result from the process. It is assumed that the reactions take place at stoichiometric quantities of reacting substances and proceed to completion, material losses are absent. The temperature of input and output substances is taken to be equal to the ambient temperature and the heat of reactions is rejected to the environment at the same temperature. It is natural that such a process proceeds with minimum consumption of energy that is unattainable for a real process. The idealized analogues of chemical and metallurgical productions should reflect the two most important factors that have an influence on energy consumption: the kind of raw material for manufacturing the

product and the technology applied. Such an analogue can be represented by a process which is described by one or several basic irreversible chemical reactions.

The approximate extent of energy perfection of the real process to the idealized one can be estimated by the relative efficiencies as:

$$\eta_{en}^{rel} = \frac{\eta_{en}^{real}}{\eta_{en}^{id}} = \frac{I_{cons}^{id}}{I_{cons}^{real}} \quad and \quad \eta_{ex}^{rel} = \frac{\eta_{ex}^{real}}{\eta_{ex}^{id}} = \frac{E_{cons}^{id}}{E_{cons}^{real}} \tag{3}$$
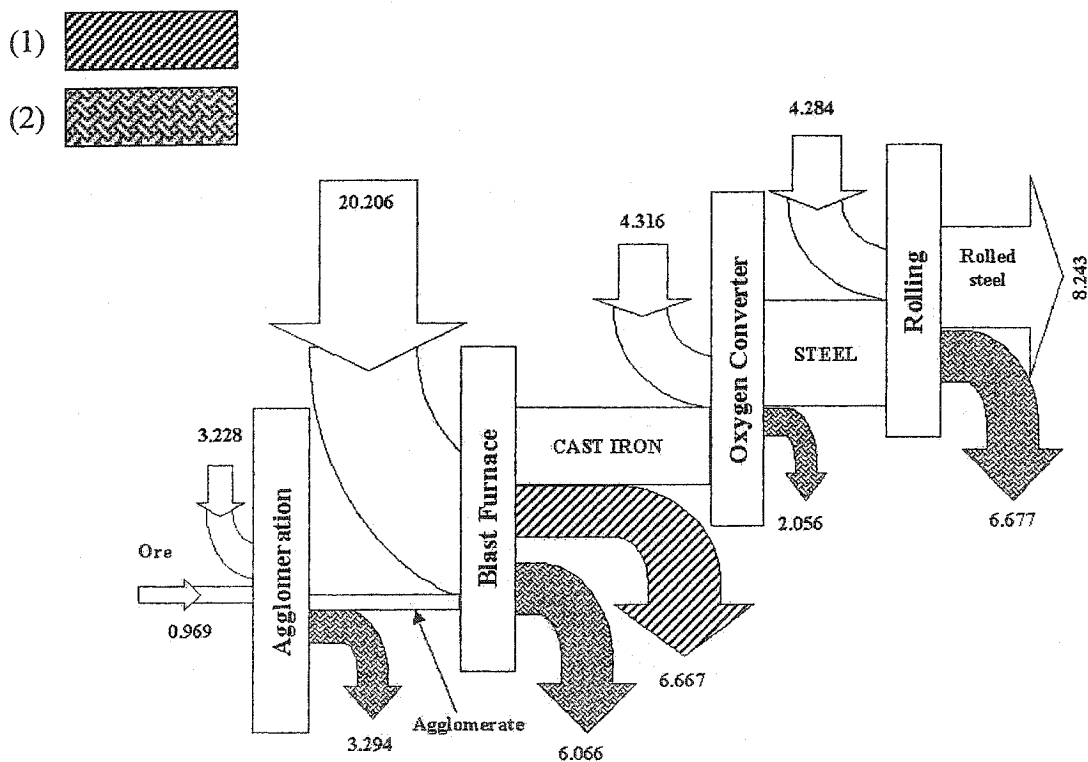
Figure 1-2. Diagram of Energy Flows for Rolled Steel production on the
Base of Oxygen Converter as an average for the Industry, GJ/t.
(1) Other useful products (blast-furnace gas, processed slag etc.);
(2) Energy/exergy losses.

Figure 1-2 [2] shows the energy and exergy flows for steel production with an oxygen converter. It presents the supplied, useful and lost energy/exergy of every production stage. Its efficiencies are η_{en} = 0.241 and η_{ex} = 0.220. From Figure 1-2, we

can clearly see a lot of the energy is lost in the different stages of the process. Thus, these stages need improvement.

The metallurgical industry is also one of the largest sources of environmental pollution. Every year it produces large quantities of gas, liquid and solid wastes. Worldwide production of four metals — aluminum, iron, copper and zinc — accounts for about 2,000 megatonnes of waste generated per year. Table 1-4 [3] indicates estimates of total emissions from metal processing operations. If discarded directly into the natural environment, such wastes would not only occupy enormous amounts of land, but also pollute air, soil and groundwater. Clearly, successful remediation efforts would greatly reduce the environmental impact.

Table 1-4. Total Emissions in Metals Processing

Emission	kg/T of metal				MT / Year			
	Al	Steel	Cu	Zn(Electrol.)	Al	Steel	Cu	Zn(Electrol.)
Carbon Dioxide								
Ancillary	7,814	486	5,124	3,589	142.3	373.1	56.7	25.48
Excl.Electricity*	4,500	1,085	2,051	NEA	81.9	833.0	22.7	NEA
Carbon Monoxide								
Ancillary	2	0.1	2.54	1.78	0.04	0.1	0.0281	0.0126
Excl.Electricity*	340	54.9	NEA	P	6.19	42.1	NEA	P
Sulfur Oxides								
Ancillary	58	3.5	37	26	1.06	2.69	0.41	0.1846
Excl.Electricity*	25	5.5	3,500	P	0.46	4.22	38.75	P
Nitrogen Oxides								
Ancillary	21	1.9	20	14	0.38	1.44	0.22	0.0994
Excl.Electricity*	2	1.1	NEA	NEA	0.04	0.87	NEA	NEA
Hydrogen Fluorides								
Ancillary	NEA	NEA	NEA	NEA	NEA	NEA	NEA	NEA
Excl.Electricity*	5	NEA	NEA	NEA	0.09	NEA	NEA	NEA
Liquid Effluents								
Ancillary	833	267	2,820	1,974	15	205	31	14.01
Excl.Electricity*	8,001	39,285	1,350,000	442	145	30,159	14,945	3.14
Solid Waste								
Ancillary	3,401	103	1,100	765	62	79	12	5.43
Excl.Electricity*	2,000	484	138,000	P	36	372	1,528	P

NEA--No estimate available;   P--Present
* Values in these rows exclude the environmental impact associated with electricity production

An allied environmental concern is the gradual depletion of nonrenewable mineral resources as metal production steadily rises. Public demand for the conservation of natural resources and for their most suitable utilization, as well as for the generation of the least possible waste, and for its reuse wherever possible, and for its proper disposal, is growing. Legislation defining standards for the protection of the environment, first enacted in the metallurgical industry during the 1960s, has become increasingly stringent.

One of the most important challenges before the metallurgical industry, therefore, is to meet or exceed these requirements while maintaining or increasing productivity. Substantial research has been carried out to identify waste emissions from metallurgical processes and develop measures for their reduction [4]. Significant achievements have been made, notably the recycling of waste water and the widely adopted practice of using SO_2 emitted during metallurgical operations such as copper and lead smelting to generate sulfuric acid for further industrial use [5].

However, many problems remain to be resolved. While many measures already exist to deal with waste gas, the recovery of waste heats in metallurgical processes demands new scientific advances. These wastes present a twofold challenge. First, they are generated in such large quantities that metallurgical operations need to be optimized and new techniques developed to substantially reduce heat pollution and increase the recover of heat energy. Second, energy consumption must be reduced. As one example, waste heat in cooling water generated by steelmaking processes are of the low grade, low temperature variety. While current techniques cannot successfully recover these heats, no integrated methods have yet been industrially applied to recover this waste heat in a single and cost-effective process.

Saving 1 kWh of energy can reduce waste generation by about 1 kg. Table 1-5 [6] illustrates the environmental impact associated with producing 1 kWh of electricity using nonrenewable resources.

If the efficiencies of energy consumption in steelmaking can rise from 0.22 to 0.5, about $2,394,610 \times 10^6$ kWh of energy can be saved annually. Simultaneously, about $2,395 \times 10^6$ tonne of waste can be cut.

7

Table 1-5. Environmental Impact of Electricity Generation

Power source	Emissions (kg/kWh)					
	CO_2	CO	SO_x	NO_x	Liquid	Solid
Coal	1.0	0.00025	0.0075	0.0027	0.00294	0.53
Oil	1.0	0.0013	0.008	0.007	1.9	0.0097
Gas	1.1	0.00013	0.007	0.0025	0.0039	0.0016
Nuclear	0.000025	Negligible	Negligible	0.000001	NEA	0.01

Therefore, to conserve energy resources and protect the environment, there is a growing need to develop new technological methods to compensate for the decline of coal, gas and oil production, and to reduce environmental pollution. We are a long way from meeting the public requirements.

Most industrial, agricultural and energy production processes involve heat and mass transfer with multiple fluid phases. In such systems, the fluids may be subjected to vaporization, condensation and transport due to pressure, temperature, or concentration gradients. Therefore, researchers in these areas are developing many suggestions for economic and efficient heat transfer devices. One such device is the heat pipe (super heat conductor) and the growing interest in it has been documented by a great number of investigations.

In this project, the cooling and heat transfer/transport method chosen for saving energy and protecting the environment is based on heat pipe technology. The heat pipe is an engineering device for transporting heat at virtually isothermal conditions.

Structurally, the heat pipe is very simple. It is normally a pressure-tight vessel fabricated, as a rule, from metal, with the atmospheric air removed from the interior of the vessel. The inner surface of such a vessel is lined with a capillary material which is wetted by the liquid that functions as the heat transfer fluid. Operation of the heat pipe is based on well-known laws of physics. When heat is applied from a heat source to one end of the heat pipe, the heat transfer fluid evaporates from the capillary material and absorbs the latent heat of vaporization. The vapor then moves toward the other (cooled) end of the

heat pipe to condense. The heat of condensation is transferred to an outer heat sink by thermal conduction. The condensed heat transfer fluid is absorbed by the capillary material to be moved back by virtue of a capillary pressure head toward the evaporation zone thereby completing the working cycle of the heat pipe. High efficiency of the heat pipe as a "heat conductor" is therefore determined by the liquid's high heat of vaporization which enables it to remove from the evaporation zone considerable heat fluxes at a relatively low consumption of the heat transfer fluid. This heat is transferred mainly by the vapor phase which moves along the pipe without the need for a high pressure differential since the hydraulic diameter of the vapor passages is, as a rule, sufficiently great.

Currently, the heat pipe is considered as an innovative device capable of transferring large quantities of heat through relatively small cross sectional areas with very small temperature differences. Because of the simplicity of design and the ease of manufacture and maintenance, these devices have found applications in a variety of areas around the world.

As a cooling device, the heat pipe is very efficient. For example, when a heat pipe with water as working fluid operates at 100 °C, the heat transfer coefficient at the inner surface of the pipe shell can be more than 10,000 W/m^2-°C, the heat flux on the pipe shell can be in excess of 1 MW/m^2, and the equivalent axial thermal conductivity of the heat pipe can be 100 to 1,000 times higher than that of pure copper. Overall, the heat transport capacity of the heat pipe with water as working fluid is comparable to that of a forced convection system with water as the cooling medium. Simultaneously, as a device transporting heat energy, the heat pipe is a very effective device for transferring heat at high rates over considerable distances with extremely small temperature drops, exceptional flexibility, simple construction, and easy control with no external pumping power.

In fact, the heat pipe as a cooling device not only has great cooling capacity to protect a furnace wall, taphole, lance and tuyere, but it also has a big advantage over the conventional forced convection method with water as the cooling medium. A heat pipe cooled device is much safer than a conventional water-cooled system in high temperature systems, since only a small amount of working fluid is used. Based on the working fluid

in the heat pipe, it may be compatible with the pyrometallurgical industry because the heat pipe cooling can be completely waterless. Furthermore, heat pipe cooling can replace conventional water-cooled systems that use forced convection cooling methods.

Although the heat pipe was invented more than three decades ago, little attention was paid to using this technology by the metallurgical industry. Therefore, in this project, an innovative heat pipe was developed to improve current technology for transporting heat and cooling equipment. It can be used especially in those systems with high temperatures and heat fluxes, such as furnace walls, lances and tuyeres found in the metallurgical industry.

The present thesis describes our contribution to innovating heat pipe technology for the metallurgical industry. It includes five parts. The literature review is presented in Chapter 2. The current status of loop heat pipes and project objectives are described in Chapter 3. Chapter 4 deals with the design criteria of heat pipes and practical considerations.

The problems associated with vertical thermosyphons and gravity-assisted heat pipes are identified and detailed in Chapter 5. In the same chapter, the explanations of the phenomena and possible solutions are presented and discussed. It also includes forced convection cooling applied on the condenser. The problems and solution of film boiling associated with gravity-assisted heat pipes are investigated in Chapter 6. The identification of the start-up problem and the solution of the flow modification associated with the newly developed gravity-assisted heat pipe are discussed in Chapter 7. Also included is a simple mathematical model for the invented heat pipe and results compared with experimental results.

The concepts, design considerations and testing results are discussed in Chapter 8. The final conclusions of this research are outlined in Chapter 9. Finally, the statement of originality of this work and the contributions of this thesis to knowledge are outlined.

CHAPTER 2. LITERATURE REVIEW

2.1 History of Heat Pipe

The heat pipe was first described by Grover, Cotter, and Erickson of Los Alamos National Laboratory in 1964 [1]. On July 24, 1963, George Grover made the following entry into his laboratory notebook under the heading: Heat transfer via capillary movement of fluids. "The 'pumping' action of surface tension forces may be sufficient to move liquids from a cold temperature zone to a high temperature zone (with subsequent return in vapor form using as the driving force, the difference in vapor pressure at the two temperatures) to be of interest in transferring heat from the hot to the cold zone. Such a closed system, requiring no external pumps, may be of particular interest in space reactors in moving heat from the reactor core to a radiating system. In the absence of gravity, the forces must only be such as to overcome the capillary and the drag of the returning vapor through its channels." [2] With this began heat pipe research at Los Alamos. Later that year Grover submitted the results of "heat pipe" experiments with water and sodium as working fluids to the Journal of Applied Physics (Vol. 35, No. 6, June 1964, pp1990-1991). In 1966, Grover, on behalf of the U.S. Atomic Energy Commission, described the phrase "heat pipe" in a U.S. patent application (U.S. patent No. 3229759). In the beginning of the patent, a description is provided, which is almost identical as that of Gaugler's (U.S. patent No. 2350348), "With certain limitations on the manner of use, a heat pipe may be regarded as a synergistic engineering structure which is equivalent to a material having a thermal conductivity greatly exceeding that of any known metal." [3]

In the patent application, Grover gave a very limited theoretical analysis of heat pipes, but presented experimental results obtained from stainless steel heat pipes incorporating a screen wick with sodium, silver and lithium as working fluids. The recognition of the heat pipe as a reliable thermal device was initially due to the preliminary theoretical results and design tools that were reported in the first publication on heat pipe analysis by Cotter (1965) [3]. Following this publication, research on heat pipes began worldwide.

Initial efforts of heat pipe research were directed towards heat transport applications in the NASA space program. The high reliability of the heat pipe and its capability for isothermal operation without the need for external power made it suitable for operation under the weightless conditions of space. It was soon realized that the unique characteristics of the heat pipe would be equally useful here on earth, and terrestrial applications began to receive considerable interest as well.

Aspects of heat pipe operation that were investigated at Los Alamos were in the following areas:

- Characterization of performance limits

- Heat pipe start-up from a frozen state

- Wetting and corrosion phenomena of various materials combinations

- Wick design

These are representative of the current research areas and trends in heat pipe studies. In fact, heat pipe design, theory, and applications have developed quickly over the 30 years since the invention of the heat pipe by Grover et al. This is evidenced by hundreds of papers published per year, ten international conferences, and the publication of a number of books on heat pipes. The majority of the references can be classified into one of the following categories.

1. Basic Study

   - Numerical analysis / heat pipe modeling

   - Heat pipe performance limits

   - Heat pipe start-up

   - Heat pipe dry-out

   - Heat and mass transfer in wicks

   - Material issues related to heat pipe construction

2. Function

   - Micro and miniature heat pipes

   - Flat plate heat pipe / disk-shaped heat pipe

   - Rotating heat pipes and thermosyphons

- Gas loaded and variable conductance heat pipes

- Multiple-heat source heat pipe

- Capillary Pumped loops (loop heat pipe)

3. Application

- Heat pipes for cooling electronics (computer chips)

- Heat pipes in heat exchangers and industrial processes

- Solar energy conversion using heat pipes

- Aircraft leading edge shaped heat pipes on the wing and tail

- Journal bearing of a rail car cooled by heat pipe

- Heat pipe ejector cooler

- Casting mold using heat pipe cooling

- Heat pipe lance

- Temperature measurement with heat pipes

This research has encompassed the full range of heat pipe operating temperatures from 2K for helium up to 2000K for silver) [4]. A wide variety of heat pipe fluids have been used from liquid hydrogen and nitrogen at cryogenic temperatures through water, ammonia, and alcohol at near-ambient temperatures, to liquid metals such as alkali metals at elevated temperatures.

The Los Alamos Heat Pipe Laboratory presented their "Heat Pipe Development Milestones" in this web site [2]:

1. Liquid metal heat pipe life tests to 45,000 hours (about 5 years) – sodium working fluid with a molybdenum container at 2060°F (1400 K).

2. Heat pipes developed from hydrogen temperature -424°F (20 K) to saturated silver temperature 3631°F (2273 K).

3. Radial power density in evaporator to 17,600 BTU/hr.in^2 (800 W/cm^2) with a National Aerospace Plane wing leading edge cooling heat pipe with a lithium working fluid and a molybdenum container operating at 2960°F (1900 K).

4. Axial power density to 5x10^5 BTU/hr.in^2 (23 kW/cm^2) with a SP-100 space reactor radiator heat pipe with lithium working fluid in a molybdenum

container operating at 2240°F (1500 K). To put this figure in perspective, the power density at the surface of the Sun is about 6 kW/cm^2.

These achievements in heat pipe applications led to the development of applications of heat pipes by some industries. The cooling of electronic components, which has seen the fastest growth in heat pipe utilization in recent years as computer and other electronic technologies grew dramatically has led to the general acceptance of heat pipes. With the adoption of heat pipes, in heat exchangers and solar collectors, one can see the maturing of heat pipe technology in some commercial applications.

2.2 Technology of Heat Pipe [1, 3, 4, 5, 6, 7, 8, 9, 10]

Figure 2-1 [2] exhibits a heat pipe made in the Los Alamos National Laboratory. It is a self-contained engineering structure whose thermal conductance greatly exceeds that which can be obtained by using a homogeneous piece of any known metal. This property is achieved within the containing envelope by the evaporation of a liquid, transport of the vapor to another part of the container, condensation of the vapor and return of the condensate to the evaporator through a wick of suitable capillary structure. The quantitative engineering theory for the design and performance analysis of heat pipes,

Figure 2-1. The Heat Pipe

alluded to but not elaborated on in the original description of these devices, is supplied herein. There are obviously many practical uses for a structure of extraordinarily large thermal conductance. The heat pipe principle is indeed applicable over a very wide range of sizes, shapes, temperatures and materials. Unlike solid heat conductors, however, heat
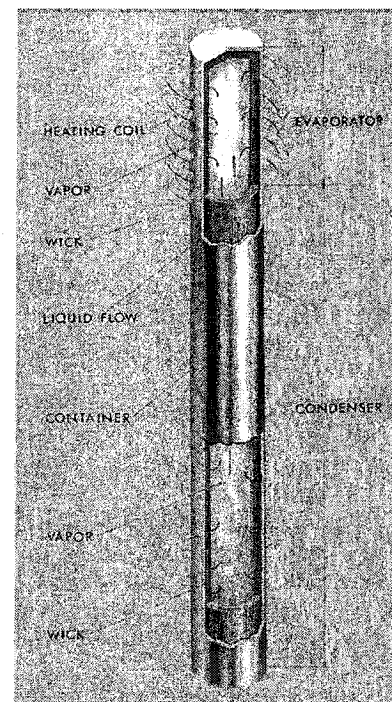
pipes cannot be characterized by a single property (an "equivalent thermal conductivity", say), since the behavior and limitations of a heat pipe are largely integral properties of the device as a whole. Furthermore, even if the size, shape, temperature and materials of a heat pipe are specified, the mass, vapor volume fraction, thermal conductance and maximum heat flux are individually (though not independently) under the control of the designer. The particular application will determine which combination of these properties is most desirable.

At the present time, certain quantitative features of heat pipe behavior have not in fact been verified experimentally, though they can be predicted with some confidence. A few properties cannot as yet even be assessed with much conviction.

This section is intended simply to offer some initial orientation in the quantitative principles of heat pipes, and to serve as a stimulus for further experimentation, applications, and improvement of the theory.

2.2.1 Structure of Conventional Heat Pipe

Conventional heat pipes are usually long and thin, that is, they take the form of long cylinders. For purposes of illustration the discussion in this section will be confined to right circular cylinders of large length-to-diameter ratios. The course of the analysis for other shapes will be evident, though not always straightforward in detail. As shown in Figure 2-2, such a heat pipe consists of a sealed container of length ℓ with outer radius r_p (pipe wall and end caps), a wick structure (an annular capillary structure saturated with a wetting liquid) with outer radius r_w, and a small amount of working fluid which is in equilibrium with its own vapor (a vapor space of radius r_v). The length of the heat pipe is divided into three parts: evaporator section, adiabatic (transport) section and condenser section. A heat pipe may have multiple heat sources or sinks with or without adiabatic sections depending on the specific application. Heat is added into the evaporator section by an external source, and the working fluid is vaporized. The resulting vapor is propelled through the adiabatic section to the condenser section as a pressure driven flow in the pipe. The vapor releases its latent heat of vaporization to the provided heat sink and condenses in the condenser section. The capillary pressure created by the menisci in the wick pumps the condensed fluid back to the evaporator section. Therefore, the heat pipe

can continuously transport the latent heat of vaporization from the evaporator to the condenser section. Since heat is added to and removed from the heat pipe through the container wall by ordinary thermal conduction, this should be as thin as other considerations permit, in order to minimize radial temperature differences. The container wall must of course sustain the difference between the internal and the ambient pressure. Heat pipes can be effective at vapor pressures as low as a hundredth of an atmosphere, and improve with increasing pressure. It is usually possible to match the ambient pressure by choosing a working fluid with an appropriate vapor pressure at the desired operating temperature. The question of the long-term compatibility of the container with the working fluid might determine its thickness, or the container might even be a structural element with other functions in the larger device of which the heat pipe is a part.
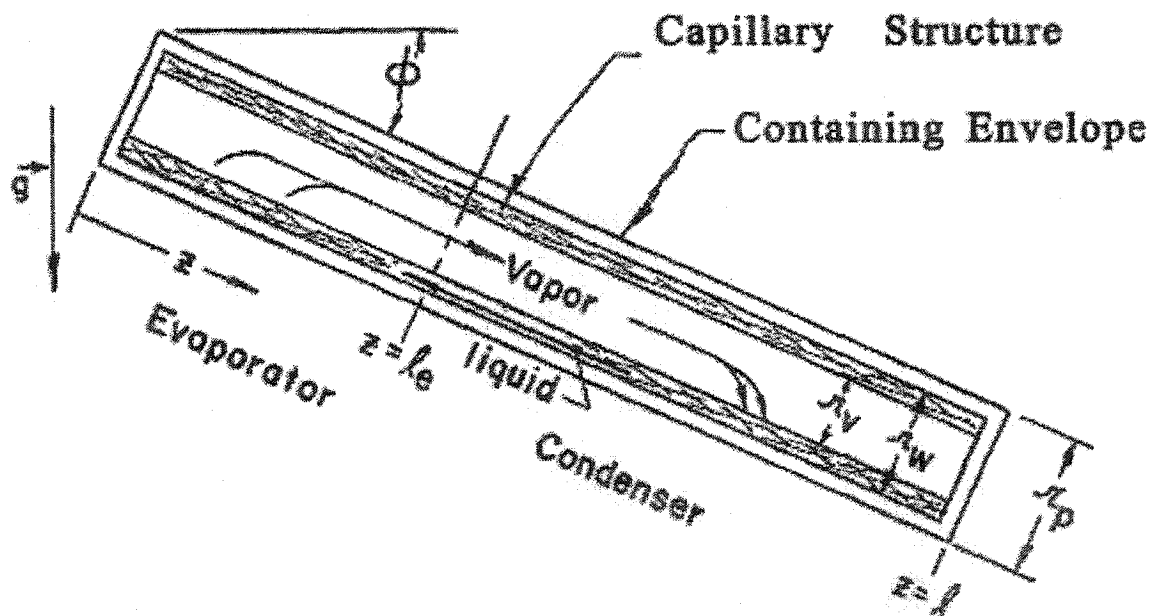
Figure 2-2. The Schematic Heat Pipe

The details of the wick can show wide variation. The wick need not be placed against the inside surface of the container as shown, though this will ordinarily be the best place for it for several reasons. Since evaporation and condensation take place at the vapor-liquid interface, this disposition of the wick allows the necessary radial heat transfer to occur through the medium of highest thermal conductance and thus minimizes

radial temperature differences. This also makes the hydraulic diameter of the vapor space as large as possible which minimizes axial pressure gradients in the flowing vapor. The wick may be a woven cloth, sinter, screens, etc., or even simply slots or grooves in the container wall. The capillary structure will be characterized by its mean pore radius, permeability and liquid volume fraction. It is desirable but not essential that the heat pipe be self-priming; that is, if the requisite amount of liquid is placed anywhere in the container it spontaneously saturates the entire wick. This is accomplished by having sufficiently small capillary pore size throughout the wick. The working fluid must wet the wick material; that is, the contact angle (the angle formed by a wedge of liquid in equilibrium contact with the solid substrate) must be less than 90°. While not essential, it is desirable that the fluid also wet the container wall as this improves the heat transfer. There is little penalty for a modest excess of liquid over the amount required to saturate wick. A deficiency on the other hand can be expected to reduce maximum heat transport by reducing the effective wick volume in the evaporator section of the heat pipe.

The vapor pressure changes along the heat pipe are due to friction, inertia and blowing (evaporation) and suction (condensation) effects, while the liquid pressure changes are mainly as a result of friction. The liquid-vapor interface is flat near the condenser end cap corresponding to the zero local pressure gradient at very low vapor flow rates. The typical axial variation of the shape of the liquid-vapor interface and the liquid and vapor pressures are shown in Figure2-3a, 2-3b, 2-3c and 2-3d, respectively. The maximum local pressure occurs near the evaporator end cap. At low vapor flow rates (see Figure 2-3b), this maximum local capillary pressure should be equal to the sum of the pressure drops in the vapor and the liquid across the heat pipe in the absence of body forces. When body forces are present, such as an adverse gravitational force, the liquid pressure drop is greater, indicating that the capillary pressure must be higher in order to return the liquid to the evaporator for a given heat input. At moderate vapor flow rates (see Figure 2-3c), dynamic effects cause the vapor pressure drop and recovery along the condenser section. The local liquid-vapor pressure difference is small, but this pressure gradient approaches zero at the condenser end cap and is similar to the low flow rate case. Again, the capillary pressure difference at the evaporator end cap should be balanced by the sum of the total pressure drop in the vapor and liquid across the heat
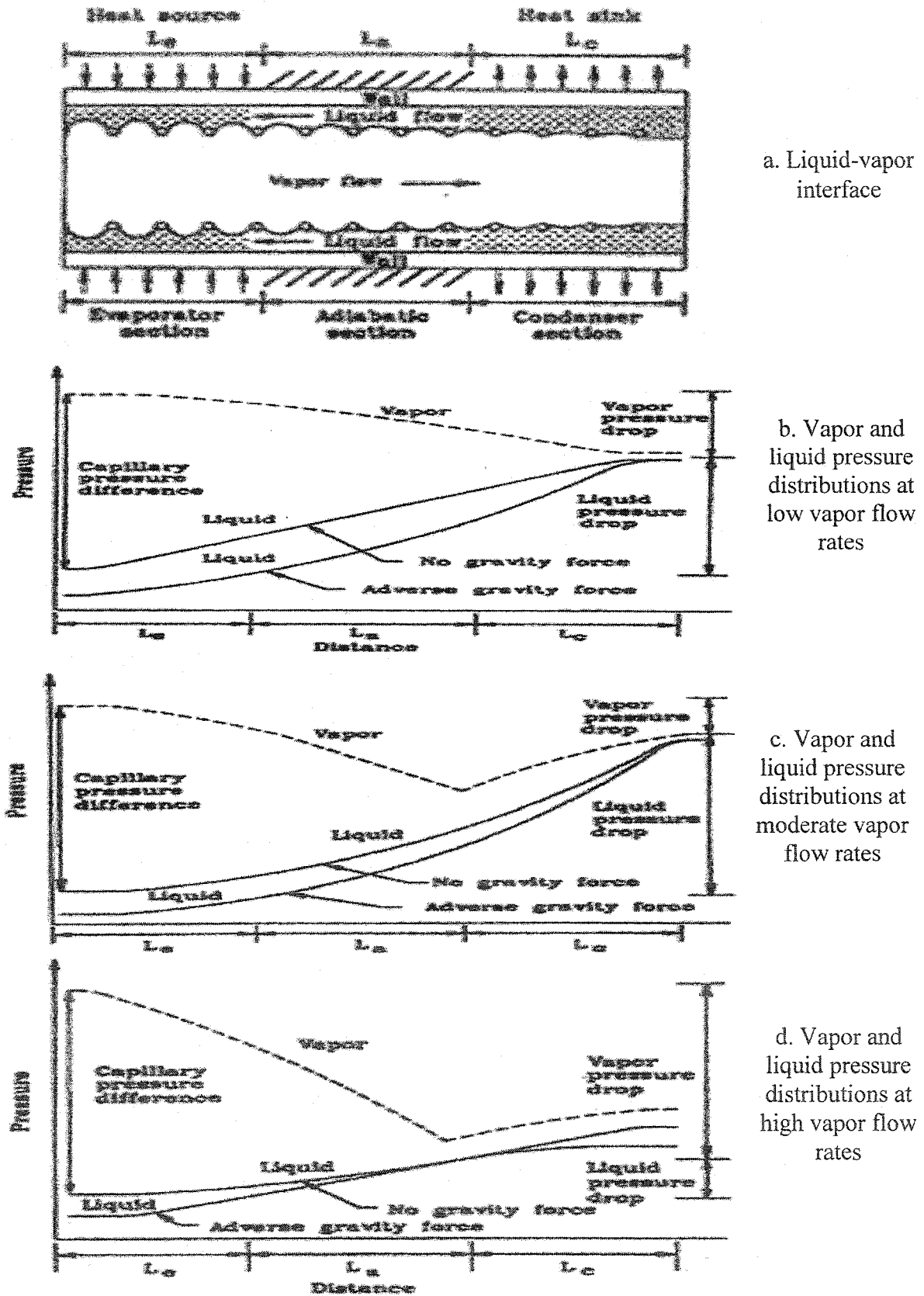
Figure 2-3. Axial Variation of the Liquid-Vapor Interface, and the Vapor and Liquid Pressures along the Heat Pipe at Various Flow Rates

pipe. The general trend at high flow rates with low liquid pressure drops is different from the other two cases, as shown in Figure 2-3d, where the vapor pressure drop can exceed the liquid pressure drop in the condenser section. In such a case, the liquid pressure would be higher than the vapor pressure in the condenser section if the pressure in the liquid and vapor are equal at the condenser end cap.

Usually, heat pipe theory focuses on fundamental analysis of the related hydrodynamic and heat transfer processes. Hydrodynamic theory is generally used to describe the axial liquid pressure drop in the wick structure, maximum capillary pumping head and the vapor flow in the vapor channel. Heat transfer theory is used to model the transfer of heat into and out of the heat pipe. Phenomena such as conjugate heat conduction in the wall and wick, evaporation and condensation at the liquid-vapor interface, and forced convection in the vapor channel and wick structure are covered. The various thermal resistances in a conventional heat pipe are shown in Figure 2-4. The thermal processes such as solidification and liquefaction, and those related to rarefied gases can play important roles in modeling transient heat pipe operation during startup from the frozen state.
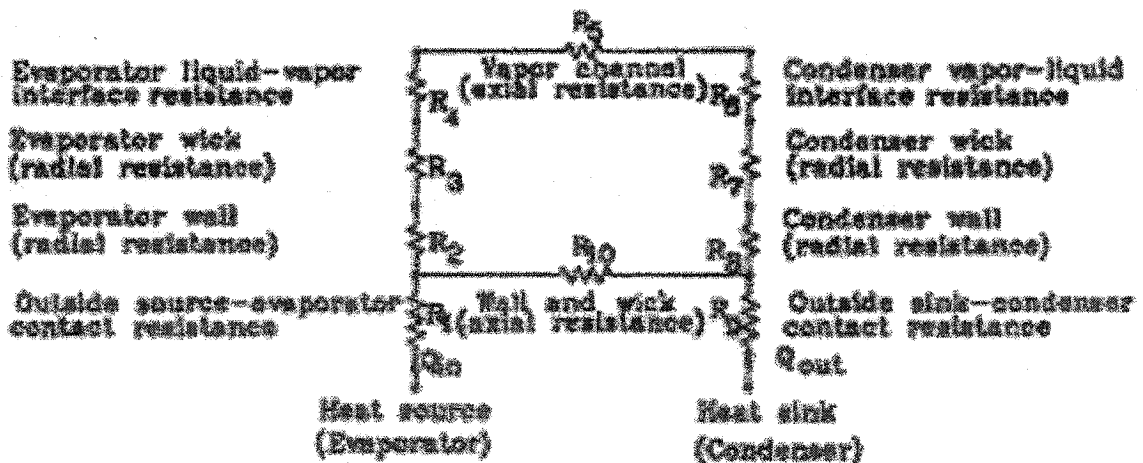
Figure 2-4. Thermal Resistance Model of a Typical Heat Pipe

Both fundamental theories will discussed in future chapters.

2.2.2 Static Condition

Suppose, first, that there is no heat addition or removal, and that the pipe is at equilibrium with its length, z, at an angle, ϕ, to a gravitational field of acceleration, g. The pressure distribution in the liquid phase, $P_l(z)$, obeys the usual hydrostatic law for an incompressible fluid:

$$P_l(z) = P_l(0) + \rho_l g z \sin \phi \qquad (2.1)$$

where ρ_l is the density of the liquid. The pressure in the vapor phase $P_v(z)$, assumed an ideal gas, has a Boltzmann distribution in the gravitational field, but the variation of pressure is entirely negligible and we may take the pressure to be constant. The interface between the liquid in the capillary structure and the adjacent vapor must assume a local radius of curvature, $r(z)$, so that surface tension, γ, supports the difference in pressure between the liquid and the vapor. Thus

$$P_v(z) - P_\ell(z) = \frac{2\gamma}{r(z)} \qquad (2.2)$$

Now the vapor pressure of the liquid depends not only on the temperature T, but also some what on the radius of curvature of the liquid-vapor interface, r. This dependence of the vapor pressure $P= P\,(T,\,r)$, is given by

$$P(T,r) = P(T,\infty)e^{-\frac{2\gamma M}{\rho_\ell RTr}}$$

Where M is the molecular weight of the vapor and R is the universal gas constant. The quantity $2\gamma M/\rho_l RT$ typically has an order of magnitude of 10^{-6} cm or less, and since the capillary pore sizes of practical interest exceed 10^{-4} cm, we may neglect this dependence and take $P = P(T)$ only. In the present equilibrium case the vapor pressure of the liquid must be equal to the pressure in the adjacent vapor, $P(T) = P_v$.

In a capillary structure of minimum pore radius r_c, containing a liquid for which the contact angle is θ, the smallest radius of curvature that the meniscus can achieve is $r_c sec\theta$. The liquid-vapor under some circumstances may be at the surface of the structure

or even outside it, so the maximum radius may be at least as large as the radius of the vapor space.

If enough liquid is present to form a pool in which the gravitational force dominates surface tension, then the radius of curvature of the interface may be essentially infinite. Thus r must lie in the range: $\infty \geq r \geq r_c sec\theta$. Using these limiting values in (2.2) and combining with (2.1) yields for the maximum height of capillary rise, $z_{max}sin\phi$, the well-known result

$$z_{max} \sin \phi = \frac{2\gamma \cos \theta}{\rho_\ell g r_c} \qquad (2.3)$$

In order to work properly the length of the heat pipe should not exceed this z_{max}.

2.2.3 Start-up

The quantitative details of the startup transient are of minor interest. Beginning with the equilibrium condition for which $r(z) > r_c sec\theta$, we consider then what happens when heat is added to the heat pipe in the evaporator section, $0 \leq z \leq \ell_e$. The temperature and consequently the vapor pressure of the liquid rises in the evaporator and falls in the condenser. This gives rise to a pressure difference in the vapor which drives it from the evaporator to the condenser. The driving pressure difference in the vapor is somewhat less than the difference between the liquid and vapor pressures at a given z, since, in order to maintain continued evaporation the vapor pressure of the liquid in the evaporator must exceed the pressure in the adjacent vapor. Similarly, in order to continue condensing, the pressure in the condenser vapor must exceed the vapor pressure of the adjacent liquid. As a result of evaporation the liquid-vapor interface in the evaporator recedes somewhat into the capillary structure and the radius of curvature of the meniscus consequently decreases there. Condensation of vapor increases the radius of curvature of the meniscus in the condenser, if it is not already essentially infinite. Thus, according to (2.2), the pressure distribution in liquid changes in the direction which drives liquid from the condenser to the evaporator. The resulting distribution of pressure is shown in Figure 2-5.

The starting transient is somewhat more complex when the material which will become the working fluid is initially below its melting point. As heat is added to the evaporator section, the material there is brought to its melting temperature and above, and vapor is formed which moves down the vapor duct to the condenser section. Material adjacent to the evaporator section is heated to the melting point partly by the condensation of vapor on its surface and partly by axial conduction of heat along the container wall and the wick. The melt zone thus moves out into the condenser section. In order for the startup to fail, liquid must continually be depleted by evaporation faster than it becomes available by melting, until all liquid formed is deposited as solid in the condenser section. In a large number of test heat pipes of various kinds, successful startup appears to be a fairly general rule as long as there are no unexpected malformations of the wick.
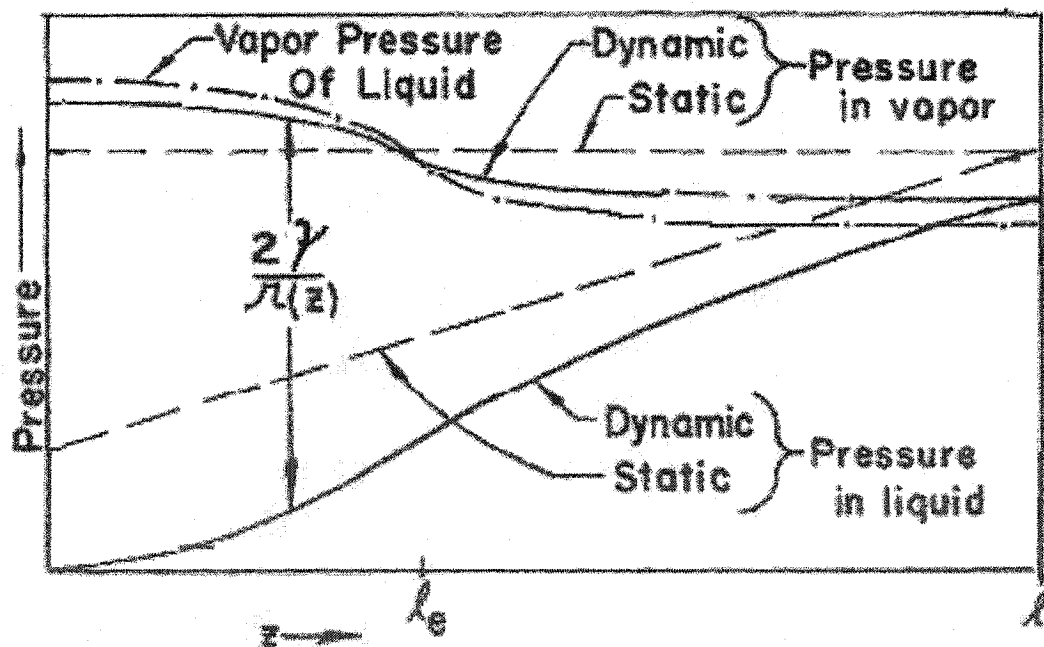
Figure 2-5. Distribution of Pressures in a Heat Pipe

2.2.4 Steady-State Heat Pipe Regime

We consider now the quantitative dynamics of the long cylindrical heat pipe in steady-state operation. We shall derive equations which determine the distribution of energy flow, material flow, and the temperature and pressure within a heat pipe when it is

placed in a specified external thermal environment. The basic working relations are obtained from the general equations of conservation of mass, momentum and energy by taking averages over the radial cross section of the pipe and making simplifying assumptions.

The conservation of mass of a fluid of density $\rho(z, r)$ in steady flow with $\vec{v}(z,r)$ velocity is expressed by

$$\nabla \bullet \rho \vec{v} = 0 \tag{2.4}$$

Since there is no flow normal to the outer boundaries of the liquid region, the velocity components v_z and v_r satisfy the boundary conditions

$$v_z(0,r) = v_z(\ell,r) = v_r(z,r_w) = 0 \tag{2.5}$$

The total axial flow of vapor, m_v, and of liquid, m_l, at axial position z are respectively

$$\dot{m}_v(z) = \int_0^{r_v} \rho_v(z,r)v_z(z,r)2\pi r\,dr; \quad \dot{m}_\ell(z) = \int_v^{r_w} \rho_l(z,r)v_z(z,r)2\pi r\,dr \tag{2.6}$$

Applying Gauss' theorem to (2.4) in a cylindrical region between 0 and z and inside r_w, and using (2.5) and (2.6), yields

$$\dot{m}_v(z) + \dot{m}_\ell(z) = 0 \tag{2.7}$$

The momentum equation for steady incompressible flow is

$$\nabla p = \rho \vec{g} + \eta \nabla \bullet \nabla \vec{v} - \rho \vec{v} \bullet \nabla \vec{v} \tag{2.8}$$

where p is the pressure and η the coefficient of viscosity. The implications of this equation for the liquid and vapor flows are quite different.

As an approximation valid for the flow of liquid through the porous structure of the wick we now obtain a version of Darcy's law. Consider the average of (2.8) over a small area with dimensions small, compared to the thickness of the wick but large compared to the average radius of a capillary pore, r_c. Since the area average velocity, v, includes regions occupied by solid wick structure, the average flow velocity within the pores is (v) /e, where e is the fraction of wick volume occupied by liquid. Since the fluid

velocity is of order (v)/e within a capillary passage and vanishes on the pore surface, then in order of magnitude,

$$(\rho_\ell v \bullet \vec{\nabla}_v) = \rho_\ell (\vec{v})^2 / er_c \qquad \text{and} \qquad \eta_\ell \nabla \bullet \nabla \vec{v} = -\eta_\ell (\vec{v}) / er_c^2$$

The ratio of magnitudes of these two terms is just the Reynold's number for the average flow in a pore, $\rho_\ell \, vr \, / \, \eta_\ell$. The final inertial term in (2.8) is therefore neglected and we have

$$\nabla p_\ell = \rho \vec{g} - b \eta_\ell (\vec{v}) / er_c^2 \qquad (2.9)$$

where b is a dimensionless constant depending on the detailed geometry of the capillary structure. For non-connected parallel cylindrical pores $b \cong 8$. For realistic capillary structures, with tortuous and interconnected pores, $b \cong 10$-20.

The average radial and axial pressure gradients will be inversely proportional to the flow areas in the radial and axial directions respectively. For long thin pipes, that is as long as $r_v 1 >> r_w^2$, the radial pressure gradient will be negligible, and we may assume that both the flow velocity and pressure in the liquid depend only on z. Thus by applying Eq. (2.9) to the axial direction and using the definition of the total liquid mass flow, (2.6), we have

$$\frac{dp_\ell}{dz} = \rho_\ell g \sin\phi - \frac{b\eta_\ell \dot{m}_\ell(z)}{\pi(r_w^2 - r_v^2)\rho_\ell er_c^2} \qquad (2.10)$$

The dynamics of the vapor flow is decidedly more complex, partly because in general an equation like (2.10) relating the local pressure gradient with the local mass flow does not even exist, and partly because of the inertial term in (2.8) is often not negligible in cases of interest. The vapor flow in the evaporator and condenser of a heat pipe is dynamically identical to pipe flow with injection or suction through a porous wall. This problem has been studied by Yuan and Finkelstein [8] for cylindrical pipes, and by Knight and McInteer [9] for flow between plane parallel walls. A summary of the partial results of these authors follows.

Both analyses assume incompressible laminar flow and uniform injection or suction. Several regimes must be distinguished, depending on the magnitude of a Reynolds number, R_r, based on the radial flow velocity at the channel wall, $v_r = v_r(z, r_v)$, the channel radius, r_v, the vapor density, ρ_v, and viscosity, η_v:

$$R_r = -\frac{\rho_v r_v v_r}{\eta_v} = \frac{1}{2\pi\eta_v}\frac{d\dot{m}_v}{dz} \qquad (2.11)$$

Note that R_r is positive for evaporation and negative for condensation. For all values of R_r solutions are found for which the axial velocity profiles are symmetric about the channel axis, with the profiles at different axial stations differing only by a velocity scale factor proportional to the distance from the axial origin of the flow. For $|R_r| \ll 1$, viscous effects dominate and the axial velocity profile is close to the usual parabolic shape for Poiseuille flow. The pressure decreases in the direction of flow, with a gradient larger than that of Poiseuille flow in the case of evaporation, and smaller if vapor is condensing. In this regime the flow properties can be calculated by a straightforward perturbation expansion in powers of the Reynolds number. The resulting pressure gradient is given approximately by [8]

$$\frac{dp_v}{dz} = -\frac{8\eta_v \dot{m}_v}{\pi\rho_v r_v^4}(1 + \frac{3}{4}R_r - \frac{11}{27}R_r^2 + \cdots) \qquad (2.12)$$

This expression is derived on the assumption that R_r as defined in (2.11) is a constant, independent of z. This will often be the case in practical applications of heat pipes.

When $|R_r|$ is large, the evaporation and condensation cases become qualitatively different. Knight and McInteer[9] show this in theory for flow between plane parallel walls. Wageman and Guevara[10] have verified the following description experimentally for cylindrical pipe flow. For high evaporation rates, $R_r \gg 1$, the radial dependence of the velocity is not parabolic but is proportional to $cos(0.5\pi)(r/r_v)^2$. The pressure decreases can be calculated by a perturbation expansion in powers of $1/R_r$. With high condensation rates on the other hand, the flow is of boundary layer type. The axial velocity is constant across most of the channel, with the transition to zero velocity occurring in a thin layer at the wall. The pressure increases in the direction of fluid motion as a consequence of

partial dynamic recovery in the decelerating flow. In this regime only limiting behavior can be described analytically, as perturbation expansions cannot be made self-consistent. In either limit, as $|Rr| \to \infty$, the pressure gradient is given by

$$\frac{dp_v}{dz} = - \frac{s\dot{m}_v}{4\rho_v r_v^4} \frac{d\dot{m}_v}{dz} \qquad (2.13)$$

where the difference in the flows enters only in the numerical coefficients: for evaporation, $s = 1$; for condensation, $s = 4/\pi^2$. As before, (2.13) is strictly correct only for constant R_r.

Nothing appears to be known about the stability of these flows, so that nothing definite can be said about the onset of turbulence. The transition criterion as well as the properties of the fully developed turbulent flow will depend also on a Reynolds number, based on the mean axial velocity v_z,

$$R_z = \frac{\rho_v r_v \bar{v}_z}{\eta_v} = \frac{\dot{m}_v}{\pi r_v \eta_v} \qquad (2.14)$$

We might, however, use (2.12) or (2.13), as appropriate, without regard to the problem of turbulence, for lack of better information, except for one case of practical interest where we may proceed on a sounder basis. If the evaporator and condenser of a heat pipe are connected by a long insulated section, then, since the returning condensate will be heated by the outgoing vapor, there will be a small but ordinarily negligible net condensation along the insulated part so that $R_r = 0$. If $R_z < 1000$, then the expression (2.12) for laminar flow is appropriate. If, however, $R_z > 1000$, and the length exceeds, say 50 r_v, then we should expect fully developed turbulent flow. In this case one should use, instead of (2.12), the empirical Blasius law

$$\frac{dp_v}{dz} = - \frac{0.0655 \, \eta_v^2}{\rho_v r_v^3} R_z^{7/4} \qquad (2.15)$$

To complete the discussion of the flow dynamics we must state the connections between the vapor and liquid mass flows. As in the equilibrium case the interface meniscus

assumes a radius of curvature satisfying equation (2.2), except that at steady state p_v also depends on z. The two mass flows are coupled with the liquid temperature at the

interface, $T(z, r_v)$, which $\dfrac{d\dot{m}_l}{dz}$

in turn determines the vapor pressure of the liquid, p. The local condensation rate is given by the gas kinetic formula

$$\frac{d\dot{m}_\ell}{dz} = -\frac{d\dot{m}_v}{dz} = \frac{\alpha r_v (p_v - p)}{\sqrt{RT/2\pi M}} \qquad (2.16)$$

The numerical factor $\alpha \approx 1$ includes both the probability of condensation of an impinging vapor molecule, and the "roughness" of the meniscus interface formed on the capillary structure. Equation (2.16) also applies for surface evaporation, but not for boiling evaporation, i.e., the formation of vapor bubbles within the capillary structure. We now discuss the transport of energy. If q is the energy flux, then at steady state and in the absence of heat sources, conservation of energy requires

$$\nabla \bullet \vec{q} = 0 \qquad (2.17)$$

The convective and conductive contributions to the steady state heat flux are given by

$$\vec{q} = h\rho\vec{v} - k\nabla T \qquad (2.18)$$

where h is the specific enthalpy of the fluid and k the thermal conductivity of the local medium. Net heat transport due to radiation ordinarily makes a negligible contribution in a heat pipe and it is therefore neglected. The total axial heat transport, $Q(z) =$, is

$$Q(z) = \int_0^{r_p} q_z(z, r)\, 2\pi r dr \qquad (2.19)$$

The desired approximation to (2.19) follows from a definition of the heat pipe regime. The device is operating in the heat pipe regime when, though the heat flow may be very large, the axial and radial temperature gradients throughout are very small, except for the

radial temperature gradient in the container wall and wick. Using the axial component of (2.18) in (2.19), assuming the heat pipe regime prevails, so that axial conduction terms are small compared to convective terms, we have

$$Q(z) = \int_0^{r_v} h_v \rho_v v_z 2\pi r dr + \int_{r_v}^{r_w} h_\ell \rho_\ell v_z 2\pi r dr \qquad (2.20)$$

The specific enthalpies of vapor and liquid depend on temperature and are related by

$$h_v(T) = h_1(T) + L(T) \qquad (2.21)$$

where $L(T)$ is the heat of vaporization at temperature T. The vapor region is at nearly uniform temperature so h_v can be taken out of the first integral of (2.20). If we define a mean specific enthalpy of liquid, h_1, by

$$\bar{h}_\ell = \int_{r_v}^{r_w} h_\ell \rho_\ell v_z 2\pi r dr \Big/ \int_{r_v}^{r_w} \rho_\ell v_e 2\pi r dr \qquad (2.22)$$

then using (2.6), (2.7), (2.21) and (2.22), the expression for $Q(z)$ becomes

$$Q(z) = L\dot{m}_v \left[1 + (h_\ell - \bar{h}_\ell) \; / L \right] \qquad (2.23)$$

Here h_1 is the liquid specific enthalpy at the temperature of the vapor-liquid interface. Since $|(h_1 - h_1)/L| < \Delta T/(L/c_1)$, where ΔT is the radial temperature difference across the wick and c_1 is the specific heat of the liquid, and for liquids $L/c_1 \sim 10^3$ K, the bracketed quantity will differ negligibly from unity in any reasonable case. Thus finally we have the somewhat obvious conclusion that the axial transport of energy is essentially entirely accomplished by the vapor convection of latent heat of condensation:

$$Q(z) = L\dot{m}_v z \qquad (2.24)$$

The heat pipe is coupled to the external environment through the net rate of heat addition per unit length of pipe, $H = H(Z, T_p, Q)$. As indicated, H may depend on: z explicitly, when heat is added with a known distribution, as might be the case with electron bombardment or induction heating of the pipe surface; $T_p = T(z, r_p)$, the temperature of

the external surface of the pipe, as in the case of radiation or conduction to a reservoir of specified temperature; and $Q = Q(z)$, as in the case of heating or cooling using parallel forced convection by an external fluid. In any case the external environment determines H as a known function of its arguments. Applying Gauss' theorem to (2.17) in a cylinder of radius r_p and length dz, and using (2.19), gives

$$\frac{dQ(z)}{dz} = -2\pi r_p q_r(z, r_p) = H(z, T_p, Q) \tag{2.25}$$

The radial heat flux through the container wall and wick to the vapor-liquid interface in the heat pipe regime is found by applying Gauss' theorem to (2.17) in an annulus, $r_p \geq r \geq r_v$, with thickness dz. Using (2.18) and (2.25), one may obtain the following relation:

$$2\pi r_v k_w \frac{\partial T(z,r)}{\partial r} r_v = 2\pi r_p k_p \frac{\partial T(z,r)}{\partial r} r_p \left[1 + (\bar{h}_\ell - h_\ell)/L\right] \tag{2.26}$$

The bracketed quantity again differs negligibly from unity, implying that convection contributes little to the radial transport of energy through the wick. The temperature at the outside of the container and the vapor-liquid interface are thus related by the standard result for radial thermal conduction in a composite cylinder:

$$T_p = T_v + H/K \tag{2.27}$$

where

$$T_p = T(z, r_p) ; \qquad \text{and} \qquad T_v = T(z, r_v);$$

$$\frac{1}{K} = \frac{1}{2\pi} \left(\frac{1}{k_p} \ell n \frac{r_p}{r_w} + \frac{1}{k_w} \ell n \frac{r_w}{r_v}\right)$$

The equations (2.2), (2.10), (2.16), (2.24), (2.25), (2.27) and one of (2.12), (2.13) or (2.15) as appropriate, provide a basis for the quantitative calculation of heat pipe properties.

Approximate solutions of the equations for steady state, which were described above, can be obtained fairly simply. In the heat pipe regime the temperature is nearly

uniform throughout the whole vapor space and the distribution of axial heat and mass flows differ little from what they would be if the vapor temperature was exactly a constant, T_0. If (2.27) is solved for T_p, we may express H in (2.25) as a function of z, T_v and Q.

$$\frac{dQ}{dz} = H(z, T_v, Q) \qquad (2.28)$$

The heat flows through the two ends of the pipe either are negligible or at worst may be known functions of the local vapor temperature, which we denote by $F_0(T_v)$ and $F_1(T_v)$ respectively. The effective average temperature, T_0, and its associated axial heat flux distribution, $Q_0(Z)$, are then obtained as the solution of

$$\frac{dQ_0}{dz} = H(z, T_0, Q_0) \qquad (2.29)$$

$$Q_0(0) = F_0(T_0); \qquad Q_0(\ell) = F_\ell(T_0)$$

Since this is a two-point boundary value problem of a first order differential equation, it can in general only be satisfied for a particular value of T_0. In a physically well defined problem $H(z, T_0, Q_0)$ will depend explicitly on T_0, and the value of T_0 satisfying (2.29) will be unique.

With this good approximation to the heat flux we may obtain the vapor and liquid mass flows from (2.24) and (2.7)

$$\dot{m}_v(z) = -\dot{m}_\ell(z) = Q_0(z)/L(T_0) \qquad (2.30)$$

The vapor mass flow in turn determines the distribution of pressure in the vapor, to within a constant, by integration of (2.12), (2.13) or (2.15) as appropriate. Using $m_v(z)$ and $p_v(z)$ in (2.16) one then determines the vapor pressure of the liquid to within an additive constant. Consistent with the accuracy of the calculation, this constant may be taken as $p(T_0)$. Since the vapor pressure is a known function of the liquid surface

30

temperature, this determines $T_v(z)$. The self-consistency of the approximate calculation is verified if the total variation of $T_v(z)$, found in this way, is small compared to T_0. Finally, the liquid mass flow determines the axial distribution of pressure in the liquid by integration of (2.10). Throughout the foregoing, all the temperature dependent properties, with the exception of the vapor pressure, are sufficiently slowly varying that they may be taken as constants evaluated at T_0.

We now obtain the total pressure and temperature variations along a heat pipe for a particular, but rather commonly met case: constant heat addition along the evaporator, and constant heat removal along the condenser. Thus

$$Q_0(z) = L\dot{m}_v(z) = \begin{cases} \dfrac{z}{\ell_e}Q_e; & 0 \leq z \leq \ell_e \\[2em] \dfrac{\ell - z}{\ell - \ell_e}Q_e; & \ell_e \leq z \leq \ell \end{cases} \qquad (2.31)$$

where ℓ_e is the length of the evaporator and Q_e is the total heat input to the evaporator. Integrating (2.12) and (2.13), neglecting the term in R_r^2 in the former, and assuming ρ_v is constant in both, gives

$$\Delta p_v = p_v(\ell) - p_v(0) = \begin{cases} -\dfrac{4\eta_v \ell Q_e}{\pi \rho_v r_v^4 L} & ; R_r \ll 1 \\[2em] -\dfrac{(1 - 4/\pi^2)Q_e^2}{8\rho_v r_v^4 L^2} & ; R_r \gg 1 \end{cases} \qquad (2.32)$$

From (2.16) one obtains

$$\Delta p = p(T_v(\ell)) - p(T_v(0)) = \Delta P_v - \frac{\ell Q_e \sqrt{RT_0/2\pi M}}{\ell_e(\ell - \ell_e)L\alpha r_v} \qquad (2.33)$$

It is a requirement for the heat pipe regime that both Δp_v and Δp be significantly smaller in magnitude than $p(T_0)$. For the small pressure differences occurring in the heat pipe regime that the Clausius-Clapeyron equation may be used to calculate the temperature difference:

$$\Delta T_v = T_v(\ell) - T_v(0) = \frac{RT_0^2 \Delta p}{MLp(T_0)} \qquad (2.34)$$

The liquid pressure differences, found by integrating (2.10), is

$$\Delta p_\ell = p_\ell(\ell) - p_\ell(0) = \rho_\ell g \sin\phi + \frac{b\eta_\ell Q_c \ell}{2\pi(r_w^2 - r_v^2)\rho_\ell er_c^2 L} \qquad (2.35)$$

As an illustration of the magnitudes of pressure and temperature drops typically encountered, we cite an experimental horizontal liquid sodium heat pipe which was reported in the original description of these devices [9]. The relevant specifications are given in the left column and various derived properties in the right:

$Q_e = 500$ watts $m_v(\ell_e) = 0.1$ g/sec

$T_0 = 920$ K $p(T_0) = 50$ mm Hg

$\ell = 90$ cm $\Delta p_v = -0.2$ mm Hg

$\ell_e = 13$cm $\Delta p = -0.5$ mm Hg

$r_v = 0.64$ cm $\Delta p_l = 2$ mm Hg

$r_w = 0.80$ cm $\Delta T_v = -0.7$ K

$r_c = 0.012$ cm

The main features of a working heat pipe are evident here: The transport of considerable heat is accomplished by the circulation of a small amount of working fluid; this circulation requires but small pressure differences; and the accompanying temperature difference is so small that its precise magnitude is not of importance in practical applications.

While the thermal conductance of a heat pipe is very large there are, however, limitations on the magnitudes of both the total and local energy fluxes. The total axial heat transport may increase only if the force of capillary origin can sustain the required circulation of fluid. As previously noted, the maximum difference in pressure between vapor and adjacent liquid that can be supported by surface tension in the capillary structure is $(2\gamma\cos\theta)/r_c$. It is therefore necessary that

$$p_v(z) - p_\ell(z) \le \frac{2\gamma\cos\theta}{r_c} \qquad ; \qquad 0 \le z \le \ell \qquad (2.36)$$

In general, the largest pressure difference will occur at the beginning of the evaporator section, $z = 0$. If the heat pipe has been prepared with a fully saturated wick, the vapor-liquid interface meniscus will have large radius of curvature at the terminal end of the condenser and, therefore, $P_v(\ell) = P_1(\ell)$. Thus if (2.36) is satisfied at $z = 0$, it will be satisfied for all z.

For the particular case of uniform heat addition and removal we may use (2.32) and (2.35) together with the preceding remarks to write down explicitly the limiting condition on the total axial heat flux:

$$\left.\begin{array}{c} \dfrac{4\eta_v \ell Q_e}{\pi \rho_v r_v^4 L} \\[2mm] \dfrac{(1-4/\pi^2)Q_e^2}{8\rho_v r_v^4 L} \end{array}\right\} + \rho_\ell g\ell \sin\phi + \dfrac{b\eta_\ell Q_e \ell}{2\pi(r_w^2 - r_v^2)\rho_\ell e r_c^2 L} \quad \leq \quad \dfrac{2\gamma\cos\theta}{r_c}; \quad \left\{\begin{array}{c} R_r \ll 1 \\[4mm] R_r \gg 1 \end{array}\right. \qquad (2.37)$$

There is a further limitation on the local radial heat flux in the evaporator section of the heat pipe. The liquid in the interior of the wick here is necessarily superheated. We should therefore expect that the limitation will be closely connected with the conditions for the onset of boiling in the capillary structure and the quantitative properties of the subsequent evaporation and heat transfer. The problems here are more complex even than those encountered in pool boiling of liquids, for in addition to the local limitations of boiling heat transfer, the undoubtedly deleterious interaction of boiling with the overall circulation of liquid throughout the capillary structure will be important. There is no generally useful experimental information available yet on this problem.

We can, however, give a conservative criterion for the nonoccurrence of boiling. The onset of boiling may be characterized by a critical bubble radius of curvature, r_b, which depends on the nature and geometry of the interface where bubbles nucleate. If the difference between the pressure of the vapor in the bubble and the pressure in the surrounding liquid is less than $2\gamma/r_b$, then the bubble will collapse. In a nucleating bubble the pressure in the vapor cannot exceed $p(T(z, r))$, the equilibrium vapor pressure of the

liquid at the local temperature. Furthermore, in the capillary structure r_b cannot exceed $r_c sec\theta$.

$$p(T(z,r)) - p_\ell(z,r) \leq \frac{2\gamma\cos\theta}{r_c} \tag{2.38}$$

Thus as long as bubbles cannot grow beyond the critical size, true boiling will not occur.

A heat pipe will commonly be required to transport the largest possible amount of heat, subject to whatever subsidiary constraints that arise in the particular application. In this case the maximum heat flux criterion (2.36) applies, in the form

$$\Delta p_\ell - \Delta p_v - \frac{2\gamma\cos\theta}{r_c} = 0 \tag{2.39}$$

If the subsidiary constraints do not involve the capillary pore size, r_c, then its optimum value may be deduced from (2.39) alone. According to (2.10) the viscous contribution to Δp_1 is inversely proportional to r_c^2. The standard extreme procedure then yields the result that r_c should be so chosen that the viscous contribution to Δp_1 is one-half the magnitude of the capillary pressure term, $(2\gamma\cos\theta)/r_c$. For example, in the case of uniform heat addition and removal, Δp_1 is given by (2.35), and the optimum choice of r_c is

$$r_c = \frac{b\eta_\ell Q_e \ell}{4\pi(r_w^2 - r_v^2)\rho_\ell eL\gamma\cos\theta} \tag{2.40}$$

If the hydrostatic contribution to Δp_1 is absent, and if the ratio r_v/r_w is not constrained by the subsidiary conditions, then the optimum value of r_v/r_w is 2/3. This follows by noting that if Δp_1 is obtained either from (2.12) or (2.13) as appropriate, and the optimal value of r_c is used for Δp_1 in (2.39) then the greatest heat transport corresponds to the maximum value of $r_v^4(r_w^2 - r_v^2)$. Under these transport conditions one finds

$$Q_e = \begin{cases} \dfrac{\pi r_w^2 L\gamma\cos\theta}{3\ell}\left(\dfrac{e\rho_v\rho_\ell}{3b\eta_v\eta_\ell}\right)^{1/2} & ; \quad R_r \ll 1 \\[4mm] \dfrac{4\pi r_w^2 L}{3}\left(\dfrac{2\rho_v\rho_\ell e\gamma^2\cos^2\theta}{(\pi^2-4)b\ell\eta_\ell}\right)^{1/3} & ; \quad R_r \gg 1 \end{cases} \tag{2.41}$$

If, for example, a fixed total volume of wick is distributed in a uniformly heated evaporator, so as to minimize the liquid viscous pressure drop in this section of the pipe, the cross-sectional area of wick should be proportional to $\sqrt{2}$, and the pressure drop is 8/9 of that of the wick of constant thickness.

2.2.5 Heat Transfer Limitations of a Heat Pipe

Heat transfer in heat pipes is limited by a number of effects, which can be divided into two groups. This is explained in Figure 2-6 [1,11], which is a schematic plot of axial heat flux for the heat pipe versus the temperature drop between the two ends of the heat pipe. Heat transport limitations for heat pipes have been studied for the last three decades.
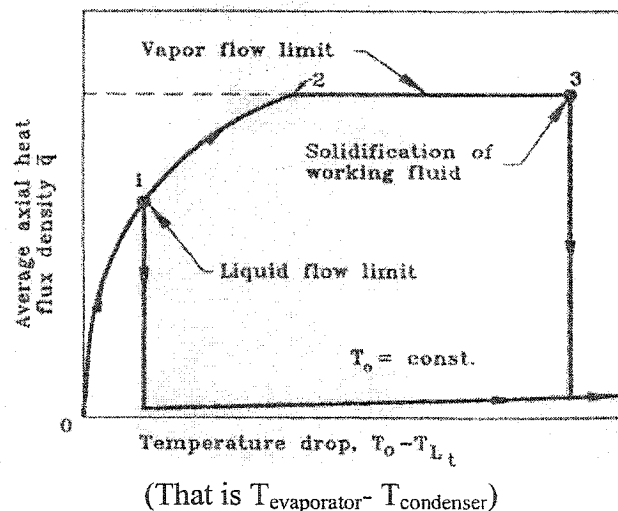
Figure 2-6. Schematic of the Heat Transport Limitations of a Heat Pipe

As shown in Figure 2-6, when no heat is transported, the temperature drop is zero and the heat pipe has a uniform temperature T_0. If one end of the heat pipe is cooled down to a temperature T_l which is less than T_0 ($T_l < T_0$) while the other end is kept at a constant temperature T_0, the heat flux increases very rapidly with $T_0 - T_l$. Continuing this procedure to an even lower cooling zone temperature one arrives at point 1, where the heat flux suddenly drops to nearly zero. This drop stems from an interruption of circulation of the working fluid due to insufficient return flow of liquid, which can be caused by insufficient capillary pressure ("wick limit") or by the formation of bubbles in the wick ("boiling limit"). Supposing that these liquid flow limitations can be overcome

by suitable design of the wick, the heat flux will increase further with decreasing cooling zone temperature, then level off on plateau 2 and finally drop to low values (at point 3) when the cold end of the heat pipe reaches the freezing temperature of the working fluid and the heat pipe is dried out by solidification of the working fluid at the cold end.

Plateau 2 is the subject of the following analysis. It stems from vapor flow limitations and presents an ultimate limit of the heat flux in the sense that it cannot be exceeded regardless of wick construction. For these vapor flow limitations several regimes can be distinguished depending on the relative magnitude of inertia-and viscous forces in the vapor.

In the limiting case of negligible viscous forces ("inertial flow regime"), the vapor flow is limited by the well known choking phenomenon. Choking occurs when the vapor pressure at the evaporator exit is as low as half of the pressure at the upstream end of evaporator. The axial heat flux can no longer be increased by a decrease of the pressure in the condenser (but only by an increase in the pressure and hence the temperature in the evaporator). For choked inertia flow the vapor leaves the evaporator with sonic speed. Therefore the related heat transfer limit is called the (inviscid) "sonic limit".

These are just three of the serious limitations. Since any attempt to increase the heat transfer above the limitations will cause dry-out in the evaporator section, it is very important to understand these limitations in heat pipe design. Following is a summary of heat transport limitations of heat pipes, which are well know.

Capillary limit

The ability of a particular capillary structure to provide the circulation for a given working fluid is limited. Thus, the capillary limit is the highest heat transport rate that can be sustained by the capillary pressure in a heat pipe wick. Higher than that the capillary force is no longer able to pump enough working fluid to cover the entire evaporator. Operating a heat pipe above its capillary limit will result in a dry out region with no working fluid wetting the inner surface. When no working fluid is wetting the surface implies that there is no cooling applied on that region, and thus the dried out region of the evaporator tends to be heated up to the environmental temperature. Thus, the dry out region is often called a hot-spot. When a heat pipe is run at a low temperature, a dry out

region usually results in a lower than the optimum heat transport ability of the heat pipe. And, when a heat pipe is operated in a high temperature environment, dry out often results in the disintegration of the pipe shell in a short time. Therefore, heat pipes, especially those operating in high temperature environments, should operate below the capillary limit. Normally, the maximum capillary pressure for a given wick structure depends on the physical properties of the wick and working fluid.

A capillary limit was proposed by Chun in 1972[12]. Since then, many researchers have adopted it as a standard [1, 3, 5]. However, the capillary limit is still a popular research topic in the many heat pipe designs.

Sonic Limit

As shown in Figure 2-1, the vapor velocity increases along the evaporator and reaches a maximum at the end of the evaporator section. If the velocity approaches the sonic velocity the flow is choked and this is referred to as the sonic limit. In fact, the sonic limit is the highest possible heat transport rate that can be sustained in a heat pipe for a specific vapor temperature at the evaporator end of the heat pipe. Such a system limitation is similar to that of a converging-diverging nozzle with a constant system mass flow rate, where the evaporator exit corresponds to the throat of the nozzle. Therefore, one expects that the vapor velocity at that point cannot exceed the local speed of sound. The sonic limit usually occurs during heat pipe startup or during steady state operation when the heat transfer coefficient at the condenser is high. The sonic limit is associated with liquid-metal heat pipes due to high vapor velocities and low densities. When the sonic limit is reached, the heat transport rate is limited for a given temperature (pressure). Increasing the evaporator end cap temperature will increase this limit to a new higher sonic limit. The rate of heat transfer will not increase by decreasing the condenser temperature under the choked conditions. Exceeding the sonic limit does not mean that the heat pipe will have a serious failure. Usually, there is a significant axial temperature drop along the heat pipe when the heat pipe is operated at the sonic limit.

Boiling Limit

The boiling limit is the highest possible heat transport rate that can be sustained in the heat pipe for a specific vapor temperature at the evaporator section of the heat pipe. It is limited by film boiling of working fluid. If the radial heat flux in the evaporator section becomes too high, the liquid in the evaporator wick boils and the wall temperature becomes excessively high. The vapor bubbles that form in the wick prevent the liquid from wetting the pipe wall, and can thus cause hot spots. This can dry out the wick in the evaporator when the boiling limit occurs. Under a low or moderate radial heat flux, low intensity stable boiling is possible without causing dry out. It should be noted that the boiling limitation is a radial heat flux limitation as compared to an axial heat flux limitation for the other heat pipe limits. The boiling limit is often associated with heat pipes of non-metallic working fluids. For liquid-metal heat pipes, the boiling limit is rarely seen.

Viscous Limit

The viscous limit is the highest heat transport rate that can be sustained in a heat pipe for a specific vapor viscosity at the evaporator end of the heat pipe. At low operating temperatures, viscous forces may be dominant for the vapor flow down the heat pipe. For a liquid-metal heat pipe, the vapor pressure at the condenser end may reduce to zero. The heat transport of the heat pipe may be limited under this condition. The viscous limit usually governs heat pipes when the system pressure is very low. Within a normal range of operating temperature the viscous limit is not an issue. The viscous limit occurs during heat pipe startup from the frozen state since the vapor pressure is very small in this case, with the condenser end cap pressure nearly zero.

Entrainment Limit

A shear force exists at the liquid-vapor interface since the vapor and liquid move in opposite directions. At high relative velocities, droplets of liquid can be torn from the wick surface and entrained into the vapor flowing toward the condenser section. If the entrainment becomes too great, the evaporator will dry out. The highest heat transfer rate at which this occurs is called the entrainment limit. The entrainment phenomenon is an

early signal of an unstable flow condition that can develop into the highest level of system instability and can be even caused by a very small disturbance or perturbation. This thus leads to the partial or total stoppage of liquid flow or dry out. The entrainment limit is often associated with low or moderate temperature heat pipes with small diameter, or high temperature heat pipes when the heat input at the evaporator is high.

2.3 Types of Heat Pipe

Heat pipes can be classified in several different ways:

(1) By operating temperature range: low temperature such as cryogenic and ambient, mid temperature such as thermex, and high temperature such as liquid metals: Sodium and Potassium.

(2) By wicking structure: arterial or composite

(3) By function: rotating/revolving heat pipes, micro heat pipes, flat plate heat pipes etc.

The following summary presents, but a few of the popular heat pipe designs. These descriptions provide information about the general concept and about the use of these different types of heat pipes.

Traditional Heat Pipe

A traditional heat pipe refers to a heat pipe with the original design, as was shown in Figure 2-1. The heat pipe is cylindrical in shape, and has three components (sealed container, wick and working fluid) and three sections (evaporator, adiabatic, and condenser sections). The basic heat pipe can work well for most applications. However, when liquid metals are employed as working fluids these heat pipes pose the problem of starting up from a frozen state. This leads to the development of variable-conductance heat pipes. NASA reported on this when 3 potassium based heat pipes were tested on the Space Shuttle in 1996.

Gravity-Assisted Heat Pipes

For terrestrial applications of heat pipes, gravity-assisted heat pipes deviate from traditional heat pipes by virtue of their orientations. For any orientation whereby the

evaporator is lower than the condenser, in the other words, that gravity assists the condensed working fluid return from the condenser to the evaporator, the heat pipe is referred to as a gravity assisted heat pipe, as shown in Figure 2-7.
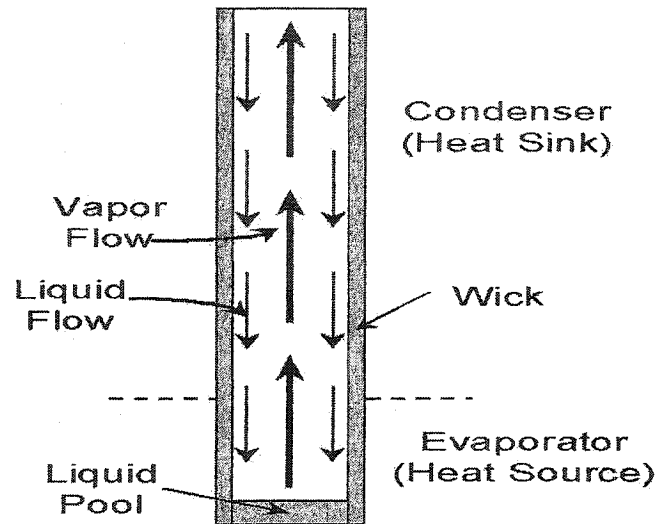
Figure 2-7. The Overall Concept of the Gravity Assisted Wick Heat

The gravity assisted wicked heat pipe has become increasingly popular in terrestrial applications because of its high heat transfer performance and less stringent requirement on the wick structure.

Heat pipe startup characteristics are of interest because the heat pipe working fluid inventory that forms a pool in the lowest part of the evaporator section behaves differently from the working fluid in basic heat pipes. Slugging of the working fluid is a unique character, which may occur during startup. Gravity assisted heat pipes have been used for a variety of terrestrial applications, such as heat recovery, energy conservation and solar energy utilization.

Variable-Conductance Heat Pipes

Variable conductance heat pipes are the most versatile modification of the basic heat pipe. This type of heat pipe not only has the three sections-evaporator, adiabatic, and condenser sections as the basic heat pipe has, but it also has one more section-the inert gas section. If the volume ratio between the inert gas section and all the other sections is

big enough, the variable conductance heat pipe is capable of maintaining a near constant temperature at the evaporator, adiabatic, and condenser sections, independent of the amount of heat energy being transported by the pipe.

The concept of the variable conductance heat pipe was first examined by Wyatt during experiments on non-condensable gas generation within sodium-stainless steel heat pipes [13]. The schematic of a variable-conductance heat pipe shown in Figure 2-8 is of the passively controlled type.
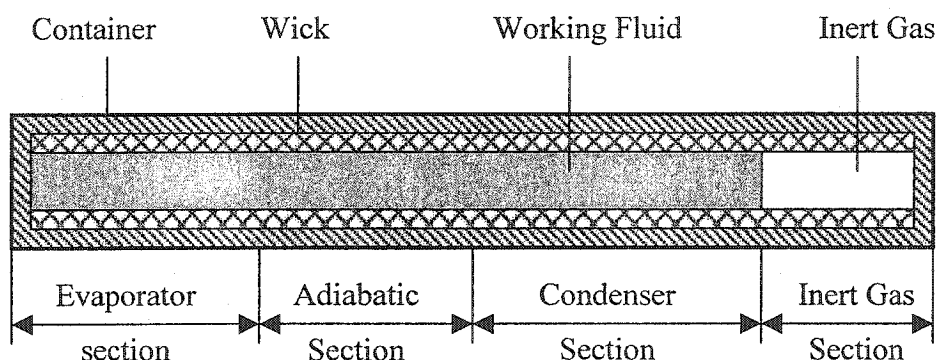
Figure 2-8. Schematic Diagram of a Variable-Conductance Heat Pipe

Typically, variable-conductance heat pipes are referred to as heat pipes with a modified design. This means that the heat pipes are still cylindrical in shape, but have four components (pipe shell, wick structure, working fluid, and inert gas) and four sections (evaporator, adiabatic, condenser, and inert gas sections). Variable conductance heat pipes are often referred to as gas-loaded heat pipes or gas buffered heat pipes.

Liquid metal heat pipes have exhibited difficulties starting up from a frozen-state. Inert gas loading is a possible solution to the frozen-state startup problem [14, 15, 16].

Rotating Heat Pipe

The rotating heat pipe, as envisaged by Gray [17], is a two phase thermosyphon in which the condensate is returned to the evaporator by means of centrifugal force, as shown in Figure 2-9. The rotating heat pipe consists of a sealed hollow shaft, having a slight internal taper along its axial length, and containing a fixed amount of working

fluid. The rotating heat pipe, like the basic heat pipe, is divided into three sections: the evaporator, adiabatic, and condenser regions. However, rotation about the axis will cause a centrifugal acceleration with a component along the wall of the pipe. The corresponding force will cause the condensed working fluid to flow along the wall back to the evaporator section.
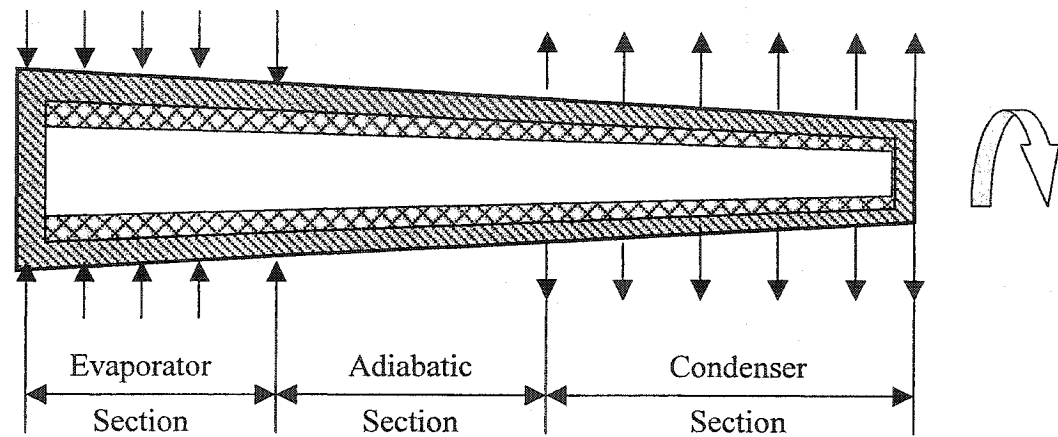
Figure 2-9. Schematic Diagram of a Rotating Heat Pipe

Polasek reported experiments on cooling of an a/c motor incorporating a rotating heat pipe in the hollow shaft [18]

Micro Heat Pipe

In 1984 Cotter [19, 20] first proposed incorporating heat pipes which are called micro heat pipes as part of semiconductor devices, and defined it as one "so small that the mean curvature of the vapor-liquid interface is necessarily comparable in magnitude to the reciprocal of the hydraulic radius of the flow channel." Since the initial conceptualization in 1984, numerous analytic investigations of micro heat pipes have been conducted, however experimental investigation of micro heat pipes have been very limited. Micro heat pipes differ from conventional heat pipes in that they are significantly smaller (characteristic dimension measured in microns) and have no formal wicking structure to assist the return of the condensate to the evaporator region. The highest heat transfer typically occurs when a pure substance or mixture undergoes a phase change. In situations where this phase change process involves evaporating or condensing fluids, the

heat transfer can be enhanced through the use of small capillary grooves which increase the effective liquid-vapor interfacial area for evaporation or the effective solid-vapor surface area for condensation. These capillary grooves allow the liquid to coalesce and promote the flow of liquid under the action of capillary forces, either away from the condensing region or towards the evaporating region.

Typically, the heat transfer enhancement of these capillary grooved surfaces can be easily controlled by the number, length, and shape of the capillary grooves. Recently, increased interest in the use of phase change heat transfer processes for the thermal control of spacecraft and electronic components, either through traditional methods or more innovative methods involving the use of micro heat pipe devices has resulted in the need for a better understanding of the liquid film behavior in these grooves.
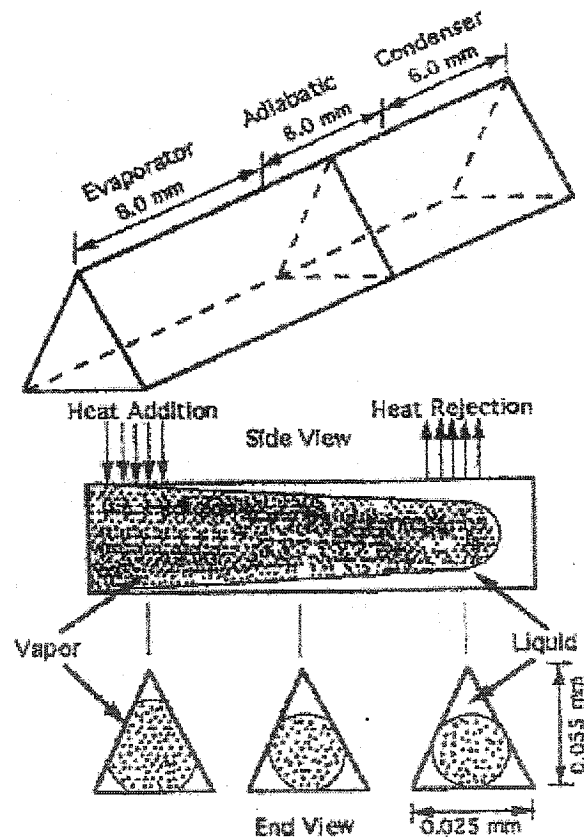
Figure 2-10. A Schematic Diagram of a Micro Heat Pipe

The evaporating meniscus in a very thin film formed on a grooved surface is shown in Figure 2-10. In such circumstance, the liquid film gets thinner and thinner and there exists an attractive force between the solid wall and the liquid at the molecular level. This phenomenon produces a pressure difference across the liquid-vapor interface due to the repulsion of the vapor phase by the solid and liquid long range intermolecular forces, i.e., van der Waals dispersion pressure. This reduction in liquid film pressure is termed the disjoining pressure. The extended meniscus formed on the heated wall is characterized by three regions. The intrinsic meniscus is formed at the base of the extended meniscus, and is described by the conventional equation of capillary while excluding the effects of disjoining pressure. The second region the evaporating thin film is above the intrinsic meniscus, and results from the combined effects of the capillary and disjoining pressures. In the adsorbed layer region (third region), the adhesion forces or disjoining pressure prevent evaporation and no heat transfer occurs from the wall. The non-evaporating adsorbed layer and the evaporating thin film meet at what is termed the interline. It is believed that most evaporation takes place at or around this interline region.

Therefore, micro heat pipes, two-phase convection devices, yield by far the highest cooling rates per unit volume in electronic systems, as evidenced by the effectiveness and large commercial impact of heat pipes in portable systems. The micro heat pipe built directly within the substrate material carries heat away from the chip much more efficiently than conduction through solid copper or transport through larger heat pipes on the substrate surface and thus allows for greater heat reduction and improved temperature control. The closer the coolant is to the circuit, the more heat can be managed. As the coolant directly underneath the operating micro chip heats up and evaporates, it moves through the capillaries to cooler areas, where it re-condenses, distributing its heat throughout the substrate. Capillary pressure on the re-condensed liquid then pulls coolant back to hotter regions where evaporation has occurred, similar to the way a candle wick draws molten wax upward to the flame.

Loop Heat Pipe

Loop heat pipes (LHPs) are a class of capillary pumped devices used for transporting heat across a distance of up to several meters in both gravity and

44

microgravity environments. They were originally developed for the terrestrial solar energy market by J. F. Maidanik and his colleagues in the former Soviet Union in the early 1980's [21].

LHPs consist of a heat-accepting evaporator, a heat-rejecting condenser, a fluid reservoir (compensation chamber) and tubing to connect the pieces. There are no moving parts, only moving fluid. Capillary pumping is produced by a small-pore wick inside the evaporator. A schematic diagram of the structure is shown in Figure 2-11, in which fluid is drawn by capillary forces from the inside to the outside surface where it evaporates due to the addition of heat. This vapor then flows to the condenser, rejects heat to the environment and returns to the reservoir as a liquid.
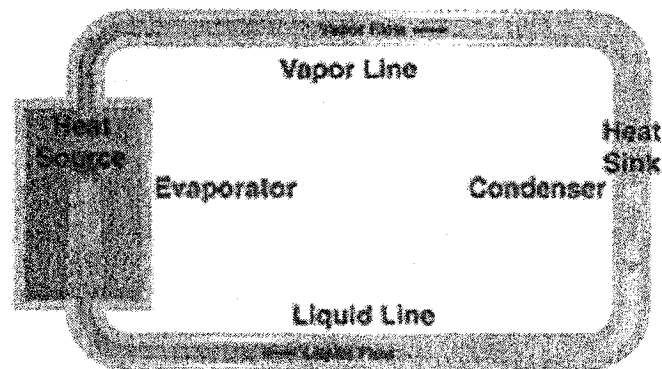
Figure 2-11. The Schematic Diagram of Loop Heat Pipe

The efficient nature of phase change heat transfer allows for the transport of kilowatts of heat with only a few degrees of temperature drop. The pressure head developed by the capillary action is inversely proportional to the square of the pore diameter in the wick material.

The advantages of LHPs over conventional heat pipes include: self-priming during startup transients, diode-action capability, increased tolerance for non-condensable gas, ability for ground testing in any orientation, and reduced mass by the elimination of wicks in the adiabatic and condenser sections. These advantages, combined with the inherent heat pipe properties of high heat transfer rates and no moving parts, make loop heat pipes attractive for many applications of interest to NASA and others.

2.4 Applications of Heat Pipes

Heat pipes were first described by Grover, Cotter, and Erickson of Los Alamos National Laboratory in 1964 [1]. Initial efforts of heat pipe research were directed towards heat transport applications in the NASA space program. The high reliability of the heat pipe and its capability for isothermal operation without the need for external power make it suitable for operation under the weightless conditions of space. It was soon realized that the unique characteristics of the heat pipe would be equally useful here on earth, and terrestrial applications began to receive considerable interest as well. At present, heat pipes are widely used (1) for heat removal in nuclear power plants (and reactors), (2) for cooling of the stagnation regions on hypersonic vehicles, (3) for cooling of electronic equipment such as computers, (4) in energy storage and waste-heat recovery units, (5) for solar energy utilization, and cookers etc. In practice, heat pipes are used over a wide temperature range (from 2K for helium up to 2000K for silver) [22]. A wide variety of heat pipe fluids have been used from liquid hydrogen and nitrogen at cryogenic temperatures, to water, ammonia, and alcohol at near-ambient temperatures, to liquid metals such as sodium and lithium at elevated temperatures. The following narrative is one way to classify the applications for heat pipes.

2.4.1 Electronic Devices Cooling

In recent years, the electronics industry has been continually improving the performance capabilities of electronic components while reducing the physical size. These improvements often result in greater power densies and increased amounts of heat that must be removed from the system. The most recent example of this is release of the Pentium microprocessor by Intel Corp. The Pentium produces 13-15 watts of heat, compared to the 3 watts produce by the 486 microprocessor. This causes computer components that use these devices to run three to five times hotter than 486 systems at twice the standard fan speed. To reduce the occurrence of electronic failures in these types of emerging electronic systems, new cooling techniques capable of rejecting larger quantities of heat must be developed that are both effective and reliable.

Most electronic components must operate with junction temperatures less than 100 °C. Additionally, the Military Handbook 217 states that failure rates of many electronic components can double for 20 °C rise in the component hot spot temperature. Although micromechanical heat sinks exist that can handle large amounts of heat, these mechanisms often produce large variability in device reliability. Experiments have demonstrated heat pipes to be extremely effective at dissipating and transporting heat while maintaining uniform temperatures across the heat source.

There exist several conventional cooling systems for electronic devices. However, heat pipes cover the complete spectrum of temperatures encountered in these heat transfer processes. Heat pipes have been used for cooling electronic systems of small and medium capacities for many years. The heat generated from the devices is transferred efficiently through the heat pipe to the radiator and dissipated to the atmosphere by other heat transfer methods.

Figure 2-12 [23, 24, 25, 26] shows some examples of using heat pipes to cool electronic components.
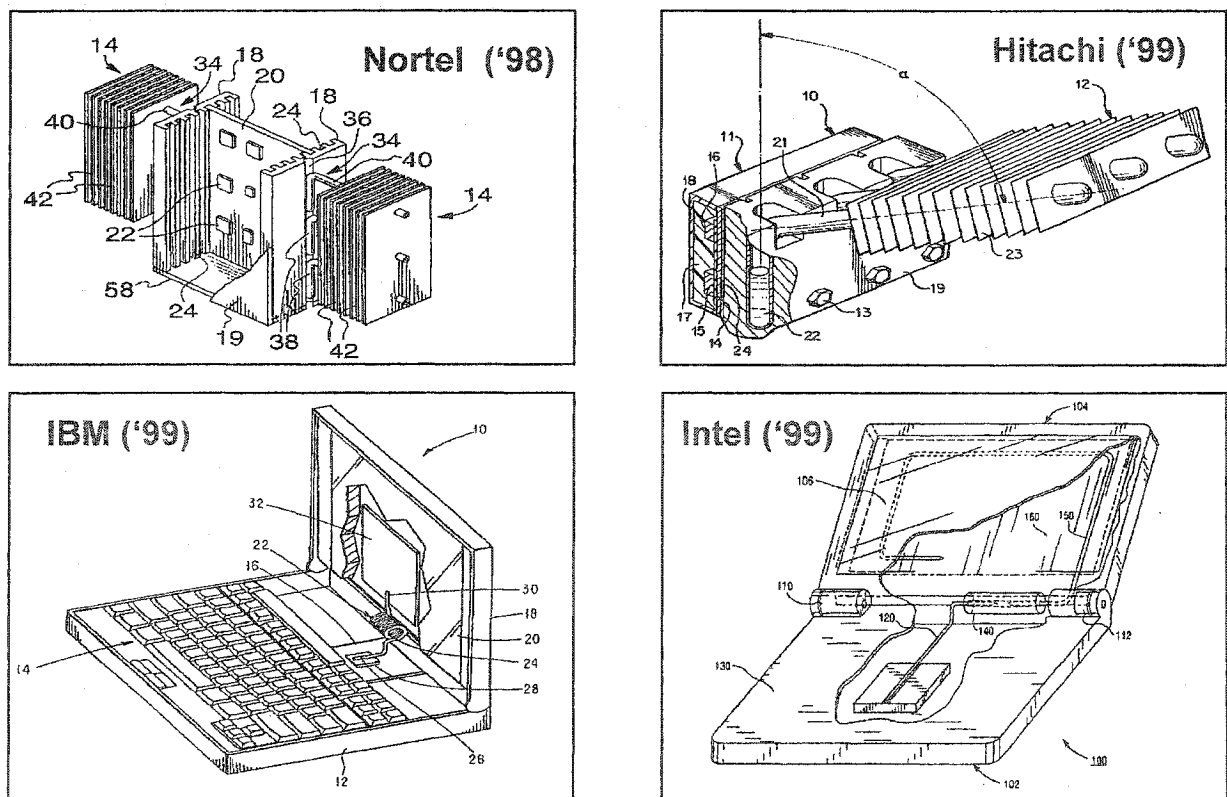
Figure 2-12. Heat Pipes Cooling Electronic Components

2.4.2 Heat Transport/Transfer in a Solar Unit

Over the past decade several programs have been initiated to develop solar dish-electric systems for terrestrial and space power generation. In these systems, a parabolic dish reflector tracks the sun and focuses concentrated solar energy on a receiving surface. The collected energy is transferred to the working fluid of a heat engine and converted to electricity. Usually, a Stirling cycle engine, with electrical power output of 25 kW for a 75 kW thermal input to the receiver, is used in many of the dish-electric systems that are currently operating. In general, tubes that carry the working fluid (typically helium or hydrogen) in these engines are directly illuminated by the concentrator. Directly heating the engine's heater tubes does have some shortcomings, though. For instance, it is usually desirable to provide a uniform heat flux to the tubes so that thermal stresses in the heater tubes are minimized and the operating temperatures are balanced in multicylinder engines. Forming heater tubers into shapes that receive a uniform flux distribution can be complicated and difficult to produce in large numbers, and tube shapes that receive a uniform flux are not necessarily well matched to the engine's geometry or flow requirements. In addition, convection currents in the receiver cavity and optical flaws in the concentrator can contribute to the nonuniform heating of an engine's heater tubes. To resolve these problems, the heat pipe receiver was introduced to couple solar concentrators to heat engines.

In a terrestrial heat pipe receiver system, liquid sodium is carried across the back side of a solar energy absorbing surface by the capillary action of a wick (see Figure 2-13 [26]). As the sodium evaporates, it removes energy from the absorbing surface. Vaporized sodium then flows to the heater tubes of the engine, where it condenses and transfers the latent heat to the engine's working fluid. Condensed sodium returns to the absorber surface by gravitational and/or capillary forces. The heat-pipe receiver is evacuated when it is constructed, so the sodium is always in a saturated state. Sodium heat pipes have a demonstrated ability to remove over 1 kW of thermal energy per square centimeter of heated surface at vapor temperatures near 800 °C. Heat fluxes are an order of magnitude lower in solar heat-pipe receiver systems, but the shape of the absorber surface can cause problems because of the pumping requirements it places on the wick. In contrast to a conventional tubular-shaped heat pipe, which is seldom required to transport liquid more

than a few centimeters against gravity, liquid sodium may be required to wick about 50 cm vertically in a heat pipe receiver. In addition, the system must work reliably for 20 years (60,000 operating hours) in a thermally cycling environment to meet system life goals [26].

A schematic of the proposed heat-pipe solar receiver is shown in Figure 2-14 [26]. Low carbon 316 stainless steel is selected as the material for both the absorber dome and the rear shell. During steady-state operation, the sodium vapor temperature will be 800 °C. The internal pressure will correspond to the saturation pressure of sodium, which varies from less than a millipascal at the triple point of sodium to 45.4 kPa at the system's operating temperature. The absorber dome is thin and fairly deep to reduce thermal and creep stresses through the operating and non-operating cycles.

Sodium vapor travels to the heater tubes of each cylinder through four separate ducts. The ducts are made of 3.8 cm (1.5 inch) stainless steel tubing, and, even though the tubes are shown straight in Figure 2-14, the actual receiver uses welded fittings to align the engine's heater tube ports with the receiver's vapor ducts. A tube is located at the bottom of each vapor duct to provide a return path for the condensed sodium. The return tubes lead to screen troughs that are placed across the evaporator surface. These troughs are intended to aid in the redistribution of sodium.
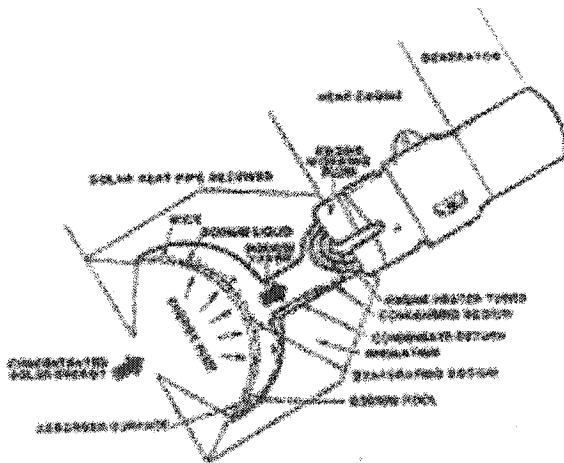
Figure 2-13. Cross-sectional View of a Heat Pipe Solar Receiver Attached to Heat Engine
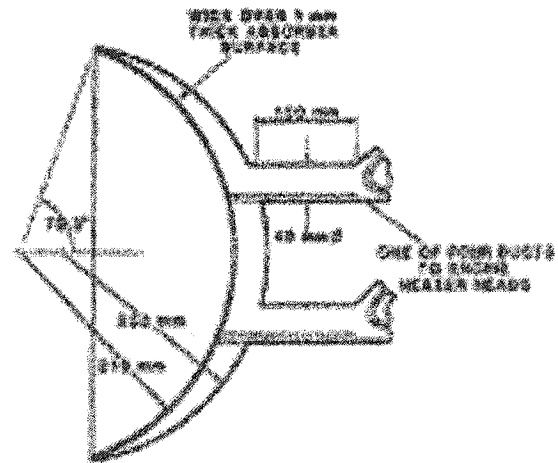
Figure 2-14. Proposed Geometry for 75-kW Solar Receiver for Testing on a 11-m Concentrator

2.4.3 Heat Pipe Heat Exchangers

(A)   (B)
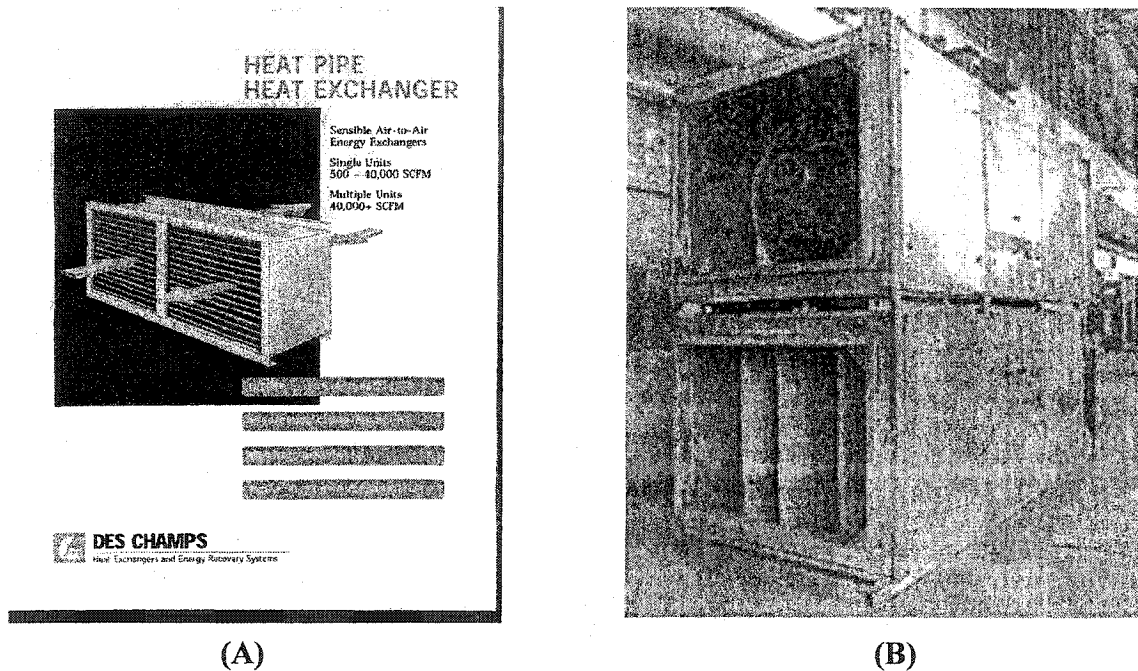
Figure 2-15. Air-condition System on Heat Pipe Heat Exchanger

Increases in the cost of energy have promoted new methods of conserving energy in industrial applications. Due to their high heat transfer capabilities with no external power requirements, heat pipes are being used in heat exchangers for various applications. In the power industry, heat pipe heat exchangers are used as primary air heaters on new and retrofit boilers. The major advantages of heat pipe heat exchangers compared to conventional heat exchangers are that they are nearly isothermal and can be built with better seals to reduce leakage. Heat pipe air heaters should also be cheaper than conventional tubular heat exchangers because they are smaller and can be shipped in a small number of modules. Heat pipe heat exchangers can serve as compact waste heat recovery systems which require no power, low pressure drop and are easy to install on existing lines. Heat pipe heat exchangers can be categorized into gas/gas, gas/liquid, and liquid/liquid type units. Among these three, gas/gas heat pipe heat exchangers have the widest application in industry. A gas/gas heat pipe exchanger consists of a group of heat pipes. Normally, gas/gas heat pipe heat exchanger units for energy recovery are divided into three types: heat recovery in air-conditioning systems (low temperature)[27], recovery

of excess process heat for space heating (moderate temperature), and recovery of waste heat from exhaust streams for reuse in the process (high temperature)[4]. Figure 2-15a and Figure 2-15b [4] are recovery units of heat pipe heat exchangers. For example, heat pipe heat exchangers are now used in metallurgy (steel producing plants) as air pre-heaters and in boilers. They save more than 10×10^3 kW of energy [4].

2.4.4 Applications in the Metallurgical Industry

Given that heat pipes are such effective cooling systems and so many components for pyrometallurgical equipment need to be cooled, the pyrometallurgical industry should be one of those industries which would be involved in the development and implementation of heat pipe technology. Unfortunately, it has not yet happened in the pyrometallurgical industry. Nevertheless, there have been a few reports and proposals on the applications of heat pipe technology in metallurgy.

Heat pipe lance

Injection of air in smelting and refining has been practiced for centuries. Since the advent of tonnage oxygen some 50 years ago, injection technology has been incorporated into numerous processes and has greatly increased productivity. Over the years, injection technology has evolved into two main avenues. One is submerged injection through tuyeres while the other is top injection through a lance positioned above the melt. Tuyere injection is practiced in many processes such as in copper (e.g. Peirce-Smith converter and Noranda reactor) and steel (e.g. Q-BOP) making. It entails injecting a reagent, usually enriched air, through a set of submerged nozzles. In general, top injection lances can be classified into two groups: consumable and non-consumable lances. The basic difference between the two groups is the cooling of the lance. If the lance is water cooled, it is non-consumable; if it is not water cooled it is consumable. While non-consumable lances are preferred for obvious reasons, they present serious safety concerns in the event of failure because of the water component. Moreover, the infrastructure costs arising from the use of recycled water can be sizeable. For these reasons, non-consumable lances, which also suffer from several major disadvantages, continue to be used. In fact, the vast majority of water cooling lances are used only in the steel industry in such units

as the BOF and the electric arc furnace. Other industries, while recognizing the advantages, have been reluctant to adopt them. Examples where consumable lances are used are the Mitsubishi and Ausmelt processes.
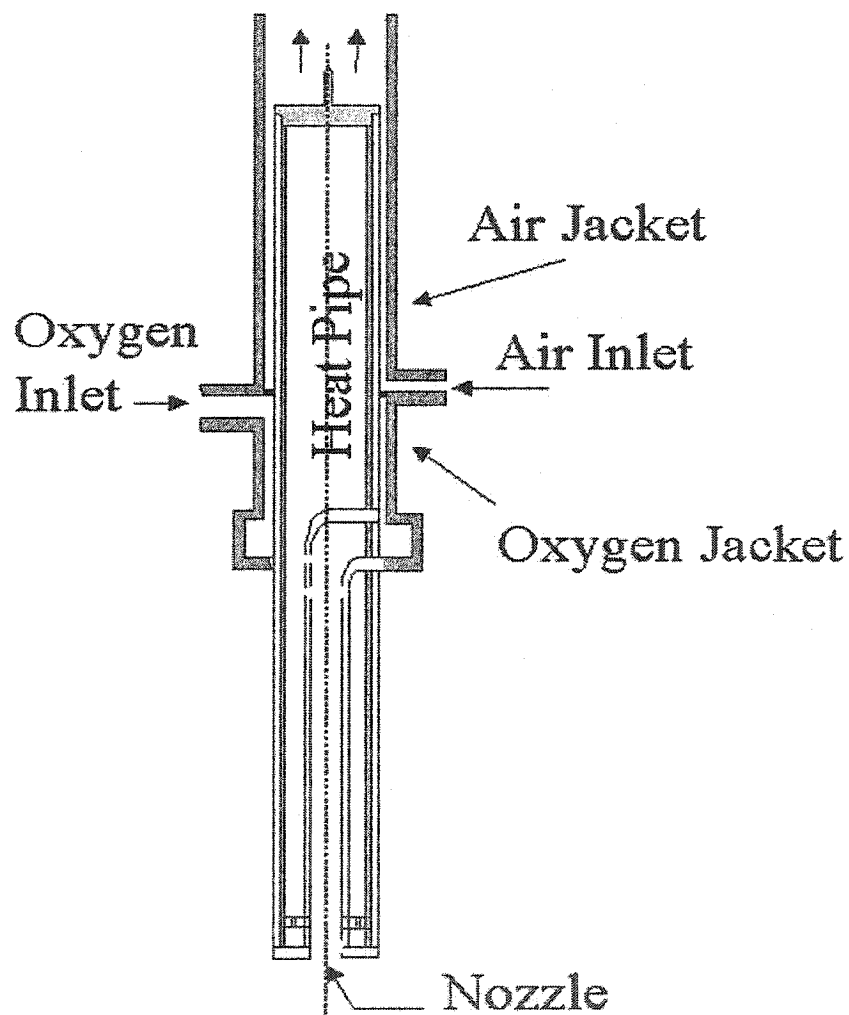
Figure 2-16. Schematic of New Heat Pipe Lance Design

A novel heat pipe lance has been developed at McGill University [28, 29, 30, 31]. This lance overcomes many of the disadvantages of both types of lances. The lance uses air cooling to replace water cooling found in non-consumable lances. In 1997, a U.S. Patent [28, 29] described this lance in detail. A schematic of the heat pipe lance is shown in Figure 2-16. One will note that the reagent is introduced into an annular jacket to both cool the

lance and preheat the reagent. The reagent travels downwards through the jacket towards the nozzle. Once sufficient preheating is achieved, it crosses to the core of the lance to be injected into the melt. The cooling air on the other hand is introduced at the bottom of the air jacket and travels upward to the exhaust. Condensation of the working substance occurs on the inner walls of both jackets.

All components of the heat pipe cooled injection lance were made of stainless steel 316L except for the tip of the lance. The lance tip was made of nickel 200 for better heat transport. The heat pipe body was made from a piece of 25.4 mm outer diameter tubing of 500 mm in length and 1.65 mm in wall thickness. Based on past experience, two wraps of 100 mesh stainless steel screen were incorporated as the wick structure in the heat pipe. The wick covered the entire inner surface of the heat pipe shell. A piece of pipe of 31.8 mm outer diameter and 260 mm in length with a wall thickness of 1.65 mm was used as the air cooling jacket. The jacket was concentric with the heat pipe shell. It covered 220 mm of condenser starting from the top cap, and the other 40 mm of the jacket stuck out from the top of the condenser to protect the sealing nipple as shown in Figure 2-16. In addition, an 80 mm length of the same tubing that was used for the air cooling jacket was employed as the reagent (e.g. oxygen) preheating jacket and was positioned immediately below the air cooling jacket in a concentric position with the heat pipe shell as shown in Figure 2-16. A piece of 6.35 mm outer diameter tubing of 200 mm in length and 0.89 mm in wall thickness was used as the central reagent conduit. It passed through the heat pipe to connect the reagent preheating jacket and the nozzle while the nozzle was of the straight bore variety with a 2 mm opening. The bottom 200 mm of the heat pipe shell was left exposed. This then was the maximum size of the evaporator. A piece of 6.35 mm outer diameter tubing of 500 mm length and 0.89 mm wall thickness was positioned axially in the heat pipe. It served as a thermocouple well with the leading end closed and in contact with the leading end of the lance. The other end was welded on the top cap and was left open.

Prior to welding on the top cap, the pipe was charged with working substance. The charge consisted of 20 g of sodium (99% purity). Subsequent testing showed that after accounting for all loses incurred prior to sealing, the remaining quantity of sodium occupied a length of about 50 mm at room temperature.

The heat pipe lance was conditioned in a hot furnace environment ranging between 750°C and 900°C. A vacuum pump was used to remove non-condensable gases within the pipe which was sealed hot. The pressure within the pipe at room temperature was estimated to be about 10^{-5} atm at room temperature. Figure 2-17 presents several pictures of the heat pipe lance as applied in copper making and steelmaking lab testing, respectively.

A. Copper Converting   **B. SteelMaking**
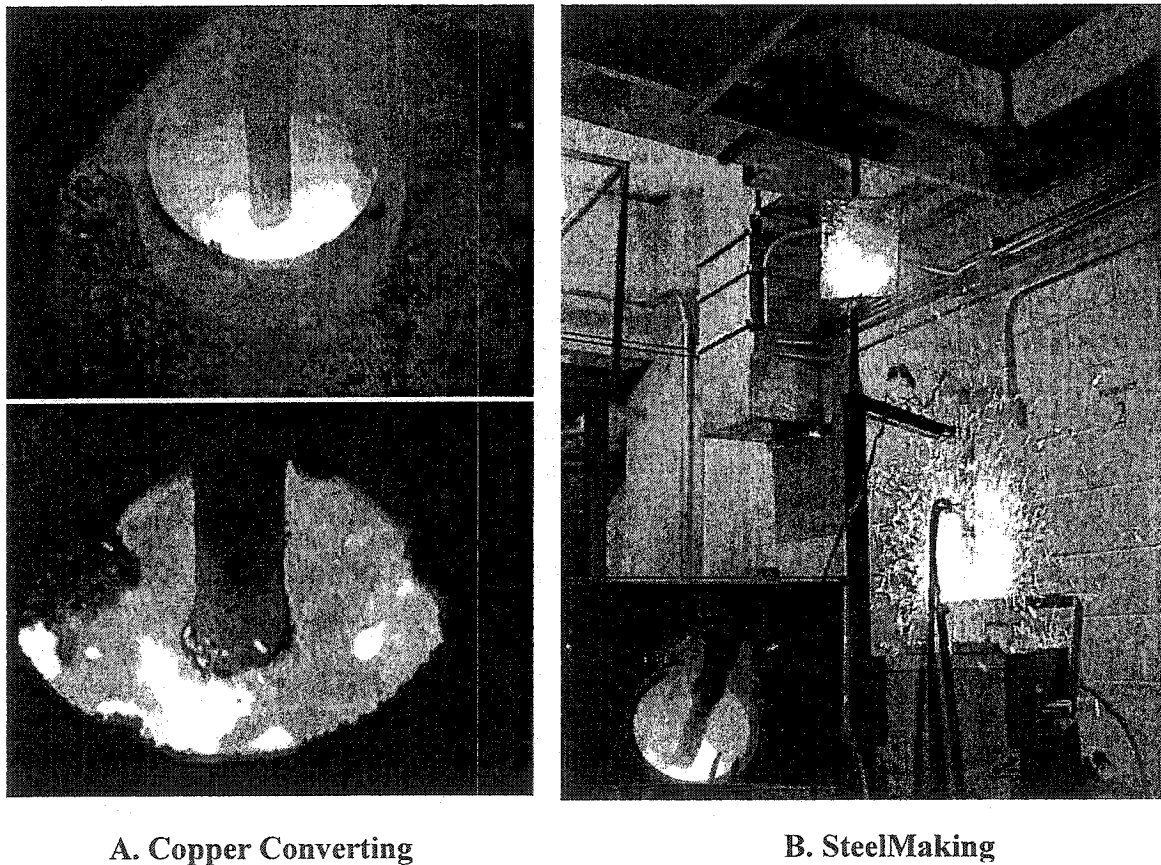
Figure 2-17. The Heat Pipe lance Applications in Copper Converting and Steelmaking

Heat pipe caster

Twin roll (or drum) casting has been the focus of numerous researchers during the last 20 years and, in particular, the last decade. All the researches have focused on the use of water cooling of the rolls to cause solidification on the rolls. Reference 32 described the only research known to the author wherein sufficient cooling is achieved with air and not water. The caster application that was developed was designed, built, tested and

modeled for the casting of copper matte at about 1200°C. For the present application, the heat pipe is configured horizontally. An outer roll defines the extremities of the heat pipe. Energy is transferred through the outer roll and is absorbed by the working substance which wets the entire circumferential area of the roll. Since it is important to have the working substance contacting the inner area, the surface is fitted with a wick to ensure uniform coverage by the liquid.

As the liquid working substance is in thermodynamic equilibrium with its vapor, the condensation of vapor creates an opportunity for liquid to vaporize. Thus, one need only produce condensation sites to create an active heat transfer system. The condensation areas that were adopted are created by horizontal cooling pipes running through the core of the outer roll. Coolant in the form of low pressure air is forced through the cooling pipes. Thus, the outer surfaces of the cooling pipes act as condensation sites (i.e. heat extraction areas) for the working substance vapor. In essence, the evaporator is formed by the inner surface of the roll while the condenser is formed by the outer surfaces of the cooling pipes. This configuration is the subject of a joint Noranda-McGill patent application and is shown schematically in Figure 2-18.
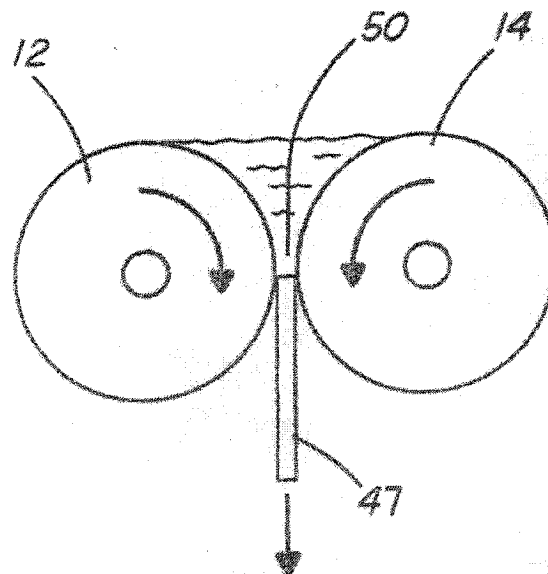
Figure 2-18. Schematic of Twin-Roll Caster as per the Noranda-McGill U.S. Patent Application

The roll was fabricated from 316L stainless steel. The unit had an outer diameter of 0.3 m and a width of 0.16 m while the thickness of the roll was 7 mm. The caster contained cooling pipes with a total condensation area of 0.39 m^2. A thermocouple was mounted in the working substance chamber. The working substance that was used in this caster was sodium. Stainless steel screen lined the inner surface of the drum to form the wick.

The drum was rotated at 10 RPM. The caster was fed matte that was initially at 1184°C. The cooling air flow, once turned on, was maintained at 103 SCFM. With the cooling air on, the temperature of the caster was stabilized and a strip averaging about 1.5 mm in thickness was produced and the rate of heat extraction by the cooling air was about 20 kW.

Heat pipes have also been used to 1) for cooling and temperature control in die-casting [33], 2) in heat exchangers in waste heat recovery [4], 3) as an in-situ, semi-continuous thermal analysis probe [34], and 4) for cooling of furnace tapholes [35, 36].

CHAPTER 3. LOOP HEAT PIPE AND PROJECT OBJECTIVES

3.1 The Concept of the Loop Heat Pipe

3.1.1 Introduction

The loop heat pipe is an extension of the conventional heat pipe. Compared with the conventional heat pipe, which is typically made of a straight length of pipe, the loop heat pipe is made by looping a piece of pipe to form a continuous entity. Therefore, loop heat pipes (LHPs) rely on geometric and other design constraints to ensure that liquid is always available to the wick. The upper liquid reservoir, also known as the compensation cavity, stores sufficient liquid that even if it were drained, the liquid would flood the vapor lines to the level of the wick which can not dry out. If the reservoir is not completely drained then liquid is directly available to the wick. The arrangement of vapor grooves and passages ensures that initial vaporization occurs within the vapor space. The configuration of the liquid return line within the compensation cavity provides the added benefit of making the LHP tolerant of the presence of non-condensable gas.

The loop heat pipe (LHP) is a two-phase thermal transport device for transporting heat over long distances in both gravity and micro-gravity environments. It was originally developed for the terrestrial solar energy market by Y. F. Maidanik and his colleagues in the former Soviet Union in the early 1980's [1, 2], parallel to the development of the capillary pumped loop (CPL) [3], which is another version of the loop heat pipe. It operates on the principal that the capillary forces developed in the wick circulate the liquid around the loop and is described in a subsequent section in which are reviewed a number of U.S. Patents that describe LHP or versions thereof.

3.1.2 The Principle of the Loop Heat Pipe [1, 2, 4, 5]

The operation of a typical LHP, as shown in Figure 3-1 [1], begins with the application of heat to the evaporative zone, which evaporates the working fluid. The vapor is then collected by grooves in the porous insert. As the vapor travels the length of the evaporator through the vapor grooves, it becomes slightly superheated because the

inner wall temperature of evaporator is higher than the saturation temperature. The vapor is forced into the evaporator line by the pressure difference between the evaporator and condenser. The working fluid then enters the condenser section and condenses on the tapered walls. The liquid flows down the length of the tapered annulus by gravity and capillary pressure where it is subcooled. The subcooled liquid returns to the reservoir (or compensation cavity) by the capillary pumping pressure of the wick structure. The subcooled liquid is distributed to the evaporator from the reservoir.
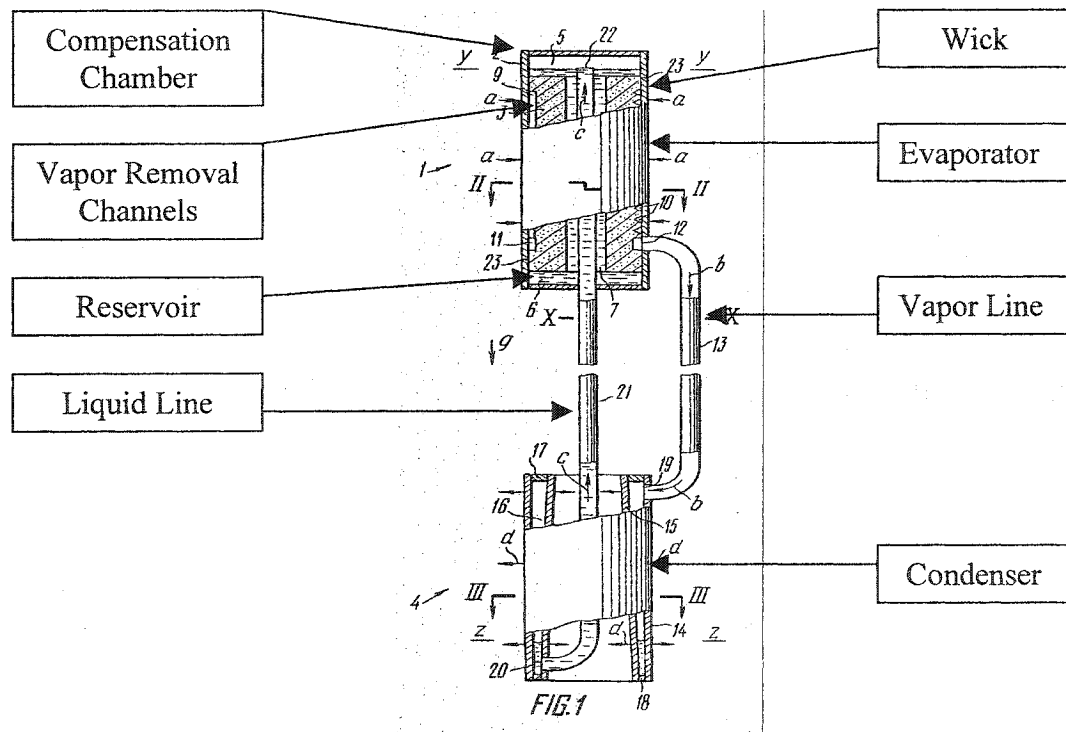
Figure 3-1. Schematic Drawing of a Typical Loop Heat Pipe

A principle equation associated with heat pipe operation is based on the balance of pressures and may be expressed as:

$$\Delta Pc \geq \Delta Pb + \Delta Pv + \Delta Pg \qquad (3.1)$$

where

58

- ΔPc is the capillary pressure head, in N/m^2 ;

- ΔPb is the pressure differential in the liquid moving in the capillary material, in N/m^2 ;

- ΔPv is the pressure differential, of the vapor in the vapor passage, in N/m^2 ; and

- ΔPg is the hydrostatic head determined by the mutual interposition of the evaporation and condensation zones of the heat pipe in a mass force field, in N/m^2.

In its simplest form the capillary pressure head for capillary pores of generally cylindrical form may be expressed by the Laplace's equation:

$$\Delta P_c = \frac{2\sigma}{r_c} Cos\,\theta \qquad (3.2)$$

where

- σ is the surface tension coefficient, in N/m;

- θ is the value of the extreme angle at which the inner wall of the capillary pore is wet by the liquid, in degrees.

- r_c is the radius of a capillary tube, in m.

This equation is true if the curvature radius of the vapor-liquid interface in the vapor condensation zone tends to be infinite, which corresponds to a flat interface, or if the wetting angle in the condensation zone is 90°. When capillary pores are of complex configuration the capillary pore radius is substituted by the effective radius which can be found experimentally. Pressure differential in a laminar flow of incompressible viscous liquid moving through a cylindrical capillary pore having a radius of r_c may be described by the Hagen-Poiseuille formula:

$$\Delta P_l = \frac{8\dot{m}\,\eta_e\,\xi}{\pi r_c^{\,4} \rho_e} \qquad (3.3)$$

where

- $\dot{m}$ is the mass consumption of liquid, in kg/cm;

- η_e is the dynamic viscosity factor, in $N \cdot s / m^2$; and

- ξ is the effective length of the heat pipe, in m; and

- ρ_e is density of the liquid, in kg/m^3.

The movement of vapor in the heat pipe is governed by more complex laws and may vary in the evaporation zone, condensation zone and the transport (adiabatic) pipe portion. Therefore, the complete pressure differential in the vapor phase, ΔP_v, is generally the total of pressure differentials at the above three portions of the heat pipe.

The last term of equation (3.1) is given by the hydrostatic head of the liquid and determined as:

$$\Delta P_g = \rho_l \cdot g \cdot \xi \cdot \sin \phi \qquad (3.4)$$

where

- ρ_l is the density of the heat transfer fluid in a liquid phase, in kg/m^3;

- g is the acceleration of gravity, in m/s^2; and

- ϕ is the angle between the longitudinal centerline of the heat pipe and the horizontal, in degrees.

Depending on the mutual position of the evaporation and condensation zones in the field of mass forces, the term ΔP_g of the equation (3.1) enters this equation either with a positive sign (+) or with a negative sign (-). When the evaporation zone is above the condensation zone, the angle of inclination of the heat pipe is considered positive, while $Sin \phi > 0$ and ΔP_g has a positive sign (+) imparting a hydrostatic resistance. As a consequence, an increase in the length of the heat pipe and in the angle of inclination will result in an increased hydrostatic pressure which attains its maximum value at $\phi = 90°$. The hydrostatic pressure ΔP_g contributes to a great extent to the total of pressure losses. Therefore, it must be taken into account even at negligible inclination angles of the heat pipe, as well as at horizontal positioning of heat pipes of larger diameter. Especially susceptible to variation in the positive inclination angle in the field of mass forces are low-temperature heat pipes wherein use is made of heat transfer fluids having a relatively

low surface tension factor. In this case, it is advisable to employ capillary materials having small radii for the capillary pores in order to attain sufficiently high values of the capillary pressure head.

The conventional heat pipe is made up of a plurality of interconnected serial sections, each of the sections being actually an independent heat pipe. The inner surface of the sections is lined with capillary material saturated with a heat transfer fluid. The sections are so interconnected that an end face wall confining the condensation zone of a serially preceding section is integral with an end face wall confining the evaporation zone of every succeeding section, and so forth. Therefore, the arrangement is such that the condensation zone of every preceding section is in thermal contact with the evaporation zone of the succeeding section of this heat pipe assembly. Because the heat transfer fluid is calculated independently in each of the sections and the length of each such section is relatively small, it stands to reason that within each of the sections the distance over which the liquid heat transfer fluid has to travel through the capillary material is rather short, which makes it possible to use capillaries with sufficiently large radii to enable the transfer of markedly larger heat fluxes with the heat transfer fluid travelling against a gravity head as compared to conventional heat pipes.

However, this heat pipe has a high thermal resistance caused by the heat transfer between the sections in light of the heat conduction through the separating walls which possess a certain amount of resistance to heat. Apparently, in order to increase the overall length of such a heat pipe, it is necessary to employ a larger number of sections. In consequence, this leads to a greater number of walls separating the sections, the total heat resistance of which makes up the overall thermal resistance of the heat pipe. It can be easily assumed that the thermal resistance of a heat pipe made up of a plurality of such sections will be higher than the thermal resistance of conventional heat pipes whereby the basic advantage of a heat transfer apparatus of this type, such as low thermal resistance, will be lost. Therefore, at a given temperature difference between a heat source and a heat sink the heat flux capacity of the above described heat pipe will be lower than that of a conventional heat pipe.

Attempts to increase the heat flow transferred through reducing its hydraulic resistance resulted in a heat transfer apparatus described in U.S. Patent 3,741,289. This

heat transfer apparatus is fashioned as a closed conduit defining an essentially circular heat link comprising at one portion thereof a vaporizer of capillary material saturated with a heat transfer fluid in thermal contact with a source of heat. A portion of the conduit remote from the vaporizer is adapted to maintain thermal contact with the heat sink. A portion of the conduit adjacent the vaporizer is provided with a liquid header. One part of the conduit disposed between the heat source and the heat sink serves to transmit the heat transfer fluid in a vapor phase, while the other part thereof is intended to carry the heat transfer fluid in the liquid phase. The apparatus is capable of providing contact of the heat transfer fluid in the liquid phase with the vaporizer under no heat load. To this end, there is provided a reservoir arranged away from the heat sink and communicating with the apparatus by way of a passage. The reservoir has a flexible diaphragm separating the heat transfer fluid from another heat transfer fluid partially in a liquid and partially in a vapor state the vapor pressure of which fluid exerted on the vaporizer under zero heat load is higher than the vapor pressure of the first heat transfer fluid and, conversely, it is lower when the temperature of the vapor of the heat transfer fluid is raised subsequent to the application of a heat load. Therefore, in the absence of heat load the diaphragm assumes a curved or arched position toward one side of the reservoir for the heat transfer fluid to be driven from the reservoir to come into thermal contact with the vaporizer. When the pressure and temperature of the vapor released by the heat transfer fluid subsequent to the application of the heat load have been increased, the heat transfer fluid is driven from the vapor portion of the conduit into the liquid portion thereof to come into contact with the outer surface of the vaporizer through the liquid header. Excess heat transfer fluid is forced into the reservoir to cause the diaphragm to assume a position curved toward the other side of the reservoir.

High heat flux capability of this apparatus is assured if the distance traveled by the heat transfer fluid in the capillary material toward the evaporation surface is relatively small. Therefore, pressure losses in this apparatus are much less than in conventional heat pipes, which then enables one to reduce the effective radius of the capillary pores and thereby increase the capillary head which provides additional force to the heat transfer fluid.

However, inherent in the above heat transfer apparatus is the disadvantage of having a relatively small surface area intended for carrying the heat transfer fluid toward the vaporizer which occupies a narrow annular portion of its outer surface. Extending the length of the vaporizer surface to convey a heat load thereto may cause insufficient feeding of remote portions of the vaporizer because of capillary resistance and, as a result, this leads to the same limitations in the travel of the heat transfer fluid against the action or mass forces as in conventional heat pipes. A second disadvantage resides in the overall bulk of the apparatus due to the liquid header and the separate reservoir arranged outside the heat link. Thirdly, the apparatus may have insufficient reliability because the movable element thereof, i.e. the diaphragm, is susceptible to residual deformations and mechanical wear.

A further reduction in the hydraulic resistance at a portion of the travel path of the heat transfer fluid in a vapor phase through the capillary material has been attained in a construction of a heat transfer apparatus [1,2]. This known apparatus comprises evaporating and condenser chambers communicable through conduits, the first of the conduits being intended to convey the heat transfer fluid in a vapor phase, the second conduit serving to carry the heat transfer fluid in a liquid phase. Accommodated in the interior of the evaporating chamber co-axially therewith is a vaporizer of capillary material saturated with the heat transfer fluid and adapted to maintain a thermal contact with a heat source. The vaporizer consists of two end portion surfaces which are tightly adjacent there between. Each portion of the vaporizer is provided with longitudinal and radial vapor release passages communicable with a vapor header incorporated into the vaporizer and having the form of an annular recess occupying a border area between the two portions of the vaporizer. The vaporizer further has a longitudinal axial passageway communicable with each of two end cavities defined by the end surfaces of the vaporizer and the walls of the evaporating chamber. Provided in the side wall of the evaporating chamber is an inlet port for a first pipe to communicate with the vapor header, whereas an end face wall facing the condenser chamber has an outlet port for a second pipe to communicate with the end cavity of the evaporation chamber. This outlet port of the second pipe is arranged either in the said cavity or in the longitudinal axial passageway of the vaporizer.

The condenser chamber is generally a shell in the form of a cup the bottom of which faces the evaporation chamber. A second co-axial shell is inside the first shell. The space between the shells handles the returning liquid. The liquid line, joined at the second shell outlet, passes through the condenser chamber and links to evaporator chamber to provide the liquid.

The heat transfer apparatus is charged with a heat transfer fluid in the amount sufficient to saturate the vaporizer, fill the second pipe, a portion of the condenser chamber, the longitudinal axial passageway, one end cavity and partially the other end cavity.

In the absence of heat load the vaporizer is saturated with the heat transfer fluid, while the balance of the heat transfer fluid occupies a certain level in the pipes as in communicating vessels. When a heat load is applied to the vaporizer, the heat transfer fluid is caused to evaporate from the surface of the vapor release passages, the surface of the longitudinal axial passage and from the end surfaces of the vaporizer. However, thanks to the thermal resistance of the layer of capillary material saturated with the heat transfer fluid which separates the said surfaces, a temperature difference and, consequently, a pressure difference occurs in the region above these surfaces.

This pressure difference may be determined according to the Clausius-Clapeyron equation as follows:

$$\Delta P = \frac{LP_v\Delta T}{RT_1^2} \tag{3.5}$$

where

- L is the latent heat of vaporization, in J/kg;
- P_v is the pressure of vapor above the evaporation surface of the vapor release passages, in N/m^2 ;
- T_1 is the temperature of vapor in the vapor release passages, in K;
- ΔT is the vapor temperature difference between the evaporation surfaces, in K;
- R is the universal gas constant, in J/K•kg.

Under the action of this pressure difference, the heat transfer fluid in the liquid phase is caused to be driven out from the first pipe of the condenser chamber to occupy the end cavities and the longitudinal axial passageway of the vaporizer wherefrom it moves essentially in a radial direction through the vaporizer to be conveyed over the evaporation surface of the vapor release passages.

As a consequence, two levels of the liquid heat transfer fluid are established in the apparatus, and in particular one in the upper end cavity at a temperature T_2 of vapor there above, and the other one in the condenser chamber at a temperature T_3 of vapor above this level. Therewith, it is necessary that the conditions $T_3 > T_2$ and $P_3 > P_2$ be complied with. These conditions are fulfilled because a cooled heat transfer fluid is admitted to the evaporating chamber, the saturated vaporizer maintaining its function of a "thermal gate". It should be noted here that the temperature T_3 is somewhat lower than the temperature T_1 due of losses caused by the travel of vapor along the first pipe and the annular space of the condenser chamber, whereas the condition $P_3 > P_2$ is realized in the case where the capillary pressure head in the vaporizer meets the following condition:

$$\Delta P_c \geq P_3 - P_2 + \Delta P_l + \alpha P_v \qquad (3.6)$$

It is therefore evident that the pressure difference $P_3 - P_2$ is approximately equal in value to the hydrostatic pressure ΔP_g which is exerted by a column of the liquid heat transfer fluid confined between free surfaces in the evaporation and condenser chambers. Accordingly, since the distance traveled by the liquid heat transfer fluid in the capillary material is relatively short and not dependent on the length of both the heat transfer apparatus and the vaporizer per se due to the predominantly radial path of travel thereof, it becomes possible to employ capillary pores that are very small in radius. This allows one to obtain a high capillary pressure head even when a heat transfer fluid with a relatively low surface tension factor is used. In addition, the before described apparatus is reliable and moderate in size because the end cavities function as a reservoir for the excess heat transfer fluid, while the moving parts are absent. The level of the heat transfer fluid is controlled by the heat transfer fluid itself through variations in the values of P_2 and P_3.

Among disadvantages inherent in the above described heat transfer apparatus are, firstly, the complicated arrangement of the system of vapor release passages which must be great in number to provide a sufficiently large evaporation surface, as well as the inconveniences in terms of providing a reliable and tight connection and accommodation of the two parts of the capillary vaporizer in the housing. Secondly, the insufficient evaporation surface of the vaporizer defined by the side surfaces of the radial vapor release passages which, as has been noted, cannot be numerous enough for purely technological considerations. This hampers vapor release with the resultant loss in pressure therein. Thirdly, another disadvantage is the location of the outlet port of the second pipe in the evaporating chamber at below the level of the liquid heat transfer fluid in the upper end cavity when the apparatus is oriented at angle of inclination $\phi > 0°$. This configuration fails to allow the admission of the "cold" heat transfer fluid directly to the upper end cavity through the longitudinal axial passageway having a cross-section by far larger than the cross-section of the second pipe due to the deceleration in the travel velocity of the heat transfer fluid. In addition, because of the direct thermal contact thereof with the walls of the longitudinal axial passageway, there results an increase in the temperature of the heat transfer fluid. As a consequence, the temperature T_2 and the pressure P_2 tend to increase in value leading to a corresponding increase in the values T_1, T_3 and P_1, P_3 and, accordingly, to increased temperature of the heat source wherefrom the heat transfer apparatus draws away heat. Fourthly, the provision of the narrow annular space in the condenser chamber having a hydraulic resistance tending to increase further due to a film of condensate flowing downwards and impaired convection when heat is transferred from the outer surface of the condenser chamber to the outside are also disadvantageous because they tend to reduce the highest heat flux capacity transferred by the above described apparatus.

The first inventors and other researchers have tried to resolve these disadvantages. A number of patents have been granted in the past two decades. Several will be briefly described in following section.

3.1.3 Review of Patents

This section reviews some of the designs as outlined in US Patents on LHP technology and what specific features have been proposed to create a circulating flow.

3.1.3.1 US Patent 4,515, 209

US patent 4, 515, 209 entitled "Heat Transfer Apparatus" was granted in May 1985 to inventors from the former Soviet Union. Since this is the most often mentioned patent on the loop heat pipe and inventor F. Maidanik was considered the first inventor of the loop heat pipe, it is necessary to discuss it in some detail.

In Figure 3-1 is shown, a heat transfer apparatus comprising an evaporating chamber #1 having arranged in the interior thereof essentially co-axially therewith a vaporizer #3 fabricated from capillary material permeable to a heat transfer fluid and adapted to maintain a thermal contact with a heat source, and a condenser chamber #4. The vaporizer is provided with vapor release passages communicable with a vapor header #11 and a longitudinal axial passage communicable with each of the two end cavities (#5 and #6). Each of the end cavities is defined by the end surface of the vaporizer and the walls of the chamber. A zone of the condenser chamber containing the heat transfer fluid in the vapor phase communicates with the vapor header of the vaporizer by way of a first pipe #13 and transmits the heat transfer fluid in a vapor phase toward the condenser chamber. The zone thereof containing the heat transfer fluid in a liquid phase communicates by way of a second pipe #21 with the evaporating chamber. The vapor release passages are defined by longitudinal recesses and a multiplicity of annular recesses intersecting with the longitudinal recesses, the recesses being arranged on the outer surface of the vaporizer between annular projections thereof and intended to prevent vapor passing from the vapor release passages to the end cavities. Start up and normal operation of the heat transfer apparatus according to the invention is guaranteed if the amount of the heat transfer fluid required for charging the apparatus is selected correctly.

This unit efficiently increases the heat flux capability by increasing the density of heat flux conveyed from the heat source to the vaporizer, by reducing the hydraulic resistance of the condenser chamber and by improving the conditions for carrying heat away from the outer surface thereof. It also improves the operating reliability of the heat

transfer apparatus when it is subjected to vibratory loads and it makes the apparatus easier to assemble by providing a flexible mechanical linkage between the evaporating and condenser chambers.

Studies at U. of Texas A&M have confirmed the viability of this unit and its design (http://two-phaseheat.tamu.edu/cpl.html). Moreover, a unit was tested on the Space Shuttle in November, 1997 under the direction of Dynatherm Inc. (a US heat pipe manufacturer). The tests confirmed the viability of this unit. A schematic of the Dynatherm unit as tested on the Space Shuttle has been extracted from the Dynatherm web home page (http://www.dynatherm-dci.com) and is shown here as Figure 3-2.
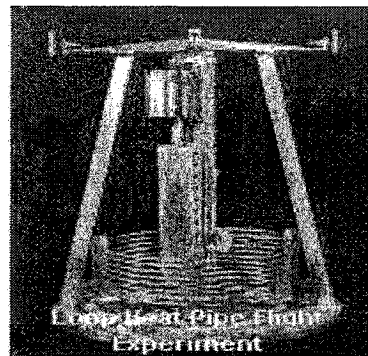
Figure 3-2. The Loop Heat Pipe Tested on the Space Shuttle Columbia

3.1.3.2 Other US Patents

Based on the first loop heat pipe as presented in above section, a number of loop heat pipes have been invented and patents granted. Description of loop heat pipes found in US Patent literature can be divided into two groups: (1) capillary loop heat pipes, (2) capillary loop heat pipe with help from a mechanical device. Figure 3-3 gives two examples of the capillary loop heat pipe. Figure 3-3a [6] is from a US patent entitled "Heat Transporting Device" (Patent No. 4,467,861), granted in Aug. 1984 to inventors from the former Soviet Union. It included an evaporating chamber with a body #2, containing a co-axially-arranged evaporator #3 in a capillary material soaked with a heat-transfer agent (e.g. cermet), which is in thermal contact with a source of heat shown by arrows. The evaporator is in thermal contact with a source of heat and having an axial bore with a transverse partition in the capillary material. A vapor-jet pump #13 served to transform the dynamic pressure of the heat-transfer agent in the vapor phase into the static pressure of the heat-transfer agent in the liquid phase, and a heat-exchanging chamber #4. The evaporating chamber is provided with two end face cavities (#5 & #6) each bounded by the corresponding end face of the evaporator and walls of the chamber.

The partition in the capillary material is located contiguously with the end face of the evaporator which faces the heat-exchanging chamber and is provided with through holes placing the end face cavities in communication with one another and is further provided with a passage. The passage was connected to a nozzle #12 of the vapor-jet pump and also to a vapor header which, in its turn, is connected to vapor outlets. The outlets are provided in the form of longitudinal grooves cut in the outside surface of the evaporator between smooth annular collars which are present on the outside surface of the evaporator at the end faces thereof to prevent vapor leaks into the end face cavities. An outlet of a first conduit is located in the axial bore of the evaporator. A zone of the heat-exchanging chamber containing the heat-transfer agent with a lower heat content is connected to the suction side of the vapor-jet pump by way of the first conduit and another zone of said chamber containing the heat-transfer agent with a higher heat content is connected to the discharge side of the said pump through a second conduit.

Figure 3-3b [7] shows the design proposed in US Patent 4,627,487. A heat pipe system #10 wherein a subcooled liquid flow tube #14 is connected to a vapor tube #12 to collect heat pipe liquid at the condenser and deliver it to the evaporator, to provide a liquid return pipe, which is separate from the flow of vapor to the condenser. Furthermore, the vapor tube is preferably interconnected with the liquid return tube over several places along its length, particularly when the length is long. Heat may be transported into or out of the heat pipe system at any location along the length thereof. In operation, heat pipe system #10 is charged with the working fluid and heat is delivered to the system from a heat source #34. The liquid is delivered to wicked material #32 and this addition of heat causes boiling of the liquid to vapor. The vapor rises in the vapor tube as indicated by a rising vapor flow arrow #36. Throughout the exposed area of the vapor tube, heat is radiantly extracted to a heat sink #38. The breadth of vapor tube is such as to permit the vapor tube to deliver heat to the heat sink through radiant heat loss. Heat sources may be coupled by other means, such as a conductive mechanical connection to the face of vapor tube but the system is particularly designed for heat rejection by means of radiation. The vapor condensing over the area of radiant heat sink is collected into the wicking material on the interior of the vapor tube and is delivered through the wicking material in the stabilizing connectors, particularly connectors #16,

#18 and #20, and delivered for flow in the liquid return tube. Since the liquid return tube contains only liquid, it can be subcooled below the condensation temperature. Therefore, there is no vapor in the liquid return tube to interfere with liquid return flow. The stabilizing connectors are required along the length of the vapor tube and liquid return tube to provide the required thermal stability there between. Liquid can move in either direction through the wicking in the stabilizing connectors for supply to the vapor tube or for collection from the vapor tube liquid state working fluid, depending on local thermal conditions.

(A)   (B)
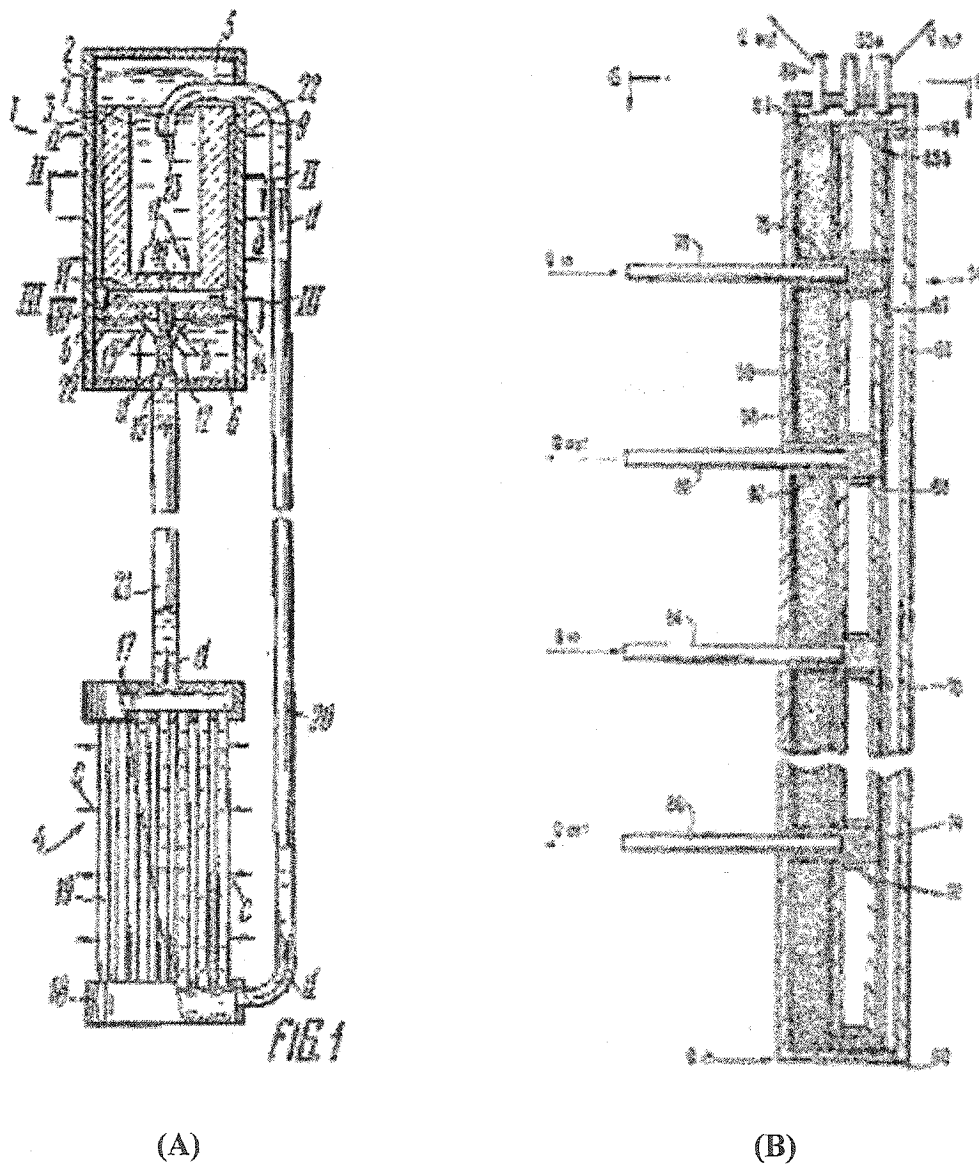
Figure 3-3. The Capillary Loop Heat Pipe with Mechanical Device

Thus, this heat pipe system features a condensing area that is connected through a separate liquid return artery, so as to provide an unobstructed vapor flow through a separate vapor tube to the condensing area. It also provides a heat pipe system wherein the vapor flowing toward the condensing zone achieves thermal stability along the length of the vapor tube and a liquid return tube that permits an especially long heat pipe system. In addition, it includes a side-flow heat pipe system wherein heat may be delivered into and extracted out of the heat pipe at different positions along the length thereof so as to achieve a thermal management system which removes heat from where it is not desired and delivers it to locations where it is desired.

Figure 3-4 shows designs from two US patents, which used various mechanical devices such as pumps and check values inside the loop heat pipe.

(A)   (B)
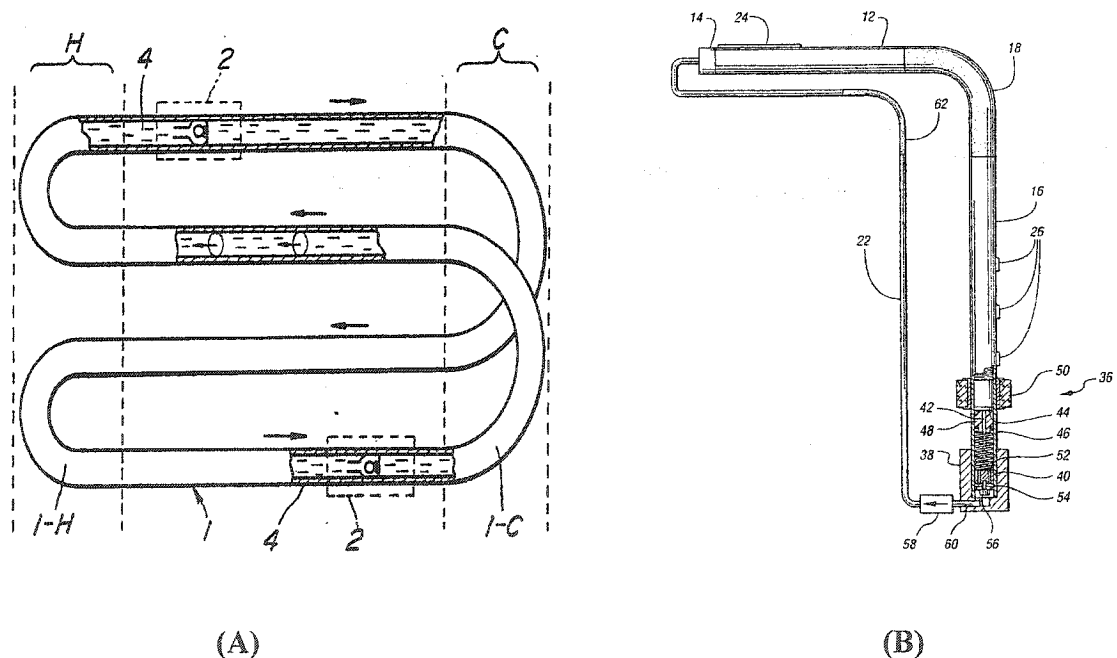
Figure 3-4. The Loop Heat Pipe with Mechanical Devices

Figure 3-4a (US patent 4,627,487) [8] is a structure of a loop-type heat pipe invented by Akachi et al in 1990. The device entitled "Structure of a Heat Pipe" includes: (a) An elongated pipe, both ends thereof being air-tight and interconnected to form a loop-type container #1 that contains the heat carrying fluid,

71

(b) At least one heat receiving portion (evaporator) #1-H. And at least one heat radiating portion (condenser) #1-C. These heat receiving, heat insulating (#4), and heat radiating portions are alternately arranged to form an endless loop.

(c) At least one check valve for limiting a stream direction of the heat carrying fluid. A check valve(s) #2 propels and amplifies forces generated by the heat carrying fluid and its vapor to move toward the stream direction limited by the check valve(s). Thus, the heat carrying fluid circulates at high speed in the stream direction through the closed-loop passage defined by the elongated pipe.

US Patent 5911272 (see Figure 3-4b) [9] shows a mechanically pumped heat pipe for spacecraft. The heat pipe evaporator section #12 is connected to the condenser section #16 by connector section #18. The condensed working fluid is collected in the condenser section. A mechanical pump #36 is attached to the condenser section for pumping the working fluid from the condenser section to the evaporator section via the return line #22 with the fluid separator #14 and the check valve #50. The mechanical pump is a cavitation-free electro-magnetically actuated pump having a piston head disposed in a pump housing attached to the condenser section of the heat pipe. The piston head has at least one through fluid passageway which is closed by a sliding valve member in response to the piston head being displaced during a pumping stroke and being open when the piston head is being retracted during a cocking stroke. The piston head is periodically reciprocated in the pump housing by a solenoid actuated armature disposed in the condenser section. A fluid separator is provided at the input end of the evaporator section, which distributes the working fluid received from the condenser section via a return line. The fluid separator may be tailored to distribute the working fluid in accordance with the requirements of each application.

3.1.4 Loop Heat Pipe Vs Conventional Heat Pipe

As the conventional heat pipe, the loop heat pipe (LHP) is also a two-phase heat transfer device, which can transfer a large amount of heat over long distances with very small temperature differences. It utilizes the surface tension forces developed in the porous wick to circulate the fluid, and does not require any external pumping power.

Therefore, it can be said that the LPH has number of characteristics of the conventional heat pipe. The following three characteristics are similar to conventional heat pipes:

- Both use passive capillary pumping and two-phase heat transfer.
- Both can transfer heat efficiently with small temperature differentials.
- Both operate passively, with no external power requirements, moving parts, vibration or maintenance.

In conventional heat pipe designs, the heat is transported along the length of the tube as the liquid vaporizes and condenses in the same tube. That is, the vapor stream from the evaporator is cooled and liquefied to form a working liquid stream. The working liquid, in turn, circulates toward the heat receiving portion by means of the capillary action of the wick in the container. In this way, the latent heat associated with the vaporization and condensation of the working liquid during such a circulation cycle causes heat transfer in the cylinder-shaped heat pipe. The working liquid and its vapor flowing in mutually opposite directions are in direct contact with each other. A loop heat pipe system can be compared to a car's cooling system. The vaporized liquid, working substances such as ammonia, water, potassium and sodium, moves through a transport line to a condenser, or a series of fins similar to a car's radiator. The liquid cools and condenses and flows through another line back to the starting point. By keeping the vapor and the cooled liquid separate, the loop heat pipe can carry more heat for greater distances than other pipes. The "pump" that moves the fluid around the loop is created by a combination of capillary forces, generated by the porous wick with extremely small pores that is located at the heat input portion of the loop, coupled with vapor momentum and gravity. The small pores act as both a capillary pump and an effective separator between the vapor and liquid phases. The efficient nature of phase change heat transfer allows for the transport of much of heat with only a few degrees of temperature drop.

On the other hand, conventional heat pipes have the following disadvantages.

(a) Less amount of heat transport because of the low limits of heat transfer.

   Mutual interference between the vapor stream and liquid stream occurs due to opposite flow directions of the vapor and working liquid streams in the case of the cylinder-type heat pipe. When the temperature difference between the heat

receiving portion and heat radiating portion is increased, speeds of the vapor stream and working liquid stream are increased respectively. At this time, the working liquid evaporates from an intermediate portion of a wick structure. The working liquid is then blown out and scattered away from the wick surface toward the heat radiating portion. The scattered vapor stream disturbs the recirculating working liquid. Thus the amount of the recirculated working liquid that makes it to the heat receiving portion is reduced. Finally, the working liquid is dried out.

In the case of a wickless-type heat pipe, the above-described phenomenon occurs at an earlier stage and more violently than the wick-type heat pipe. Therefore, the previously proposed cylinder-type heat pipe has a disadvantage of reaching a limit of heat transfer operation with relatively small amounts of heat transportation. If the heat pipe is lengthened or if the inner diameter of the heat pipe is small, the above-described phenomenon occurs at an earlier stage.

To avoid the above-described phenomenon, a heat insulating portion of the container can be constructed in a double pipe structure.

(b) Inevitable presence of a wick limit.

In the case of the wick-type heat pipe, if the thermal resistance value is low and the heat input is low, the pipe exhibits good performance characteristics. However, if the heat input becomes large, boiling and vaporization of the working liquid are generated inside the wick. Therefore, since the recirculated working liquid cannot flow into the heat receiving portion of the wick, it consequently becomes dried out. This is called the wick limit. Such a phenomenon will be easier to occur as capillaries of the wick become thinner and the thickness of the wick increases.

(c) The occurrence of abnormalities due to a water hammer action.

If the quantity of working liquid is increased as in the case of the wickless-type heat pipe, the maximum heat transfer rate can become larger by a sizeable factor as compared with the wick-type heat pipe. However, if an abrupt heat input or a large heat input is applied, the working liquid boils violently. Consequently, the working liquid still in the liquid phase is blown up toward the

heat radiating portion and violently collides with the end surface of the heat pipe. In this case, the heat transportation of the wick-type heat pipe becomes intermittent. In addition, an abnormal sound and an abnormal vibration are generated. In the case of the violent collision, the heat pipe container is often damaged. Such a phenomenon as described above is generated if the quantity of working liquid is too much.

(d) Presence of limits in the length and diameter of the heat pipe.

As the inner diameter of the heat pipe becomes smaller due to the mutual actions of liquid resistance and wick limit in the heat insulating portion, the limiting length of the heat pipe becomes shorter.

(e) Limited mounting orientations of the whole heat pipe during its application.

When the conventional heat pipe is used under a top heat situation, i.e., in a state where the water level of the heat receiving portion is higher than that of the heat radiating portion, even the wick-type heat pipe has a remarkably reduced heat transportation capability.

If the water level difference is lowered below a certain level, the heat pipe becomes dried out and cannot be used any more. The thermal resistance value is doubled even in the horizontal position. If the heat input is increased, dry out of the working liquid occurs easily. Hence, the heat pipe is commonly used in a bottom heat state (i.e., the water level of the heat receiving portion is lower than that of the heat radiating portion) with a tilting angle of 15 to 20 degrees with respect to the horizontal direction. The wickless-type heat pipe cannot be used in the horizontal direction. It is noted that the wickless-type heat pipe cannot function when the mounting orientation thereof is under the top heat situation.

(f) Difficulty in mounting on heated and cooled objects.

No flexibility is present in conventional heat pipe containers and it is almost impossible to use a product of the heat pipe without the product being bent. Hence, it is difficult or impossible to mount on the heated object and on the cooled object. If the container is formed in a corrugated-pipe configuration to provide the flexibility for the heat pipe, the heat pipe not only becomes

expensive but also fluidity of the working liquid becomes reduced. Consequently, the performance of the heat pipe becomes worsened.

(g) Difficulty arises in the sealing operation of the working liquid in the container.

In the case when a non-condensable gas is generated or mixed in the container, the non-condensable gas during the operation of the heat pipe stays within the heat radiating portion and the performance of the heat pipe can, thus, be reduced remarkably. To prevent such reduced performance, attention needs to be paid to maintain a high vacuum state of the heat pipe during the sealing-in operation of the working liquid.

It is, therefore, an objective of the novel, relatively simple structure of a loop heat pipe to solve all of the problems (a) to (g) described in the above, so that it can be applied to many fields requiring such heat pipes. Some characteristics of the new LHP's are:

- A LHP is arranged as a loop.

- Wick structure need only be in the evaporator.

- High capillary pumping and low-flow impedance results in very high heat transport power densities and reduced sensitivity to gravitational acceleration.

- Fine pore wick structure can achieve high capillary pumping against gravity.

- Smooth-walled, low-impedance tubing can be used throughout the loop, and tubing may be flexible.

- In a typical loop heat pipe, the fluid is drawn by capillary forces from the inside to the outside surface where it evaporates due to the addition of heat. This vapor then flows to the condenser, rejects heat to the environment and returns to the reservoir as a liquid. Thus, the liquid takes another route to return to the evaporator.

3.1.5 Loop Heat Pipe Vs Capillary Pumped Loops

Three capillary-driven thermal management systems have been developed with space-based applications: heat pipes, capillary pumped loops (CPLs), and loop heat pipes (LHPs). As mentioned in Chapter 2, heat pipes were invented by Gaugler and then reinvented in the 1960s at the Los Alamos National laboratory of US. Heat pipes are

relatively simple devices that have been used in many space-based and terrestrial applications. The CPL was developed by Stenger [3] and is significantly more complicated. It is still in the developmental stage and has been applied to many situations while the LHP was developed in Russia. Over the past few years there has been much confusion as to the similarities and the differences between the two technologies. The LHP operates under the same principles as CPLs. However, unlike traditional CPLs, the LHP has the reservoir (compensation chamber) both thermally and hydrodynamically tied to evaporator. This tie is the primary distinguishing feature between the two technologies and results in different operational and control characteristics for the LHP.
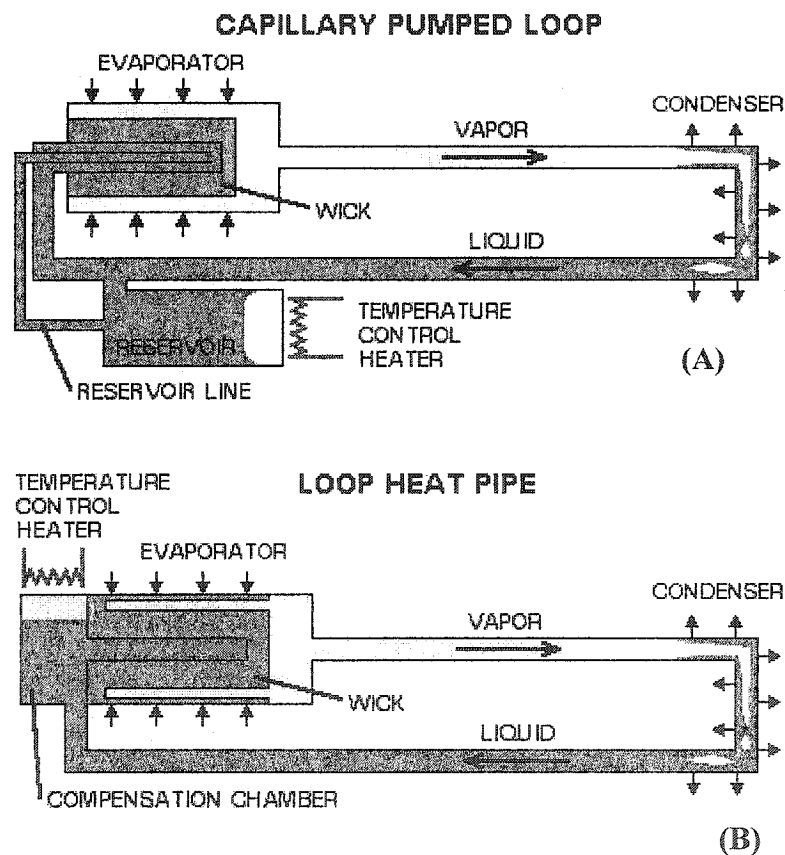
Figure 3-5. CPL and LHP Schematically Diagrams

Figure 3-5 presents schematic diagrams of the CPL and the LHP. Structurally, loop heat pipes are similar to a competing technology called Capillary Pumped Loops (CPL). The CPL invented in the US in the 1960's has only recently (early 1980's)

received much attention. A review and comparison of the two devices is presented in reference 5 from the theoretical point of view. Both achieve pumping by capillary action and feature similar operating curves of thermal power transport versus evaporator temperature.

Since the LHP evaporator and compensation chambers are integrated together, the system performance becomes a function of the evaporator heat load in addition to the subcooling delivered to the evaporator and the gravity gradients. A portion of the heat applied to the evaporator results in vaporization of the working fluid. However, because of the conductive coupling of the evaporator to the compensation chamber and the conductive path through the wick to the core, a portion of the applied heat also flows into the compensation chamber and must be eventually offset by increased subcooling. This is demonstrated by the characteristic increase in the loop temperature difference. At low powers, the conductive coupling becomes more significant hence the upward turn in the loop temperature differential as the power approaches the low power limit. A similar increase in loop temperature differential can be induced by loss of subcooling coming to the evaporator (via parasitic heating of liquid return line). Decreased loop conductance also occurs under adverse orientations, which increase the back conduction by increasing the pressure (and therefore saturation temperature) gradient across the wick. In all cases, the effects of back conduction degradation are more noticeable at low powers (and therefore low flow rates).

Conversely, traditional CPLs have a reservoir in the loop which is not thermally nor hydraulically tied to the evaporator. Indeed, the reservoir need not be thermally connected to the loop at all, although in practice the liquid return line is used to provide cold biasing. If the CPL reservoir is designed to retain two-phase fluid under normal operating conditions, it is a variable conductance device due to its ability to control the saturation temperature of the loop with no influence from the evaporator heat load or gravity loads placed on the loop. CPLs can be designed to have the reservoir. It is hardly filled with liquid during hot conditions (or under most circumstances) at which point the system will transform to a fixed conductance device similar to a LHP.

Table 3-1 [10] summarizes many of the operational and integral differences between LHPs and traditional CPL technologies, at least when restricting the comparison

to single evaporator units. Please note that not all developers agree on the specifics of this comparison.

Table 3-1: Comparison of Single-Evaporator CPL and LHP Technologies

Criterion	CPL	LHP
Definition	Reservoir is not flow-through, and is not necessarily thermally connected to the flow, usually two-phase (variable conductance) but may be hard-filled (fixed conductance)	Usually in-line (flow-through) reservoir, or at least thermally and hydraulically well-connected to evaporator; never allowed to hard-fill nor empty: almost always two-phase.
Key Advantage	Reservoir can be remote from evaporator, and is usually smaller. Performance (W/K) not sensitive to environmental influences. More easily customized. More applicable to larger scale applications.	Easy start-up. Generally robust. Great as a retrofit (thermal strap).
Main Difficulties	Lacks turn-key start-up: requires heating of reservoir (preconditioning). Sensitive to bubble formation in liquid lines and evaporator: less robust. Sensitive to pressure oscillations (unless fixed conductance)	Reservoir is relatively large and must be co-located with evaporator, yet is sensitive to heat leaks. Performance is sensitive to environmental conditions (more difficult to analyze and integrate). Limited acquisition/rejection footprint.

Similarly, both devices can be controlled to maintain fixed evaporator temperatures for a range of power levels by thermostatically controlling the reservoir or compensation chamber temperature.

Typically, the power required to maintain the compensation chamber temperature constant is less than 10 watts for ammonia based LHPs [10]. This feature is very attractive for systems requiring active temperature control over a wide range of power dissipation scenarios such as high power laser based systems. One disadvantage of the LHP over the CPL is that the compensation chamber of a LHP must be physically near the evaporator to share fluid directly or through a weak capillary link. This may cause some integration and packaging difficulties.

3.2 Research Objective

Although the heat pipe was invented more than three decades ago and the first loop heat pipe was invented about twenty years ago, little attention was paid to using this technology with high heat fluxes until three years ago. As the comparisons above show, the conventional heat pipe can have many problems in high temperature circumstances due to its structure. The start-up of the CPL and its sensitivity to bubble formation limits its applicability for high heat flux and high temperature cases. Therefore, the loop heat pipe was selected as the heat transfer device for high temperature and high heat flux industries such as the metallurgical industry, combustion, and other pyro-processes. To develop a suitable LHP for these industries, the following tasks (the research objectives) were performed:

- Identify the problems associated with the conventional heat pipe, and develop and test possible solutions;
- Identify the problems associated with the capillary loop heat pipe, and develop new loop heat pipe and test possible solutions;
- Improve the performance of the loop heat pipe by applying forced convection cooling on the condensers;
- Investigate the film boiling problems of gravity-assisted loop heat pipes, and develop and test a method which can eliminate the film problems;
- Investigate the start up problems of gravity-assisted loop heat pipes, and develop and test a method which can eliminate the startup problems;
- Develop a viable design of the loop heat pipe.

CHAPTER 4. HEAT PIPE DESIGN AND PRACTICAL CONSIDERATIONS

The introduction of a new product or changing an old model involves carrying out a variety of activities including:

- Feasibility study;

- Making designs;

- Reaching economic decisions;

- Selecting optimum materials and processes;

- Planning and scheduling of manufacturing activities;

- Developing the market;

- Selling the product;

- Arranging for after-sales service.

These diverse activities are interdependent and should not be performed in isolation from each other. This is because it is not sufficient that the design of the product should satisfy the technical, safety, and legal requirements; it must also be possible to manufacture it economically, to sell it at a competitive price, and to dispose of it satisfactorily at the end of its useful life. Therefore, the above outlines the activities in developing a new product, starting from the conception of the idea and ending with the marketable product. In fact, an industrial product is normally expected to satisfy a certain need, to give satisfaction to the user, and to comply with the prevailing safety and environmental laws. A product usually starts as a concept which, if feasible, develops into a design, then a finished product. While each engineering product has its own individual character and its own sequence of development events, there is a general pattern for the various stages that accompany the introduction of a new product, as shown in Figure 4-1.

With regards to the case of a novel heat pipe, stage 1 and stage 2 have been illustrated in Chapters 1 to 3. This chapter will discuss the design, materials and process selection of the heat pipe (stage 3).

Stage 1	Concept Development and Function Definition

Stage 2	Feasibility Study

Stage 3	Design, Materials, and Process Selection

Stage 4	Planning and Scheduling

Stage 5	Prototype Preparation, Market Testing, Pilot Production

Stage 6	Large-scale Production, Market Development, Sales

Stage 7	Production Modification and Development

Stage 8	Obsolescence, Disposal, Recycling

Figure 4-1. Stages of Product Development

As mentioned in Chapter 2, the physical process occurring during the transport of the heat input imposes a number of constrains on the heat pipe operation. The limitations of a conventional heat pipe can also appear in a novel heat pipe. Short descriptions of these limitations are summarized by the following:

A. Capillary limit

It describes the ability to circulate or pump the given working fluid inside the loop heat pipe. Sometimes it is called the *Hydrodynamic Limitation*. It is also defined as the maximum circulation inside the heat pipe in order to obtain the maximum heat capability. The capillary limitation of heat pipes occurs when the capillary pressure difference in the liquid phase is not great enough to overcome the sum of the pressure drops associated with the liquid flow, vapor flow, and phase change phenomena. Loop heat pipes are in almost all cases capillary limited in their performance.

B. Sonic limit

It occurs when sonic velocities are reached in the vapor flow, leading to a chocked flow condition in some parts of the pipe, usually at the start of the condensation zone. The possibility of attaining this limit in the loop heat pipe is less due to its geometry.

C. Viscous limit

This limit appears when the vapor flow occurs at a low temperature and thus the reduced pressure limits the circulation of the working fluid. It occurs when the vapor pressure is not sufficient to drive the vapor phase from the evaporator region to the condenser region of the heat pipe.

D. Boiling limit

It is the disruption of the liquid flow by nucleate boiling in sharp corners and the like at intense heat flux levels in the evaporator region. This can lead to the formation of insulating vapor films. Due to the small amount of working fluid in a loop heat pipe, this limit can be a major limit in the operation of a loop heat pipe. It will be discussed in a subsequent Chapter in detail.

E. Entrainment limit

The entrainment limit is characterized by the tearing of liquid off the liquid-vapor interface by vapor flowing at high velocity. It is reached when the vapor shear stresses tend to remove liquid from the liquid flow channel, leading to premature dry out of the evaporator region.

These limits depend on the container design, type of working fluid, operating temperature, and heat load. The axial heat flux in heat pipes is limited in principle for two reasons: (1) insufficient return flow of condensate, and (2) vapor flow limitations. If the liquid return flow is guaranteed by a suitable wick design or gravity or a combination, the axial heat flux is ultimately limited by vapor flow effects. For this ultimate limit of heat transfer, several vapor flow regimes can be distinguished depending on the relative magnitude of inertial and viscous forces in the vapor.

The following sections discuss the general criteria of heat pipe design and the optimum design concept of a heat pipe. Specific and important criteria of loop heat pipes such as the boiling limit will be discussed in a later chapter.

4.1 Optimum Design of a Heat Pipe [1-6]

Heat pipes, as simple heat transfer devices, have a high effective thermal conductivity and are capable of transporting large quantities of heat over considerable distances. Because of the simplicity of design and ease of manufacture and maintenance, these devices have found applications in a wide variety of areas. Finding an optimum design, which can be used in practical applications, is not easy since heat pipe geometry, wick, and working substance can be changed.

The conventional methods of design do not ensure that the design is optimum. Even though a number of models (linear or nonlinear) are presented in the literature, they cannot be used for our intended design since they are too theoretical to easily implement in practice and most of them are focused on low temperature and low heat flux. Thus, they cannot be used directly in the high temperature industries such as the metallurgical, and the combustion and heat recovery industries. It is necessary to derive a simple and easily implemented design method. As mentioned at the beginning of this Chapter, the maximum heat transport capacity is limited by various factors: (1) capillary limit--the maximum capillary pumping pressure must be greater than the total pressure drop in the heat pipe; (2) thermal resistance limit; (3) boiling limit; and (4) entrainment limit. In addition, there is (5) the viscous limit at low temperature and (6) the sonic limit at high temperature.

Previous investigators have studied various problems associated with heat pipes [2,3,4]. Some design equations associated with these investigations have been selected and summarized in the following.

4.1.1. Formulation of the Problem

The heat pipe consists of an evacuated container, the interior of which is lined with a wick which is saturated with a working fluid. The heat is essentially transferred as latent energy by evaporating the working fluid in a heating zone called the evaporator and condensing the vapor in a cooling zone, called the condenser. The circulation is completed by the return flow of the condensate to the evaporator through the wick under the driving action of capillary forces. The section connecting the evaporator and the condenser is termed as the adiabatic section.

The total weight of the heat pipe is the sum of the weights of: (1) pipe container, (2) end caps, (3) wick structure and (4) working fluid. The design of the first two is controlled by the vapor pressure inside the container. The wick has to be designed to develop sufficient capillary pumping pressure and to provide passage for heat and fluid flow. The selection of the working fluid depends on the operating temperature of the heat pipe and its compatibility with the wick and container materials.

Depending upon the requirement, compatible combinations of 1) fluid, 2) wick structure, 3) wick material and 4) container material should first be selected. The thicknesses of the container and end caps depend on the difference between the internal and environmental pressures. The amount of working fluid depends on the porosity of the wick structure. The weight of the wick structure can be brought down by reducing the diameter of the wick wire, the mesh number, the thickness of the wick, and the lengths of the evaporator and condenser sections for a constant adiabatic section length. The thickness of the pipe container is assumed to be 10% of the inside diameter.

The design variables, therefore, are (1) mesh number. (2) diameter of wick wire, (3) diameter of vapor core, (4) thickness of wick structure, (5) length of evaporator section, and (6) length of condenser section. Thus there are six independent variables in this problem.

The design criterion is, as stated earlier, to minimize the weight of the heat pipe. For this, it is sufficient to minimize the weight of the wick structure, since the thickness of the container is not taken as an independent variable. As the density of wick material is constant, the criterion therefore becomes the minimization of the volume of wick material expressed by

$$F = 2\pi r_v t_w (L_e + L_a + L_c)$$ (4.1)

The minimization is to be achieved subject to the constraints in the problem, which include both functional and side constraints. The functional constraints are as below:

- **Capillary limit:** The capillary pumping pressure developed in the wick must be sufficient to compensate for the liquid, vapor and gravitational pressure drops. The capillary limit is expressed as,

$$Q_c = \frac{P_C + P_G}{(F_l + F_v) L_{eff}}$$ (4.2)

Definitions for the terms used in the above equation are given in the Appendix at the end of this chapter. The constraint for this limit becomes,

$$g(1) : Q\text{-}Qc \leq 0$$ (4.3)

- **Thermal resistance limit:** The heat carried by the heat pipe has to cross the evaporator wall, pass through the wick structure at both the evaporator and the condenser sections, through the vapor core and finally across the condenser wall. By neglecting the resistance to heat flow at the liquid-vapor interface, through the vapor core and the conduction along the heat pipe wall, the overall total thermal resistance to heat flow can be expressed as follows:

$$R = R_{eo} + R_{co} + R_{et} + R_{ct} + R_{ew} + R_{cw}$$ (4.4)

(See the appendix for details)

The wall thermal resistance limit can be expressed as follows:

$$Q_R = \frac{T_{so} - T_{si}}{R}$$ (4.5)

and the constraint becomes

$$g(2) : Q - Q_R \leq 0$$ (4.6)

- **Boiling limit:** The working fluid shall not reach the boiling limit. This constraint is expressed by,

$$Q_B = \frac{2\pi L_e k_{eq} T_g}{h_{fg} \rho_g \ln(r_i / r_v)}\left(\frac{2\sigma}{r_n^*} - P_C\right)$$ (4.7)

Where, r_n^* is the nucleation radius and is approximately equal to 2.5×10^{-7} m. This constraint becomes operational when the solution algorithm tries to reduce the length of evaporator and condenser sections, *ie.*,

$$g(3) : Q\text{-}Q_B \leq 0$$ (4.8)

- **Entrainment limit:** This limit becomes significant when the mesh number is extremely small. The entrainment limit is expressed as,

$$Q_E = A_v h_{fg}\left[\frac{\sigma \rho_g}{2r_{hs}}\right]^{1/2}$$ (4.9)

where, r_{hs} is the hydraulic radius. The expression for r_{hs} is given in Appendix. The constraint expressing this limit is,

$$g(4) : Q\text{-}Q_E \leq 0$$ (4.10)

- **Viscous limit:** At low temperatures, viscous forces are dominant in the vapor flow. This limit can be written as,

$$Q_V = \frac{\pi r_v^4 \rho_g h_{fg} P_g}{16\mu_g L_{eff}}$$ (4.11)

ie., $\qquad g(5) : Q - Q_V \leq 0$ (4.12)

- **Sonic limit:** At somewhat higher temperatures chocking at the evaporator exit may limit the power handling capability of the heat pipe. This is given by,

$$Q_S = A_v \rho_g h_{fg}\left[\frac{\gamma_g R_g T_g}{2(\gamma_g + 1)}\right]^{1/2}$$ (4.13)

Therefore, $g(6) : Q - Q_S \leq 0$ (4.14)

The values of F_l and F_v given in equation (4.2) are valid only when the vapor flow is laminar and incompressible. ie. when $Re \leq 2300$ and $Mv \leq 0.2$. These two constitute two more constraints.

- **Mach number limit:**

$$g(7): \left[\frac{20Q}{\pi \rho_g h_{fg} (\gamma_g R_g T_g)^{1/2}} \right]^{1/2} - 2r_v \leq 0 \qquad (4.15)$$

- **Reynolds number limit:**

$$g(8): \frac{4Q}{\pi \mu_v h_{fg} 2300} - 2r_v \leq 0 \qquad (4.16)$$

In addition to the above functional constraints, there are additional side constraints so that the dimensions will all be physically acceptable.

g(9) : d-$1/N$ ≤ 0 ; (width between wires; where d is the diameter of wick wire)   (17)

g(10) : d_{min} - d ≤ 0 ; (diameter of the wick wire)   (18)

g(11) : $2d$-t_w ≤ 0; (thickness of the wick structure)   (19)

g(12) : 1-N ≤ 0; (mesh number)   (20)

g(13) : -d_v ≤ 0; (vapor core diameter)   (21)

g(14) : -Le ≤ 0; (length of the evaporator section)   (22)

g(15) : -Lc ≤ 0; (length of the condenser section)   (23)

Thus, the present optimization problem can be stated in a condensed form as:

Find X which minimizes the objective function $F(X)$.

Subject to the constraints $g_j(X) \leq 0; j = 1, 2, \ldots m$

Where, $X = [N, d, dv, t_w, Le, Lc]^T$

$F(X)$: is the volume of the wick material

$g_j(X)$: are the functional and side constraints

m : is the number of constraints

4.1.2. Solution Procedure

The present problem is a nonlinear programming problem with nonlinear inequality constraints. The Interior Penalty Function Method is used to convert this constrained problem into an unconstrained problem. A sequential search method namely Modified Powell's Method is used for the unconstrained optimization and the Quadratic Interpolation Technique for the one dimensional search. The gradient based algorithms

are found to be unsuitable for solving this problem due to serious ill conditioning of the penalty function. To arrive at a global minimum, the search has been carried out from different starting points. Almost all searches converged to the same final point.

It is found that the combination of Interior Penalty Function, Modified Powell's Method and Quadratic Interpolation Technique work very efficiently for this problem. However, the thickness of the heat pipe container can be included in the set of design variables by incorporating suitable failure criteria as additional constraints in the optimization problem. The optimum solution cannot be physically realized. However, this difficulty can be overcome easily by specifying a tolerance limit for the feasible region. The method illustrated by the example can be used with the necessary modification for the design of other types of heat pipes also.

4.2 Heat Pipe Design Considerations

In the actual heat pipe design, those influencing factors such as working fluid, container material, wick materials and structures and heat transport limits are all thought out. Each of these aspects is described in a subsequent section.

4.2.1 Working Fluid

The working fluid should satisfy as many of the following criteria as possible.

- Chemical compatibility with wick and wall materials.
- Good thermal stability.
- Wet-ability of wick and wall materials.
- Vapor pressures not too high or low over the operating temperature range.
- High latent heat of vaporization.
- High thermal conductivity.
- Low liquid and vapor viscosities.
- High surface tension.
- Acceptable freezing or pour point.

Almost any fluid that satisfies the above criteria may be used as working fluid in a conventional heat pipe. Other details of working fluids will be discussed in the next chapter.

4.2.2 Container Materials

Generally, the container materials should satisfy as many of the following criteria as possible. The best suitable one may be chosen for a given system.

- Compatibility (with the working fluid).
- Compatibility (with the reagent).
- Compatibility (with the external environment).
- High strength to weight ratio.
- High thermal conductivity.
- Ease of fabrication, including weldability, machinability, ductility.
- Low porosity.
- Wet-ability by the working fluid.

The container materials have to be compatible with the working fluid. The most useful container materials are listed in Table 4.1 [5].

In this project, stainless steel SS-304, and SS-316L were chosen as the container materials.

Table 4.1. Recommended heat pipe wall and wick materials

Working fluids	Recommended Materials
Ammonia	Aluminum, Carbon, Nickel, Stainless Steel
Acetone	Copper
Methanol	Copper, Stainless steel
Water	Copper, Monel
Mercury	Stainless steel
Potassium	Nickel, Stainless steel, Inconel, Titanium,
Sodium	Stainless steel, Nickel, Inconel 800, Haynes
Lithium	Niobium-1% zirconium,Molybdenum, TZM
Silver	Tungsten-26% rhenium

4.2.3 Wick Materials and Structures

Generally, the materials and structures should satisfy as many of the following criteria as possible.

- Compatibility with working fluid.
- High thermal conductivity.
- High porosity;
- Wet-ability by the working fluid.

The wick can be made of the same material as that of the container. Some of them are given in Table 4.1.

Many wick structures have been suggested in the literature [3,4,5]. The most available wick structures are listed in Table 4.2.

In this project, the wick structure is the single wick, the type of wick is woven mesh screen, and the materials of the wick are SS-304 and SS-316. The wick structure influence will be discussed in detail in the next chapter.

Table 4.2 Wick Structures

Wick Structure	Type of Wick
Single Wick	Woven mesh screen, sintered metal powder, sintered metal fibers, grooves
Combined Wick	Two woven mesh screens, grooves covered with one woven mesh screen
Artery Wick	One artery wick, two artery wicks

4.2.4 Heat Transport Limits

All the heat transport limits have to be calculated once all the three components and dimensions of a heat pipe have been initially sized. This part of the design may need to be modified if the calculations show that the actual heat transport rate for the pipe will exceed one or more of the limits. In the end, the final design must ensure that the actual heat transport rate is less than all the limits. The equations which are used to evaluate the limits are denoted as g(1) to g(15) as presented above.

4.2.5 Sample Design Procedure

Based on the above description of heat pipe limitations, any attempt to increase the heat transfer above the limitations will cause dry-out in the evaporator section. Therefore, these design constraints must be satisfied in the heat pipe design. Normally, the design of the heat pipe must include the following three major entities: (1) pipe container, (2) wick structure, and (3) working fluid. The design of the first is controlled by the vapor pressure inside the container. The wick has to be designed to develop sufficient capillary pumping pressure and to provide passage for heat and fluid flow. The selection of the working fluid depends on the operating temperature of the heat pipe and its compatibility with the wick and the container materials.

Depending upon the requirement, matching combinations of fluid, wick structure, wick material and container material should first be selected. The thickness of the container and end caps depends on the difference between the internal and environmental pressures. The dominant thermal resistance in the heat pipe, and hence almost the entire temperature drop, occurs across the wall and wick thickness. If the condenser is much longer than the evaporator, the radial heat flux at the condenser will be much smaller than that at the evaporator. In this event, which is not uncommon in heat pipe design, most of the temperature drop will take place in the evaporator section. If the wall and wick thicknesses are a significant fraction of the heat pipe radius, curvilinear geometry should be used in calculating temperature drops. If the thickness does not exceed 10% of the radius, rectilinear geometry is usually sufficient for design purposes. Working liquid is determined by application temperature, wick structure and material. Its amount depends on the porosity of the wick structure.

Although the heat pipe is easy to fabricate, the hydrodynamic and heat transfer phenomena make the design quite complex. Therefore, every combination of container type and size, wick type, mesh and material, and working fluid and amount are chosen to suit a particular application.

For this research project, heat pipes including a loop heat pipe were required for laboratory experiments. In one set of experiments heat pipes were designed and constructed to extract heat from baths of molten Zn and Cu. The particular design dimensions for these

heat pipes, wick structures, working fluids and other parameters will be described in the following chapters.

4.3 Heat Pipe Fabrication

The overall process of fabricating a heat pipe includes preheating, cleaning, assembling, charging, conditioning, sealing, and final testing. Given that this is a novel application, many of the procedures had to be developed specifically for this project. Any mistake can lead to a failure of the heat pipe or a shortening of its life.

4.3.1 Preheating

Preheating is a procedure in which the materials of the container and wick are treated under a condition similar to that which the heat pipe will encounter in actual use. The purpose of this procedure is to reduce internal stresses and to increase wetting capability.

This procedure is important when container and wick are made of metallic materials.

4.3.2 Cleaning

Cleaning is a procedure in which the materials of the container and wick are cleaned by following a sequence of steps in order to eliminate any foreign substance and to avoid contaminating the working fluid which may change the properties of the heat pipe shell, the wick, and the working fluid. It is a necessary procedure for all heat pipes.

In our practice, acetone and alcohol are employed to clean all parts of the heat pipe container and wick.

4.3.3 Assembly

Assembly of the heat pipe is a procedure in which all the parts are assembled into the final product. Usually, spot welding, arc welding and some other welding methods need to be used. Particular attention has to be paid to the different expansion and thermal stresses especially when stainless steel is chosen as the container material.

A most difficult and also most important stage in the assembly procedure is to insert and fix the wick in place. For a cylindrical system, the following procedures are very important:

- Maintain the integrity of the wick.
- Leave the gap between the inner surface and the wick and between different layers as small as possible.
- Use spot welding machine or spring to fix the wick.

4.3.4 Charging

Charging is a procedure in which the working fluid is put into the pipe by following safety procedures for the working fluid without contaminating it. The working fluid can be charged in solid or liquid states. Safety should be a great concern in this procedure when alkali metals are employed.

4.3.5 Conditioning

Conditioning is a procedure in which the heat pipe is operated under a condition similar to one it will ultimately encounter in actual trials. The purpose of conditioning is to allow any reactions between the working fluid and pipe to occur and to evacuate the heat pipe of any extraneous inert gases and gaseous reaction products. For high temperature heat pipes this procedure may take at least several hours. When this procedure is completed the connections between the pipe and the environment have to be cut off while maintaining an evacuated state.

4.3.6 Sealing

Sealing of the heat pipe is a procedure in which the pipe is sealed either permanently or temporarily. Obviously, for permanent sealing the quality of the seal is extremely important. Welding is typically employed for permanent sealing.

In this project, permanent sealing was applied to the liquid metal heat pipe cooled injection lances, and temporary sealing was applied to the water heat pipes.

4.3.7 Final Testing

Final testing is a procedure in which the heat pipe is operated under a condition similar to that which the heat pipe is going to be exposed. Abnormal operation during the test is usually indicative of a problem in the sealing procedure or otherwise. It may require that one repeat the procedures from 4.3.5 to 4.3.7.

4.3.8 Coating

Coating is the final procedure on the list. It entails coating the evaporator of the pipe with materials which are compatible with the external environment by CVD, PVD or some other method. This is not essential but may be carried out to reduce wear of the pipe body.

4.4 Heat Pipe Operational Considerations

The operations of a heat pipe can be classified into two categories: unsteady-state operation (start-up) and steady-state operation.

4.4.1 Unsteady-State Operation

Transient or start-up operation is an important stage. Any improper implementation can cause a problem or even destroy the pipe. Improper implementation refers to the following operation for those heat pipes when alkali metals are employed as working fluids: the pipe is heated up too slowly or too quickly. When the pipe is heated up too slowly, the working fluid will tend to freeze on the condenser instead of flowing back to the evaporator. When the pipe is heated up too quickly, the pipe will hit one or more heat transfer limits.

4.4.2 Steady-State Operation

Steady-state is the operating state in which the pipe spends the majority of its time. Most types of heat pipes are capable of running for quite a long period of time at the designed operating temperature.

4.4.3 Loop Heat Pipe Operation

The loop design avoids the limitations of conventional heat pipes. As illustrated in Chapter 3, the liquid and vapor flow in series, not against each other. The wick is confined to the evaporator portion of the LHP, rather than running the entire length of the device. This avoids the liquid flow losses in the wick experienced in a conventional heat pipe. With such a small length of wick, very small pore-size wicks can be used in applications with high thermal transport requirements and/or where the heat must be transported over a long distance against gravity. Since there is no wick in the liquid or vapor lines, they can be made of standard or flexible tubing.

Loop Heat Pipe Design and Performance Features:

- Simple design, a totally passive heat transport system with no moving parts.

- Easy, reliable startups, starts by simply applying heat to the evaporator.

- Operation even at large adverse elevations with high pumping head.

- Routable, flexible, small-diameter transport lines.

- Operation as constant or variable conductive device, with seamless transition between modes.

Appendix

Expressions for various terms used in the equations:

Q: Heat load (W)

R: Thermal resistance (k/W)

$Pc = \sigma / r_c$ Pc: capillary pressure [N/m^2]; σ: surface tension [N/m]; r_c: condenser radius [m]

$r_c = 1/2N$ N: mesh number [m^{-1}]

$r_{hs} = (1/2N)-(d/2)$ r_{hs}: hydraulic radius of wick surface pores[m]; d: diameter [m]

$P_G = \rho_l\, g\, \{[La + Le + Lc]\, sin(\alpha) - d_v\, cos(\alpha)\}$ P_G : gravitational Pressure [N/m^2];

ρ_l: saturated liquid density [kg/m^3]; g: acceleration due to gravity [m/s^2];

La, Le and Lc: the length of adiabatic zone, evaporator and condenser [m];

α: angle of inclination to the horizontal [rad]; d_v: vapor core diameter [m];

$F_l = \mu_l / (K A_w \rho_l h_{fg})$ F_l: saturated liquid frictional coefficient [Nm^{-2}/Wm];

μ_l: saturated liquid dynamic viscosity [Ns/m^2]; K: wick permeability [m];

A_w: wick area [m^2]; h_{fg}: latent heat of vaporization [J/kg];

$F_v = 8\mu_g / (\pi r_v^4 \rho_g h_{fg})$ F_v: vapor core frictional coefficient [Nm^{-2}/Wm];

μ_g: saturated vapor dynamic viscosity [Ns/m^2]; r_v: vapor core radius [m];

ρ_g: saturated vapor density [kg/m^3]; h_{fg}: latent heat of vaporization [J/kg];

$K = d^3 \varepsilon^3 / [122(1-\varepsilon)^2]$ ε: porosity

$\varepsilon = 1-(1.05\pi Nd/4)$

$L_{eff} = La + (Le + Lc)/2$ L_{eff}: effective length [m];

$k_{eq} = k_l[(k_l+k_w)-(1-\varepsilon)(k_l-k_w)]/[(k_l+k_w)+(1-\varepsilon)(k_l-k_w)]$ k_{eq}:equivalent thermal conductivity[W/mK]

k_l and k_w: saturated liquid and wick thermal conductivity[W/mK]

$R_{eo} = 1/(2\pi r_o Le\, h_e)$ R_{eo}: convective resistance at out wall of evaporator;

r_o: container outer wall radius [m];

h_e: evaporator covective heat transfer coefficient [W/m^{2}K];

$R_{co} = 1/(2\pi r_o Lc\, h_c)$ R_{co}: convective resistance at out wall of condenser;

r_o: container outer wall radius [m];

h_c: condenser covective heat transfer coefficient [W/m^{2}K];

$R_{et} = ln(r_o/r_i)/(2\pi Le\, k_t)$ R_{et}: conduction resistance across container at wall of evaporator;

r_i: container inner wall radius [m];

k_t: container thermal conductivity [W/mK];

$R_{ct} = ln(r_o/r_i)/(2\pi Lc\, k_t)$ R_{ct}: conduction resistance across container at wall of condenser;

$R_{ew} = ln(r_i/r_v)/(2\pi Le\, k_{eq})$ R_{ew}: conduction resistance across wick structure at evaporator;

r_v: vapor core radius [m];

$R_{cw} = ln(r_i/r_v)/(2\pi Lc\, k_{eq})$ R_{cw}: conduction resistance across wick structure at condenser;

CHAPTER 5. EXPERIMENTAL INVESTIGATION OF A CONVENTIONAL HEAT PIPE

5.1 Efficiency of Wick

5.1.1 Wickless Heat Pipe

The wick is not essential for those heat pipes using the gravity force as the driving force to restore the working fluid from a cooling section located at the upper part to the heating section at the lower part. Wickless heat pipes are often called thermosyphons. They can operate over a wider range of heat input and temperature, since they are free from the disadvantages of a normal heat pipe such as a large flow resistance and low maximum heat transfer rate by bubble packing in the wick region. However, current evaluation techniques are not valid enough for a thermal design over wide operating conditions even for steady-state operation, since the thermosyphon shows complex behavior such as changes of two-phase flow. For example, most of the applications have been for relatively low pressure and low heat flux conditions.

Ning Jin [1] reported hot-spot generation and explained the reasons for it. In his experiment, a cylindrical heat pipe with 20g of sodium, made of 304 stainless steel, with a length of 1000 mm, O. D. of 25.4 mm and a 1.65 mm wall thickness was tested. The testing furnace temperature was 850 °C. The length of the evaporator section was 300 mm, and the length of the condenser was about 400 mm. A hot spot on the evaporator section was clearly observed, as shown in Figure 5-1 [1].

A similar case was observed by Mucciardi [2]. In his experiment, the wickless heat pipe was tested in a furnace using a burner as a heat source. The heat pipe ran well when the burner had a medium flame. When the flame intensity was increased, a hot spot was generated on the heat pipe wall where the flame was impinging. This caused a dry out of the liquid of the evaporator. The heat pipe failed quickly. The photo in Figure 5-2 [2] illustrates this situation.

Hot spot formation is not a new occurrence in the heat pipe field. The hot spot is a well known problem during the starting up from a frozen-state for basic heat pipes with

liquid metals such as K and Na as the working fluids. Lack of working fluid covering the entire evaporator section is the reason for the generation of hot spots. However, during steady state a basic heat pipe usually does not encounter the hot-spot problem. This hot spot on a wickless gravity assisted pipe was observed during steady state.
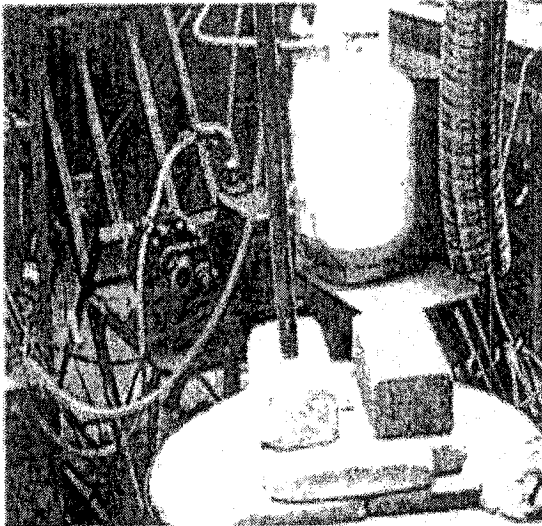
Figure 5-1. Hot-spot on the
Evaporator section of Heat Pipe
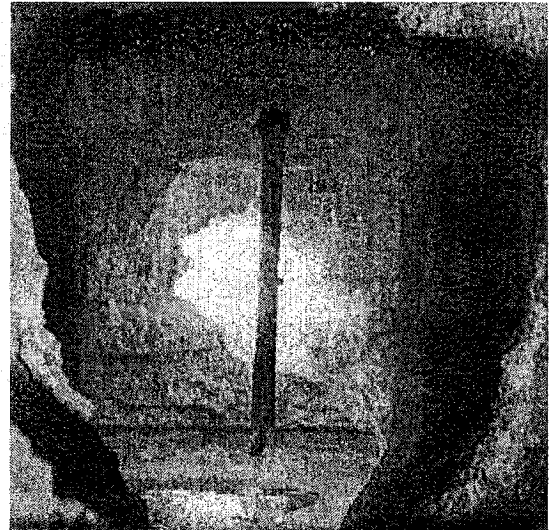
Figure 5-2. The Heat Pipe
Failed due to Hot-spot

Based on the definition of the basic heat pipe and the wickless heat pipe, the differences between both are the wick structure. The basic heat pipe uses capillary force (sometimes combined with gravity force) to restore the working fluid from the condenser to the evaporator while the wickless heat pipe only relies on the gravitational force to recycle the working fluid. Evidently, the gravitational force is not enough for the wickless unit. Surface tension forces cause beading of the liquid. In both cases, it is not the lack of the working fluid on the evaporator section since the condition in both cases is one of steady state. The issue is how to evenly redistribute the working fluid over the entire evaporator section. It is in this setting that the gravitational force does not have the same capacity of redistributing the working fluid uniformly as the wick structure does. Therefore, it is clear that the assumption of the working fluid flowing down uniformly from the condenser section to the evaporator section under gravity in a wickless heat pipe

is not valid, especially at low vapor pressures or high heat fluxes. In actuality, the working fluid tends to flow down from the condenser to the evaporator unevenly as droplets. In the extreme, some places on the evaporator section are not covered by any working fluid at all during normal operation. Sections not covered by working fluid will forego the cooling which should be provided by the heat pipe and they will be heated up to the hot furnace environment temperature.

Generally, there are two possible solutions available for resolving the problem of hot spot formation on the evaporator section. They are outlined as follows:

The first possible solution for the hot spot problem is to fill the entire evaporator section with working fluid. This solution can be implemented very easily. However, it raises another concern that too much working fluid will reduce the efficiency of the heat pipe as well as the operating stability of the heat pipe. This is the downside of this solution. Therefore, it is not encouraged.

The other possible solution for the hot spot problem is to employ a wick structure in the heat pipe. The working fluid in the wick can be redistributed evenly on the inner wall of the evaporator section by capillary forces. Although this solution cannot be implemented as easily as the first solution, it has no side effect on the performance of the heat pipe.

5.1.2 The Selection of Wick Structure and Materials

The wick structure within the heat pipe has two functions. It is both the vehicle and the mechanism through which the working fluid returns from the condenser to the evaporator section. While small pores are needed at the liquid-vapor interface to develop high capillary pressures, large pores are preferred within the wick so that the movement of the liquid is not restricted too greatly. Another function of the wick ensures that the working fluid is evenly distributed circumferentially over the entire evaporator surface. As mentioned above, the wick is employed if a hot spot is generated in a thermosyphon heat pipe since it can redistribute liquid to uniformly wet the whole evaporator wall of the heat pipe. For these reasons, many different types of wick structures have been developed in order to optimize the performance of the capillary heat pipe. Usually, the types of wick structures are divided into two categories: homogeneous and composite wicks.

Homogeneous wicks have the benefit of being relatively simple to design, manufacture and install. Composite wicks, however, can significantly increase the capillary limit of the heat pipe, but have the drawback of high manufacturing costs.

Homogeneous Wicks

Homogeneous wicks, some of which are listed in Table 5-1 [3], are constructed with one type of material or machining technique. The screen wick is probably the simplest and most common type of wick structure. It consists of a metal or cloth fabric which is wrapped around a mandrel and inserted into the heat pipe. After placement, the mandrel is removed, leaving the wick held by the tension of the wrapped screen, in the case of a metal fabric. For a cloth fabric, a spring may be inserted into the heat pipe to hold the wick against the inside of the pipe wall. The capillary pressure generated by a screen wick is determined by the size of the rectangular pores between the individual threads. The permeability is determined by the number of wraps and the looseness of the wraps, which creates annular gaps through which the condensate can flow.

Sintered metal wicks are manufactured by packing tiny metal particles in powder form between the inner heat pipe wall and a mandrel. This assembly is then heated until the metal spheres are sintered to each other and to the inner wall of the heat pipe. Special materials are used for the mandrel so that it can be removed, leaving an open vapor space. This type of wick is obviously more difficult to manufacture compared to the simpler screen wick. However, the capillary pressure developed by the sintered metal wick (and therefore capillary limit) is more easily predicted because the annular gaps present in a screen wick create uncertainties in the permeability. Also since a metal powder is sintered, the effective thermal conductivity is much higher than a comparable screen wick due to the poor thermal contact between the screen wraps.
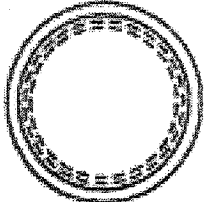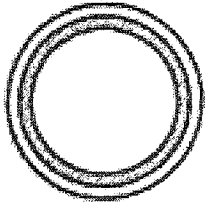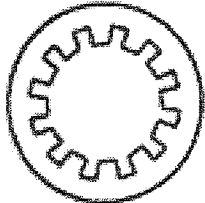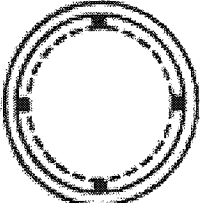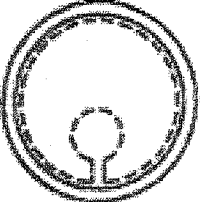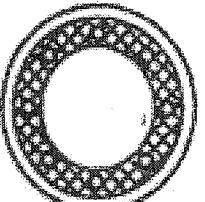
Axial groove wicks are formed by extrusion or broaching of grooves onto the inner radius of the heat pipe. Several different types of grooves have been used and proposed, which have rectangular, triangular, trapezoidal, or nearly circular cross sections. Trapezoidal grooves are the most common type these days. The performance of axial groove wicks is excellent, provided that the application does not call for a significant adverse elevation against gravity. Since the sizes of the grooves are large compared to

those of a screen or sintered metal wick, the capillary pumping pressure is quite small. However, the permeability and the effective thermal conductivity are very high. Drawbacks to this type of wick are the difficulty in machining the grooves for long heat pipes, which proves to be excessively expensive. Another concern is the liquid-vapor interaction at the opening of the groove at high vapor velocities. Other attractive features of axial groove wicks include the field-tested performance, reliability, and simplicity of design.

The open annulus wick is simply a single-wrap screen wick, which is held away from the inner pipe wall by stand-offs. This provides an unimpeded return flow path between the screen and the pipe, which greatly increases the permeability over the simple screen wick, while maintaining a high capillary pressure. However, the effective thermal conductivity of this wick is very low for most working fluids due to the low liquid thermal conductivity. Difficulties in priming during startup, and depriming during near-dryout operation are common in this type of wick. The idea of an open condensate return path is also present in the artery wick, but the problem of low effective thermal conductivity, as is present in the open annulus wick, is again of concern.

The artery wick combines the two necessities of having a small pore radius for capillary pressure generation and having a large pore radius for high permeability. In the artery wick structure, the interior of the heat pipe is covered by a screen wick or by a sintered metal powder in the usual manner, but a hollow passage(s) running the length of the pipe is fashioned and is in communication with the rest of the wick structure. Condensate is collected within this passage(s) or artery and is pumped back to the evaporator section by the capillary forces generated at the liquid vapor interface. Since the inner diameter of the artery is much larger than the effective pore radius of the wick, the liquid is able to easily traverse the length of the heat pipe with a minimum pressure drop. As with any design, there are difficulties associated with the artery wick. First, problems associated with the manufacture of arteries must be addressed. Also, the startup of artery wick heat pipes is critical due to the inevitable presence of vapor bubbles within the artery, which effectively block liquid return. Methods of collapsing these bubbles are complicated and are not always effective.

Table 5-1. Typical Homogeneous Wick Designs
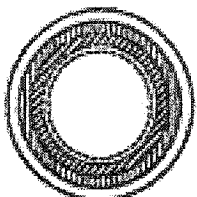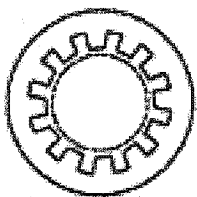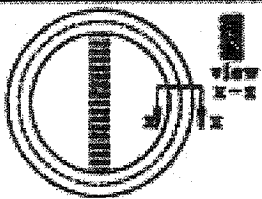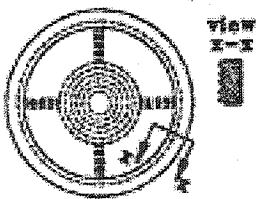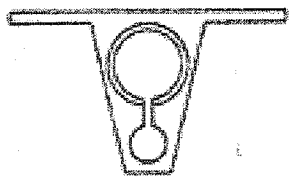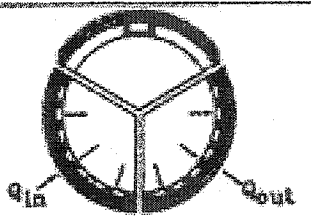
Wick type	Capillary pumping	Thermal conductivity	Permeability	Comments
A. Wrapped Screen	High	Low	Low-average	Multiple wraps of wire screen mesh
B. Sintered Metal	High	Average	Low-average	Packed spherical particles, felt metal fibers or powder
C. Axial Grooves	Low	High	Average-high	Rectangular, circular, triangular, or trapezoidal grooves
D. Open Annulus	Low	Low	High	Wire screen mesh spaced from wall
E. Open Artery	Low	High	High	Wire screen mesh formed into artery and wall lining
F. Integral Artery	High	High	Average-high	Homogeneous material with built-in arteries

Composite Wicks

Composite wick structures, listed in Table 5-2 [3], employ the benefits of having small pores for generating, high capillary pumping pressures and having large pores for increasing the permeability of the liquid return path. Again, the simplest type of composite wick is the screen wick, except that two screens with different pore sizes are used. Several wraps with a large pore size are applied against the inner pipe wall for the liquid return path, and a single wrap of screen with a much smaller pore size is placed adjacent to the vapor space to develop high capillary pressures. Similarly, axial grooves covered by a single wrap of a small pore screen can solve many of the problems associated with the homogeneous axial groove wick. Since the screen effectively separates the liquid and vapor flows, the entrainment of the liquid into the vapor flow by the interfacial shear is nearly eliminated. Also, this composite wick can be used in adverse gravity fields because the screen generates the needed capillary pressures.

A slab wick in conjunction with circumferential grooves is often used for applications where vapor velocities are generally low. The slab wick, which is usually a felt or several layers of screen, is made in the shape of a bar with a rectangular cross section. The longest side of the cross section is the same as the inner diameter of the heat pipe. Circumferential grooves distribute the condensate around the entire circumference. Obviously, this type of wick is not appropriate for very long heat pipes due to the difficulty in machining circumferential grooves on the inside of the pipe. The tunnel or spiral artery also uses a felt or several layers of screen, but is fashioned in the shape of a tube, which is smaller than the inside diameter of the pipe. The artery is then located on the pipe axis by slab wick stand-offs, which provide condensate communication between the hollow artery and the circumferential grooves on the inside diameter of the pipe. In the monogroove heat pipe design, the vapor and liquid condensate flow in different channels separated by a narrow groove. As with arterial type wick designs, circumferential grooves in the vapor channel help distribute the condensate. The double-wall artery consists of an inner tube with external grooves, and is perforated at the evaporator and condenser sections to allow vapor to escape into the interior. This inner tube is concentrically placed in an outer tube with a screen mesh wick at the inner wall. The double-wall artery wick design produces high capillary pressures, and since condensate returns to the evaporator by both a screen

Table 5-2. Typical Composite Wick Designs

Wick type	Capillary pumping	Thermal conductivity	Permeability	Comments
A. Composite Screen	High	Low-average	Average	Two or more layers of homogeneous material. The material next to wall has largest pore size
B. Screen Covered Grooves	High	High	Average-high	Axial grooves covered with one screen.
C. Composite Slab	High	High	High	Slab of homogeneous or non-homogeneous material with circumferential grooves
D. Spiral Artery	High	High	Average-high	Spiral wire screen mesh and circumferential grooves
E. Monogroove	Average	High	High	Slab of non-homogeneous material with circumferential grooves
F. Double-walled artery	High	High	Average-high	Concentric perforated externally grooved inner tube wall. Inner-annuli screen mesh wick.

105

wick and arteries on the exterior of the inner pipe, total blockages of the liquid return is unlikely.

Therefore, when selecting a wick structure for a particular application, one must keep in mind the benefits and drawbacks of each type of wick.

The following three properties of wicks are important in heat pipe design:

- Minimum capillary radius: this parameter should be small if a large capillary pressure difference is required, such as in terrestrial operation for a long heat pipe with the evaporator above the condenser or in the case where a high heat transport capability is needed.

- Permeability: permeability is a measure of the wick resistance to axial liquid flow. This parameter should be large in order to have a small liquid pressure drop and therefore higher heat transport capability.

- Effective thermal conductivity: a large value for this parameter gives a small temperature drop across the wick, which is a favorable condition in heat pipe design.

A high thermal conductivity and permeability, and low minimum capillary radius are somewhat contradictory properties in most wick designs. For example, a homogeneous wick may have a small minimum capillary radius and a large effective thermal conductivity, but have a small permeability. Therefore, the designer must achieve a balance between these competing factors to obtain an optimal wick design.

Since most of the heat pipes are used in the earth's gravitational field, the heat pipe can be aided by the gravity force when capillary force is not enough. Thus, the expensive composite heat pipe was not considered as necessary for our design.

5.1.3 Liquid Distribution in the Wick

A summary of recommended wall and wick materials for various heat pipe liquids is given in Table 5-3. These recommendations are based on extensive life testing of heat pipes, in most cases covering periods of 10,000 or more hours [4]. The lifetime tests were usually conducted at moderate temperatures and heat transport rates for the heat pipe fluid involved.

Selection of a particular type is dependent on the design requirements of the specific application. In general, the simplest wick structure that is appropriate to a particular design situation is preferable.

After our comprehensive survey, the simplest, cheapest and easiest wick to manufacture is the screen wick. Thus, this was used in our experiments. Because the heat pipes are used at high temperature and the container is made of 304/316 stainless steel, 304/316 stainless steel screen was employed in all heat pipe designs.

There are numerous papers that have been published on the various capillary wicks in heat pipes. Some models of capillary wick design can help meet the design requirements [3,5] for a particular application. In our experiments, we were concerned with the capability of evenly distributing the return fluid from the condenser to the evaporator to avoid hot spot generation in a high temperature environment or at a high heat flux. Since the distribution of liquid inside a heat pipe is hard to observe, especially at high temperature, a similar and simple set of experiments were performed in an open space. The experimental setup is shown in Figure 5-3. It consisted of an aluminum foil with two wraps of 316 stainless steel screen (100 Mesh) tightly stuck at the support. A glass filled with water which was dyed with red food coloring was used to provide the liquid into the screen via a plastic tube of 1 mm inner diameter. The whole experimental process was recorded using a video recorder.

Table 5-3. Recommended Heat Pipe Wall and Wick Material

Heat Pipe liquid	Recommended Material	Heat Pipe liquid	Recommended Material
Ammonia	Aluminum	Potassium	Nickel
	Carbon steel		Stainless steel
	Nickel		Inconel
	Stainless steel		Titanium
Acetone	Copper		Refractory metal and alloy
Methanol	Copper	Lithium	Niobium-1% zirconium
	Stainless steel		TZM molybdenum
Sodium	Stainless steel		Tungsten
	Nickel		Tungsten-26% rhenium
	Inconel 800		SGS tantalum
	Hastelloy X	Silver	Tungsten-26% rhenium
	Haynes 188	Water	Copper
	Molybdenum		Monel
	Tungsten		Stainless steel

In order to observe the distribution of liquid at a variety of inclination angles, a number of experiments were run from vertical to horizontal (see Figure 5-4).
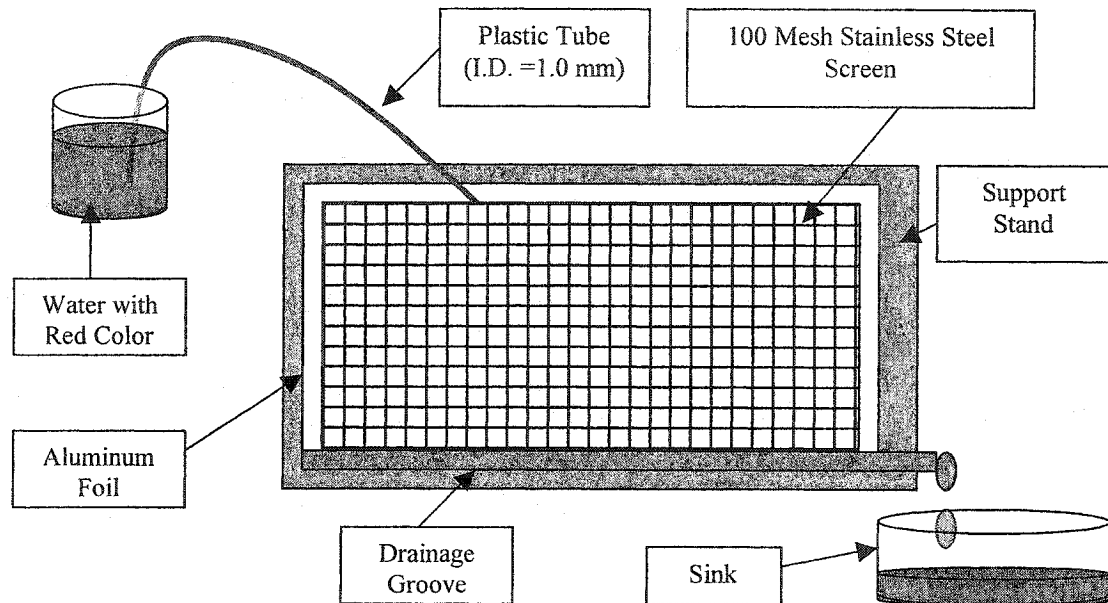
Figure 5-3. The Experimental Setup of Fluid distribution on Screen

a. Vertical   b. Angle   c. Horizontal
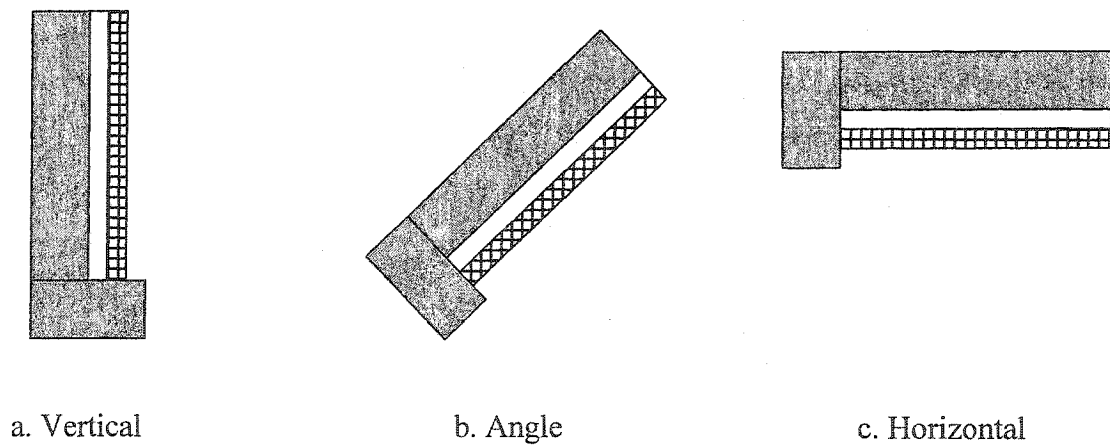
Figure 5-4. The Testing Position of Liquid Fluid Distribution in Screen

In the experiments, water droplets, which were continuously provided to the surface of the screen at 50 ml/min, directly touched the screen surface via a very small tube. They were adsorbed quickly, and then scattered and disappeared inside the screen (Figure 5-5). Simultaneously, they flowed out of the screen bottom (Figure 5-5a and b). In the screen surface between the water inlet and outlet, no water was observed. Even when the plate (the screen is under the plate) was near horizontal, the above phenomenon still occurred.

Feeding Plastic Tube

Screen with liquid

Drainage of fluid the screen end

a. Vertical   b. Angle
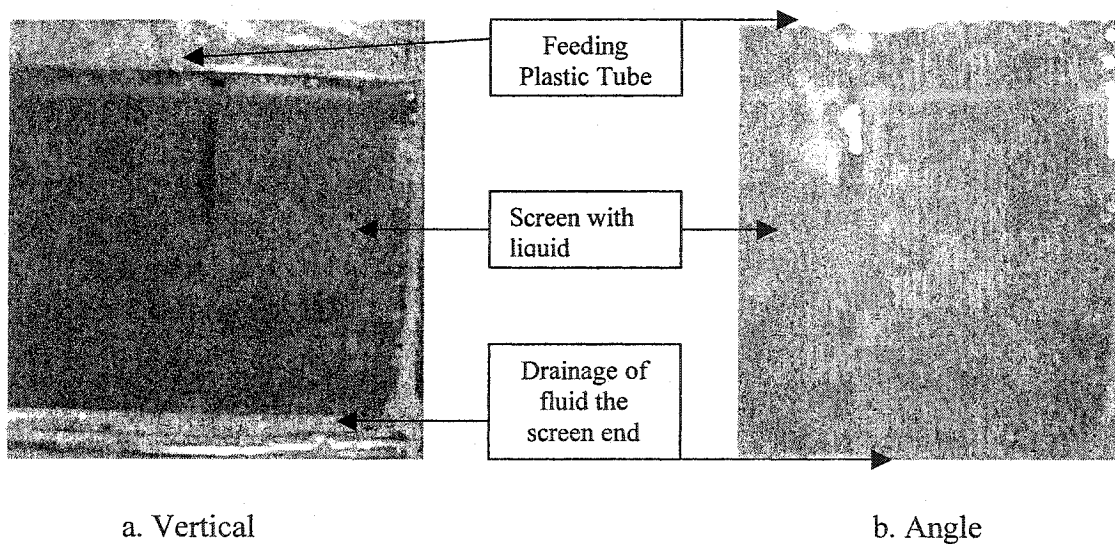
Figure 5-5. The Pictures of Fluid Distribution Experiments

Therefore, a screen stuck to a metal wall satisfies the requirement of redistributing the return fluid inside a heat pipe. A 100 mesh stainless steel screen also has a good capillary force. Thus, it can be used in our heat pipe design.

5.2 Comparison and Selection of Working Liquids

Because the basis for operation of a heat pipe is the vaporization and condensation of working fluid, selection of suitable working fluid is perhaps the most important aspect of the heat pipe design and manufacturing process. Factors that affect the selection of an appropriate working fluid include the operating temperature range, the

vapor pressure, the thermal conductivity, the compatibility with the wick and case materials, the stability, and the toxicity.

5.2.1 Working Fluid and Temperature Ranges

Each heat pipe application has a particular temperature range in which the heat pipe needs to operate. Therefore, the design of the heat pipe must account for the intended temperature range by specifying the proper working fluid. Table 5-4 [3, 5] lists some of the commonly used and proposed working fluids, their melting and boiling points at atmospheric pressure, and their useful ranges. As a rule of thumb, the useful range extends from the point where the saturation pressure is greater than 0.1 atm and less than 20 atm. Below 0.1 atm, the vapor pressure limit may be approached. Above 20 atm, the container thickness must increase to the point where the heat pipe becomes limited by the thermal resistance through the container.

Longevity of a heat pipe can be assured by selecting a container, wick and welding materials that are compatible with each other and with the working fluid of interest. Performance can be degraded and failures can occur in the container wall if any of these parts (including the working fluid) are not compatible. For instance, the parts can react chemically or set up a galvanic cell within the heat pipe. Also, the container may be soluble in the working fluid or may catalyze the decomposition of the working fluid at the expected operating temperature. A compilation of the most up-to-date information concerning compatibility of metals with working fluids for heat pipes is given in Table 5-5 [3].

Figure 5-6 [3] presents various working fluid boiling points and classifies them into four categories: cryogenic, low, medium and high temperature ranges. The working fluid inventory of a heat pipe is the sum of the masses of vapor and liquid phases, assuming the wick is full of liquid. This criteria is slightly over the optimum requirement because the meniscus recedes into the evaporator wick during normal operation. However, this situation is more advantageous than under-filling the heat pipe, which may significantly reduce the maximum heat transfer. With extreme over-fill, however, excess fluid might collect as liquid in the condenser section and increase the thermal resistance, thereby decreasing the heat transport capability of the heat pipe.

Table 5-4. Working Fluids and Temperature Ranges

Working Fluid	Melting Point, K At 1 atm	Boiling Point, K At 1 atm	Useful Range, K
Helium	1.0	4.21	2-4
Hydrogen	13.8	20.38	14-31
Neon	24.4	27.09	27-37
Nitrogen	63.1	77.35	70-103
Argon	83.9	87.29	84-116
Oxygen	54.7	90.18	73-119
Methane	90.6	114.1	91-150
Krypton	115.8	119.7	116-160
Ethane	89.9	184.6	150-240
Freon 22	113.1	232.2	193-297
Ammonia	195.5	239.9	213-373
Freon 21	138.1	282.0	233-360
Freon 11	162.1	296.8	233-393
Pentane	143.1	309.2	253-393
Freon 113	236.5	320.8	263-373
Acetone	180.0	329.4	273-393
Methanol	175.1	337.8	283-403
Flutec PP2	223.1	349.1	283-433
Ethanol	158.7	351.5	273-403
Heptane	182.5	371.5	273-423
Water	273.1	373.1	303-473
Toluene	178.1	383.7	323-473
Flutec PP9	203.1	433.1	237-498
Naphthalene	353.4	490	408-478
Dowtherm	285.1	527.0	423-668
Thermex	285	530	423-623
Mercury	234.2	630.1	523-923
Sulphur	385.9	717.8	530-947
Cesium	301.6	943.0	723-1173
Rubidium	312.7	959.2	800-1275
Potassium	336.4	1032	773-1273
Sodium	371.0	1151	872-1473
Lithium	453.7	1615	1273-2073
Calcium	1112	1762	1400-2100
Lead	600.6	2013	1670-2200
Indium	429.7	2353	2000-3000
Silver	1234	2485	2073-2573
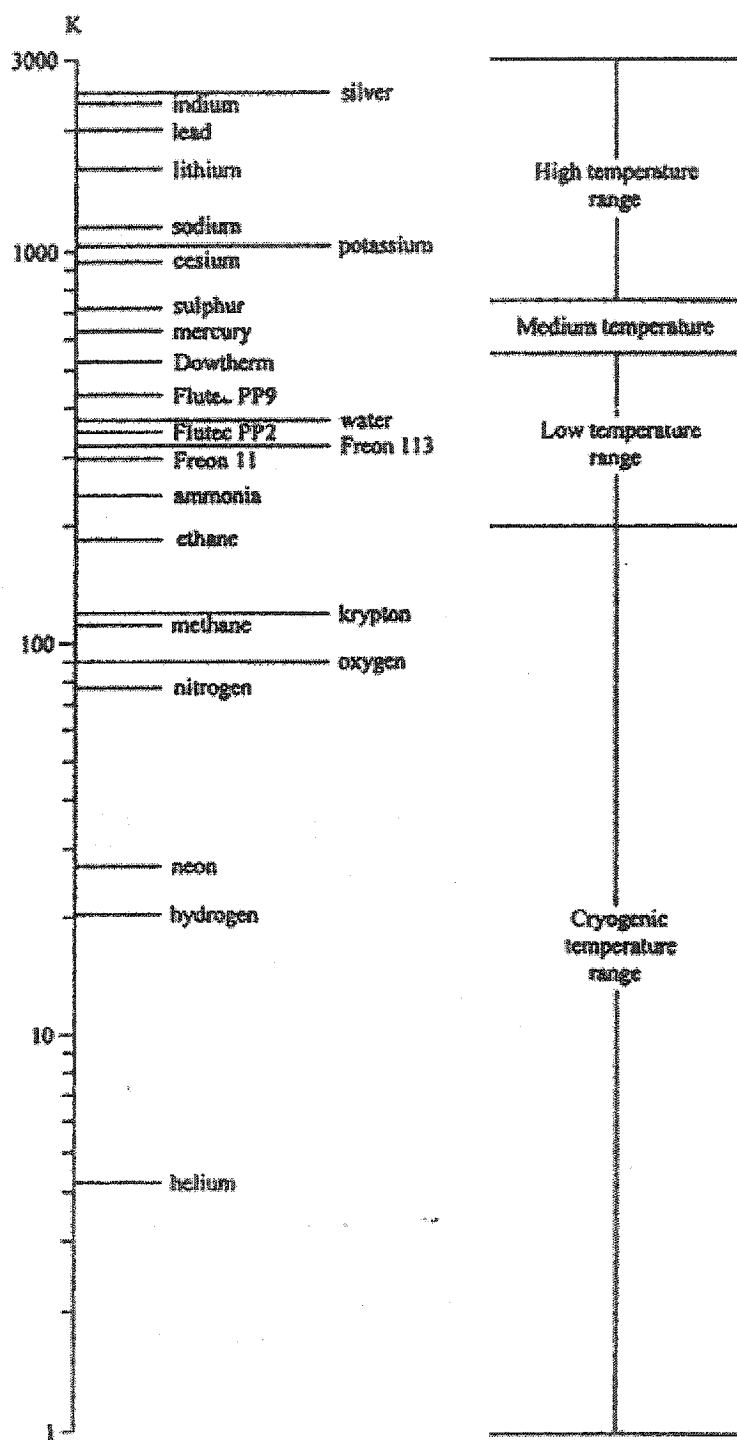
Figure 5-6. Operating Temperature Ranges of Various Working Fluid
on a Logarithmic Temperature Scale

Table 5-5 Generalized Results of Experimental Compatibility Tests

Working Fluid	Compatible Material	Incompatible Material
Water	Stainless steel, copper, silica, titanium	Aluminum, inconel
Ammonia	Aluminum, stainless steel, cold rolled steel, iron, nickel	Copper
Methanol	Stainless steel, iron, copper, brass, silica, nickel	Aluminum
Acetone	Aluminum, stainless steel, copper, brass, silica	
Freon-11	Aluminum	
Freon-21	Aluminum, iron	
Freon-113	Aluminum	
Heptane	Aluminum	
Dowtherm	Stainless steel, copper, silica	
Lithium	Tungsten, tantalum, molybdenum, niobium	Stainless steel, nickel, inconel, titanium
Sodium	Stainless steel, nickel, inconel, niobium	Titanium
Cesium	Titanium, niobium	
Lead	Tungsten, Tantalum	Stainless steel, nickel, inconel, titanium, niobium
Silver	Tungsten, Tantalum	Rhenium

Cryogenic Temperature Range

Cryogenic heat pipes operate between 4 to 200 K. Typical working fluids include helium, argon, oxygen, and krypton. The amount of heat that can be transferred for cryogenic heat pipes is quite low due to the small heats of vaporization, high viscosity, and small surface tensions of the working fluids.

Low Temperature Range

The low temperature range is from 200 to 550 K. Most heat pipe applications fall within this range. Commonly used fluids are ammonia, acetone, the Freon compounds, and water. Compounds such as Thermex or Dowtherm (Diphenyl-Diphenyloxide Eutectic) are employed in the upper portion of this range. Water, which is probably the most widely used working fluid, has good thermophysical properties such as heat of

vaporization and surface tension, and has the added benefit of being safe to use during handling.

Medium Temperature Range

The working fluids in the medium temperature range, 550 to 750 K, are mercury and sulphur. Mercury has extremely attractive properties inherent in a liquid metal such as its high thermal conductivity. However, problems with wetting the wick and wall present difficulties in using mercury in capillary heat pipes. The toxicity of mercury is also a significant problem.

High Temperature Range

Potassium, sodium, lithium, silver and a sodium-potassium compound (NaK) are often used in the high temperature range (750 K and above). The heat transport rates for liquid-metal heat pipes are generally much higher than those in the other temperature ranges because the surface tension coefficient, latent heat of vaporization, and thermal conductivity of liquid metals are very high.
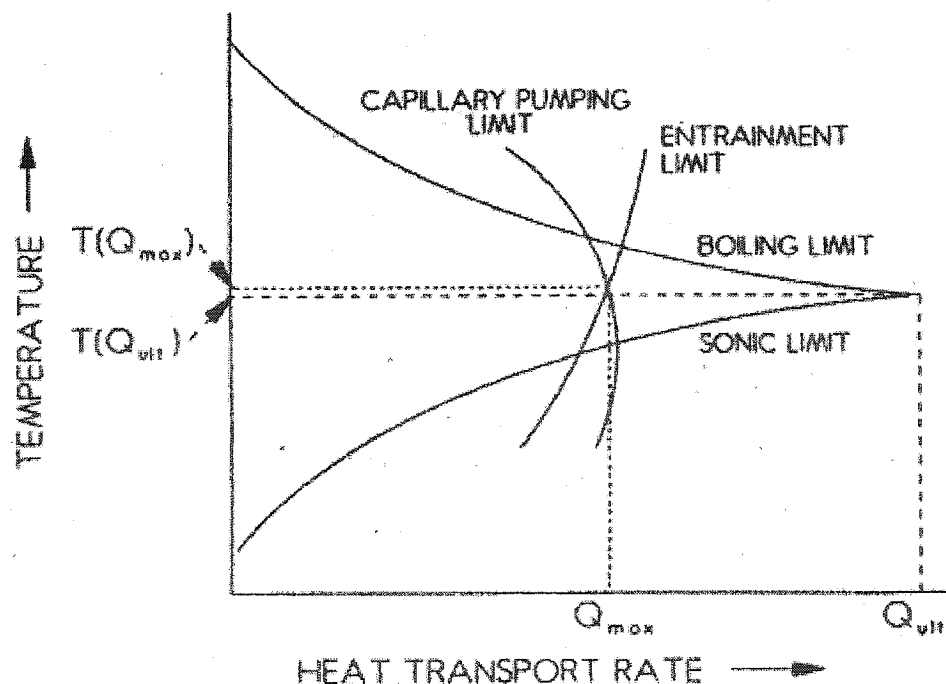
Figure 5-7. Heat Pipe Operating Temperature Range Versus Heat Transport Rate

For a given heat pipe fluid and heat pipe design, there is a range of operating temperature over which the heat pipe will be functional. The operating temperature range is determined by the heat transport limits of the heat pipe at a particular heat transport rate, as shown in Figure 5-7 [4].

At low heat pipe transport rates, the operating temperature range is relatively large, with the upper temperature limit usually determined by the boiling limit and the lower temperature limit by the sonic limit. The operating temperature range narrows as the heat transport rate increases. At higher heat transport rates, the operating temperature range may be limited by the cessation of capillary pumping or the onset of entrainment, as well as by the onset of sonic velocity or boiling.

If the lower operational temperature limit is determined by the sonic heat transport limit, operation of the heat pipe in the regime below this limit will not be physically possible. The temperature can then be lowered only by reducing the heat transport rate.

A heat transport rate will ultimately be reached at which the operating temperature range is reduced to a single point, denoted as $T(Q_{max})$ in Figure 5-7. This is the maximum attainable heat transport rate, and is denoted as Q_{max} in Figure 5-7. Any attempt to operate the heat pipe at a heat transport rate above Q_{max}, or to operate Q_{max} at a temperature other than $T(Q_{max})$, either will be impossible or will result in heat pipe operation failure.

It is evident from Figure 5-7 that determination of the operating temperature range for a particular heat pipe and heat transport rate requires that the temperature-dependent heat transport limits be known. Although the sonic limit, expressed as an axial heat flux, is dependent only on temperature, the other limits depend on the heat pipe geometry as well. Therefore, the operating temperature range varies with the specific heat pipe design as well as the heat transport rate.

As mentioned before, for most heat pipes, the vapor pressure usually lies in the range between 0.1 ~ 7 atm. For vapor pressure below 0.1 atm, heat transport capability is increasingly limited by the low density of the heat pipe vapor. The low vapor density in turn restricts the allowable axial heat flux for isothermal operation to relatively low values. For vapor pressure above 7 atm, heat transport capability is increasingly limited

by the low superheat for boiling in the heat pipe liquid, as well as by the thicker and heavier heat pipe wall needed to contain the pressurized vapor. The 0.1 to 7 atm of vapor pressure range represents a convenient basis for initial estimates of operating temperature ranges for various heat pipe fluids, as well as for selection of candidate fluids for preliminary heat pipe design studies. However, the design requirements of a particular application may require selection of a vapor pressure outside this range.

When more than one fluid is applicable to a particular temperature or temperature range, selection of the preferred fluid should be made on the basis of heat transfer, structural, and integratability criteria appropriate to a particular application.

Although Table 5-4 and Figure 5-6 provides a basis for selection of heat pipe fluids to meet a given operating temperature requirement, no information is supplied about relative heat transport capabilities. A convenient measure of heat transport capability is the liquid heat transport parameter P_{ht} defined as [4]:

$$P_{ht} = \rho_l \sigma \kappa / \mu_l$$

Where ρ_l is the density of the heat pipe liquid, σ is the surface tension, κ is the heat of vaporization, and μ_l is the liquid viscosity.

Thus, the heat pipe heat transport capability is directly proportional to the liquid heat transport parameter ($Q_c \propto P_{ht}$). In Figure 5-8 [4], the value of the liquid heat transport parameter at the boiling point corresponding to a vapor pressure of 1 atm (14.7 psia) is plotted as a function of boiling point temperature for selected heat pipe liquids. The data fall along two distinct curves--one corresponding to the liquid nonmetals and one corresponding to the liquid metals. For each curve, the liquid heat transport parameter is an increasing function of the boiling point. The liquid heat transport parameter for a given liquid varies with temperature, and tends to reach a maximum value at temperatures corresponding roughly to vapor pressures in the 0.1 to 0.7 atm range.

Comparisons of the liquid heat transfer parameter can be made when the following conditions are met:

- The vapor pressure drop is negligible.
- Liquid flow through the wick structure is laminar.
- The liquid hydrostatic head is negligible.

116

- The maximum heat transport rate is established by the capillary pumping limit.

These conditions are frequently satisfied for heat pipes operating at sub-ambient and ambient temperatures, which have been designed for space applications. Even when one or more of these conditions are not satisfied, the liquid heat transport parameter is still a reasonable, but more approximate indicator of relative heat transport capacity. Therefore, it can still be used to estimate the relative heat transport capability of a given heat pipe design with various heat pipe fluids when at a vapor pressure of 1 atm. For example, the heat transport of a water heat pipe is almost 4 times greater than that of an ammonia heat pipe, almost 20 times greater than that of a methanol heat pipe. It is also about 2.4 times that of a cesium heat pipe and almost 70% that of a potassium heat pipe.
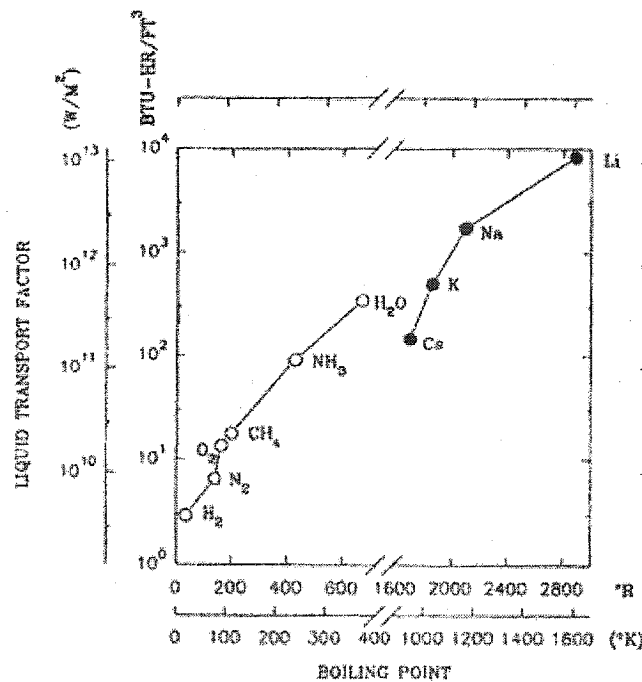
Figure 5-8. Liquid Transport Factor at Boiling Point Versus Boiling Point

5.2.2 Selection of Working Fluid

As discussed previously, the theoretical operating temperature range for a given heat pipe is typically between the critical temperature and triple state of the working fluid. After considering the applications, four kinds of working fluids have been chosen

for the present study to represent the three application temperature ranges. Low temperature is water, medium temperature is Thermex and high temperature is Potassium and Sodium.

Water

Water was selected as the most desirable heat transfer fluid for this investigation since it possesses the substantial advantages of having (1) well-known properties, (2) relatively low boiling point, (3) convenient working fluid characteristics, e.g. it is nonflammable, inexpensive, non-corrosive, and non-toxic, and (4) is available at high purity levels.

Thermex

From Table 5-4, the working fluids in the medium temperature range, 550 to 750 K, are mercury and sulphur. Because of the toxicity of both, they are rarely used in actual applications. Thus, Thermex, Diphenyl-Diphenyloxide (1/3) Eutectic, is employed instead as a working fluid in the medium temperature range because it is in the upper portion of the low temperature range.

Potassium and Sodium

Inexpensive and low melting point metals, such as Potassium (K) and Sodium (Na) are used extensively as working fluids in the high temperature range. They are present in many applications of heat pipes. Their melting points and vaporization heats are ideal and are the most common heat pipes used by the high temperature industries such as the metallurgical industry, chemical industry and energy industry.

The physical and chemical properties of selected working fluids are listed in references 3, 4, and 5. Figure 5-9 shows the vapor pressure vs. temperature for the 4 fluids used in the present study.

5.3 Forced Cooling of the Condenser

For a given heat pipe, its normal operating temperature range is defined by its working fluid. The normal operating temperature ranges of four selected working fluids

are shown in Figure 5-9. Below the low end of the range, the pressures corresponding to the saturation temperatures are too low to allow the heat pipe to maintain its properties. Above the high end of the range, the pressures corresponding to the saturation temperatures are too high to allow the working fluids to be confined in the heat pipe shell safely. Therefore, the heat pipe effect is controlled by the ratio of the condenser to the evaporator area. For a given evaporator area of the heat pipe with a particular working fluid, the extracting (transporting) heat is determined by the condenser area if the working fluid has a high enough vaporization latent heat. This translates to the operating temperature of the pipe. In order to obtain a suitable operating temperature range for a given application, one can adjust the ratio of the condenser to the evaporator area. This by itself is difficult for most applications. In addition, a large ratio of the condenser to the evaporator area is required to sustain high heat loads. Since self-cooling of the condenser cannot satisfy these application requirements, forced cooling of the condenser was employed in our experiments. In this section, the investigation results of forced cooling are presented.
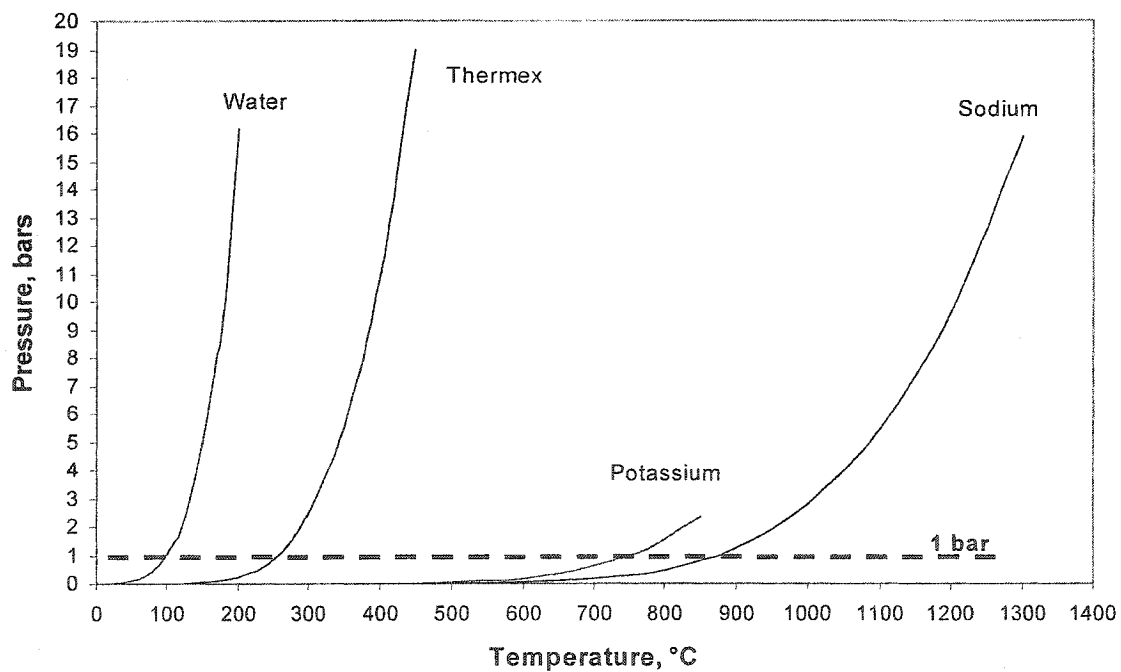
Figure 5-9. The Pressure Vs. Temperature Relation for Selected Working

5.3.1 Experimental Setup and Heat Pipe Structures

Steady-state testing and evaluation procedures for heat pipes are typically designed to measure the maximum heat transport capacity, the end to end temperature drop, the thermal resistance, and/or the effect of variations in the local gravitational acceleration on the overall thermal performance [5]. All of the measurements can be accomplished using a single, relatively simple test facility and straightforward test procedure. Normally, the testing facility consists of four principal sub-systems: a test heat pipe, a heat source, a heat sink, and a temperature measurement system. If cooling air is used, an additional measuring system of air flow rate is necessary. The test facility can be constructed for use in an air environment, but should be adjustable so that the evaporator section of the heat pipe can be elevated above or below the condenser to determine the effect of the gravitational body force on the transport capacity. Figure 5-10 shows a schematic diagram of our experimental setup. The temperature regulation of the furnace is achieved by the temperature controller. The cooling air is regulated by a metering valve and measured with an electronic flow meter. Entry and exit temperatures of the cooling air, and working substance temperatures are measured with thermocouples. All data are recorded by the computer. The working temperature of the heat pipe is easily controlled by adjusting the flow rate of the cooling air.
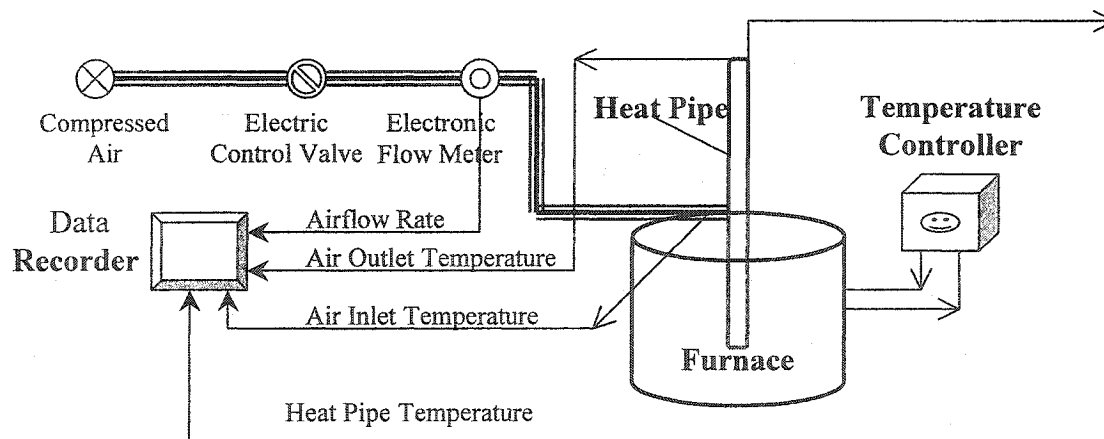
Figure 5-10 Schematic of the Experimental Setup for the Cylindrical Pipe

Four kinds of experimental programs were designed to evaluate the performance of cooling air in the traditional cylindrical heat pipe with a cooling jacket. The primary

intent of these studies was to understand and compare their thermal capabilities. These results will be used to help us choose a suitable structure, and the material and working liquid for subsequent heat pipe designs. For the setup, the design of the heat pipe plays a key role. As described above, the three major components: container, wick and working liquid need to be thought of in designing a heat pipe even if one temporarily ignores the heat pipe structure. Like past heat pipe research at McGill, 304 and 316 stainless steels were used as container materials and as wicks in these primary designs while water was used as the working fluid. The internal structure of a heat pipe will now be discussed as it has a major influence on the behavior of a heat pipe.

Figure 5-11 Schematic Diagram of Cylindrical Heat Pipe with a Double Jacket

A typical test procedure consisted of setting the heat source temperature (i.e. furnace) and cooling air flow rate. These values were recorded in addition to the temperature of the air inlet and the air outlet, and the temperature of the heat pipe.

Figure 5-11 is a schematic diagram of a cylindrical heat pipe with a cooling jacket. This heat pipe has double jackets. There are two inlets for the cooling air. These allowed us for the testing of both a top inlet and a bottom inlet for the cooling air. When introduced from the top, the air moves down the outer jacket and then passes into the inner jacket and moves up the outer wall of the heat pipe. For bottom entry, the air simply moves up the inner jacket. A removable copper coil was placed between the heat pipe and the inner jacket. A thermocouple well is placed inside the heat pipe. This well allows for the free movement of the thermocouple in order to measure the whole heat pipe temperature. The air outlet temperature is measured in the air flow from the cooling jacket just above the top of the heat pipe. A thermocouple holder is used to stabilize and hold the thermocouple at the air outlet.

Based on this heat pipe, the next version (No. 2) of the heat pipe was designed with just one jacket and a bottom inlet. Since this new version was to be used in a test program with liquid zinc, it had a thicker evaporator and a smaller condenser. Some parameters of the design are shown in Table 5-6, as No. 2. Also shown are the characteristics of version No.1. In both designs, 316 stainless steel was used as the container material of the heat pipe while 304 stainless steel was used to make the cooling jacket.

Table 5-6 Design Parameters of the Cylindrical Heat Pipe

No	Cooling Jackets: Condenser			Evaporator	Air Inlet		Heat Pipe	Wick	Working Liquid
	Layer	Outer-- Diameter, Thickness,	Inner-- Diameter, Thickness,	Length, OD*, Thickness,	Bottom	Top	Length, OD*, Thickness,	Material, Mesh, Layers,	Type, Quantity,
1	2	60.32 mm 2.77 mm	42.16 mm 2.77 mm	304.8 mm 26.67 mm 3.91 mm	yes	yes	1829 mm 26.67 mm 3.91 mm	Steel 100mesh 2	Water 150 ml
2	1	42.13 mm 2.77 mm		150 mm 50.8 mm 15.97 mm	yes		850 mm 26.67 mm 3.91 mm	Steel 100mesh 2	Thermex 50 ml

*. OD----Outer Diameter.

Since the energy transferred by heat flowing through the pipe cannot be directly measured, it is determined by computing enthalpy changes using temperature measurements that are readily made for a variety of experimental conditions. Usually, to design or to predict the performance of the heat pipe, it is essential to relate the total heat transfer rate to quantities such as the inlet and the outlet coolant temperatures, the overall heat transfer coefficient, and the total surface area for heat transfer. Such relations can be readily obtained by computing the enthalpy change of the cooling air. In particular, the total rate of heat transfer between the cooling air and the condenser wall assumes that there is negligible heat transfer between the heat pipe and its ambient surroundings in the forced cooling case, as well as negligible potential and kinetic energy change. The following four equations (5.1 to 5.6) [6] have been used to treat the primary experimental results.

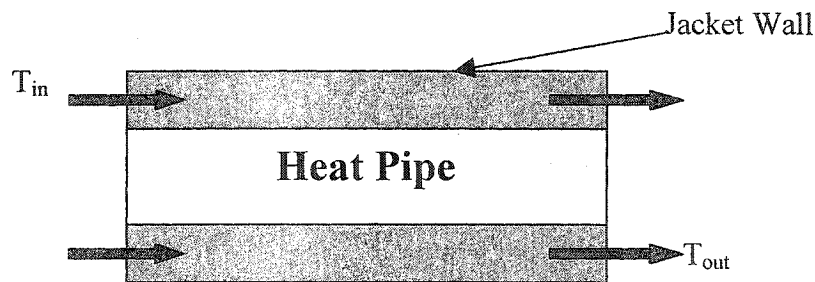Consider the flow of a fluid over an isothermal surface of known temperature and surface area. Figure 5-12 depicts such a case.

Figure 5-12. Schematic Diagram of Fluid Flow Pass an Isothermal Surface

- **Experimental Heat Transfer Rate**

$$Q_{exp} = \dot{m} C_p (T_{out} - T_{in}) \qquad (5.1)$$

where:

$\dot{m}$ air flow rate (l(STP)/s) x (28.8 g/mole/22.4 l/mole)

C_p the specific heat of air (J/g °C)

T   temperature °C

- **Theoretical Heat Transfer Rate (Radiation)**

$$Q_{theo} = \sigma A \varepsilon (T_{furnace}^4 - T_{wall}^4) \tag{5.2}$$

where:

σ Stefan-Boltzmann constant (5.67×10^{-8} W/m^{2}K^4)

A   Surface area of the black body (m^2)

T   Temperature of black body (K)

ε Emissivity of the body (0.8)

- **Heat Transfer Coefficient (h) in the Cooling Jacket**

$$h = -\frac{\dot{m}C_p}{RL} \ln\left[\frac{T_{wall} - T_{out}}{T_{wall} - T_{in}}\right] \tag{5.3}$$

where:

R   perimeter of cross sectional area cooled by air

L   length of passage cooled by air

T_{wall} temperature of heat pipe wall

T_{out} temperature of outlet cooling air

T_{in} temperature of inlet cooling air

- **Thermal Efficiency of Heat Pipe**

The thermal efficiency is defined as the accomplished temperature change for the cooling air.

$$Thermal \;\; Efficiency = \frac{(T_{out} - T_{in})}{(T_{heat\,pipe} - T_{in})} \times 100 \tag{5.4}$$

5.3.2 Experimental Results and Discussion

Various experimental parameters are used to investigate forced cooling effective for the following configurations.

5.3.2.1 The Heat Pipe without a Copper Coil

In this experiment, the heat pipe without a copper coil, which was shown in Figure 5-11, is tested under two conditions: air entering from top air inlet and from the bottom air inlet. Figure 5-13 presents experimental data from another test wherein the heat pipe is operated at steady-state. In this case, the heat pipe temperature didn't change for a given furnace temperature and cooling air flow rate. This situation avoids startup problems and can be used to evaluate the effect of the cooling air.

Normally, we chose a safe operating pressure, which for water is around 1 atm at 100 °C. The experimental plan (data recording) was then implemented by adjusting furnace temperature and air flow rate. When the three parameters: furnace temperature, air flow rate, and heat pipe temperature were stable (lasting at least 10 minutes without changing), the furnace temperature, air flow rate, heat pipe temperature and inlet/outlet temperatures of the cooling air were recorded as the experimental results for that case. Figure 5-13 lists these recorded data points (1 to 5). After the data was recorded, the furnace temperature and flow rate of cooling air were changed to the next testing conditions based on the experimental plan.

Figure 5-14, Figure 5-15 and Figure 5-16 present these experimental results. All these results were obtained under steady-state. Figure 5-14 shows a comparison of the heat extracted in the experiment (calculated via equation 5.1) when the air inlet was alternated between the top (Figure 5-14a) and the bottom (Figure 5-14b). From this figure, it is observed that heat extraction increased as the flow rate of cooling air was increased for both cases. Also, it increased with increasing heat pipe temperature. However, heat extraction in case of bottom air inlet is greater than that of the air inlet at the top when the air flow rate was the same.

Figure 5-15 presents heat transfer coefficients (calculated by equation 5.3) for both cases of air input. For a given heat extraction, the heat transfer coefficients increased as the flow rate of cooling air increased for a fixed heat pipe temperature. Also, the coefficient for the bottom case (Figure 5-15b) is greater than that for the top (Figure 5-15a). But, the heat transfer coefficients show a peak in the curves. In some of the low flow rates, only decreasing trends were observed. It is clear that the heat transfer coefficient, with air input from bottom air inlet (Figure 5-15b), is almost two times that for the top air inlet (Figure 5-15a).
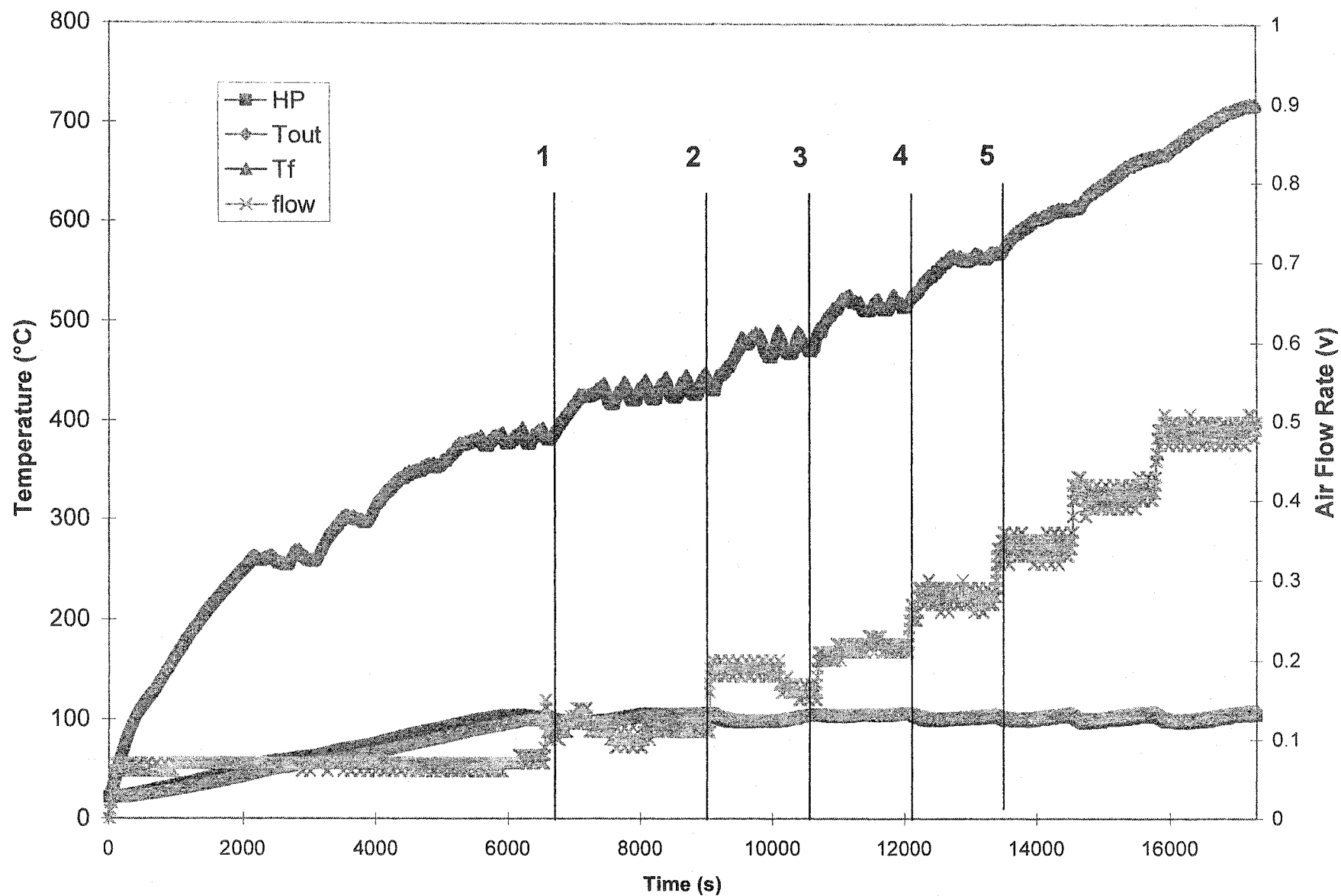
Figure 5-13. A Type of Recording Curve of Experimental Conditions

Figure 5-14. The Comparison of Extracting Heat between Air Inlet from Top and Bottom

Figure 5-15. The Comparison of Heat Transfer Coefficient between Air Inlet of Top and Bottom

Heat Pipe Efficiency (Top Air Inlet, Without Coil)

Heat Pipe Efficiency (Bottom Air Inlet, Without Coil)

Figure 5-16. The Comparison of Heat Pipe Efficiency between Air Inlet of Top and Bottom

Figure 5-16 presents the results of heat pipe efficiency, which were calculated using equation 5.4. The heat pipe efficiency increased as the flow rate of cooling air first increased. When the flow rate reached a certain value, the efficiency stopped increasing. In our experiments, the values of heat pipe efficiencies were almost the same for flow rates of cooling air at 10.26, 8.64 and 6.84 Nl/s, respectively. Thus, with a particular heat pipe, there is an optimum value of cooling air flow. Similarly, heat pipe efficiency also has a peak in the curves, shown in Figure 5-16a and b. It was not possible to obtain higher heat pipe efficiency by raising the operating temperature of the heat pipe. With a particular working fluid, an optimum operating temperature range existed in our experiments. Figure 5-16 also shows that the efficiency of the heat pipe in top air inlet mode is less than that in bottom air inlet mode

Therefore, heat extraction and the heat transfer coefficient, as well as heat pipe efficiency increased as the flow rate of cooling air was increased. The results of the bottom air inlet case are much better than the results of the top air inlet case. Thus, in formulating a new heat pipe design, introducing cooling air from the bottom air inlet was selected.

5.3.2.2 Testing of the Heat Pipe with a Copper Coil

In order to improve the heat transfer by the cooling air, a copper coil was placed in the cooling jacket for another series of experiments. The relative results are shown in Figure 5-17, Figure 5-18 and Figure 5-19. A general comparison was made, and it was shown that the trends were the same as those in the tests of the heat pipe without the copper coil. The bottom inlet case was the best one. However, these two sets of figures also indicated some differences. The results of heat extraction, heat transfer coefficient and heat pipe efficiency for the heat pipe with a copper coil were much better than those for the heat pipe without a copper coil. For instance, the presence of the coil almost doubled the heat extraction rate since it improved the turbulence of the cooling air. Therefore, the use of a coil in the heat pipe design is warranted to improve the heat transfer of the cooling air.

5.4 Cooling Panel with Internal Condenser

Extracting Heat Flux (Top Air inlet, Coil in)
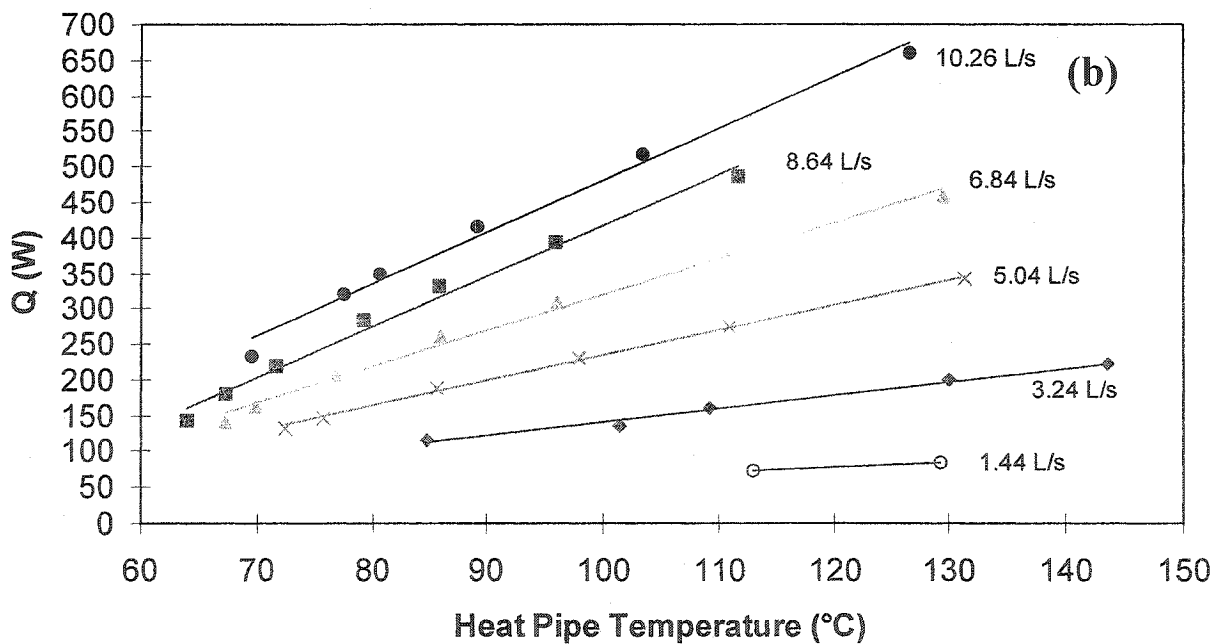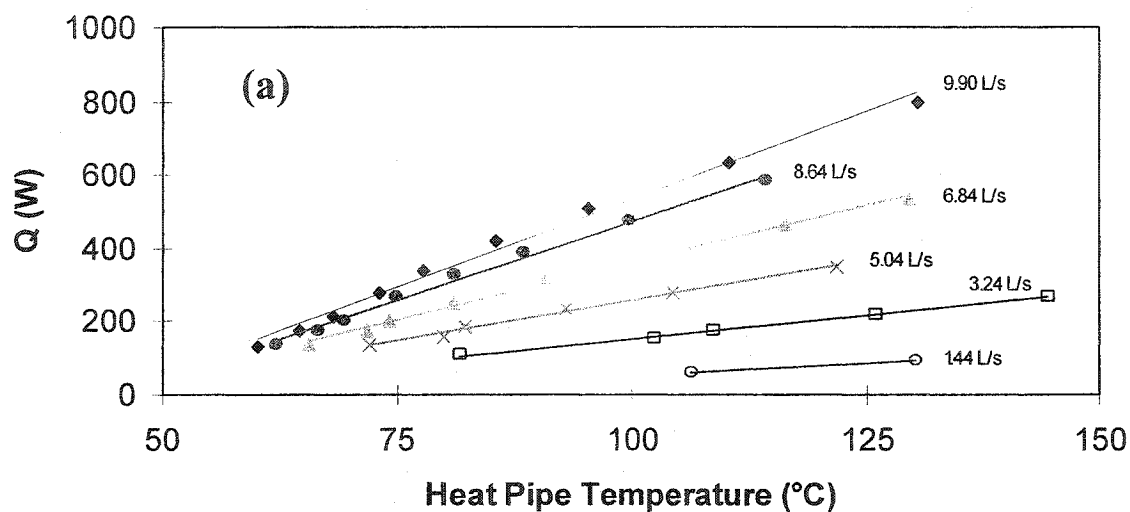

Extracting Heat Flux (Bottom air inlet, Coil in)

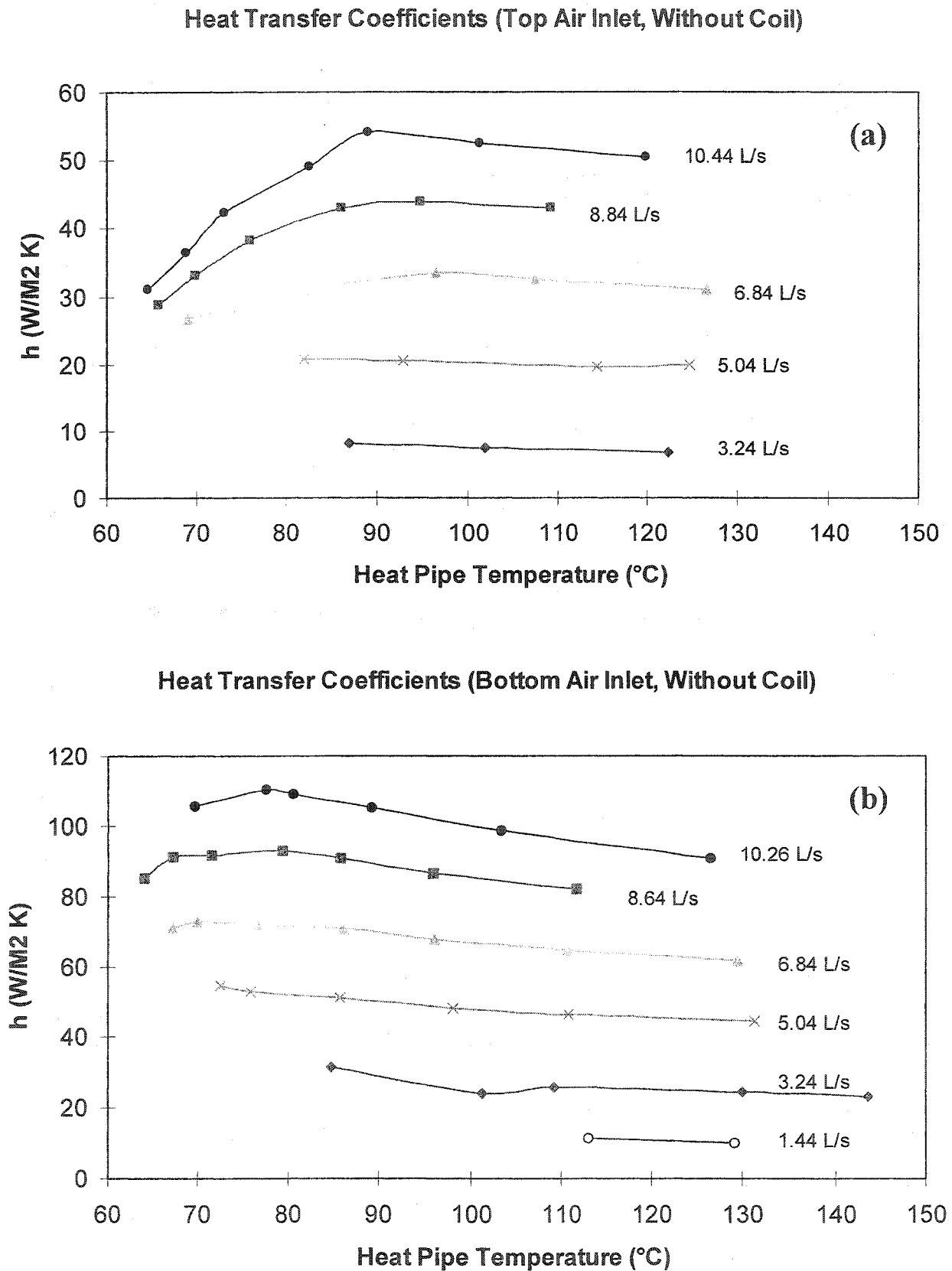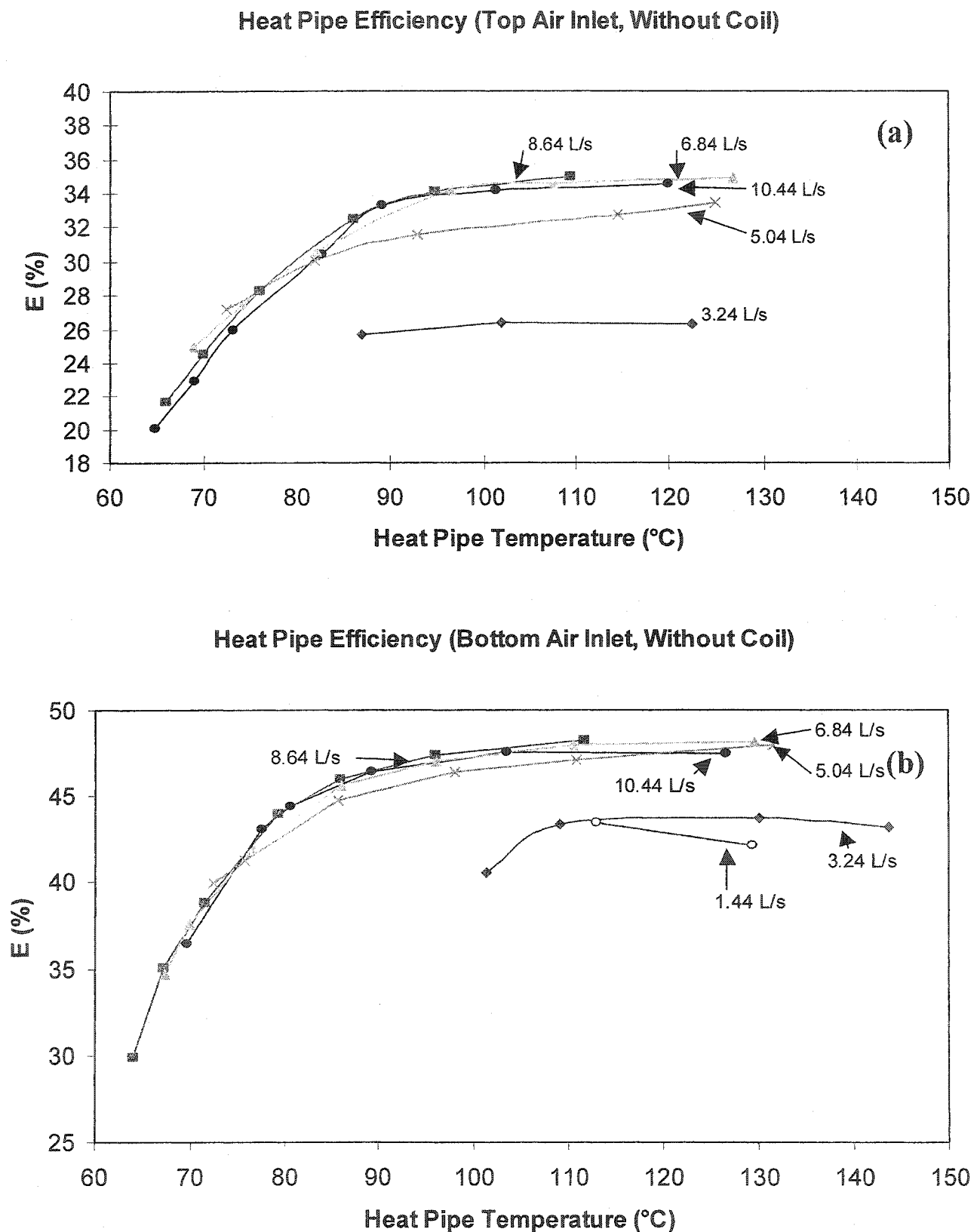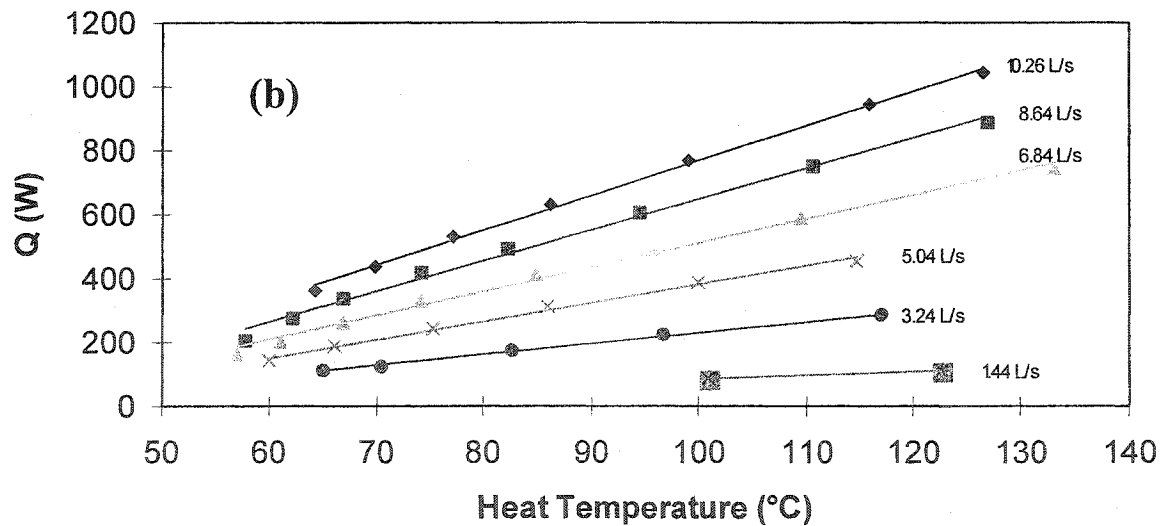Figure 5-17. The Comparison of Extracting Heat between Air Inlet of Top and Bottom
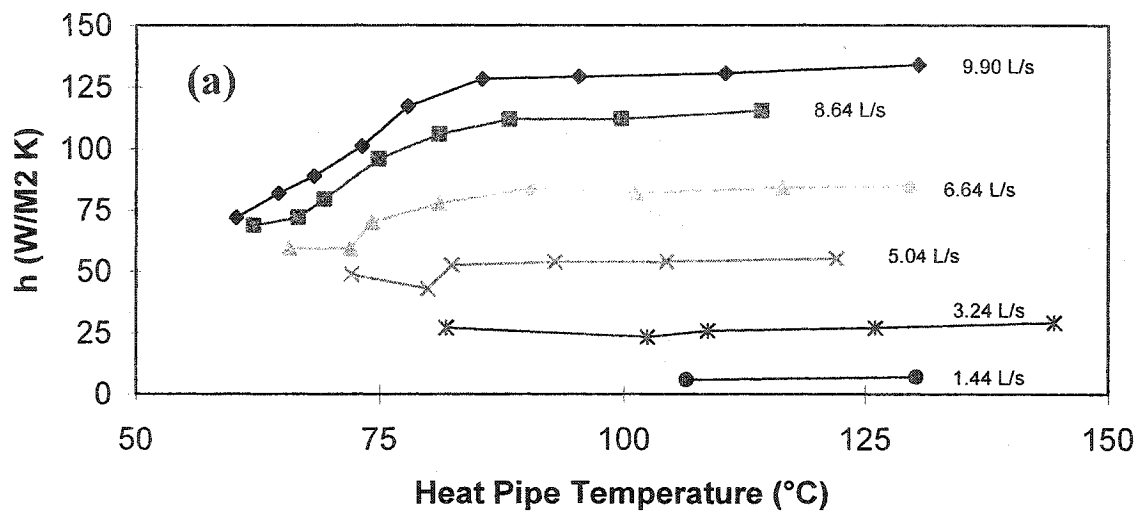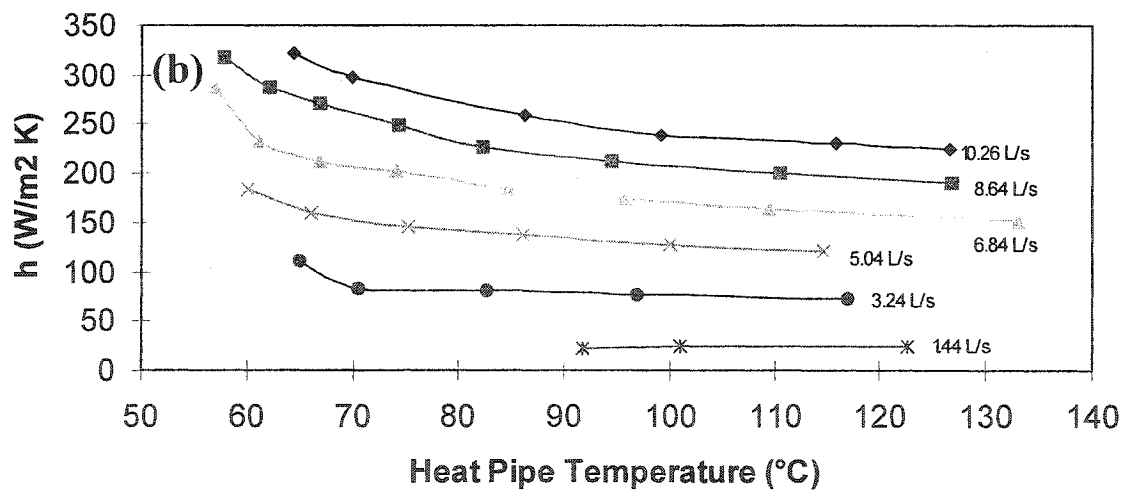
Figure 5-18. The Comparison of Heat Transfer Coefficient
Between Air Inlet of Top and Bottom

Efficiency (Top Air Inlet, Coil in)

Heat Pipe Efficiency (Bottom Air Inlet, Coil in)

Figure 5-19. The Comparison of Heat Pipe Efficiency
between Air Inlet of Top and Bottom

133

Unsealed
Cooling Panel
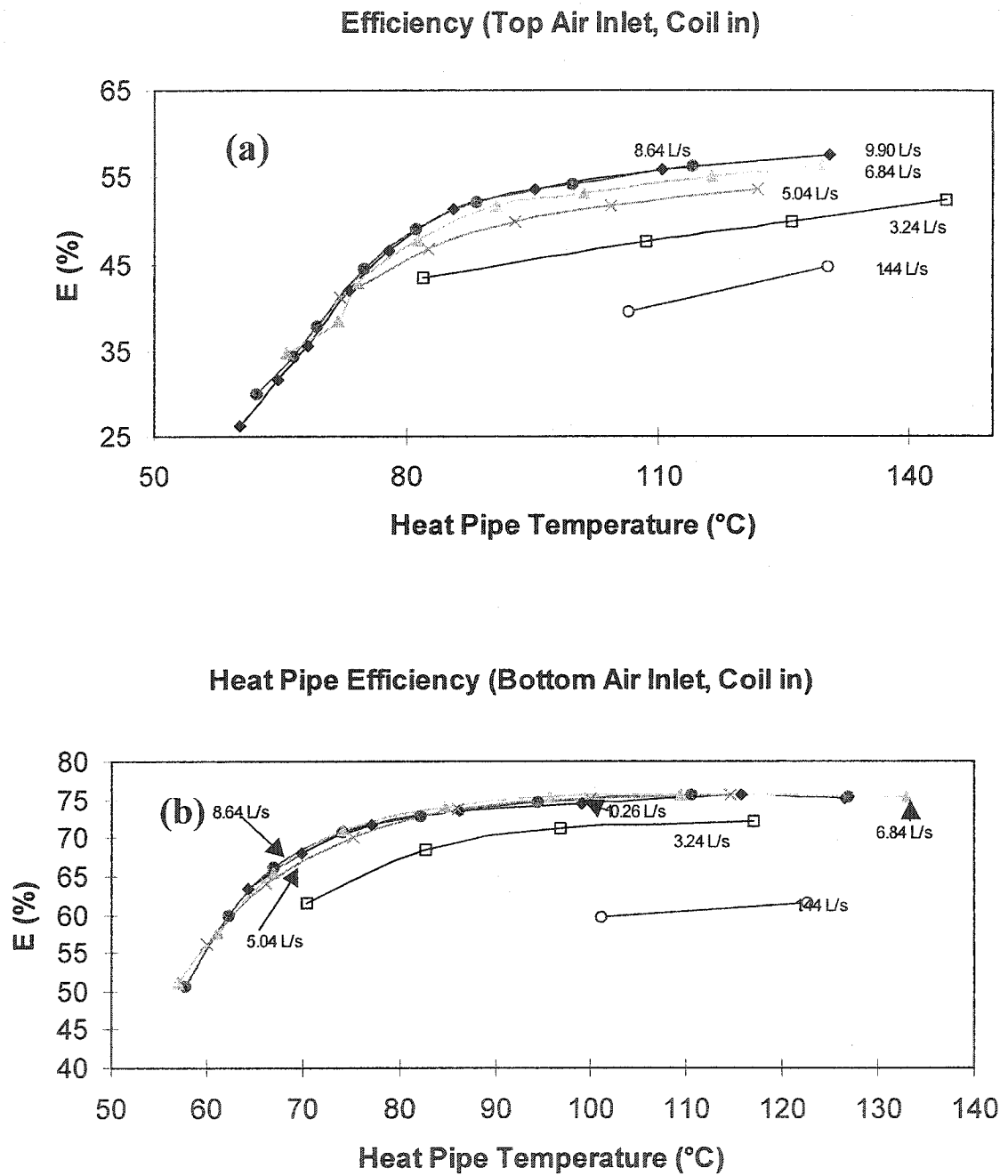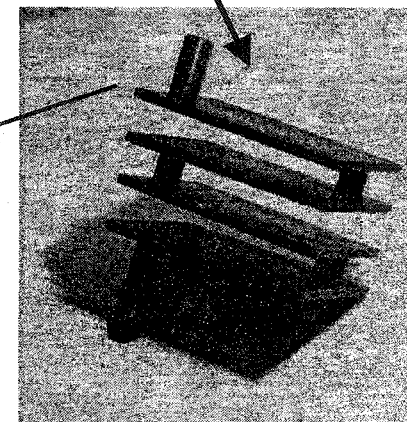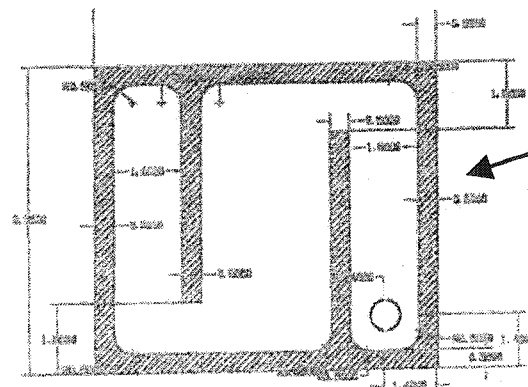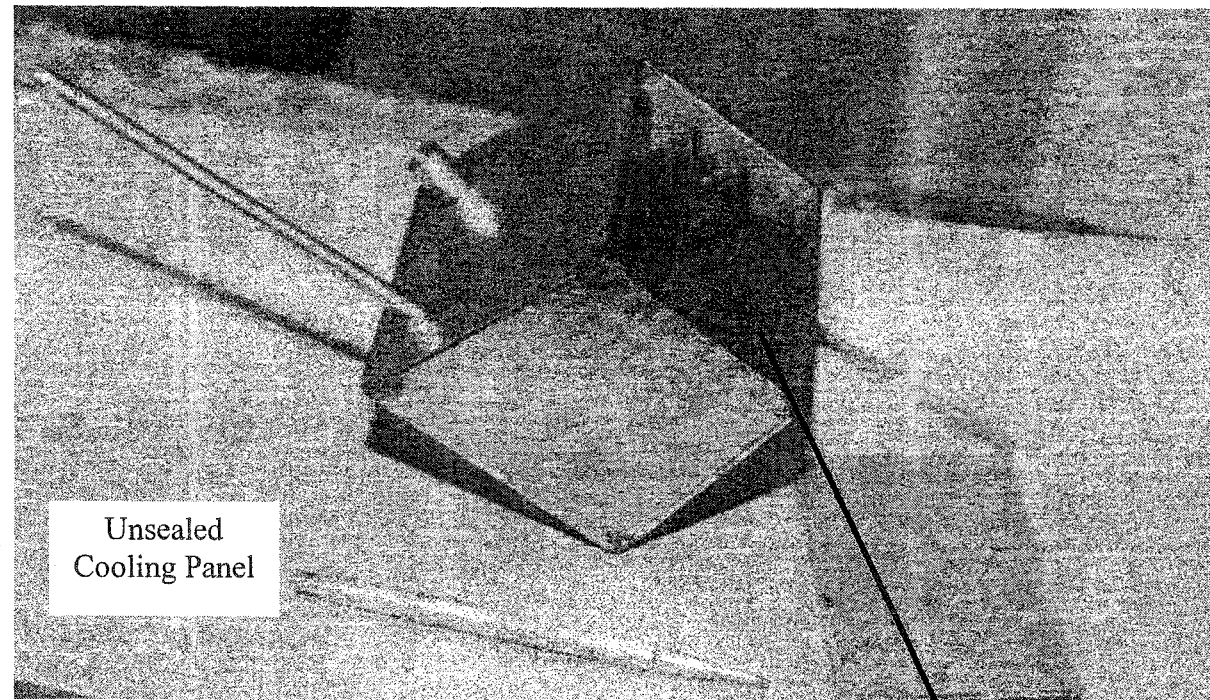
Condenser Plate
(Bottom)

Internal Condenser

Figure 5-20. Views of the Cooling Panel with Internal Condenser

Figure 5-20 shows a picture of a heat pipe cooling panel with an internal condenser [7]. The design criteria are listed in Table 5-7. In this design, 304 stainless steel was used for the box container, the condensing plates and the tubes. To ensure that the working substance in liquid form would run down the condensing plates onto the front plate, the cooling plates were fixed in the panel at an angle of 15°. There was a 0.5 cm gap on each side of the plates to let excess water vapor rise inside the box and condense on the upper plates. The interior of the plates was designed to ensure a maximum area to be cooled by the cooling air. The "S"-shaped channel (Figure 5-20(c)) forces the cooling air to cool most of the condenser plate area. Four layers of 100 mesh stainless steel wick were then tack-welded on the inside surface of the front box face (evaporator). The number of layers were determined using a trial and error approach: wick layers were added on top of one another until the gap existing between the end of the condensing plates and inside surface of the front face became negligible [7].

This was done to make sure that the condensing liquid flow could contact the wick surface on the inside of the evaporator face.
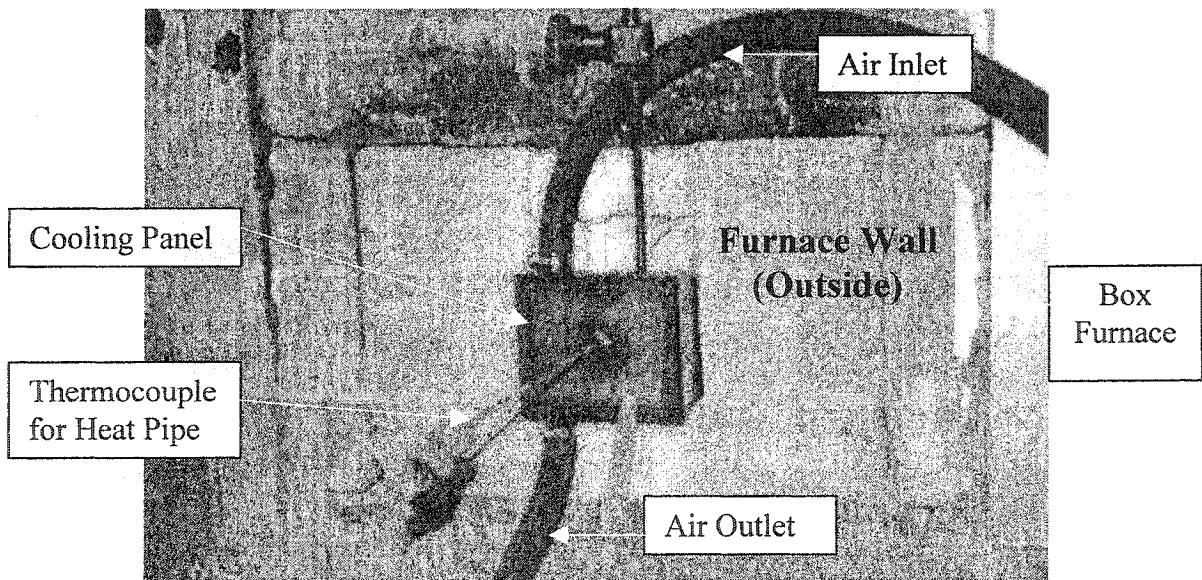
Figure 5-21. Picture of Cooling Panel Setup as Seen from the Outside of the Furnace

Table 5-7. Design Parameters of Heat Pipe Cooling Panel

Box of Heat Pipe Cooling Panel					Condenser	Evaporator	Wick	Working Liquid
Bottom	Front	Back	Top	Sides*	8 faces	1	4 layers	Water
8 × 10 cm	7 × 10 cm	9.07 × 10 cm	8 × 10 cm	8 × 8.04 cm	8 × 9 cm	7 × 10 cm	100 mesh	80 g

*. It has two pieces of by-sides. There is an angle of 15° in its top. Thus, it is not a square.

Since the cooling panel has a flat shape, it can be incorporated into a furnace wall, as shown in Figure 5-21. The box furnace was used as the heat source in the schematic of our experimental setup (Figure 5-10).

5.4.1 Extracted Heat

The total heat extraction rate for the cylindrical heat pipe and the cooling panel exceeded 1000 W and 450 W in our testing range, respectively. A comparison of some results is listed in Table 5-8. The heat flux (W/m^2) on the cooling panel was about 4 times that on the cylindrical heat pipe. In this comparison, the best case (bottom air inlet and with copper coil) of the cylindrical heat pipe is selected.

Table 5-8. Comparison of the Testing Results for the Cooling Panel and Cylindrical Pipe

Cooling Panel Air Flow Rate = 4.41 Nl/s					Cylindrical Heat Pipe (Bottom, Coil in) Air Flow Rate =5.04 Nl/s				
$T_{furnace}$ (°C)	T_{out} (°C)	T_{HP} (°C)	Q_{exp} (W)	Q (W/m^2)	$T_{furnace}$ (°C)	T_{out} (°C)	T_{HP} (°C)	Q_{exp} (W)	Q (W/m^2)
850	110.45	107.14	456.15	65164	555	91.71	114.65	458.20	17557
790	103.45	99.08	416.46	59494	506	80.35	99.96	384.59	14737
730	94.76	90.04	367.19	52455	453	68.95	85.94	310.72	11906
670	84.76	82.88	310.49	44355	404	59.03	75.27	246.43	9443
610	73.95	72.79	249.20	35599	356	49.86	66.14	187.01	7166
550	65.8	65.62	202.99	28998	305	43.01	60.1	142.62	5465

Because of the limitation of the experimental furnace, these results are still lower than the design capacity of the heat pipe, especially for the cooling panel. As the flow rate of the cooling air was increased, the rate of heat extraction was also increased.

5.4.2 Efficiency of Heat Pipe

From our experimental results of the cooling panel and the cylindrical heat pipe, the thermal efficiency strongly depends on the structure of the heat pipe, the flow rate of the coolant and the inlet position of the cooling air. With the cylindrical heat pipes, the efficiency using the bottom air inlet is higher than that using the top air inlet because of the recycling of heat. Some heat from the inside jacket was absorbed by the coolant when the top air inlet was used as shown plotted in Figures 5-22(a) and (b). In this case, for example, the efficiency of the heat pipe went from 75% to 55% with the change in inlet entry. Given that the heat pipe had a double jacket to allow for top or bottom entry, only the bottom entry could be compared to the cooling panel which had only one jacket. The efficiency of both kinds of heat pipes increased with increasing flow rate. However, when it reached a certain level, the trend changed slowly or even showed no change. The case of the cooling panel is somewhat unique. In most of the tests we observed, its efficiency exceeded 100% ($T_{out} > T_{HP}$, as listed Table 5-8). This was due to exit air passing through the bottom liquid pool which is superheated. Compared with both heat pipes, the cooling panel with internal condenser (100%) was more efficient than the cylindrical heat pipe with the external condenser (75%) because the internal condenser improved heat transfer as it provided more contact area. Of course, increasing the flow rate of the cooling air at a constant furnace temperature decreased the operating temperature of the heat pipe. The coil in the cylindrical pipe also improved heat extraction. It raised the efficiency of the heat pipe by 25% when it was added inside the cylindrical jacket as a result of the change in flow of the cooling air.

From Figure 5-23, we can see that at a low operating temperature, the active volume of the condenser of the heat pipe shrinks as the overall pressure drops and the inert gas expands. As a result, the efficiency of the heat pipe decreases. Thus, the optimum combination of operating conditions including furnace temperature, operating temperature of the heat pipe and flow of cooling air can be determined by experiments to obtain the highest efficiency of the heat pipe.
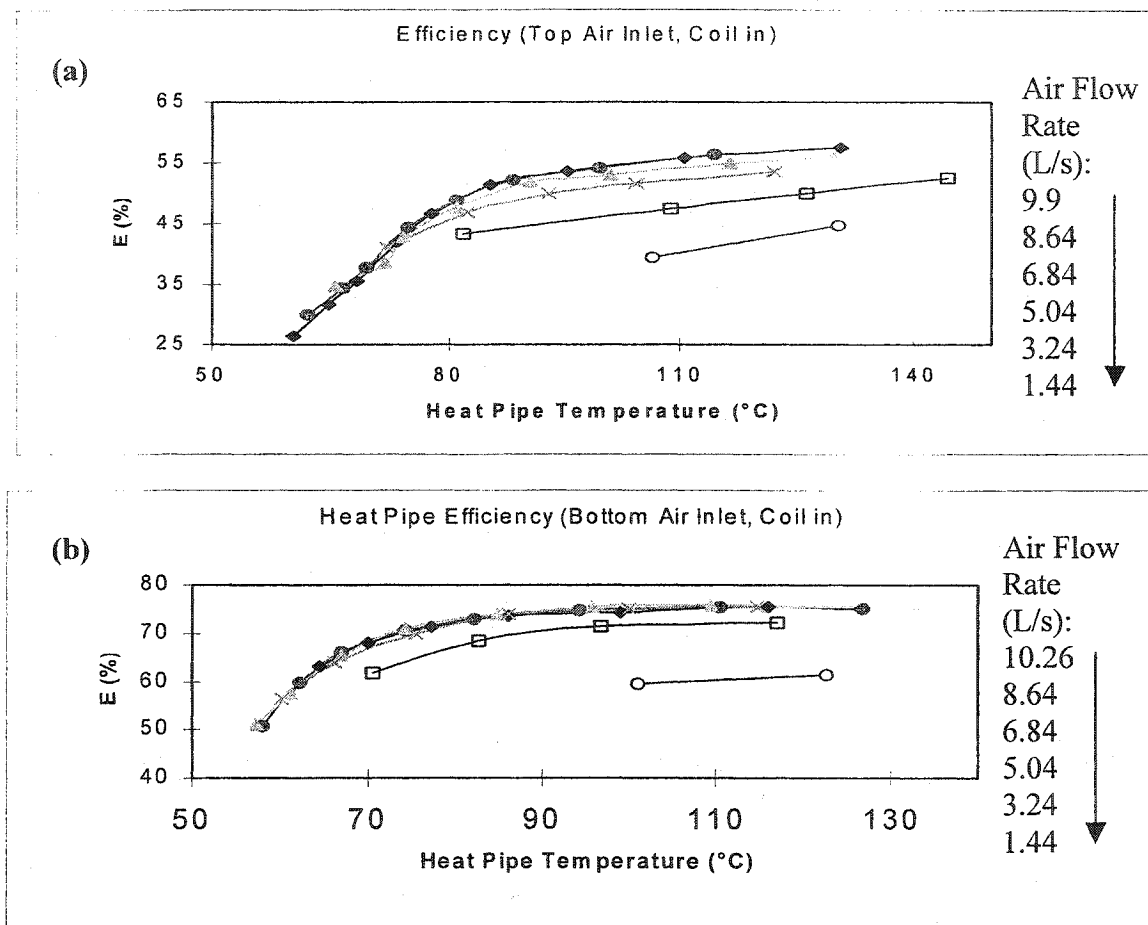
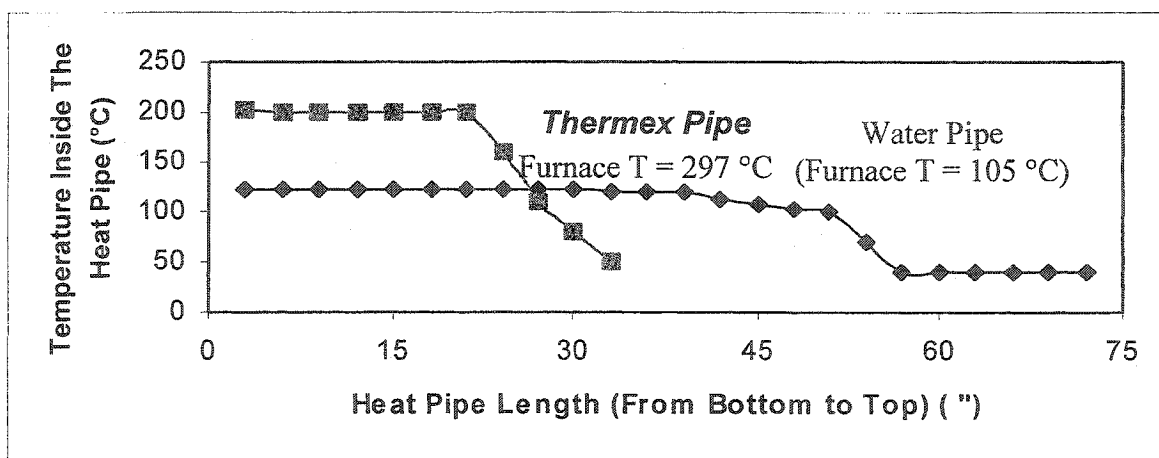Figure 5-22. Comparison of Efficiency of the Heat Pipe

Figure 5-23. Temperature Distribution inside the Heat Pipe

4.2.3 Heat Transfer Coefficients

The heat transfer coefficient is one of the most important factors that influences the thermal situation of the heat pipe. It can be computed based on experimental data. Since the experimental data were taken in a relatively steady situation, we considered the system as being at steady state. Therefore, to calculate heat transfer coefficients, we developed a model using a finite differences numerical analysis. Due to the symmetry of the heat pipe about its vertical axis, only the radial and longitudinal axes were considered (i.e. 2-D). A heat balance equation for every node was developed and solved by TK Solver which is produced by Universal Technical Systems, Inc., USA. This program can easily solve a series of non-linear equations.

Some calculation results of computed heat transfer coefficients, h, are plotted in Figure 5-24. As the flow rate of cooling air increased, the heat transfer coefficient, h, increased. In the thermex pipe without a coil, this trend slows down at high flow rates. The increase in h is strongly dependent on the operating temperature of the heat pipe. With increasing operating temperature, the h showed a sudden drop at a certain operating temperature. This is indicated clearly in Figure 5-24(c). We suspect that this phenomenon was a result of the air flow changing from turbulent to laminar, and thus an overall reduction in its heat transfer ability. The water pipe showed a similar phenomenon (Figure 5-24(b)), but the trend was gentler in change. In addition, the higher "apparent" h's at low heat pipe temperatures were that the condenser area is less than the total (see Figure 2-23) and h is computed with the total area. The h appears to increase. In reality, it is the area that is decreasing.

From these figures, we can see that the h of the heat pipe with the coil is much higher than that without the coil. Therefore, the use of a coil in the heat pipe jacket efficiently improves heat transfer. The coil can transform laminar flow into turbulent flow. Usually, with a certain flow rate of cooling air, the heat transfer coefficient should be constant. But in Figure 5-24a a changing trend is noticeable at low operating temperatures of the heat pipe. A possible explanation for this is that the heat pipe used in experiments did not have a relatively high vacuum; there was still some inert gas inside the heat pipe. When the heat pipe was operated at low temperature, the low vapor pressure was choked by the gas inside the heat pipe, which resulted in a decrease in the

active condenser length. This phenomenon was observed and measured in experiments (Figure 5-22). The lower the operating temperature of the heat pipe, the larger was the shrinking condenser. At this point our calculation algorithm for h does not fully take this effect into account. Future work should incorporate this feature.

For the cooling panel, we did not compute the heat transfer coefficients. Before developing a model of the cooling panel and a simulation of the thermal behavior inside the cooling panel, we found that the cooling panel can experience a serious problem in high heat flux environments, this will be discussed in the next chapter. In addition, its manufacture is complex. It is relatively expensive to machine. Thus, we abandoned this plan and chose instead to use a loop heat pipe to replace it.
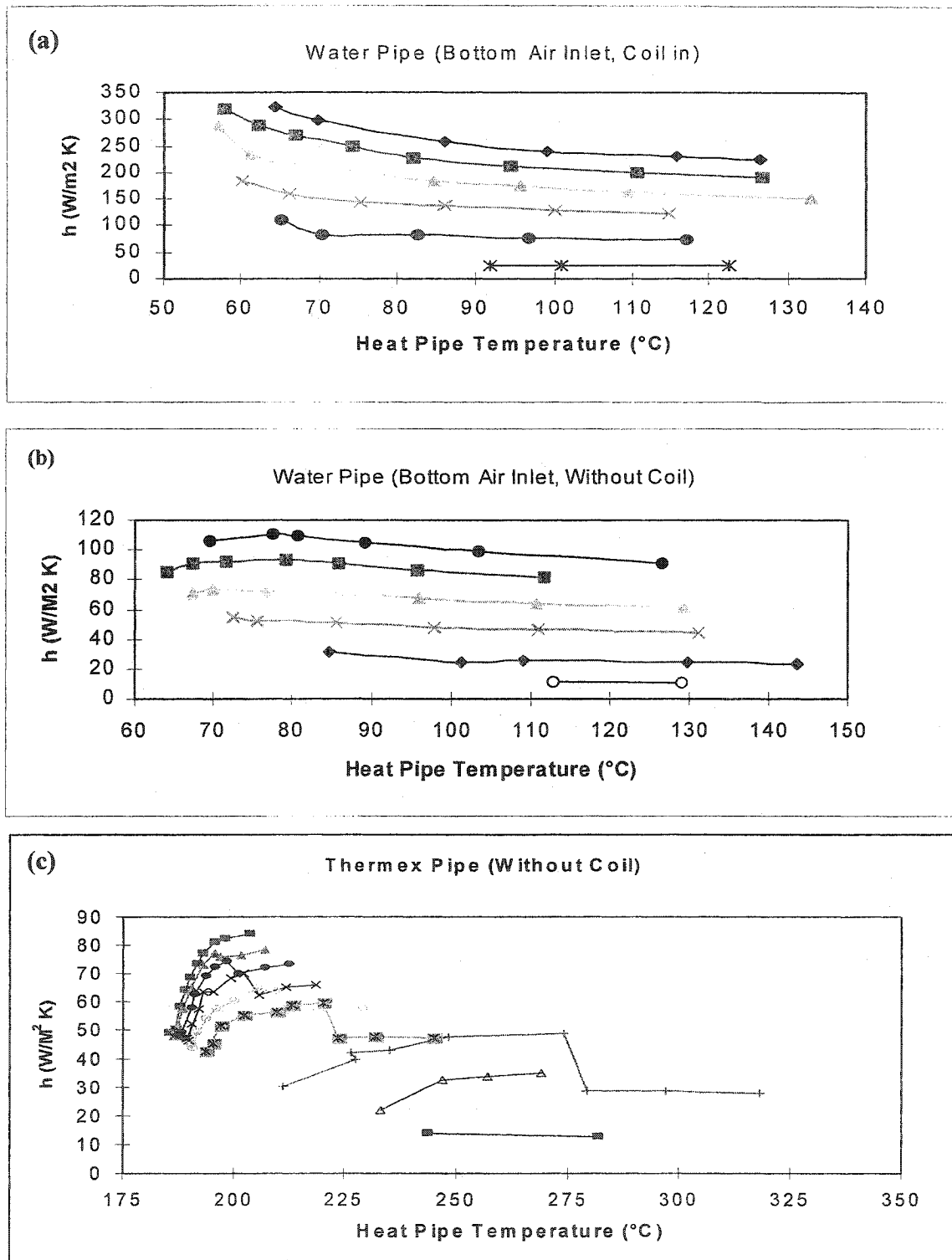
Figure 5-24. Comparison of Heat Transfer Coefficients in Both Cylindrical Heat Pipes

CHAPTER 6. THE ISSUE OF FILM BOILING WITH HIGH HEAT FLUXES

6.1 Heat Pipe Behavior In a Radiation Furnace and in Liquid Zinc

6.1.1 Structure of the Heat Pipe

The heat pipe was used to extract heat from molten zinc. Some zinc properties are shown in Table 6-1. From Table 6-1, the zinc melting point is 420 °C. Thus, the operating temperature of the heat pipe must be lower than this temperature to freeze zinc. As described in Chapter 5, the operating temperature range of the heat pipe is usually determined by the working fluid.
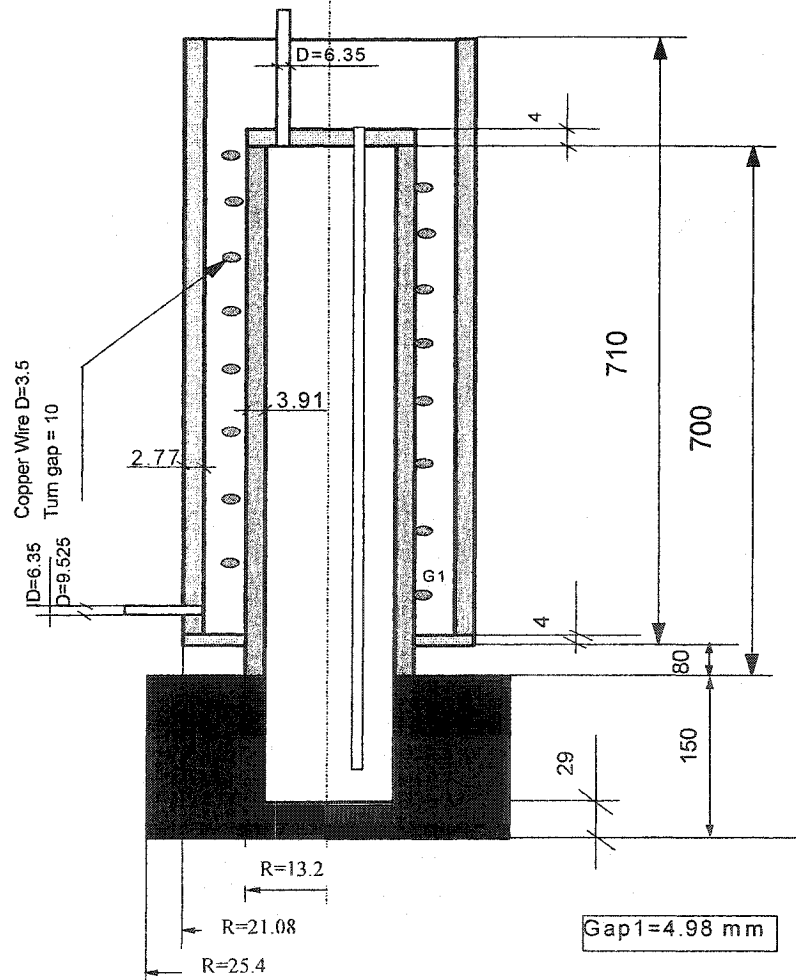
Figure 6-1. The Structure of Our First Thermex Heat Pipe

Thus, Thermex, which can be used in the corresponding temperature range (see section 5.2.2.), was selected as the working fluid. Its operating temperature range is $150 \sim 350$ °C, as shown in Table 5-4. Table 6-2 presents some thermophysical properties of Thermex. These will help in understanding the behavior of Thermex in this application.

Table 6-1. Technical Data of Zinc

ATOMIC NUMBER	30
ATOMIC WEIGHT	65.37
DENSITY 25°C 419.5 °C (liquid) 600 °C	7140 kg/m^3 6921 kg/m^3 6808 kg/m^3
MELTING POINT	419.5°C (692.7 K)
BOILING POINT (1 atm)	907°C(1180 K)
MODULUS OF ELASTICITY	$7 \times 10^4 \text{ MN/m}^2$
SPECIFIC HEAT 20°C 419.5 °C (liquid) 600 °C	0.382 kJ/kg.K 0.502 kJ/kg.K 0.490 kJ/kg.K
LATENT HEAT OF FUSION (419.5°C)	100.9 kJ/kg
LATENT HEAT OF VAPORIZATION (906°C)	1.782MJ/kg
HEAT CAPACITY: Solid (25 - 419.5 °C) Liquid Gas	$C_p = 22.40 + 10.5 \times 10^{-3} \text{ TJmol}^{-1}$ $C_p = 31.40 \text{ Jmol}^{-1}$ $C_p = 20.80 \text{ Jmol}^{-1}$
LINEAR COEFFICIENT OF THERMAL EXPANSION (polycrystalline 20-250°C)	39.7 μm/m.K
VOLUME COEFFICIENT OF THERMAL EXPANSION(20-400°C)	0.89×10^{-6}/K

THERMAL CONDUCTIVITY :
Solid   18°C
       27 °C
       127 °C
       327 °C
Liquid 500 °C
       600 °C
	113 W/m.K
	116 W/m.K
	111 W/m.K
	103 W/m.K
	57.7 W/m.K
	56.8 W/m.K

Table 6-2. The Thermophysical Properties of Thermex [1]

Temperature (°C)	Latent Heat (kJ/kg)	Liquid Density (kg/m^3)	Vapor Density (kg/m^3)	Liquid Thermal Conductivity (W/m °C)	Liquid Viscosity (cP)	Vapor Viscosity (cP, x 10^2)	Vapor Pressure (Bars)	Vapor Specific Heat (kJ/kg °C)	Liquid Surface Tension (N/m x 10^2)
100	354.0	992.0	0.03	0.131	0.97	0.67	0.01	1.34	3.50
150	338.0	951.0	0.22	0.125	0.57	0.78	0.05	1.51	3.00
200	321.0	905.0	0.94	0.119	0.39	0.89	0.25	1.67	2.50
250	301.0	858.0	3.60	0.113	0.27	1.00	0.88	1.81	2.00
300	278.0	809.0	8.74	0.106	0.20	1.12	2.43	1.95	1.50
350	251.0	755.0	19.37	0.099	0.15	1.23	5.55	2.03	1.00
400	219.0	691.0	41.89	0.093	0.12	1.34	10.90	2.11	0.50
450	185.0	625.0	81.00	0.086	0.10	1.45	19.00	2.19	0.03

A schematic of the conventional heat pipe that was built is shown in Figure 6-1. The evaporator portion of the heat pipe was made by drilling a hole 19 mm in diameter in a solid 316L stainless steel (SS) bar of 50.8 mm outer diameter. The bottom of the bar was left with a 29 mm thickness of SS. A condenser measuring the same internal diameter with a wall thickness of 3.9 mm and a length of 70 cm was welded onto the opening of the bar. The combination of pipe and bar together formed the heat pipe chamber. An air cooling jacket was welded onto the pipe. The gap in the jacket was about 5 mm. The inside of the pipe was fitted with 2 wraps of 100 mesh SS wick.

The heat pipe was made with a thermocouple well extending to within 2 cm of the bottom of the evaporator chamber. The pipe was charged with 60 g of Thermex and evacuated.

In designing this particular heat pipe, the solid bar was used to increase the thickness of the evaporator. The intention was to operate the heat pipe so that the outer temperature of heat pipe was close to the zinc freezing temperature (420 °C). This would create a temperature gradient in the boundary layer of the liquid zinc. The objective was to cool the zinc in the vicinity of the heat pipe wall to cause impurities to come out of solution without freezing the zinc. This will be explained in a following section.

6.1.2 Testing in a Radiation Furnace

The pipe was first tested in a radiative environment to determine the range of heat fluxes it was capable of handling. In the next set of experiments it was tested in a high heat flux environment that was produced by immersing the evaporator into molten zinc of varying superheat.

The heat pipe was tested vertically in a radiation furnace in the 400 to 750 °C temperature range. In these tests, the entire length of the evaporator was exposed to the radiative flux from the furnace walls. The steady state results for these tests are shown in Figure 6-2 to Figure 6-4. Values for the rate of heat extraction were computed by determining the enthalpy change of the cooling air (equation 5.1). One can see from these results that at a given heat pipe operating temperature, the rate of heat extraction increases as the furnace temperature and the flow rate of cooling air are increased.

Extracted Heat Flow (Coil In)

Extracted Heat Flow (Without Coil)
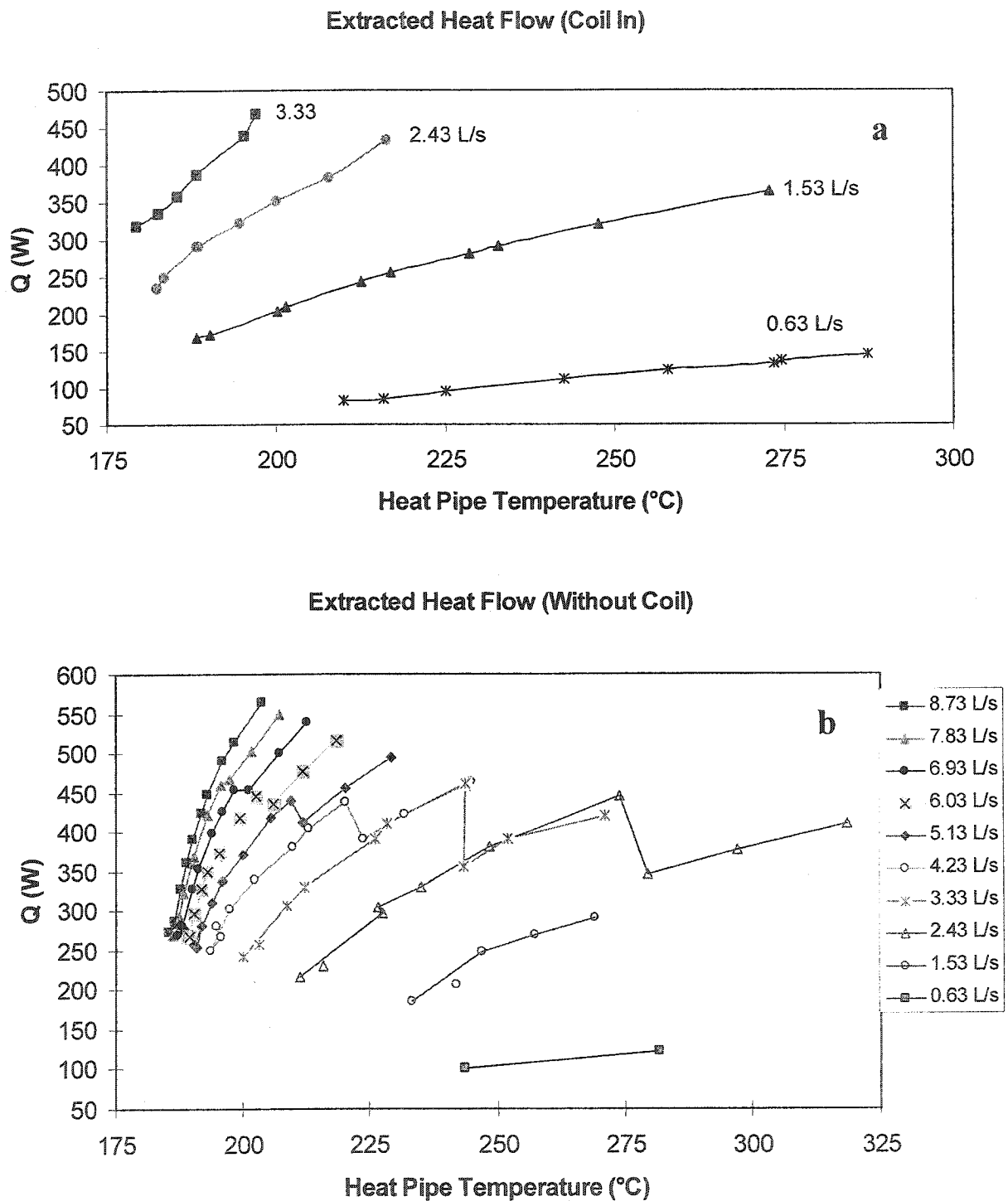
Figure 6-2. The Extracted Heat Flow of Thermex Heat Pipe

Heat Transfer Coefficients (Coil In)

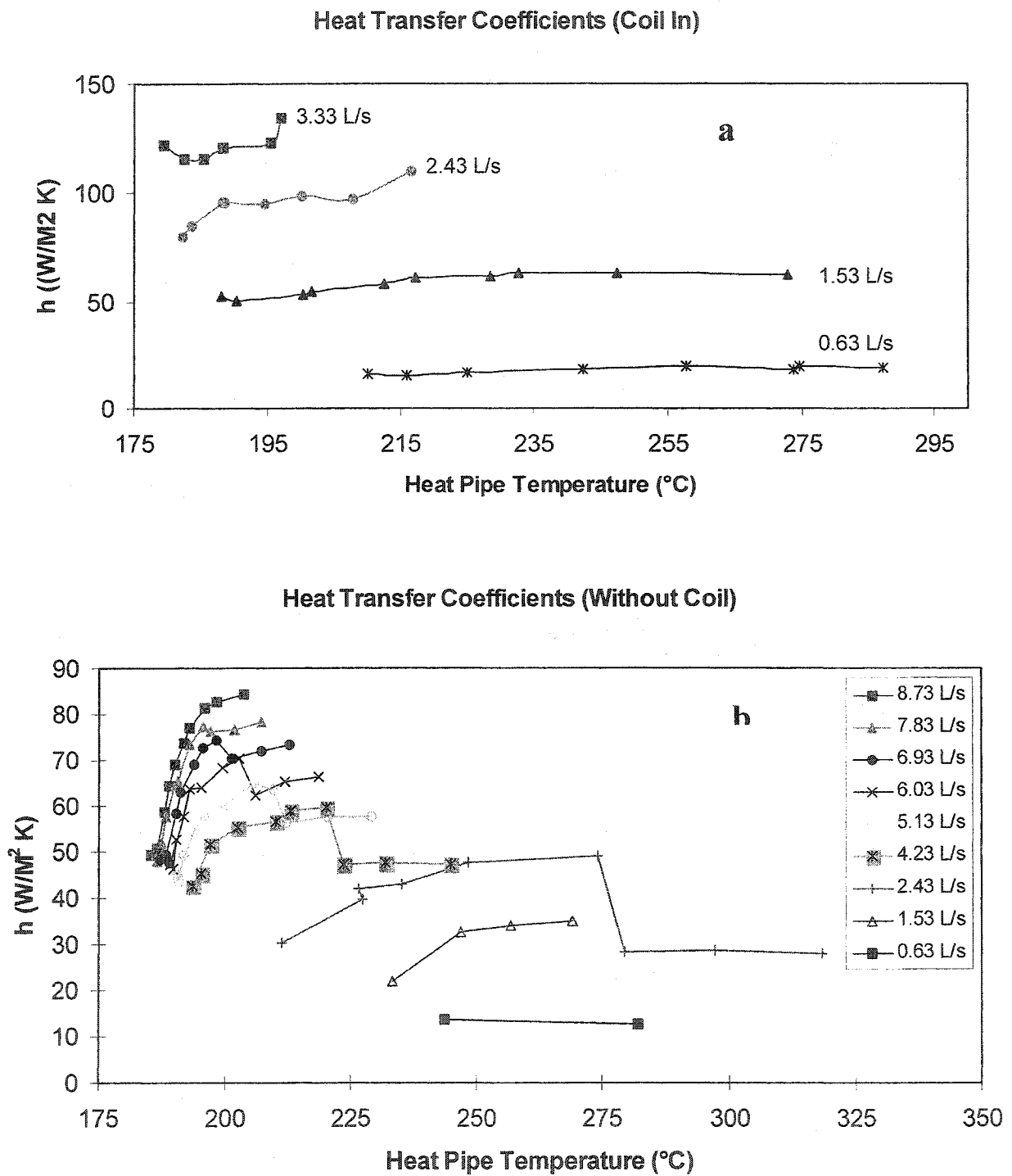**Heat Transfer Coefficients (Without Coil)**

Figure 6-3. Heat Transfer Coefficients in the Cooling Jacket of the Thermex Heat Pipe

Heat Pipe Efficiency (Coil In)

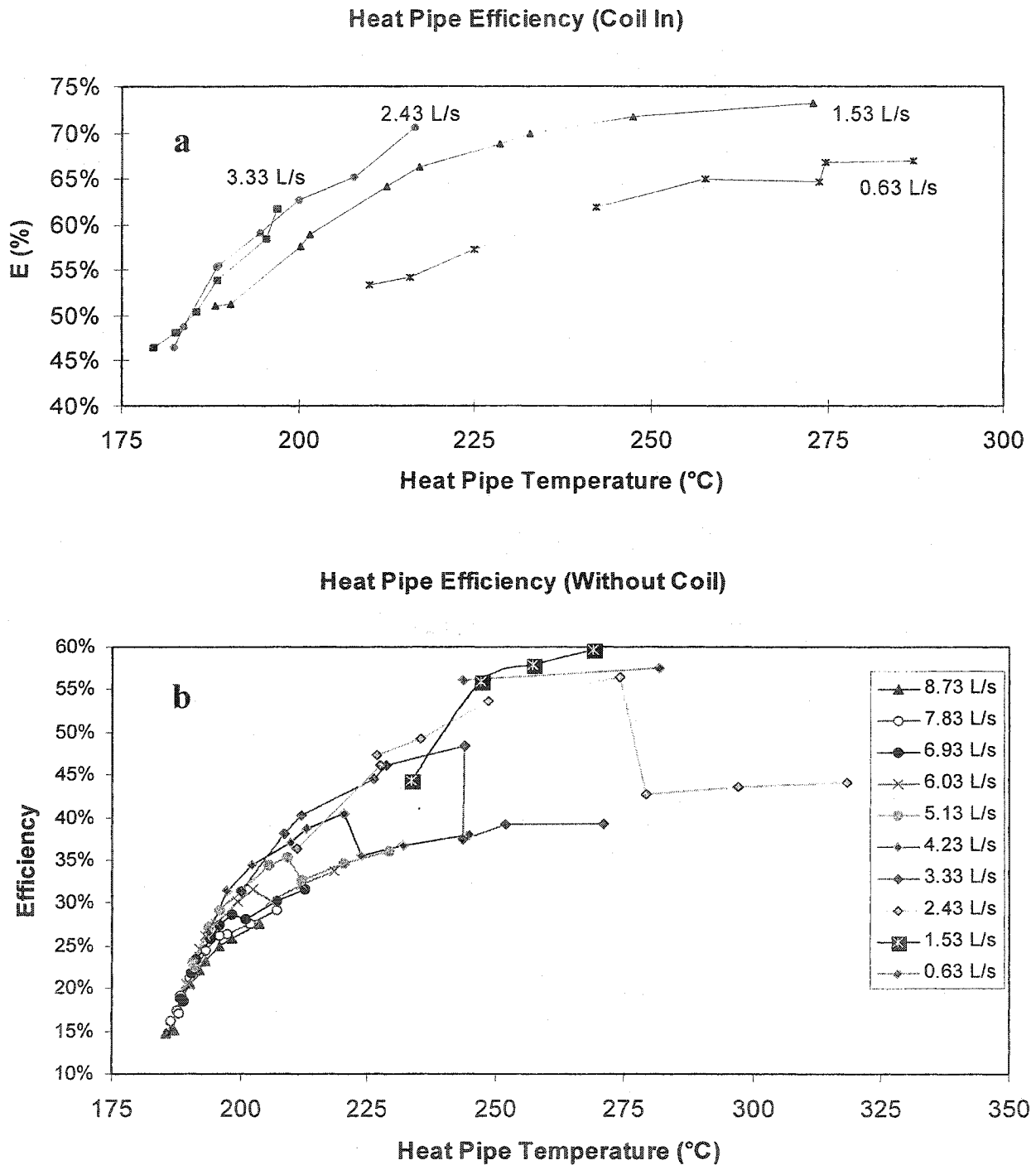## Heat Pipe Efficiency (Without Coil)

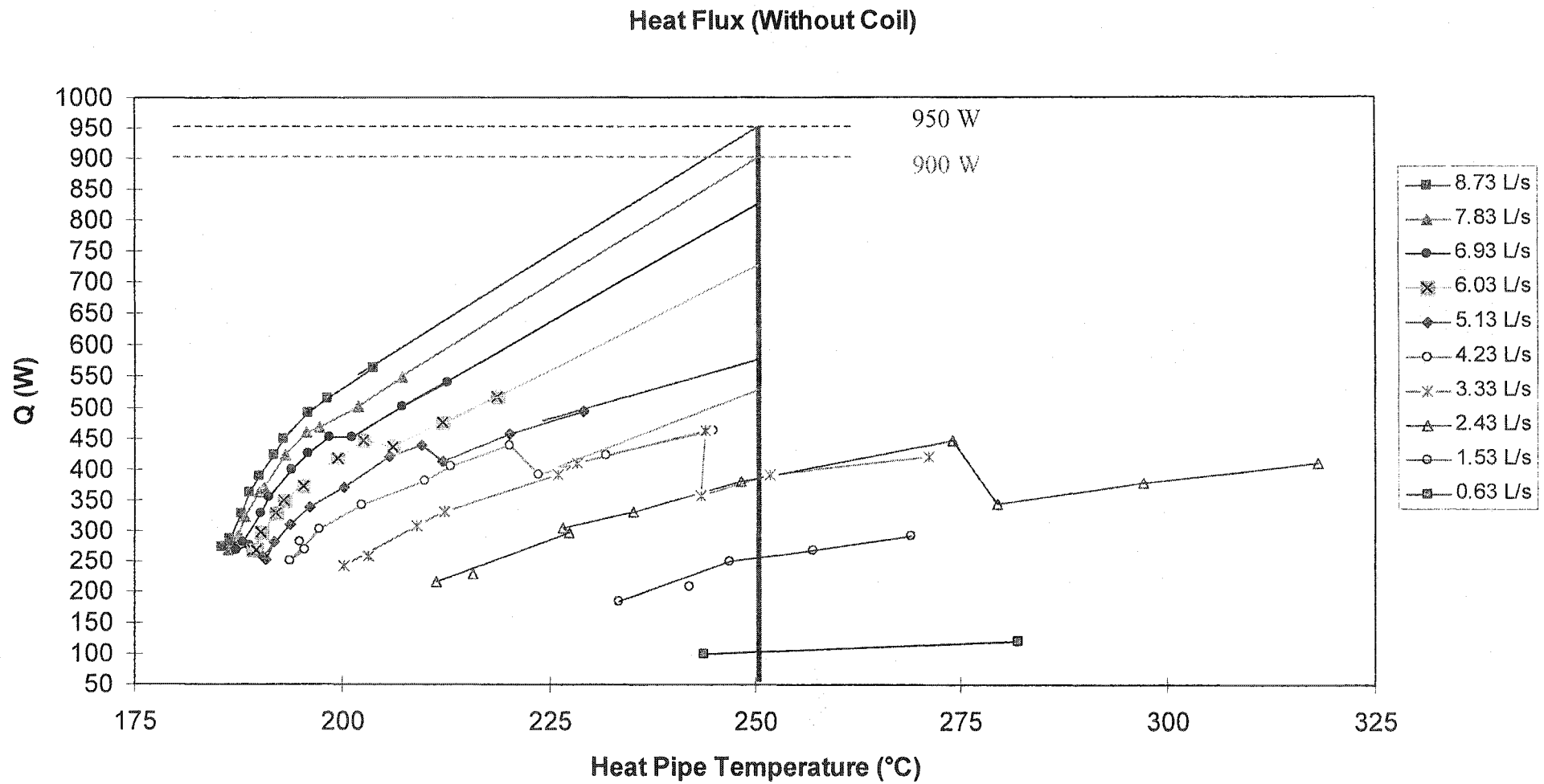Figure 6-4. Heat Pipe Efficiency of the Thermex Heat Pipe

Figure 6-5. The Heat Extraction for the Thermex Heat Pipe at Various Cooling Air Flow Rates

Because of the temperature limit of the radiation furnace, we could not further increase the flow rate of cooling air beyond what is reported. This heat pipe had a copper coil inserted into the gap of the cooling air for some of the tests. As mentioned in the previous chapter, the coil improved the heat transfer of the cooling air. Comparing curves a and b in Figure 6-2 to Figure 6-4, one can see that the conclusion which states that the coil improves heat transfer is reaffirmed.

Figure 6-5 indicates the rate of heat extraction of the heat pipe without the coil. Extrapolating to 250 °C for the heat pipe operating temperature, one finds heat flows of 950W and 900W for air flow rates of 8.37 and 7.83 Nl/s. As was mentioned previously, heat extraction by the heat pipe, when the coil is used is better than the case when no coil is used. In Table 6-3 is shown a comparison of heat extraction for both cases. With these data was drawn the curve in Figure 6-6, which shows the relationship of the ratio of the heat extraction with the coil to without the coil for varying cooling air flow rates. These results were calculated based on the experimental data, shown in Figure 6-2, with the trend lines extending to flows of 8.73 and 7.83 Nl/s of cooling air. From this curve one can read the ratios of $Q_{with\text{-}coil}$ / $Q_{without\text{-}coil}$ as 4.25 and 3.90 for the 2 air flow rates. Therefore, the estimated values of heat extraction for the heat pipe with the coil in place are 950 x 4.25 = 4037.5 W and 900 x 3.90 = 3510 W. These values are very high. Since the area of the outer wall of heat pipe evaporator, which all sits inside the radiation furnace, is 0.0259 m^2, heat fluxes at these points are 15.6 W/cm^2 and 7.8 W/cm^2, respectively. Heat fluxes at the working substance / evaporator wall interface are approximately double these values.

Table 6-3. The Comparison of Extracting Heat at 250 °C of Heat Pipe Temperature

Items	Flow Rate of Cooling Air (Nl/s)			
	3.33	2.43	1.53	0.63
$Q_{without\text{-}coil}$ (W)	385	385	255	105
$Q_{with\text{-}coil}$ (W)	900*	650*	325	125
Ratio = $Q_{with\text{-}coil}$ / $Q_{without\text{-}coil}$	2.21	1.69	1.27	1.14

* estimated value using trend line in Figure 6-2a

Fourier's law of conduction (equation 6.1) is used to calculate the conduction heat transfer through the evaporator wall.

$$Q = \frac{2\pi kL}{\ln\dfrac{r_0}{r_i}}(T_i - T_0) = \frac{2\pi kL}{\ln\dfrac{r_0}{r_0 - \Delta r}}\Delta T \qquad (6.1)$$

Where Q: Rate of heat transferred by conduction (W), 4028 W

K: Thermal conductivity (W/m °C). For stainless steel, 13.4 W/m K.

r_0: outer radius = 25.4 mm. L: Evaporator length=150 mm

ΔT: Temperature gradient (°C). Here $\Delta T = T_{zn} - T_{heatpipe} = 420 - 250 = 170$ K

Δr: Thickness of evaporator wall.
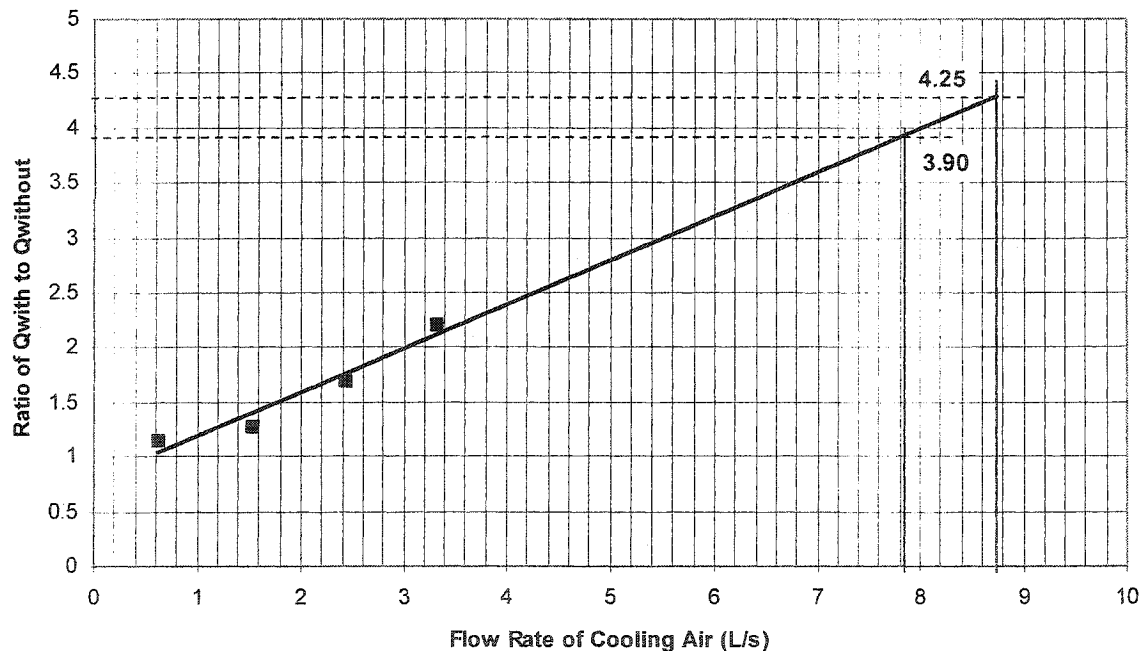
Figure 6-6. The Ration of $Q_{with\text{-}coil}$ to $Q_{without\text{-}coil}$ Vs. Flow Rate of Cooling Air

Substituting these data into the equation 6.1, one obtains that Δr is 10.5 mm. With this thickness of heat pipe wall, one can impose the zinc melting point (420 °C) on one side and the operating temperature of the heat pipe (250 °C on the other side), with a corresponding pressure of 0.88 bar.

In our design, the thickness of evaporator wall was 16 mm instead of the calculated 10.5 mm. This allowed us to work with a lower operating temperature for the heat pipe. In actual fact, the freezing of a zinc layer on the surface of the heat pipe evaporator will be automatic and adjust to the evaporator thickness and will be based on the temperature of the liquid zinc and the operating temperature of the heat pipe.

Throughout the testing temperature range of the radiation furnace (400 - 750 °C), all experimental results clearly indicated that the Thermex heat pipe significantly satisfied the design requirements and worked very well. Therefore, we decided to use this heat pipe to freeze molten zinc at the Noranda Technology Center (NTC).
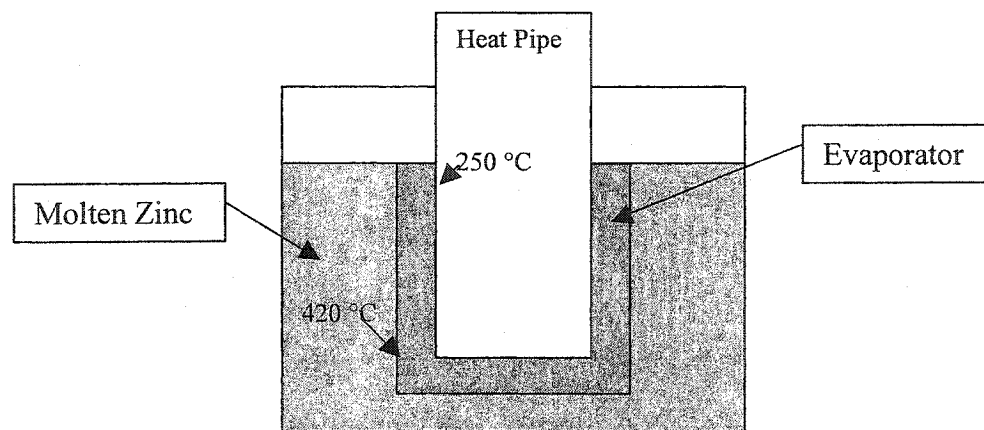
Figure 6-7. The Schematic Diagram of Heat Pipe Immersing Zinc

6.1.3 Testing in Molten Zinc

The NTC experimental setup was similar to the previous setup. The only difference was that the relatively small wire radiation furnace was replaced by a relatively large radiation furnace with Si-Mo bar elements. 50 kg of zinc metal was melted in a container which was placed inside the furnace. The heat pipe was then immersed in the molten zinc until the whole evaporator was immersed in the liquid zinc

(see Figure 6-7). As the heat pipe was heated to its steady state, the testing results were recorded and are shown in Table 6-4.

Table 6-4. Steady State Results for Immersion in Liquid Zinc

Furnace Temperature (°C)	Heat Pipe Temperature (°C)	Flow Rate of Cooling Air (Nl/min)	Air Inlet Temperature (°C)	Air Outlet Temperature (°C)	Calculated rate of Heat Extraction (W)
482	214	118	20	111	230

The value of heat extraction was much less than the estimated or designed value. Even when the experimental conditions, such as the flow rate of cooling air, evaporator length inside the liquid zinc, and so on, were changed, the test results were still much worse than the estimates which had been anticipated based on the tests in the radiation furnace. The heat flows were remarkably low. Something differed between the 2 sets of tests. In an attempt to identify what was limiting the heat transfer, two additional thermocouples were placed in the evaporator wall at 2 mm and 7 mm distance from the outside wall. The evaporator diameter was machined to 46 mm to clean the outer evaporator wall.

The heat pipe was tested again in the same molten zinc bath. The test results are shown in Table 6-5. From this table, the values are very low compared with the experimental values obtained in the radiation furnace.

Actually, some data for the three experimental conditions are presented in Table 6-6. The average values for each experimental condition (a) T_{Zn} = 460 °C, air flow rate = 1.75 Nl/s; b) T_{Zn} = 482 °C, air flow rate = 1.75 Nl/s; c) T_{Zn} = 480 °C, air flow rate = 2.48 Nl/s) were used to draw the curves shown in Figure 6-8.

Figure 6-8 illustrates the comparison of temperature between the measured values of the experiments and the calculated values using equation (6.1) at 2 mm and 7 mm, respectively. It is a clear that the experimental data is lower than the calculated values. These temperature differences ($T_{experiment}$-$T_{calculated}$) at 2 mm and 7 mm are displayed in Figure 6-9. The range of temperature difference is about 2 to 3 °C.

Table 6-5. The Test Results in Liquid Zinc for the Second Trial

Furnace Temperature (°C)	2 mm thermocouple Temperature (°C)	7 mm thermocouple Temperature (°C)	Heat Pipe Temperature (°C)	Flow Rate of Cooling Air (Nl/min)	Air Inlet Temperature (°C)	Air Outlet Temperature (°C)	Calculated Extracting Heat (W)
459.8	456	452.6	214	105	20	115	214
459.8	456	452.9	214	105	20	114	212
482	477	473.8	224	105	20	119	223
482	478	474.7	225	105	20	121	227
483	479	475.5	209	149	20	102	262
480.9	477	473.5	208	149	20	100	255
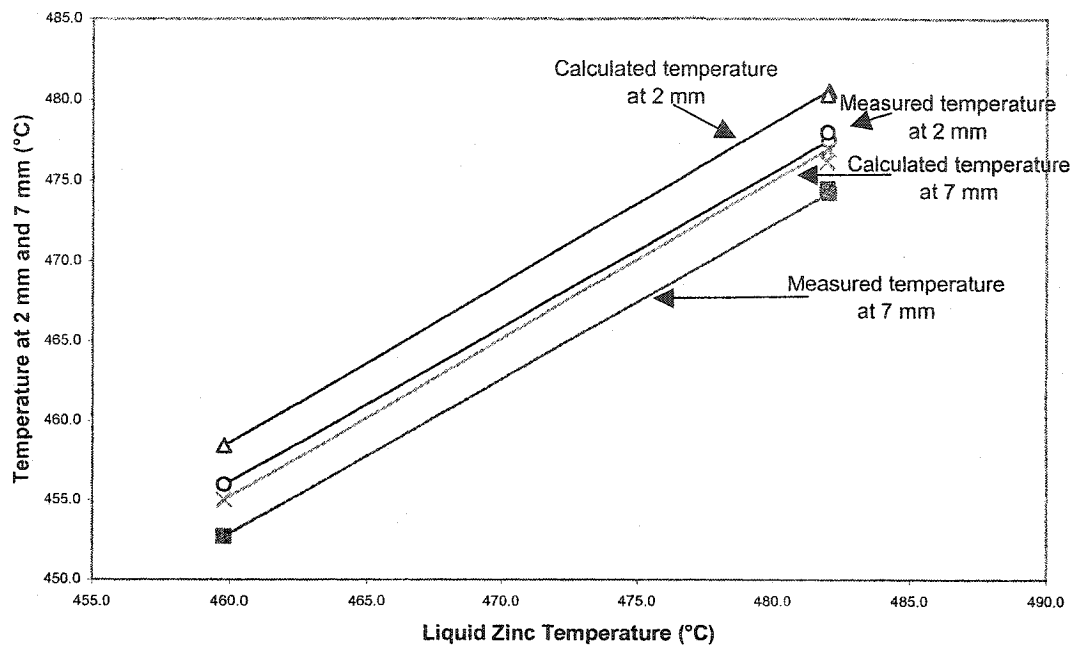
Figure 6-8. Comparison of Temperature at 2 mm and 7 mm

The calculated heat flow, using the measured temperature at 2 mm and 7 mm and liquid zinc temperature by equation (6.1), and the experimental heat flow (equation 5.1) are shown in Figure 6-10. The calculated values are higher than the experimental data. And then, the calculated value at 2 mm is higher than that at 7 mm. From theory, the transferred heat passing across the evaporator wall of the heat pipe is the same at any radial displacement at steady state. Therefore, there must exist a resistance between the inner wall of the heat pipe and the vapor of the working fluid to block the heat transfer.

From Figure 6-10, one finds an interesting phenomenon. For a liquid zinc temperature of 482 °C, the calculated values decreased as the flow rate of cooling air increased. The results are the reverse of the results obtained in the radiation furnace. It is thus worth noting that there exists a resistance in the heat pipe and that it increased as the flow rate of cooling air was increased.

6.1.4 Re-testing in Radiation Furnace

In order to find out what was happening inside the heat pipe, it was brought back to the laboratory, and re-tested in the radiation furnace. Unfortunately, the heat pipe could not be started appropriately. In the low operating temperature range that was used the

Figure 6-9. Temperature Difference between Calculated Data and
Experimental Data

Figure 6-10. Comparison of Transferred Heat between
Calculated and Experimental Values

first time, the whole condenser was now lost. This meant that some gas existed inside the heat pipe. This gas expanded since the vapor pressure is low at a low operating temperature of the heat pipe. Therefore, that made the heat pipe lose the condenser.
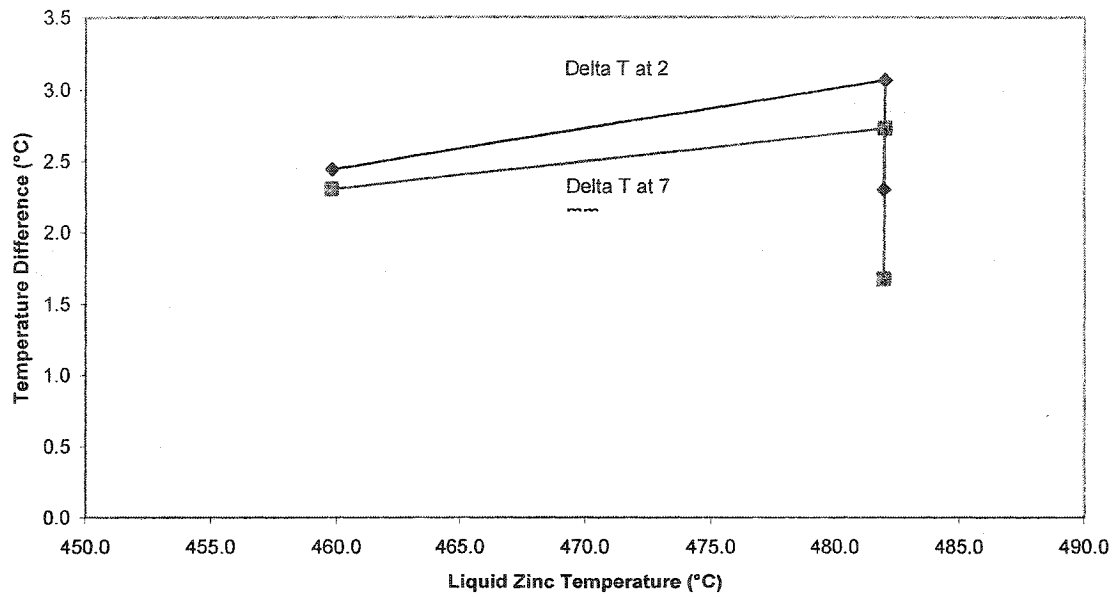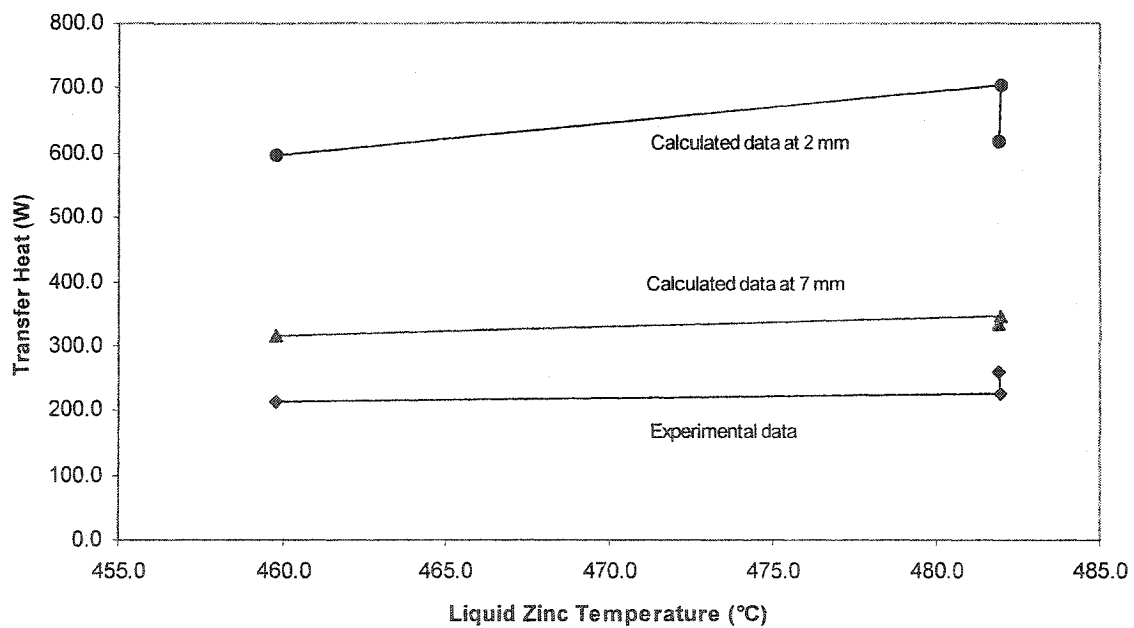
A look at the thermal conductivity shows that thermex has a much lower thermal conductivity (0.113 W/m °C at 250 °C, Table 6-2) compared with liquid zinc (57.7 W/m °C, Table 6-1) and 316L stainless steel (13.4 W/m °C), which would make it susceptible to film boiling. This film with lower thermal conductivity blocked the heat transfer from the heat pipe wall to the liquid. Some part of the evaporator dried out due to high heat flux. The working fluid--Thermex decomposed and generated the gas, which made the heat pipe fail due to losing the condenser, since Thermex is an organic. Heat extraction by the heat pipe is reduced as the condenser of the heat pipe shrinks. Therefore, in order to overcome the decomposition of working fluid, it was decided to use water to replace the organic Thermex. 100 grams of water was used as working fluid in the same heat pipe. This water quantity is higher than the regular design quantity. Nonetheless an excess was deemed appropriate to avoid drying out of the evaporator. This heat pipe was tested again in the radiation furnace. After testing in the radiation furnace, it also was tested in liquid zinc at NTC. Both testing conditions and results are shown in Table 6-6. Items 1 and 2 are results for the radiation furnace tests, while items 3 to 5 are the experimental results for the tests in liquid zinc at NTC.

Table 6-6. Testing Results of Water Heat Pipe in Radiation Furnace and Liquid Zinc

No	Furnace / Liquid Zinc T (°C)	Heat Pipe T (°C)	Air Inlet T (°C)	Air outlet T (°C)	Flow Rate (Nl/s)	Extracted Heat Q (W)
1	634	103.65	20	84	11.61	955.3
2	658	108.76	20	88	11.61	1015.0
3	461	84	20	64	8.08	457.3
4	459	117	20	91	5.28	482.3
5	457	161	20	124	4.63	619.5

Comparing both sets of test results, it is obvious that values obtained in the radiation furnace are much higher than the values obtained in the liquid zinc. It is the reverse of what would typically be expected. The heat flow from the zinc should have been substantially higher than the heat flow obtained in the radiation furnace.

The results of items 3 to 5 in Table 6-6 were obtained while the heat pipe was tested in liquid zinc. These values clearly illustrate that the rate of heat extraction of the heat pipe decreased as the air flow rate increased. This was not expected for us, and it goes against the results from the radiation furnace, which we have shown in Chapter 5. Therefore, it would appear that the higher heat flux of the liquid zinc caused the heat transfer inside the heat pipe to change. It is quite different from the heat transfer when the pipe is in the radiation furnace. Because water was used as the working fluid in the heat pipe, it is clear that there is no decomposed gas, like happened with organic thermex, to reduce the heat extraction. Thus, there must be a thermal resistance between the inner wall of the heat pipe and the working fluid to resist the vaporization of the working fluid. The resistance appears for the high heat flux case. After assessing the results, we concluded that film boiling inside the heat pipe was responsible for the phenomenon we observed.

6.2 Film Boiling Problem

6.2.1 Introduction

Boiling heat transfer occurs when a liquid with a saturation temperature, T_{sat}, contacts a surface with an interfacial temperature, T_w. The saturation temperature of the liquid is the equilibrium temperature at which the fluid develops a vapor pressure that equals the pressure of the system. Numerical values can be determined from the well-known pressure-temperature correlation referred to as the Clausius-Clapeyron equation.

For instance, water exposed to atmospheric pressure may boil at approximately 100 °C. Boiling occurs when the heat flow into the liquid cannot be completely transported to a free surface. In this case vapor forms at the interface and turns into bubbles--hence boiling. When the rate of vapor generation is high enough, a stable film of vapor appears between the liquid and the solid surface. Heat transfer then occurs mainly by radiation across the gap (i.e. film). This mode of heat transfer is termed film

boiling and typically can be as little as 10% of the heat extraction for fully developed nucleate boiling.

Usually, boiling heat transfer can be divided into several stages: from convection boiling, nucleate boiling, partial film boiling, and film boiling. Boiling heat transfer data is normally shown plotted as the logarithm of the heat flux to the surface against the logarithm of the temperature difference, T_w-T_{sat}. This excess temperature differential represents the driving force for boiling. If the wall temperature is less than the saturation temperature, boiling will not occur. However, if the wall temperature exceeds the saturation temperature of the liquid by a sufficient amount, boiling heat transfer will be dominant. A typical boiling curve is shown in Figure 6-11[2]. And Figure 6-12 [5] is a magnification from the right bottom corner of Figure 6-11.

To fully appreciate the boiling phenomenon, one must be aware of the regimes that comprise the boiling curve. Consider the lower boiling curve shown in Figure 6-12 and denoted by the label, 'natural convection'. Up until point B, the excess temperature differential does not lead to the formation of vapor bubbles. Natural convection within the liquid is sufficient to move heat from the wall to the bulk of the liquid. At point B, vapor bubbles begin to nucleate on the surface. As the wall temperature is increased, the rate of bubble nucleation increases as does the heat flux from the surface. This regime, as denoted by the labels B-C, is referred to as the nucleate boiling regime. At point C, the maximum heat flux for nucleate boiling is reached. This is referred to as the critical heat flux (CHF). At the CHF, the wall temperature exceeds the saturation temperature by a fixed amount. If the wall temperature is increased, the heat flux from the wall surface decreases until point D is reached. The reason for the declining heat flux is the formation of a vapor film over the surface area of the wall. This film acts as a heat transfer barrier and prevents the liquid from contacting the wall. This phenomenon occurs as a progressive event in that the greater is the wall temperature, the greater is the coverage of the wall by the film and the more stable the film becomes. This regime, as delineated by the labels C-D, is referred to as partial film boiling.

At point D, coverage of the surface by the film is complete and heat transfer by film boiling becomes dominant. The film boiling regime extends from point D to point E. The reason why heat transfer increases in this region relates to the fact that radiation

across the vapor film dominates. Given that radiative heat transfer increases by the fourth power of temperature, the heat flux from the wall increases in the film boiling regime. The set of curves in the upper left hand quadrant of Figure 6-11 correspond to the boiling curves for forced convection systems wherein the liquid flows over the wall surface. As the bulk velocity of the liquid is increased, the boiling curve is shifted upward. Thus, increasing velocities allow for greater heat extraction for a given excess temperature, T_w-T_{sat}. In addition, the forced convection set of curves is for a constant pressure. If the pressure is increased, then T_{sat} also increases. As a result, one can operate in the nucleate boiling regime at higher wall temperatures without experiencing film boiling with higher system pressures.

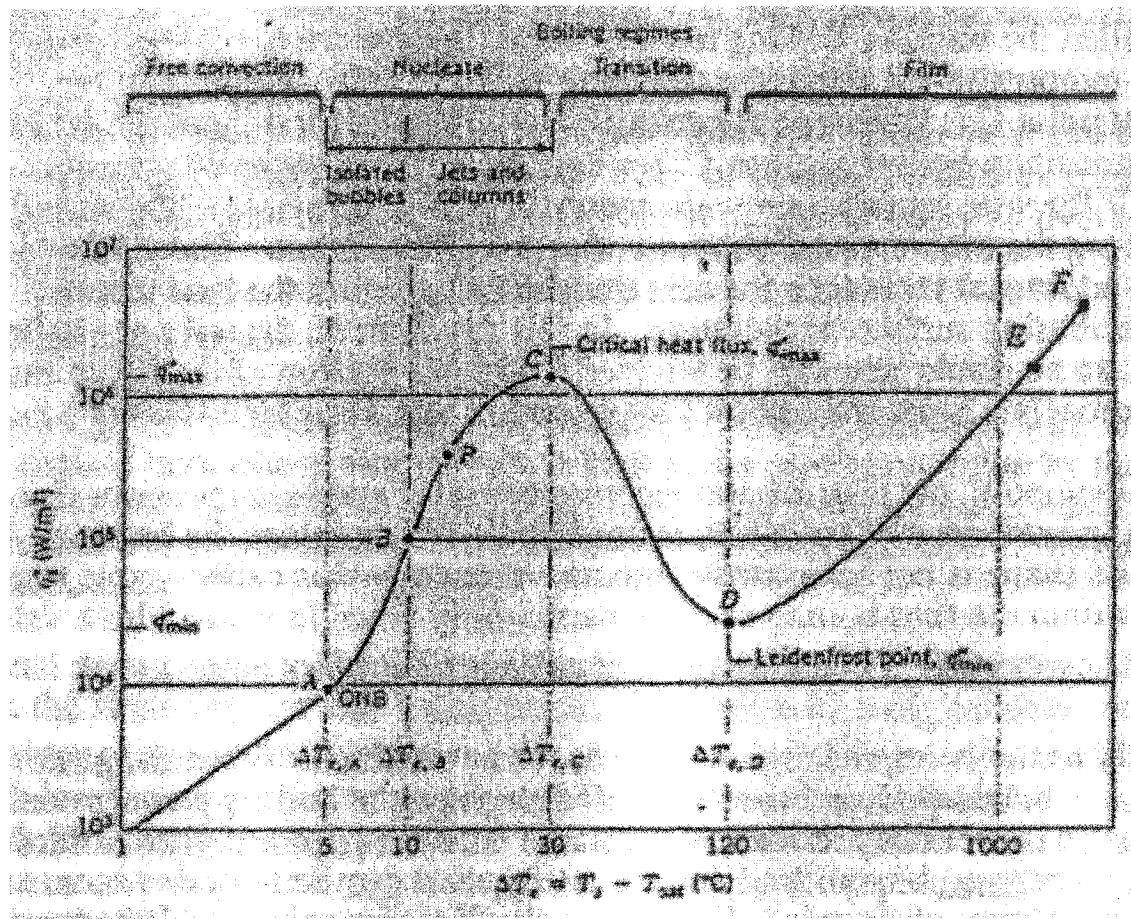Figure 6-11. Typical Boiling Curves for Natural and Forced Convection.

Figure 6-12. Typical Boiling Curve for Water at One Atmosphere: Surface
Heat Flux q"s as a Function of excess Temperature, $\Delta T \equiv Ts - Tsat$

As an illustration of natural convection boiling heat transfer, Figure 6-13 presents
the boiling curve for water on a horizontal, electrically heated wire [2]. Also shown are the
corresponding heat transfer coefficients. Boiling is sensitive to configuration and as such
these results are only included to illustrate how the regimes of boiling interact with each
other.

Water cooling dominates many metallurgical processes. When heat fluxes are
relatively large, it is important to prevent film boiling by imposing water velocities and
pressures that correspond to nucleate boiling for the system. Otherwise, if a portion of the
system experiences film boiling, the wall in that region will be subjected to dramatic
increases in temperature and may ultimately fail. Classical metallurgical examples where
water cooling predominates are the continuous casting of steel, the DC casting of

aluminum, and rolling in general. The pictures, shown in Figure 6-14, clearly show the film boiling phenomenon in the casting of copper anodes.
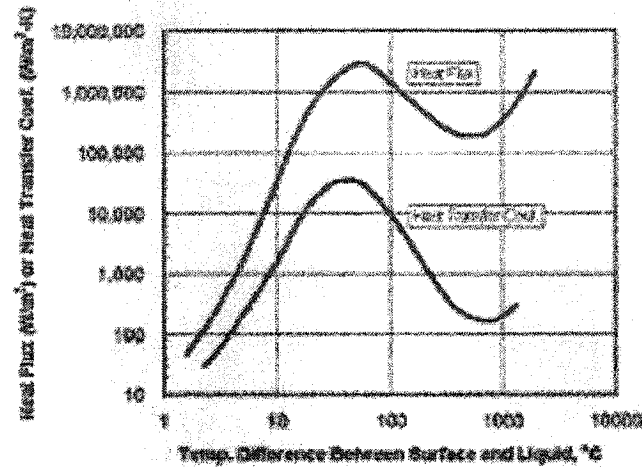
Figure 6-13. Boiling Curve for Water on a Heated Wire.

6.2.2 The Minimum Film Boiling Point

Once the critical heat flux is exceeded, the heater surface is blanketed by a continuous vapor film, i.e., film boiling. Under this condition one must find the heat transfer resistance of this vapor film as well as consider the additional effect of radiation heat transfer at very high heater surface temperatures through this vapor film. Bromley [3] used the approach first developed by Nusselt for film condensation to predict the film boiling heat transfer coefficient for a horizontal tube.

Film Boiling

Figure 6-14. Film Boiling in Casting of Copper Anodes

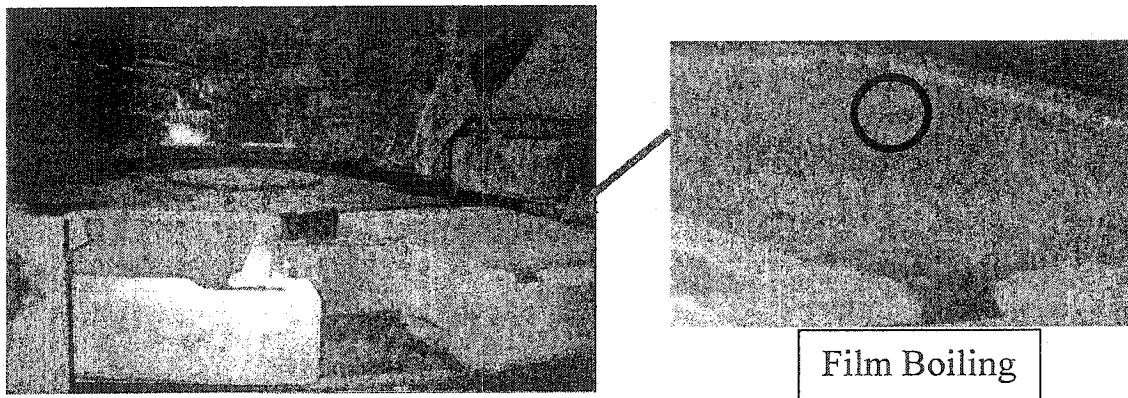$$h_{fb} = 0.62 \left[\frac{k_g^3 \rho_g \Delta \rho g}{D \mu_g \Delta T} \left(h_{fg} + 0.4 C_{pg} \Delta T \right) \right]^{\frac{1}{4}} \qquad (6.2)$$

where ΔT is the difference in temperature between the heater wall and the saturation temperature. Bromley also considered the film boiling heat transfer coefficient for a vertical wall.

This simplest of solutions is obtained assuming the vapor film is laminar and that the temperature distribution through the film is linear. For a vertical flat surface various boundary conditions may be imposed:

(1) zero interfacial shear stress ($\tau_i = 0$)

(2) zero interfacial velocity ($u_i = 0$)

(3) zero wall shear stress ($\tau_w = 0$)

For the first of these boundary conditions, the local heat transfer coefficient $h(z)$ at a distance z up the surface from the start of film boiling is given by

$$\frac{h(z)z}{k_g} = \left[\frac{z^3 g \rho_g (\rho_f - \rho_g) h_{fg}}{4 k_g \mu_g \Delta T} \right]^{\frac{1}{4}} \qquad (6.3)$$

The average coefficient $h(z)$ over the region up to a distance z is given by:

$$\frac{h(z)z}{k_g} = 0.943 \left[\frac{z^3 g \rho_g (\rho_f - \rho_g) h_{fg}}{k_g \mu_g \Delta T} \right]^{\frac{1}{4}} \qquad (6.4)$$

If one defines

$$P_r^* = \frac{\mu_g h_{fg}}{k_g \Delta T} \quad \text{And} \quad G_r^* = \left[\frac{z^3 g \rho_g (\rho_f - \rho_g)}{\mu_g^2} \right] \qquad (6.5)$$

$$Nu_z = \frac{h(z)z}{k_g} \qquad (6.6)$$

then
$$Nu_z = CP_r^* G_r^{*1/4}$$
(6.7)

Where: h_{fg} = latent heat

ρ_g = density of saturated vapor

ρ_f = density of saturated liquid

σ = surface tension

g = gravitational acceleration

μ = viscosity

k = conductivity

Note the analogy with natural convection. The values of C for the first of the above boundary conditions is 0.943 and for the second is 0.667. This thin vapor film over a horizontal surface is unstable and large bubbles form and break away. The characteristic spacing of these bubbles (λ_c) is determined by a balance of surface tension and gravitational forces and is given by:

$$\frac{\lambda_c}{2\pi} = \left[\frac{\sigma}{g(\rho_f - \rho_g)} \right]^{1/2}$$
(6.8)

where one substitutes this length scale, (λ_c), for the tube diameter or wall length.

The final point to discuss is what happens if one decreases the heat flux while in film boiling. Once the continuous vapor film is formed it is hydro-dynamically stable even if the heat flux decreases below the critical heat flux. In fact, this hysteresis effect persists until the heat flux decreases to a point where the superficial velocity of the vapor formed at the heater surface is too low to "levitate" the liquid above the "continuous" film. In fact, the film oscillates substantially and this physical picture may only be qualitatively correct. Zuber [4] developed the expression for the minimum film boiling heat flux based on the concept of minimum superficial vapor velocity in a saturated pool and resulted in

$$q''_{MFB} = C\rho_g h_{fg} \left(\frac{g\Delta\rho\sigma}{(\rho_f + \rho_g)^2} \right)^{1/4}$$
(6.9)

164

The constant, C = 0.09, has been experimentally determined by Berenson [5]. This result is accurate to approximately 50% for most fluids at moderate pressures but provides poorer estimates at higher pressures. A similar result has been obtained for horizontal cylinders [4].

Notice that this expression is similar in form to the CHF model except the density in the velocity term is the liquid density and comes about from a force balance on vapor bubbles leaving the interface. This minimum film boiling heat flux can be combined with the heat transfer coefficient to predict the minimum film boiling ΔT_{MFB} for a saturated liquid pool. Note that once again it is the intersection of a horizontal stability line and the film boiling regime.

6.2.3 Film Pool Boiling [5]

At excess temperatures beyond the Leidenfrost point, a continuous vapor film blankets the surface and there is no contact between the liquid phase and the surface. Because this condition of a stable vapor film bears a strong resemblance to that of laminar film condensation, it is customary to base the film boiling correlation on the results obtained from condensation theory. One such result, which applies to film boiling on a cylinder or sphere of diameter D, equation 6.4, is rewritten to:

$$\overline{Nu}_D = \frac{\overline{h}_{conv}D}{k_g} = C\left[\frac{g(\rho_f - \rho_g)h'_{fg}D^3}{u_g k_g (T_w - T_{sat})}\right]^{1/4} \qquad (6.10)$$

The correlation constant C is 0.62 for a horizontal cylinder and 0.67 for a sphere. The corrected latent heat h'_{fg} accounts for the sensible energy required to maintain temperatures within the vapor blanket above the saturation temperature. Thus, it may be approximated as:

$$h'_{fg} = h_{fg} + 0.80 C_{p,g}(T_w - T_{sat}) \qquad (6.11)$$

It is known to depend weakly on the Prandtl number of the vapor. Vapor properties are evaluated at the film temperature, $T_f = (T_w + T_{sat})/2$, and the liquid density is evaluated at the saturation temperature.

At an elevated surface temperature ($T_w \geq 300$ °C), radiation heat transfer across the vapor film becomes significant. Since radiation acts to increase the film thickness, it is not reasonable to assume that the radiative and convective processes are simply additive. Bromley [3] investigated film boiling from the outer surface of horizontal tubes and suggested calculating the total heat transfer coefficient from a transcendental equation of the form

$$\bar{h}^{4/3} = \bar{h}_{conv}^{4/3} + \bar{h}_{rad}\bar{h}^{1/3} \tag{6.12a}$$

If $\quad \bar{h}_{rad} < \bar{h}_{conv} \quad$, a simpler form may be used

$$\bar{h} = \bar{h}_{conv} + \frac{3}{4}\bar{h}_{rad} \tag{6.12b}$$

The effective radiation coefficient is expressed as

$$\bar{h}_{rad} = \frac{\varepsilon\sigma(T_w^4 - T_{sat}^4)}{T_w - T_{sat}} \tag{6.13}$$

Where ε is the emissivity of the solid and σ is the Stefan-Boltzmann constant.

Note that the analogy between film boiling and film condensation does not hold for a small surface with high curvature because of the large disparity between vapor and liquid film thickness for the two processes. The analogy is also questionable for a vertical surface although satisfactory predictions have been obtained for liquid conditions.

6.2.4 Analysis of Experimental Data

With a steady state situation, the heat passing through the evaporator wall must be constant. According to the conduction heat transfer equation (6.1), the inner wall can be analyzed by following equation:

$$\Delta T_2 = \frac{\ln\dfrac{r_0}{r_0 - \Delta r_2}}{\ln\dfrac{r_0}{r_0 - \Delta r_1}} \Delta T_1 \tag{6.14}$$

Where $\Delta T_2 = T_{Zn} - T_w$

$\Delta T_1 = T_{Zn} - T_{2mm}$

Δr_2 = thickness of evaporator, 13.7 mm

Δr_1 = distance from surface, 2 mm

r_0 = outer radius, 25.4 mm

Table 6-7. The Calculated Results Based on Experimental Data

Liquid Zn T (°C)	At 2 mm T (°C)	ΔT_1 (°C)	ΔT_2 (°C)	T_w (°C)	Heat Pipe T (°C)	ΔT_e
461	454.7	6.3	43.2	417.8	84	333.8
459	452.1	6.9	47.3	411.7	117	294.7
457	448.6	8.4	57.6	399.4	161	238.4

The calculated results are listed in Table 6-7. Here, excess temperature $\Delta T_e \equiv T_w - T_{sat}$, where the temperature of the saturated vapor (T_{sat}) is the operating temperature of the heat pipe. According to the boiling curve of Figure 6-12, film pool boiling conditions are exceeded. Therefore, these points are located in range of the Leidenfrost point (q''_{min}).

Heat is transferred from the solid surface to the liquid, and the appropriate form of Newton's law of cooling is [5]:

$$q''_w = h(T_w - T_{sat}) = h\Delta T_e \qquad (6.15)$$

Written on a transferred heat rate for a cylindrical surface of Leidenfrost point D.

$$q_w = q''_w A_2 = \bar{h} A_2 \Delta T_e \qquad (6.16)$$

The heat transfer coefficient h is calculated from 6.12a or b while the convection and radiation heat transfer coefficients follow from equation 6.10 and 6.13, respectively. For the convection coefficient:

$$\bar{h}_{conv} = 0.64 \left[\frac{k_g^3 \rho_g (\rho_f - \rho_g) g (h_{fg} + 0.8 c_{p,g} \Delta T_e)}{\mu_g D \Delta T_e} \right]^{1/4} \qquad (6.17)$$

Here

$$D = \lambda_c = 2\pi \sqrt{\frac{\sigma}{g(\rho_f - \rho_g)}}$$

167

Since the average $h_{conv} > h_{rad}$, equation 6.12b was used to calculate average h. The results are shown in Figure 6-15 and Figure 6-16. Figure 6-15 presents the average heat transfer coefficient vs the temperature of the heat pipe while Figure 6-16 is the heat flux and heat flow vs temperature of the heat pipe. Comparing these data with heat extraction data in Table 6-6 (items 3, 4, 5) as obtained from experimental data, the experimental values are almost double the calculated values for film boiling. This is reasonable. Since there was a wick inside the heat pipe, it may have not allowed the whole evaporator to be located in the film boiling range due to wick capillary force. It caused some areas to be in nucleate boiling or free convection boiling. Therefore, the experimental data is higher than the data calculated from film boiling. The main area of film boiling should be the bottom area of the heat pipe evaporator. Shown in Figure 6-17 is the evolution of film boiling formation. In Figure 6-17a, the liquid spreads on the whole surface area of the evaporator. When heat was applied with a high heat flux, the vapor bubbles formed and grew under the liquid (film boiling) to block the heat transfer directly from the wall to the liquid, as in Figure 6-17b, c and d. Each bubble separated from the film after it grew enough (Figure 6-17e). Once the first bubble left the film, a second one was formed, as shown in Figure 6-17f.

These processes continuously repeat to keep the vapor film on the bottom surface of the heat pipe evaporator. The vapor film prevented the liquid from touching the bottom of the evaporator. This phenomenon has been observed in our experiments, which will be discussed in the next chapter. Therefore, it is necessary to study film boiling in a heat pipe and to determine a method to improve heat transfer inside the heat pipe, so as to increase heat pipe efficiency.
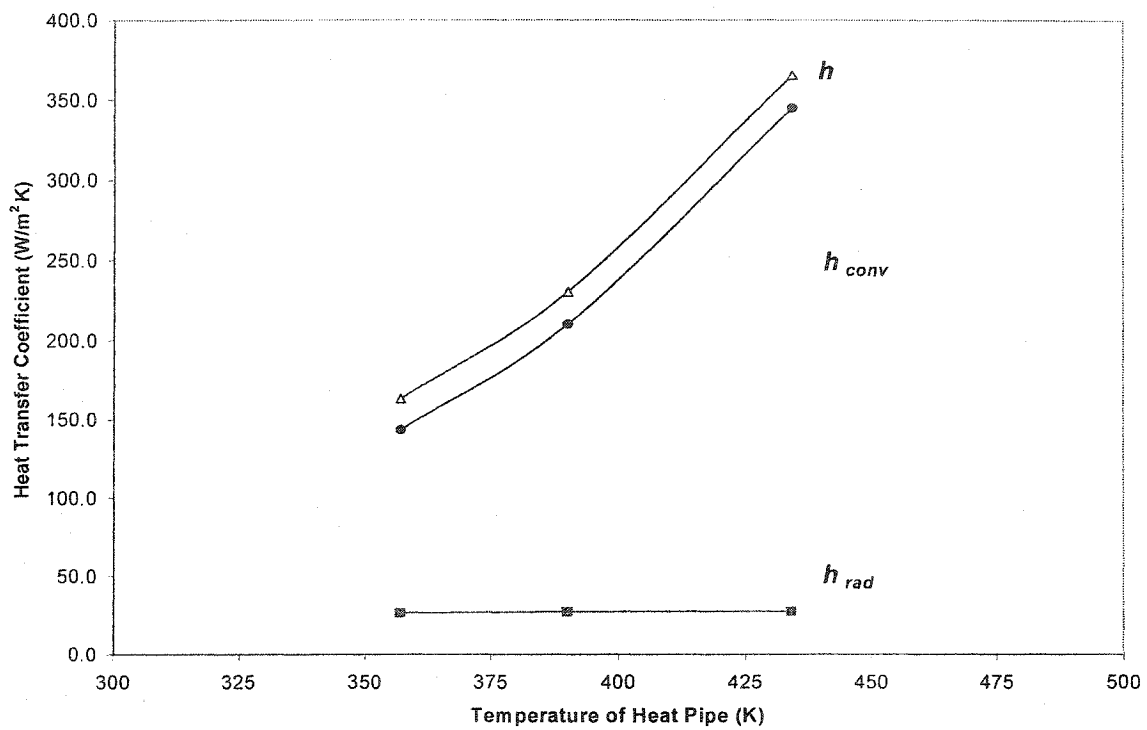
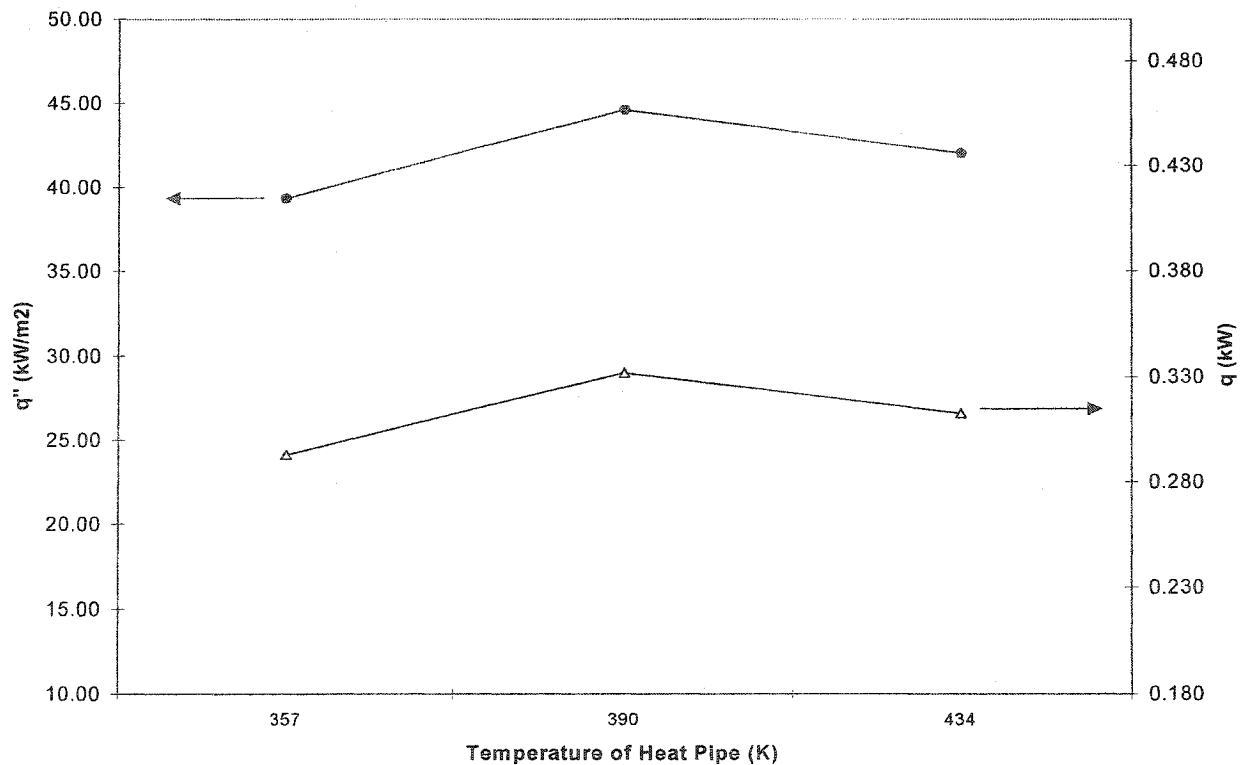Figure 6-15. Heat Transfer Coefficient Vs Temperature of Heat pipe

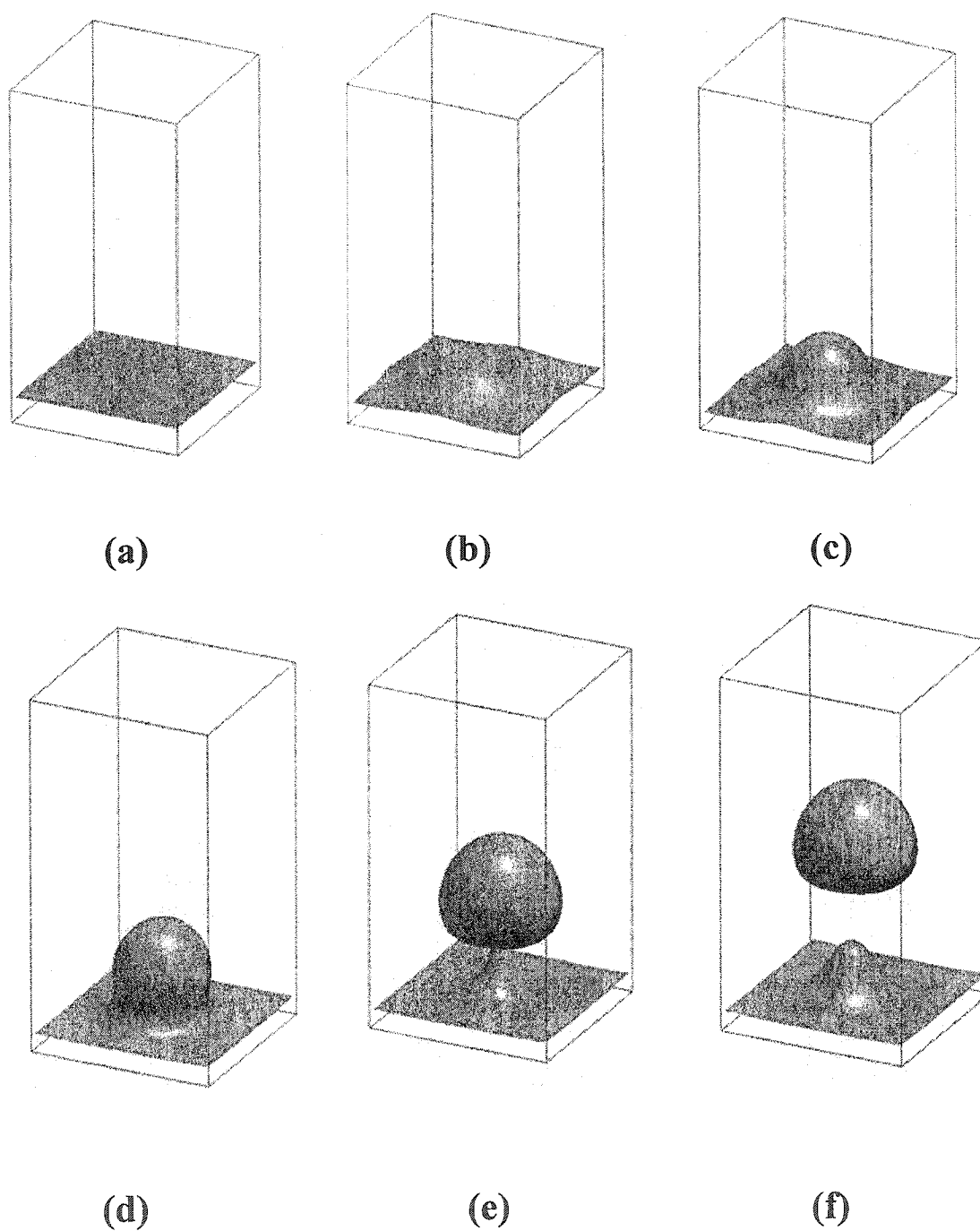Figure 6-16. Heat Flow and Heat Flux Vs. Temperature of Heat Pipe

169

(a)   **(b)**   **(c)**

(d)   **(e)**   **(f)**

Figure 6-17. The Process of Film Boiling inside a Heat Pipe

CHAPTER 7. FLOW MODIFIED HEAT PIPE

The vast majority of experimental work performed to date regarding film boiling has utilized conventional heat pipes that were large compared to individual bubble sizes, making it difficult to look at details of the boiling process. These experiments usually used a simple heat pipe structure operated in a constant heat flux mode, making it difficult to study transition boiling effects beyond the critical heat flux. Other experiments have utilized surfaces held in open systems. Even when local measurements were obtained, the local heat flux and temperature were not comparable with heat pipe systems.

It must be remembered that boiling behavior on small heat pipe areas can differ from that on open system heated areas. First, the total number of nucleation sites is much smaller due to the heat pipe itself. This can result in heat transfer which is smaller than the corresponding average distance between nucleation sites on open system heaters. Boiling can be delayed because of higher wall superheats or the number of nucleation sites may not be statistically representative. Second, the Taylor wavelength, which is significant at the CHF and the transition to film boiling, can be larger than the heat pipe size. Third, edge-effects can become significant.

Enhancement of the boiling heat transfer mechanism is being widely pursued because of its importance in the design of compact and high performance heat pipes.

Therefore, as presented in Chapter 6, film boiling has become a significant barrier to heat transfer in a heat pipe. It is necessary to develop a technique to overcome this obstacle. This chapter will show the technique we developed to overcome film boiling. And, the results from an experimental and theoretical study will also be presented.

7.1 Introduction [1, 2, 3, 4, 5, 6]

Many different techniques have been considered for increasing the rate of heat transfer in forced convection while reducing the size of the pipe and efficiency. However, many of these have not been used in heat pipes. One focus of our work was to incorporate heat transfer knowledge into heat pipe technology. These techniques for enhancing heat transfer can be divided into two main groups: passive techniques and active techniques.

Passive techniques, which do not need additional external power, include the use of treated surfaces, rough surfaces, extended surfaces, displaced enhancement devices, swirl flow devices and additives for liquids and gases. Active techniques, which require an extra external power source, include mechanical aids, surface vibration, fluid vibration, electrostatic fields, injection or suction of fluid and jet impingement.

Since swirl flow is one of the widely used methods for enhancing boiling heat transfer and increasing the critical heat flux inside tubes, swirl flow devices form an important group of passive augmentation techniques.

Swirl flow in pipes may be classified into two essential types: continuous swirl flow and decaying swirl flow. In continuous swirl flow, the swirling motion persists over the whole length of the duct, while in decaying swirl flow, the swirl is generated at the entry section of the duct and decays along the flow path. Continuous swirl flow in a duct is generated by inserting coiled wires, twisted tapes, helical vanes, or by making helical grooves in the inner surface of the duct.

Gupta et al. classified the methods of generating swirl into three main categories: (i) tangential entry, (ii) guide vanes and (iii) direct rotation. Tangential entry of the fluid into a duct stream can be achieved by a single tangential entry, tangential inlet duct (circular or rectangular at different angles to the pipe axis) or more than one tangential entry, tangential inlet nozzles, tangential machined slots and tangentially drilled slots. Generally, tangential entry swirl generators have been used as a combination of axial plus tangential entry. With these types of swirlers, the degree of swirl can be controlled by adjusting the proportion of fluid admitted by the axial and tangential fluid inlets. Guided vane swirl generators may be grouped into two types: radial guide vane and axial guide vane. Axial guide vane swirl generators consist of a set of vanes fixed at a certain angle to the axial direction of the duct, which give a swirling motion to the fluid. Generally, the vanes are mounted on a central hub, and they occupy space in an annular region. Even one single helical vane or twisted tape can be used as a means of generating decaying swirl flow. Radial guide vane swirl generators are generally mounted between two disks, and the vanes are constructed to be adjustable to obtain the desired initial degree of swirl. Since tangential entry into a duct generates a highly unsymmetrical swirl motion about

the axis and since the pressure drop requirements of tangential swirl generators are relatively high, commercial burners tend to adopt the guided vane system.

Swirl flow improves heat transfer not only by increasing overall flow turbulence, but also by promoting the exchange of fluid between the bulk flow and the flow near the wall. However, the removal of scale from wall protrusions requires special cleaning methods. The twisted tape inserts can be designed for easy removal and the empty tubes cleaned by more conventional methods. Thus, the twisted tape is one of the most important members of this group.

Actually, twisted tape inserts have been used to enhance heat transfer since the 19th century. Marine steam boilers were fitted with "retarders" (twisted tapes) to reduce coal consumption. Research began to appear in the literature around this time. In one of the first studies, Whitham showed that twisted-tapes resulted in a 18.4% fuel saving for a coal-fired, horizontal, tube boiler of a Philadelphia railway station. In a more recent study, Marner and Bergles reported 300% enhancements over the heat transfer of empty tubes for single phase flow with twisted-tape inserts. In the time between the Witham (1896) and the Marner and Bergles (1978) publications, 90 manuscripts were published on the enhancement of single phase convection with swirl flow devices. As of 1995, the number of publications on the subject had grown to 261. Over the years, the vibrant interest in the study of twisted tapes for heat transfer augmentation has been sustained by its affordability and its suitability for retrofitting existing shell-and-tube heat exchangers.

The flow enhancement of the twisted tape arises primarily from increased flow path length and swirl mixing. Swirl flow and increased path length are expected to also benefit two-phase heat transfer. For example, Royal and Bergles surveyed horizontal, convective condensation with twisted tapes and found improvements in heat-transfer coefficients by as much as 30% over empty tube condensation. In addition, the most popular use of twisted tapes in flow boiling is to delay the occurrence of burnout. Yet, relatively few two-phase heat transfer studies with twisted tapes exist: approximately ten convective condensation and possibly 60 flow boiling. Furthermore, to the best of author's knowledge, no two-phase heat transfer studies of heat pipes with twisted tapes exist. This is interesting considering that using twisted tapes is as an inexpensive way to simplify heat pipe structure and improve the heat pipe efficiency at high heat flux.

Consequently, there is a need for phase change heat transfer data that provides information that can be used to design heat pipes with twisted-tape inserts for alternative conventional heat pipes, which have film boiling problems at high heat fluxes.

7.2 Experimental Results and Analysis of a Flow Modified Heat Pipe

7.2.1 Structure of a Flow Modified Heat Pipe

To achieve comparable uniform and large heat fluxes, it was decided to use a bath of molten zinc as the heat source for a water based heat pipe. By immersing the evaporator into the zinc one can create the potential for producing high heat fluxes. A new heat pipe was constructed, it had the identical dimensions of the conventional heat pipe, as was shown in Figure 6-1. A schematic of the flow modified (new) heat pipe is shown in Figure 7-1.
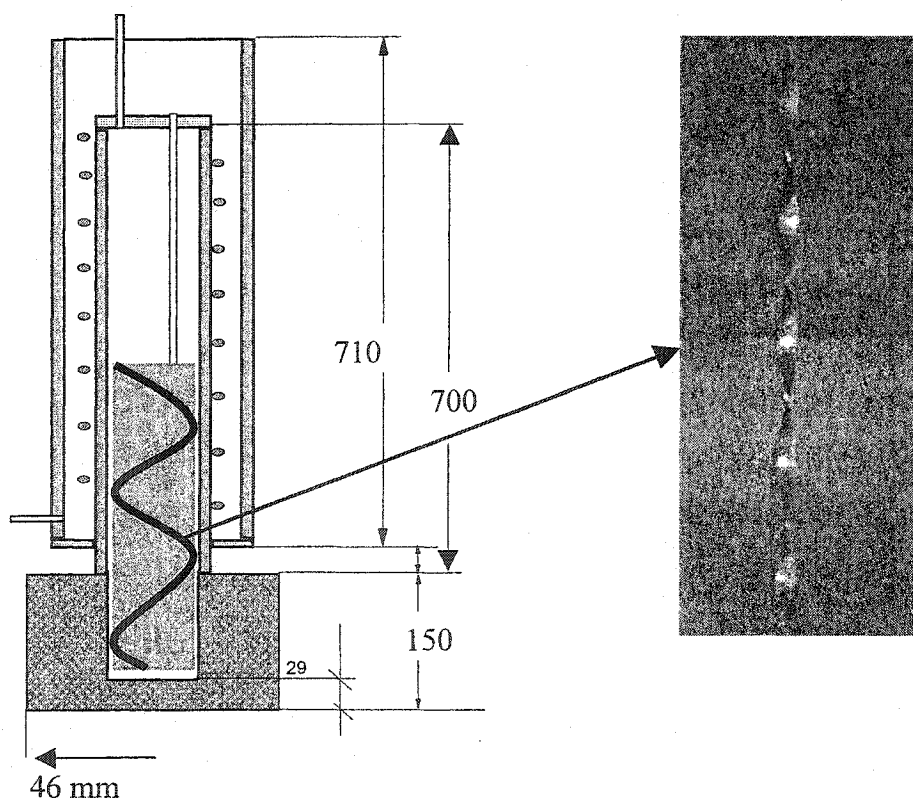

Figure 7-1. A Schematic of the Flow Modified Heat Pipe with a
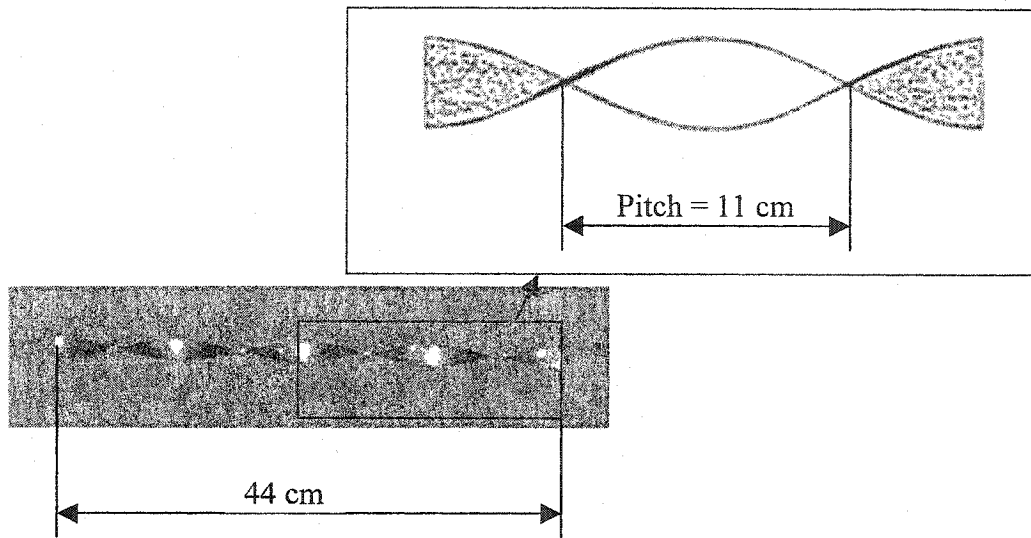Twisted Tape Insert

Figure 7-2. Twisted Tape Insert

a. 4-way groove
twisted bar
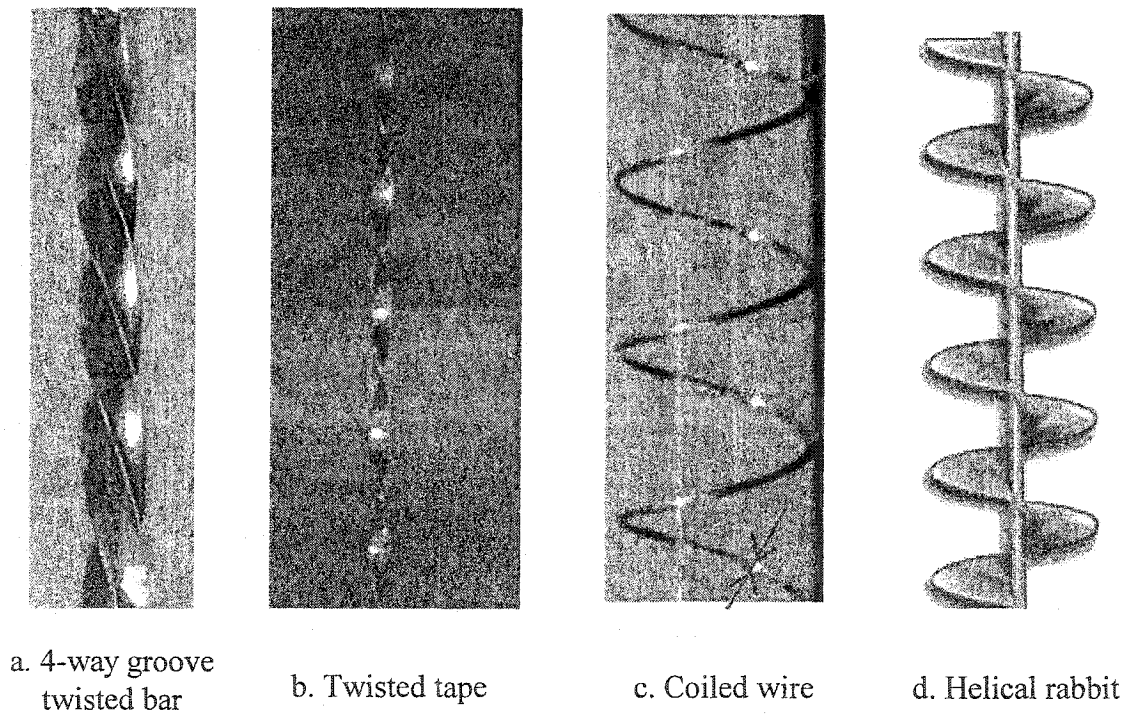
b. Twisted tape

c. Coiled wire

d. Helical rabbit

Figure 7-3. The Various Types of Swirlers

Like the conventional heat pipe, the evaporator portion of the heat pipe was made by drilling a hole 18 mm in diameter in a solid 316L stainless steel (SS) bar of 46mm diameter. The bottom of the bar was left with a 29 mm thickness of stainless. A condenser, including an air cooled jacket, was welded onto the opening of the bar. The inside of the pipe was fitted with 2 wraps of 100 mesh SS wick. The pipe was charged with 40 g of distilled water and evacuated.

The new heat pipe was identical with the exception that the inside of the evaporator was fitted with a twisted tape insert, which made a complete turn over a length of 11 cm. The thermocouple well, extending to within 40 cm of the bottom of the evaporator chamber, was shortened and extended up to the top of the twisted tape. It didn't affect the measurement of heat pipe temperature. A photograph of the twisted tape element is shown in Figure 7-2. The pitch of the twisted tape is 11 cm when 44 cm of total length has 4 turns.

In fact, before the twisted tape was finally selected as the flow modifier element to improve the heat transfer inside the heat pipe, the various types of swirlers such as coiled wire, 4-way twisted groove bar and helical rabbit, shown in Figure 7-3, were tested in experiments of extracting heat from the outer heat pipe wall. It was observed coiled wire (spring) didn't reach expected results because it could not generate enough momentum in the experiments. It was also observed the 4-way twisted groove bar and helical rabbit were not different from twisted tape insert in the test results. But they are more expensive to manufacture compared with simple twisted tape inserts. Therefore, the twisted tape inserts were finally chosen.

7.2.2 Testing Results of Flow Modified Heat Pipe in Radiation Furnace

Before testing the heat pipe in molten zinc, it was tested vertically in a radiation furnace in the 440 to 740 °C temperature range, as our other experiments. In these tests, the entire length of the evaporator was exposed to the radiative flux from the furnace walls. The steady state results for these tests are shown in Figure 7-4. Values for the rate of heat extraction were computed by determining the enthalpy change of the cooling air (equation 5.1). One can see from these results that at a given heat pipe operating

temperature, the rate of heat extraction increases as the furnace temperature and cooling air flow rate are increased.
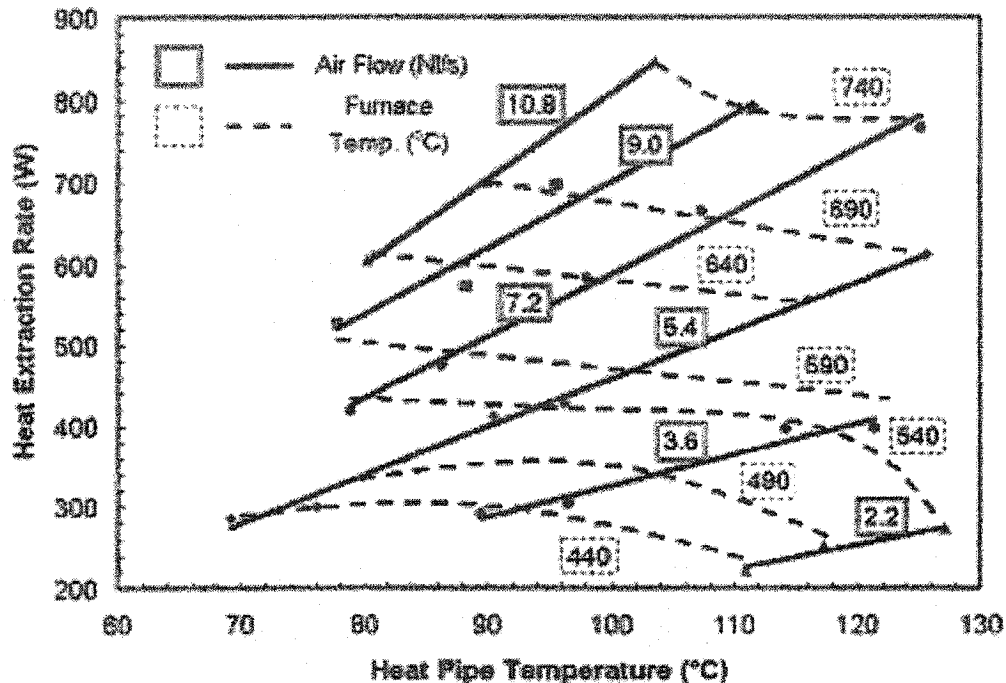

Figure 7-4. Summary of Flow Modified Heat Pipe Results in a Radiation Furnace

Similar plots to those shown in Figure 7-4 could have been drawn for the outlet air temperature. Conclusions drawn from such a plot would have been comparable to those arrived at when the data is plotted against the heat pipe temperature. These conclusions of flow modified heat pipes are not different from the results obtained in the tests of the conventional heat pipe in the same furnace, as shown in Chapter 6.

7.2.3 Testing Results and Analysis of Flow Modified Heat Pipe in Liquid Zinc

The flow modified heat pipe was also tested in a bath of molten zinc. In fact, the pipe was originally designed with this intent – thus, the relatively thick evaporator walls. As the zinc is conductive and dense, the effective heat transfer coefficient at the solid/liquid interface for a stagnant bath is about 4,000 W/m^2-K as determined in a parallel project [7]. Thus, the heat pipe can be subjected to very large heat fluxes.
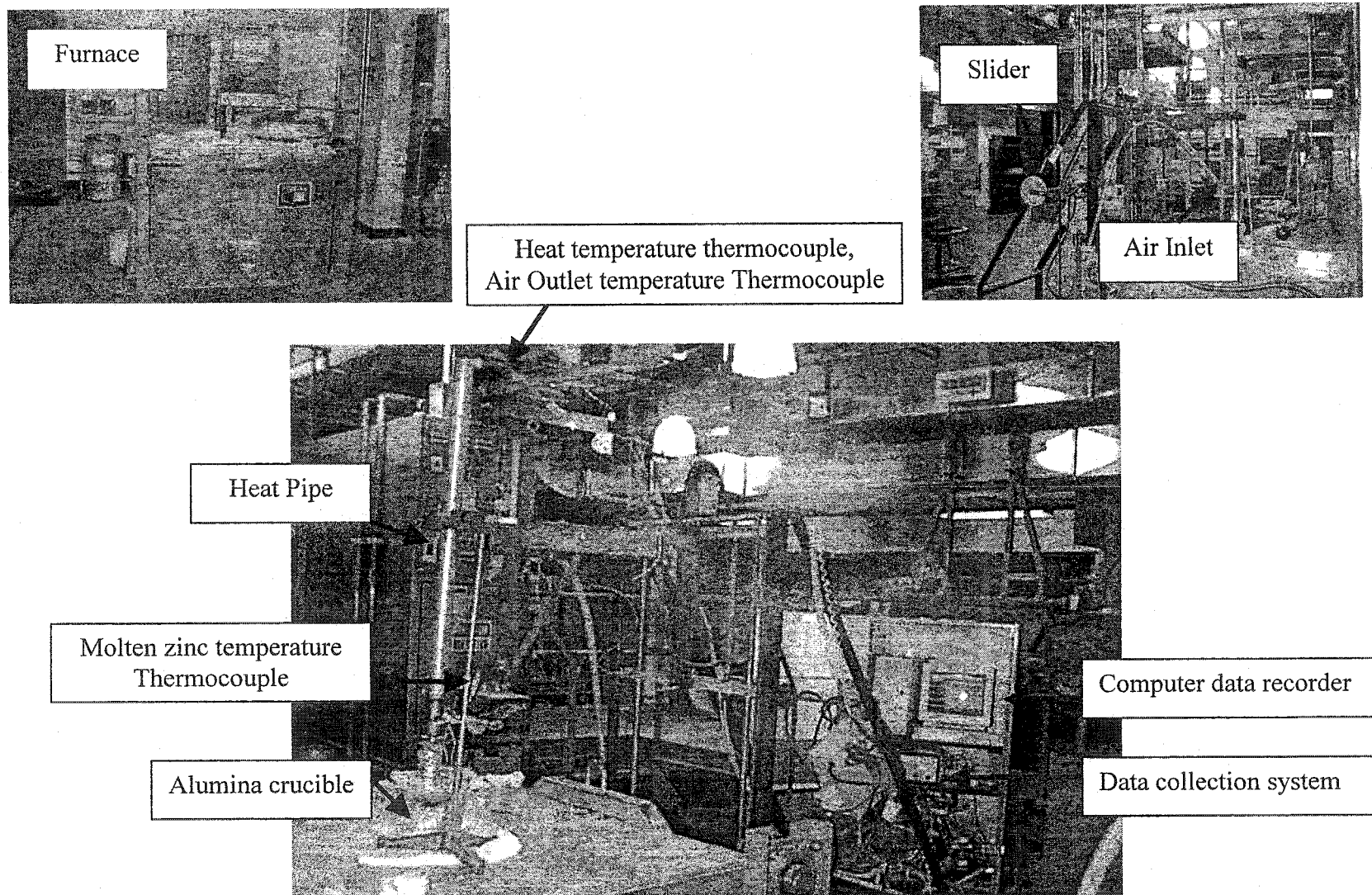
Figure 7-5. Experimental Set-up For Heat Pipe Testing in Molten Zinc

A photo of the experimental setup is shown in Figure 7-5. In this experimental set up, the heat pipe was attached to a lifting mechanism, which allowed us to move the heat pipe in and out of the molten zinc quickly. Besides the heat pipe thermocouple and the air outlet thermocouple, there was another thermocouple, which was placed inside the molten zinc, and was used to measure the liquid zinc temperature. An alumina crucible with zinc metal sat inside the furnace.

The tests were conducted by immersing varying lengths of the leading end of the evaporator into the molten zinc. For each immersion tested, the temperatures of the heat pipe, the zinc melt and the outlet cooling air were recorded as a function of time. Also recorded was the flow rate of cooling air. The inlet temperature of the cooling air was relatively constant and only noted at the start of each experiment. Several deviations of the above procedure were also used. These will be described as the results are presented. All the immersion trials were conducted in a melt of about 22 kg of commercial purity zinc with a melting point of about 420 °C. The melt was contained in an alumina crucible of 15 cm internal diameter.

A typical testing process of the heat pipe can be classified into 3 stages: start up, heat extraction and removal from the zinc melt. The following sections give explanations and discussions of the startup and the heat extraction stages in detail. The removal stage just simply refers to the removal of the heat pipe from the liquid zinc melt.

Start-up Stage

It was very surprising when the start up phenomenon was observed in the heat pipe with water as the working fluid. Normally, this situation could be observed in metals, such as K and Na, as the working fluids of the heat pipes. Usually, heat pipes using high vapor pressure working fluids (such as water and ammonia) typically exhibit uniform temperature startup, whereas those using fluids with low vapor pressures (such as the liquid metals, K, Na) do not since they are in the solid state at room temperature. This start-up is called frozen start-up. It proceeds as follow [8]: Heat is first conducted through the pipe wall and into the wick structure, increasing the temperature in the evaporator section only. After the working fluid in the evaporator wick is liquefied, evaporation begins to fill the vapor core section with vapor. The vapor travels to the adiabatic section and condenses, releasing its latent heat and increasing the adiabatic

section temperature. This front continues along the length of the pipe until it reaches the condenser end cap. At that time, the axial temperature distribution starts to become uniform, and the startup process is completed. The presence of large axial temperature gradients indicates that the sonic limit is occurring during frozen startup. In actuality, this is not a limit per se, since the heat pipe will not be damaged during this process. Another more important limit is the frozen startup limit. This occurs when more working fluid is evaporated than can be re-supplied by the wick structure, due to the fact that the working fluid in the adiabatic and condenser sections is completely frozen. When this occurs, the evaporator section is depleted of liquid and overheats due to dryout.

The frozen startup of low temperature heat pipes with water is rare. J. Tournier and M. El-Genk [9, 10] give their experimental results and analysis of the frozen startup. The frozen startup characteristics of low temperature and high temperature heat pipes differ significantly due to differences in the vapor pressure of the working fluid near the melting point. In low temperature heat pipes, the vapor pressure is large enough to allow significant migration of the working fluid to colder regions in the heat pipe. Once the solid working fluid is melted in the evaporator, dryout may occur due to immediate vaporization of the fluid. In the case of high temperature working fluids, the vapor flow in the heat pipe remains in the free-molecule regime for temperatures well above the melting temperature. This has the beneficial effects of preventing migration of the solid working fluid to the condenser, and allowing for melting the working fluid by conduction heat transfer before large scale evaporation of liquid occurs. The startup of a low temperature heat pipe from a frozen state can be divided into several periods. Initially, the frozen working fluid sublimates and is transported as a continuum flow to the condenser where it re-solidifies. Sublimation-resolidification depletes the frozen working fluid in the evaporator and accumulates it in the condenser. As the evaporator wall temperature continues to increase, the working fluid begins to melt. When the melting front reaches the liquid-vapor interface, the following processes take place:

(i) Evaporation of working fluid in the evaporator, which can cause the wick to dryout; and

(ii) A thin liquid film from vapor condensation forms on a frozen substrate in the condenser;

(iii) Melting of frozen working fluid occurs in the condenser and adiabatic sections at the liquid film/solid interface and proceeds radially outward.

Eventually, the thaw of the heat pipe is completed and proper liquid circulation in the wick is fully resumed.

But, startup of the water heat pipe with film boiling is quite different from either the metals heat pipe or frozen startup of low temperature heat pipe since it is caused by film boiling due to high heat flux transfer and it only happens at around room temperature. Several experiments were done to understand the behavior of the startup of a flow modified heat pipe and to characterize the process of startup.

A typical example is shown in Figure 7-6. It illustrates when the heat pipe was directly slid into the superheated molten zinc. The operating temperature of the heat pipe was kept low and stable, and the heat pipe didn't work as expected. It was pumping out much less heat than it could have based on simple heat transfer calculations The heat pipe was moved out of the liquid zinc and cooled until it reached a "turning point". The heat pipe was slid into the zinc again. This time, the heat pipe started to work (i.e. extracted much more heat). The operating temperature of the heat pipe increased fast until it reached a new balance level. Figure 7-6b shows a close look at the change point. This start-up problem was caused by film boiling inside the heat pipe. Since a huge amount of heat transferred into the heat pipe at the beginning when the heat pipe was initially inserted into the liquid zinc, the flow modifier element (twisted tape) inside the working fluid of heat pipe didn't have enough time to form a swirl flow, which would have caused the liquid to generate nucleate boiling. Instead, the superheated bottom of the evaporator led to the formation of a film that blocked the heat transfer from the evaporator surface to working fluid. Thus, the operating temperature of the heat pipe was constant and low. When the heat pipe was moved out of the liquid zinc and allowed to cool to the changing point, the formed film collapsed due to the lowering of the superheat. The working substance fell back into the bottom of the evaporator, and the twisted tape started to create swirl flow although the vapour pressure was still low. Now, the heat pipe was inserted into the liquid zinc again. The twisted tape used momentum of the vapour to speed the swirl flow as extraction of heat from the heat pipe increased. When stable heat extraction was reached, the heat pipe was at steady state.

In fact, this phenomenon was not only observed at the beginning. Figure 7-7 shows a case when the heat pipe worked well when the heat pipe was immersed 1 cm into the liquid zinc. After the operating temperature was stable, the heat pipe was quickly immersed to 8 cm inside the liquid zinc. The heat pipe temperature first increased. However it then decreased until it reached a new low level. The pipe was removed from the melt. After the changing point was reached, 8 cm of the evaporator of the heat pipe was put into the liquid zinc again. The heat pipe was now working again. It was permitted to continue until the operating temperature of the heat pipe was too high and it was taken out of the molten zinc because of insufficient cooling air flow in the laboratory. In the case, when the heat pipe was quickly inserted into the liquid zinc from 1 to 8 cm, a large amount of heat was transferred into the heat pipe from the side. The momentum arising from extra vapor chocked the normal swirl flow, which had been created by the twisted tape when 1 cm was inside the molten zinc. A new swirl flow was not formed. Therefore, a consistent flow could not efficiently remove the film formed on the evaporator wall.

Other methods of start up were investigated. When the temperature of the liquid zinc is not too high, the heat pipe can be directly started up. It is not necessary to move it out to collapse the formed film. Figure 7-8 indicates this situation. The heat pipe temperature increased first, and then decreased. The film then collapsed (first try) and the temperature increased again. However, it could not completely remove the film, thus the heat pipe temperature decreased again to cut the film again (second try). The heat pipe successfully removed the film this time, so the heat pipe started to work. Therefore, when the superheat of the liquid zinc is low, the heat transfer into the evaporator can be low because of the interfacial contact resistance at the pipe/zinc interface. The twisted tape can then form a swirl flow to remove the film. Of course, the evaporator area inside the liquid zinc should also not be too big. In another case, when the heat pipe had been previously coated with a large mass of frozen zinc and when it was heated back up in molten zinc, the heat pipe could also start up appropriately. The experimental data will be presented in latter sections in detail.

For the heat pipe without a twisted tape, a similar phenomenon was observed. In Figure 7-9 is presented a typical temperature of the conventional heat pipe. When this heat pipe was immersed in liquid zinc, the operating temperature increased. When it
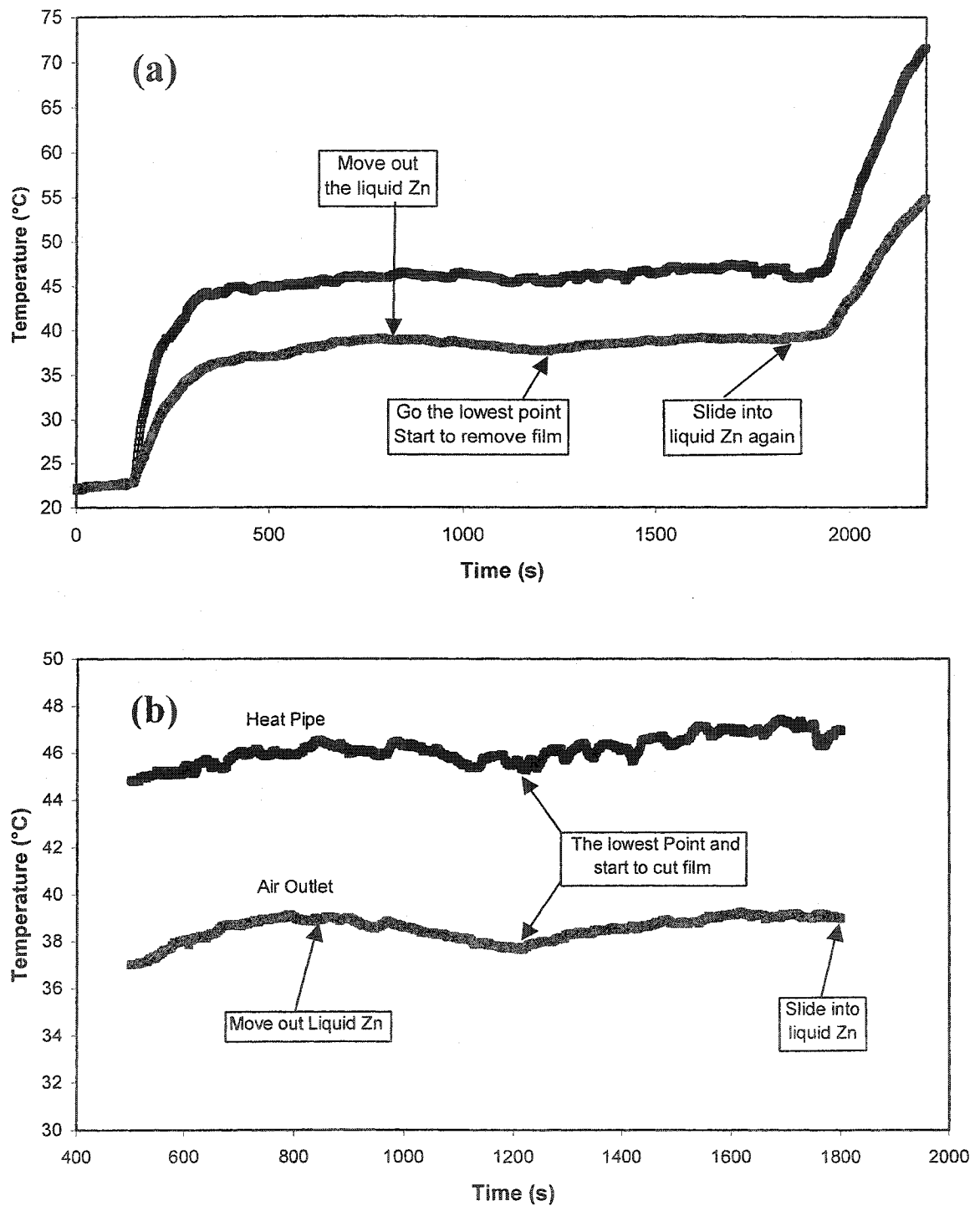
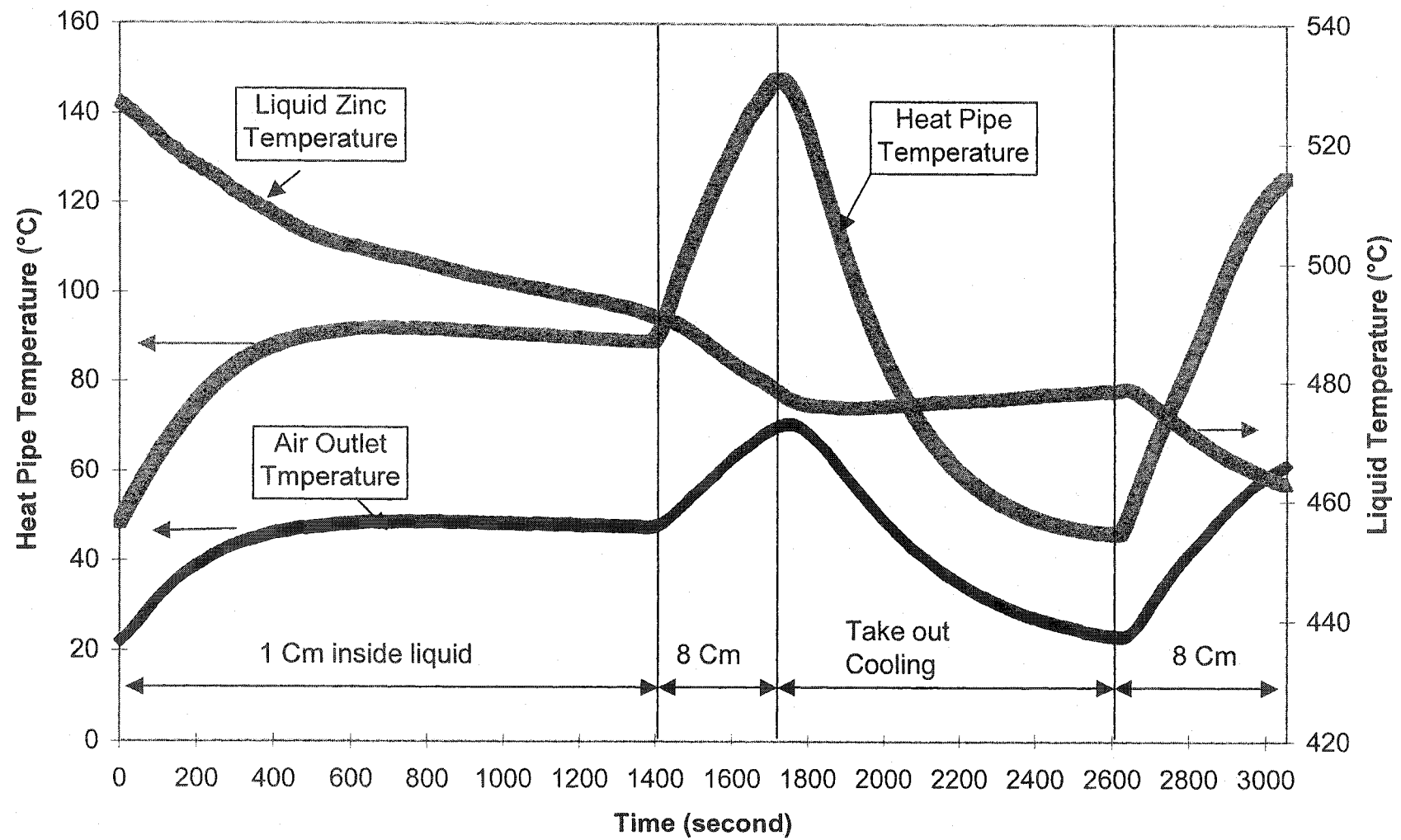Figure 7-6. The Start-up of Flow Modified Heat Pipe

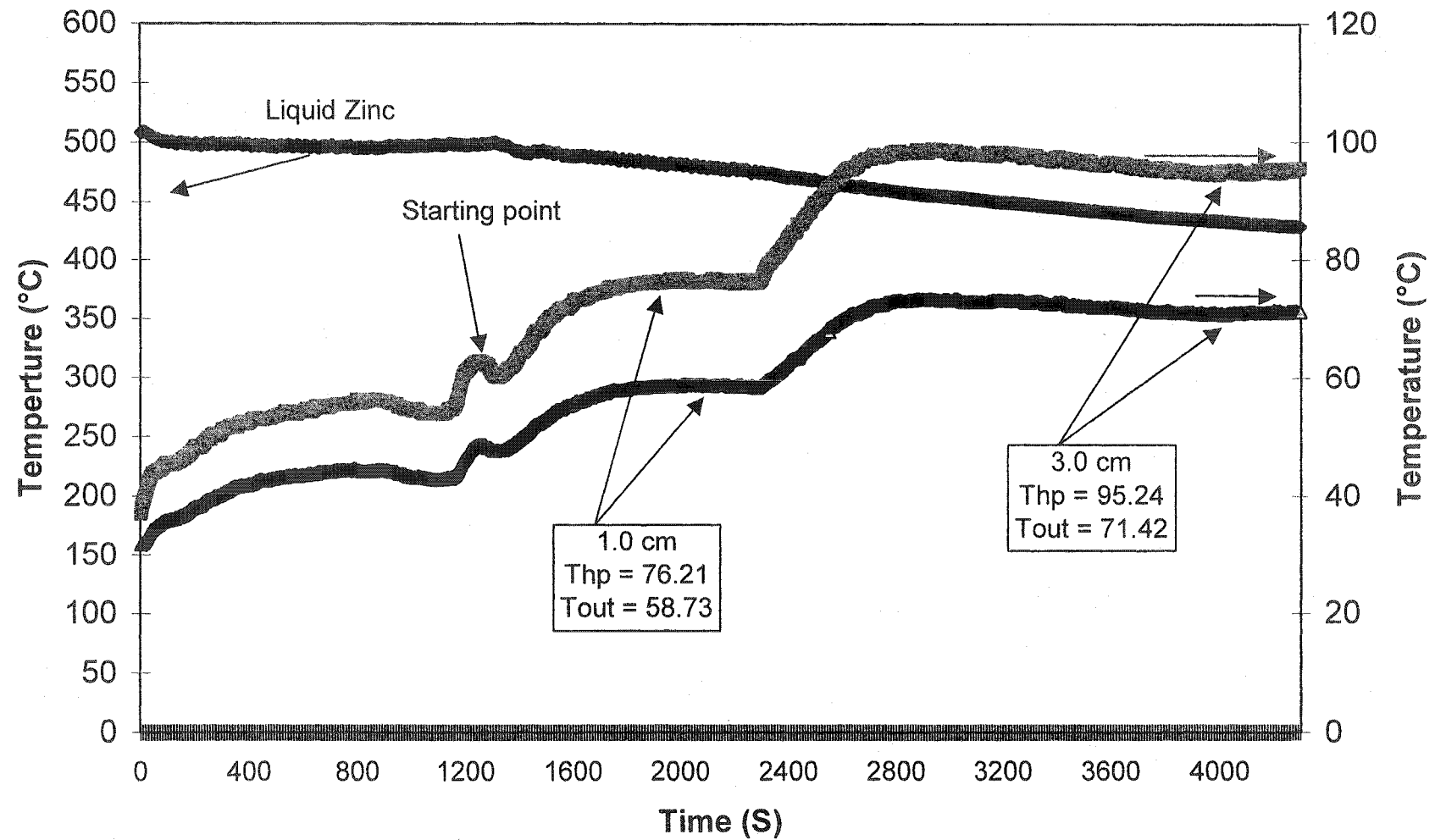Figure 7-7. Film Boiling Caused by Sharply Increasing Heat

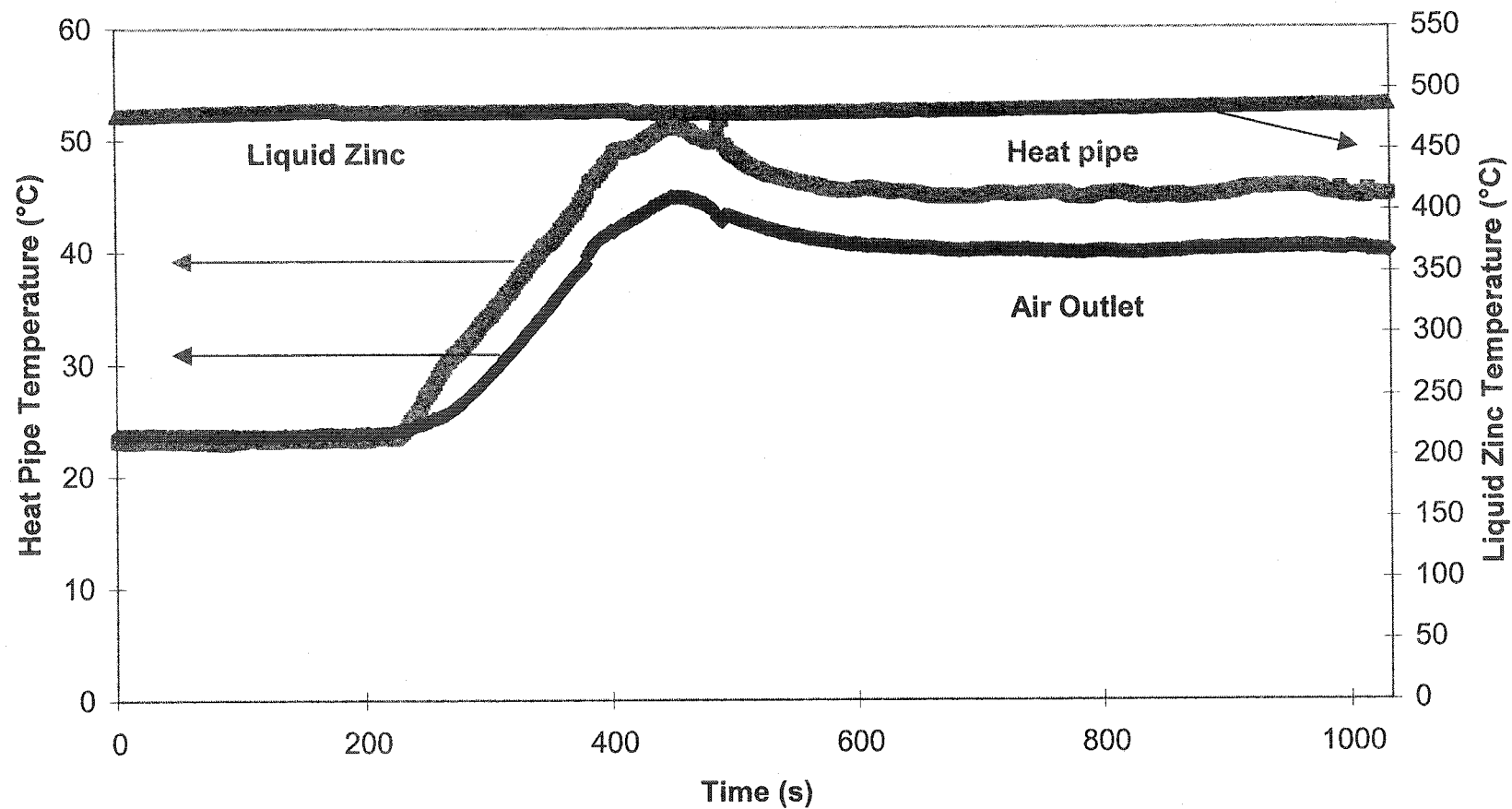Figure 7-8. Direct Start-up of the Heat Pipe at Low Molten Zinc Temperature

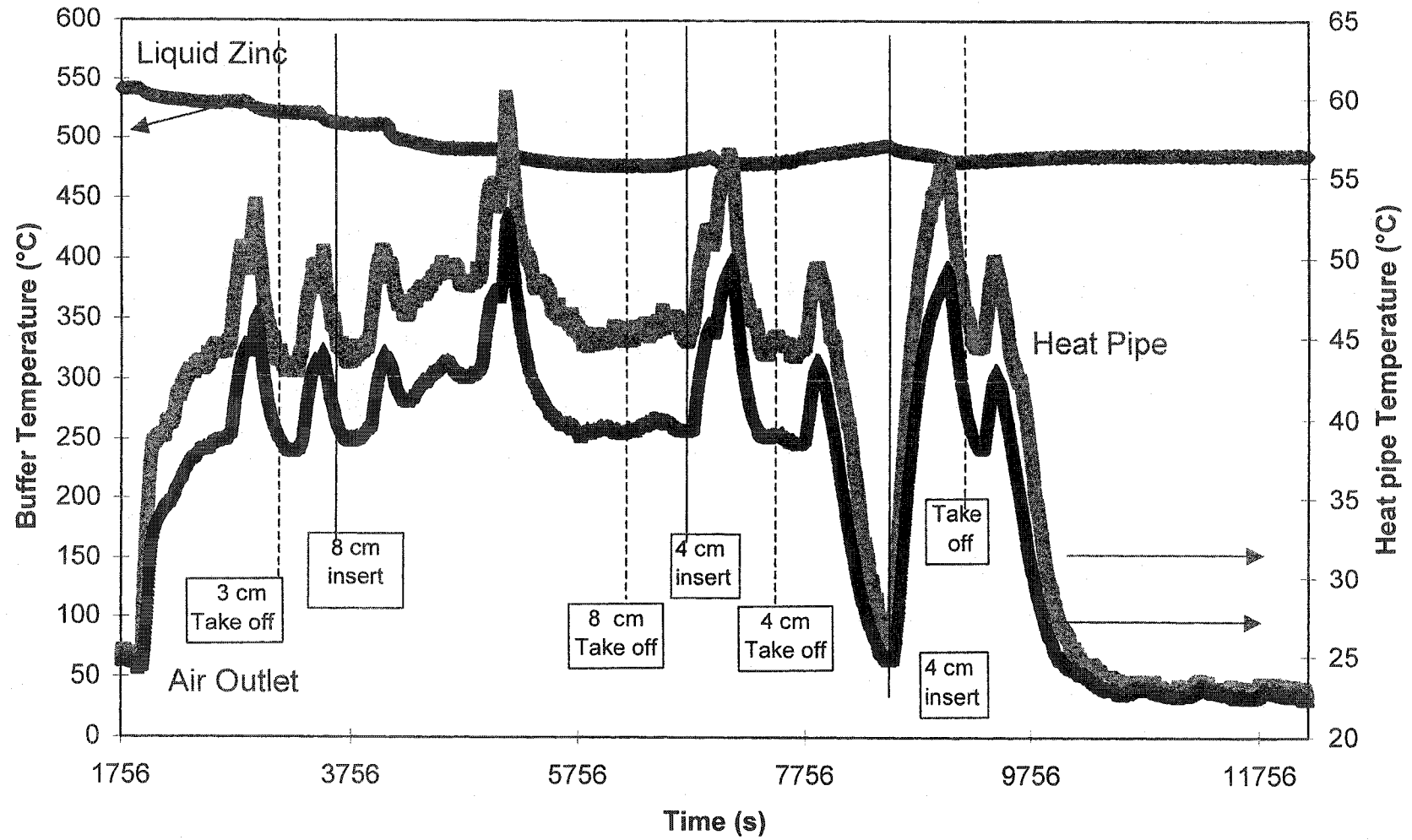Figure 7-9. Typical Temperature Changes of Conventional Heat Pipe

Figure 7-10: The Experimental Data of Startup of Conventional Heat Pipe

reached about 50 °C, the operating temperature would not increase any more. Film boiling significantly reduced the heat transfer. Since it is not the same as the modified flow heat pipe with a twisted tape, it can't cut (i.e. strip) the formed film. Therefore, it never got working although the formed film was cut when it was moved out of the liquid zinc. However, the film formed again when it was re-immersed into liquid zinc. This is clearly shown in Figure 7-10. More comparisons of both heat pipes will be discussed in following sections.

To summarize, the startup of a flow modified heat pipe with a twisted element can be divided into several periods. Initially, the working fluid—water is vaporized. Since the amount of vapor is too small to form a swirl flow via the twisted element inside the heat pipe, some parts of the heat pipe evaporator generate film boiling at the interfaces between the superheated wall of the evaporator and the working substance. As the amount of vapor generated in the evaporator increases, a swirl flow is formed in the lower part. The initial swirl flow is very unstable. It may be killed by a disruptive force. When the swirl flow becomes stronger, the vapor flow travels up via the twisted element. The swirl flow eliminates film boiling and cuts the film formed in the initial period in the evaporator. Thus more heat is transferred into the heat pipe and more vapor is generated. The amount of vapor further increases, consolidates and strengthens the swirl flow. Simultaneously, the vapor is transported to the condenser and is condensed. The condensed working substance may be forced to leave the swirl flow via a centrifugal force, which is created by the swirl flow, and then accumulates in the condenser wick. Therefore, the working fluid in the condenser returns to the evaporator under the help of gravity and the capillary force of the wick. When the swirl flow reaches full development and stabilization, the following processes take place:

(a) Evaporation of working fluid in the evaporator, which can cause the wick to dryout; and

(b) Swirl flow continuously eliminates film boiling, and forces the condensed liquid to firmly penetrate in the wick structure, where the liquid working fluid is redistributed via wick capillary.

(c) The working fluid in the wick is restored to the evaporator.

Finally, the startup of the heat pipe is completed and proper liquid circulation in the wick is fully resumed.

Heat Extraction

When the swirl flow is fully developed, the operating temperature of the heat pipe reaches a stable point, and the heat extraction per unit time is stable. Figure 7-11 shows the temperatures of heat pipe operation, the outlet of the cooling air and the liquid zinc. These data were obtained with 20 Nl/s of cooling air flow rate, which is the maximum flow obtained in the laboratory. When the heat pipe started to work normally after startup, the temperatures of the heat pipe and air outlet increased until they reached steady state under this experimental condition. Initially only 1 cm of the pipe was immersed into the molten zinc. Then, this was increased to 4 cm. Thus, the evaporator area was changed from 2.79×10^{-4} m^2 to 9.3×10^{-4} m^2. In calculating the area, the inner radius of the heat pipe is 0.94 cm. For the case of 1 cm immersed inside molten zinc, the area of the evaporator is πr^2 since the heat pipe had 2.9 cm solid bar in the bottom of the evaporator and the area equals to $\pi r^2 + 2\pi r(4-2.9)$ for 4 cm immersed in liquid zinc. The corresponding heat extraction was 720 W and 1106 W, respectively. Therefore, the average heat flux to the water was: 2580 kW/m^2 and 1190 kW/m^2, respectively.

When the immersed length of the heat pipe evaporator was increased to 6 cm. The heat extraction at this time was computed to be about 1,560 W. When the heat pipe was removed from the melt, as shown in Figure 7-12, it was evident that a fairly large accretion had formed over the immersed portion as also shown in right small pictures of Figure 7-12. It is instructive to compute the average heat flux to the water working substance. Thus, the total inner area for unidirectional heat flow was 2.114×10^{-3} m^2. As has been stated, the heat extraction rate was 1,560 W. Thus, the average heat flux to the water was 740 kW/m^2. This still is a huge heat flux; in fact, it approximates the heat flux one associates with a Hazelett caster for copper anodes [11]. Moreover, it demonstrates the capability of the heat pipe in high heat flux applications.

It will be noted that the heat flux to the water working substance decreased as the length inside the molten zinc increased, as indicated in Figure 7-13. There are two reasons for this change. First, with the solid bar of the evaporator bottom, the outside

a. **Heat Extracting (1 cm evaporator)**

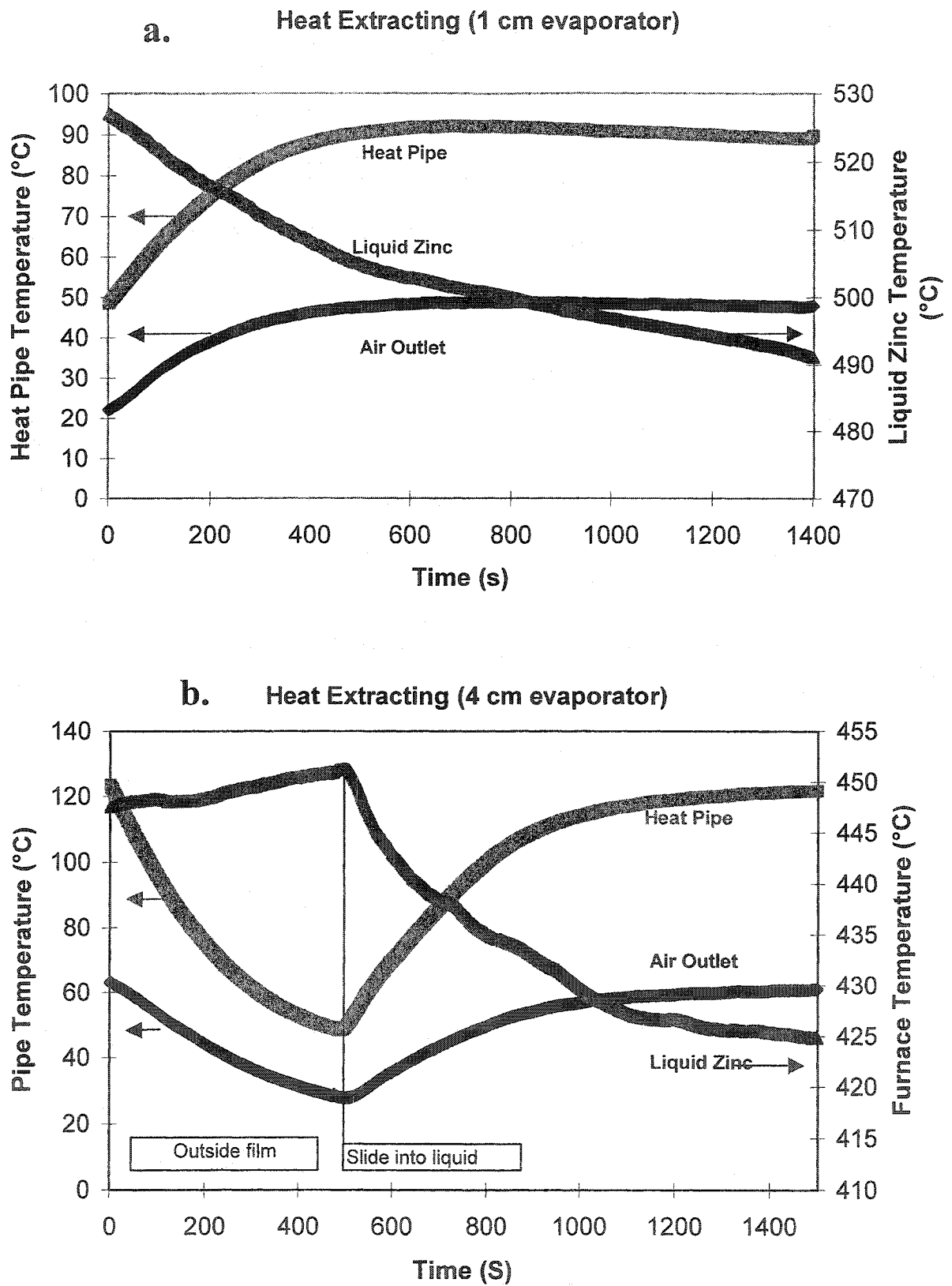**b.** **Heat Extracting (4 cm evaporator)**

Figure 7-11. Typical heat Extracting Curves of Modified Flow Heat Pipe

evaporator area that actually touched the molten area was higher than the inner evaporator area used in the calculations. As the length immersed into molten zinc (1, 4, and 6 cm) increased, the ratio of real outside contacted area to inner area (11, 8, and 5) decreased. More heat is actually extracted from the evaporator with a higher area ratio. Therefore, one can expect the net heat flux to decrease. Secondly, as the liquid zinc temperature went down, the driving force for conduction heat transfer also decreased and thus the heat flux decreased. The thermal conductivity of zinc increases as the zinc temperature decreases. Especially for the 6 cm case, the frozen zinc covered the evaporator area, and it reduced the heat transfer because of the imperfect contact at the interface. Figure 7-14 displays actual results for these three cases.

These two influencing factors lead to the phenomenon that the heat flux for 1 cm was much higher than one for 6 cm.
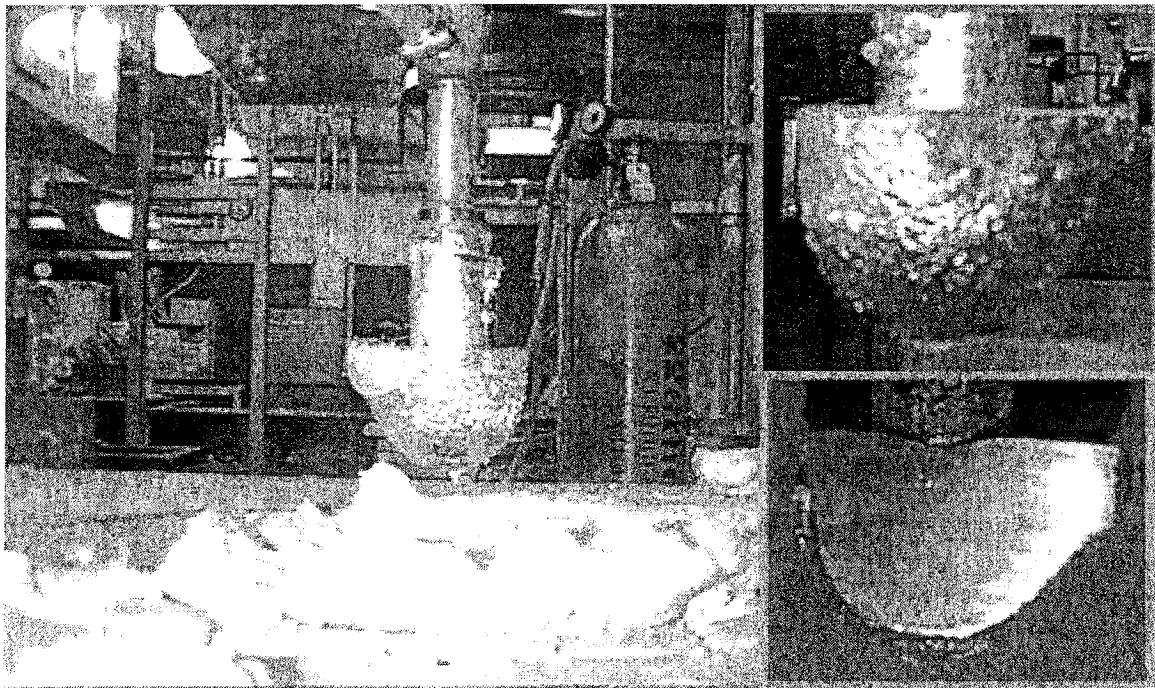

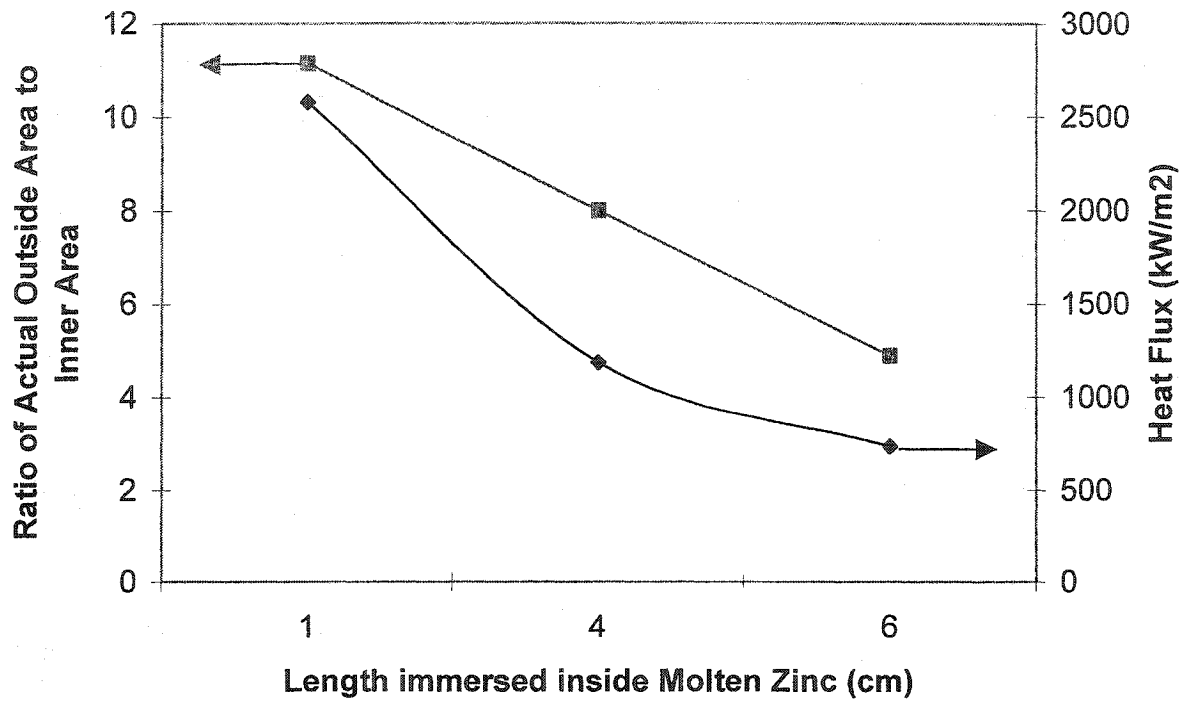Figure 7-12. The Heat Pipe as It Was Removed from the Zinc Melt

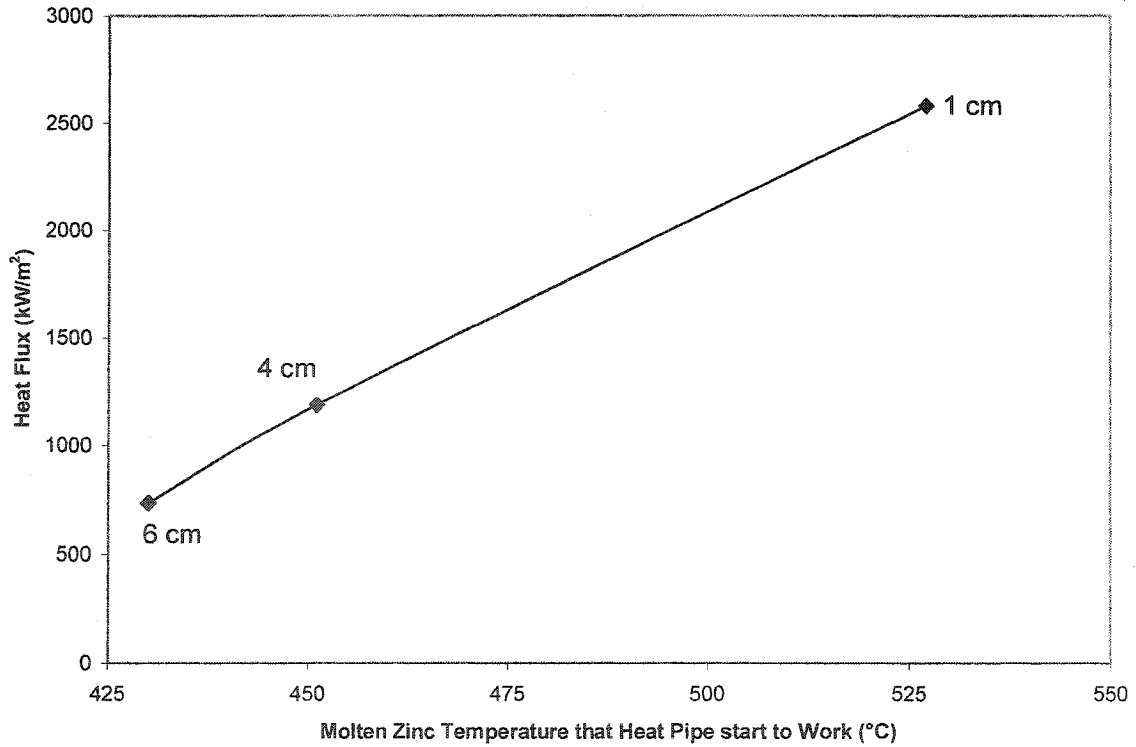Figure 7-13. The Comparison of Heat Flux in Different immersed Length

Figure 7-14. Liquid Zinc Temperature Vs Heat Flux

A series of similar tests with different flow rates of cooling air were also carried out. The results are summarized in Figure 7-15 wherein the heat extraction rate is shown plotted against the difference between the heat pipe temperature and the exhaust cooling air temperature for several flow rates of cooling air. The differences in these curves are attributable to the dependence of the heat transfer coefficients on the air flow. Thus, as the flow rate is increased, the forced convection heat transfer coefficient for air also increases. The results agreed with the results obtained in the radiation furnace, which were shown in Figure 7-4. Of course, these results are different from the results of the conventional heat pipe, which were presented in Chapter 6.

At the same time, Figure 7-15 illustrates that the heat load increased as the temperature difference between the heat pipe and the air outlet increased. This means that the driving force for the large temperature difference is bigger than that for the small difference. Therefore, the heat extraction increased as the driving force increased.
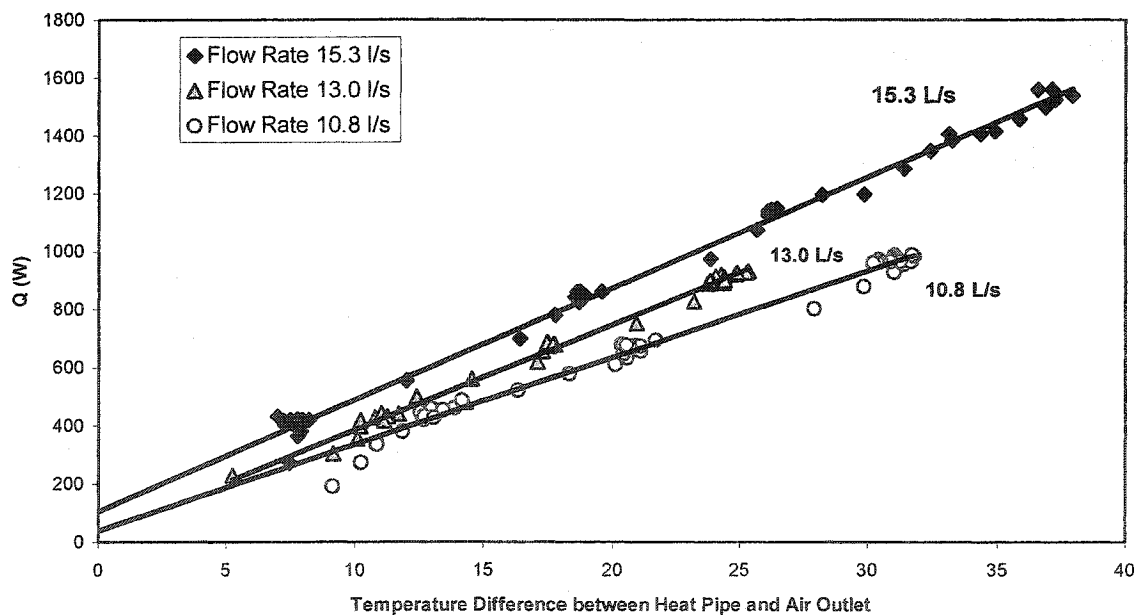

Figure 7-15. Correlation of Experimental Data for 3 Air Flow Rates

7.3 Comparison of Both Heat Pipes

In order to compare the modified flow heat pipe and the conventional heat pipe, many experiments were done and a large amount of experimental data were obtained. Here, a sampling of the results will now be presented to illustrate how the new heat pipe with the internal flow modifier compared with the conventional heat pipe. The tests are divided into 4 categories: a) immersion, d) cooling, c) heating, and d) removal from the melt. Each of these stages is used to illustrate the effect of internal flow modification on heat pipe performance compared with the conventional heat pipe [11].

7.3.1 Immersion Into Molten Zinc

The conventional heat pipe with no flow modifier was immersed in molten zinc in 4 stages. Initially, 2 cm were immersed. This was then increased to 3 cm and then to 4.5 cm and finally to 6 cm. The results of this test are shown in Figure 7-16. One can see from these results that after the initial immersion of 2 cm, the gains in heat extraction as more of the pipe was inserted were modest. The bath temperature changed little following the 2 cm immersion. The total change of the melt temperature during the experiment was only 12 °C.

Contrast these results to those obtained under similar conditions with the heat pipe that was fitted with an internal flow modifier—twisted tape as shown in Figure 7-17. One can see that the heat pipe extracted substantially more heat. In fact, the rate of heat extraction was sufficient to cause the melt to cool an appreciable amount. The change of melt temperature during the experiment reached 68 °C. This is significantly higher than the change of the conventional heat pipe without modified flow, as shown in Figure 7-16. Because of the declining melt temperature, the rate of heat extraction, as computed from the cooling air outlet temperature, did not increase in proportion to the length immersed. A photograph of the heat pipe after removal from the melt is shown in Figure 7-12. A layer of zinc had frozen on the pipe because of the low superheat of the melt at the end of the test. Also apparent is the smooth contour of the zinc layer, which indicates that heat extraction was uniform.

It is to be noted that the outlet temperature of the cooling air is directly proportional to the rate of heat extraction. Clearly, the flow modifier had a profound effect on the rate of heat extraction and thus on the heat flux the water was able to absorb.

Even though only one set of results for each pipe is presented, the tests were repeated on numerous occasions with similar results. The difference between the heat extraction capabilities of the two heat pipes was ascribed to the fact that the mode of boiling in the two pipes differed. Whereas the conventional pipe was operating in the film boiling regime, the new pipe with a flow modifier was operating in the nucleate boiling regime.

This conclusion is also proven by an interesting phenomenon which arises when the pipes are removed from the melt. In Figure 7-16, one can clearly see a jump in the curves of the heat pipe temperature and the air outlet temperature after the heat pipe was taken out of the molten zinc. This is similar to the startup situation, as discussed in a previous section. When the heat pipe was cooled down to a certain point, the superheat $(\Delta T = T_w - T_{sat})$ between evaporator wall and saturation liquid was lowered. Thus, the heat transfer of the heat pipe switched from film boiling regime to the nucleate boiling regime because the film was broken (film cutting). The heat extraction rate increased. Therefore, temperatures of the heat pipe and the air outlet went up as in Figure 7-16. Since there is no film boiling in the flow modified heat pipe, the jumping point is not seen in Figure 7-17. The temperature curves of the heat pipe and the air outlet drop quickly and smoothly after the heat pipe was removed from the molten zinc and can be verified in Figure 7-12.

Figure 7-18 compares the rates of heat extraction between a flow modified heat pipe and a conventional heat pipe without flow modification. It also displays the comparison of heat flux between the flow modified heat pipe and the conventional heat pipe without flow modification. One can clearly see that the heat pipe with the twisted tape is much better than the heat pipe without the twisted tape because film boiling is eliminated by the swirl flow that the twisted tape created in the flow modified heat pipe.

7.3.2 Freezing in Zinc

Given the different modes of boiling in the two heat pipes, it was postulated that if the pipes were allowed to freeze in the zinc after the power to the furnace was switched off, it would be possible to determine if film boiling was a factor. Thus, the conventional heat pipe immersed to a depth of 3 cm was allowed to freeze in the zinc as the temperatures were recorded. The results are shown in Figure 7-19.

An examination of the curves shows that when the zinc had cooled down to about 340 °C, the heat pipe and cooling air outlet temperatures both increased sharply. This indicates that film boiling was prevalent prior to this point. When the film became unstable and collapsed, the heat flux into the pipe showed a sudden increase as reflected by the curves. In addition, the cooling rate of the frozen zinc also showed a sudden increase.

A repeat of this test with an immersion depth of 5 cm produced the results shown in Figure 7-20. Once again the presence of film boiling is discernible. At a zinc temperature of about 250 °C, the heat pipe and cooling air temperatures showed dramatic increases. This indicates the collapse of the film and the resumption of nucleate boiling.

A similar test was carried out with the heat pipe fitted with the flow modifier. In this case, the pipe was immersed 3 cm into the melt. The results are shown in Figure 7-21. For this case it was clear that there was no film boiling. The heat pipe and outlet air temperatures followed the same trend as the zinc temperature. Once again the results show that the flow modifier was successful in eliminating film boiling.

It is not necessary to solidify the heat pipe in the zinc to determine if film boiling is dominant. One can simply remove the pipe from the zinc and allow the pipe to cool in the air. This was done for the conventional pipe and the results are shown in Figure 7-22. Prior to removing the pipe, the readings were stable. When the pipe was raised from the melt, a decline in both the heat pipe and cooling air temperatures was noted. However, at some point both temperatures began to increase until a maximum was reached. This increase is similar to that shown in Figure 7-19 and 7-20. Thus, this pipe had been operating in the film boiling regime. Similar tests with the flow modified heat pipe do not exhibit this reversal in the cooling curves.

7.3.3 Heating in Zinc

Given that film boiling is discernible during the cooling of the zinc, the reverse should be true. Thus, if the heat pipe is allowed to solidify in the zinc and cool, one can then study the reheating of the system when the furnace is switched back on.
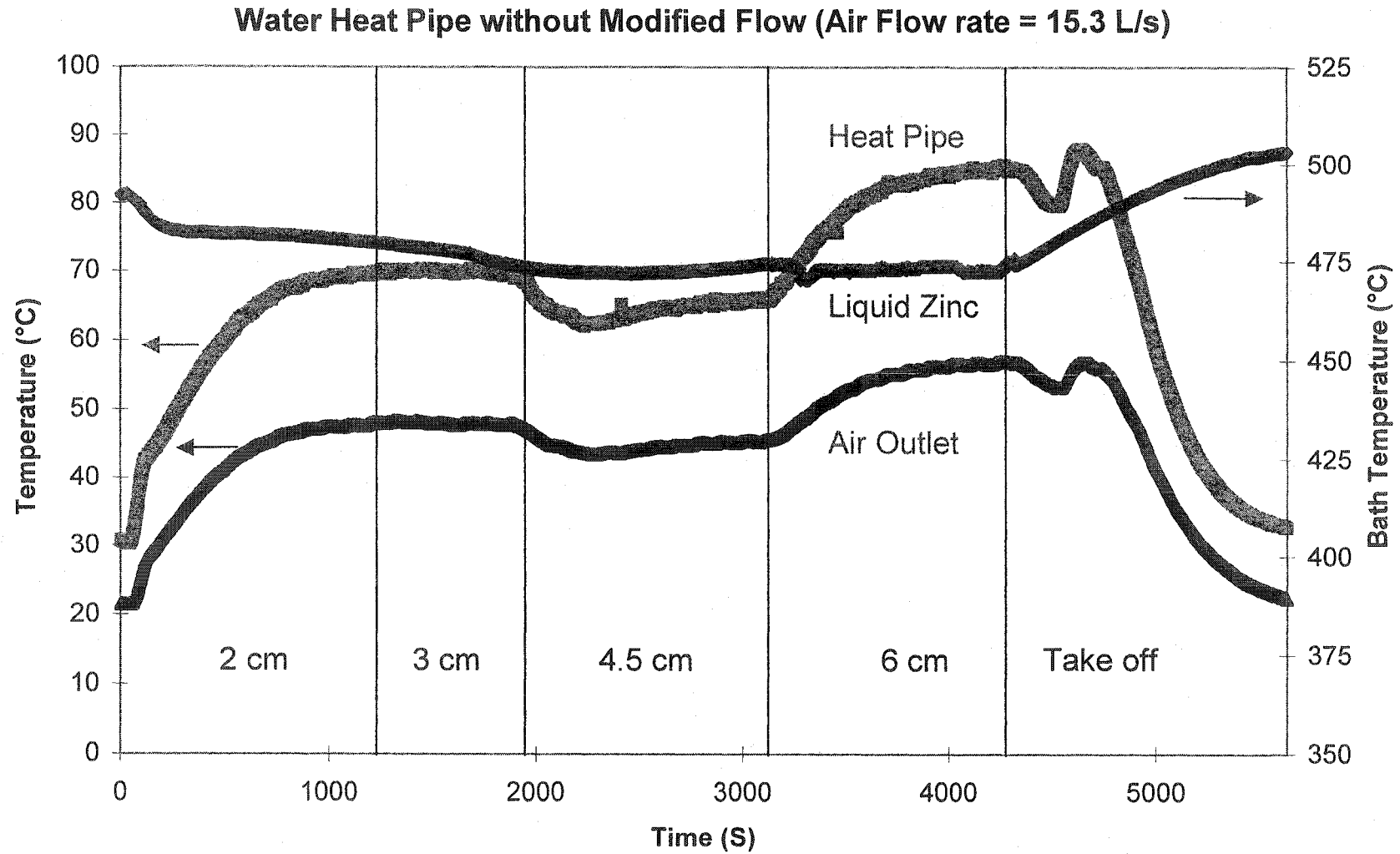
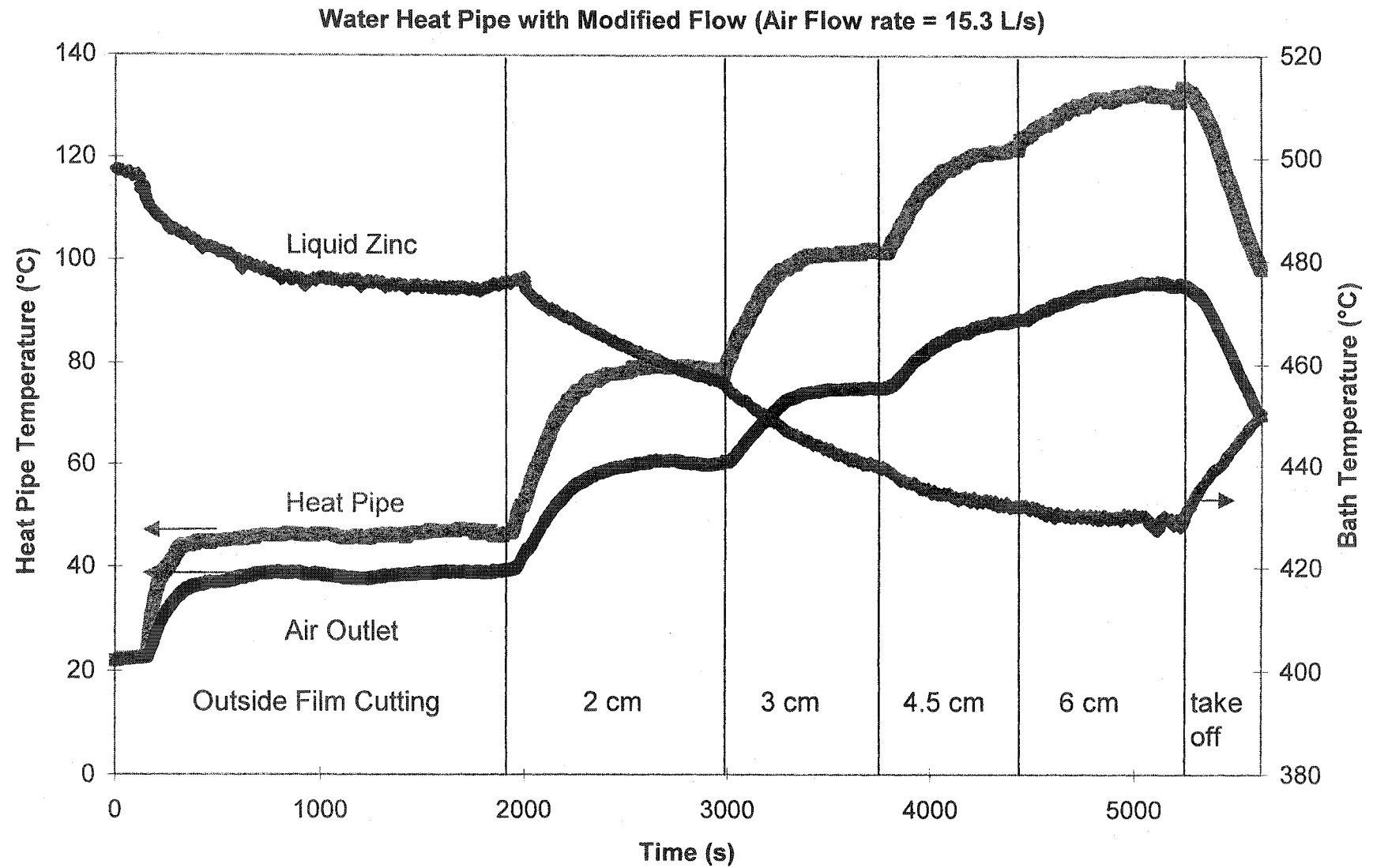Figure 7-16. Staged Immersion of Conventional Heat Pipe in Molten Zinc.

Figure 7-17. Staged Immersion of Modified Flow Heat Pipe in Molten Zinc.
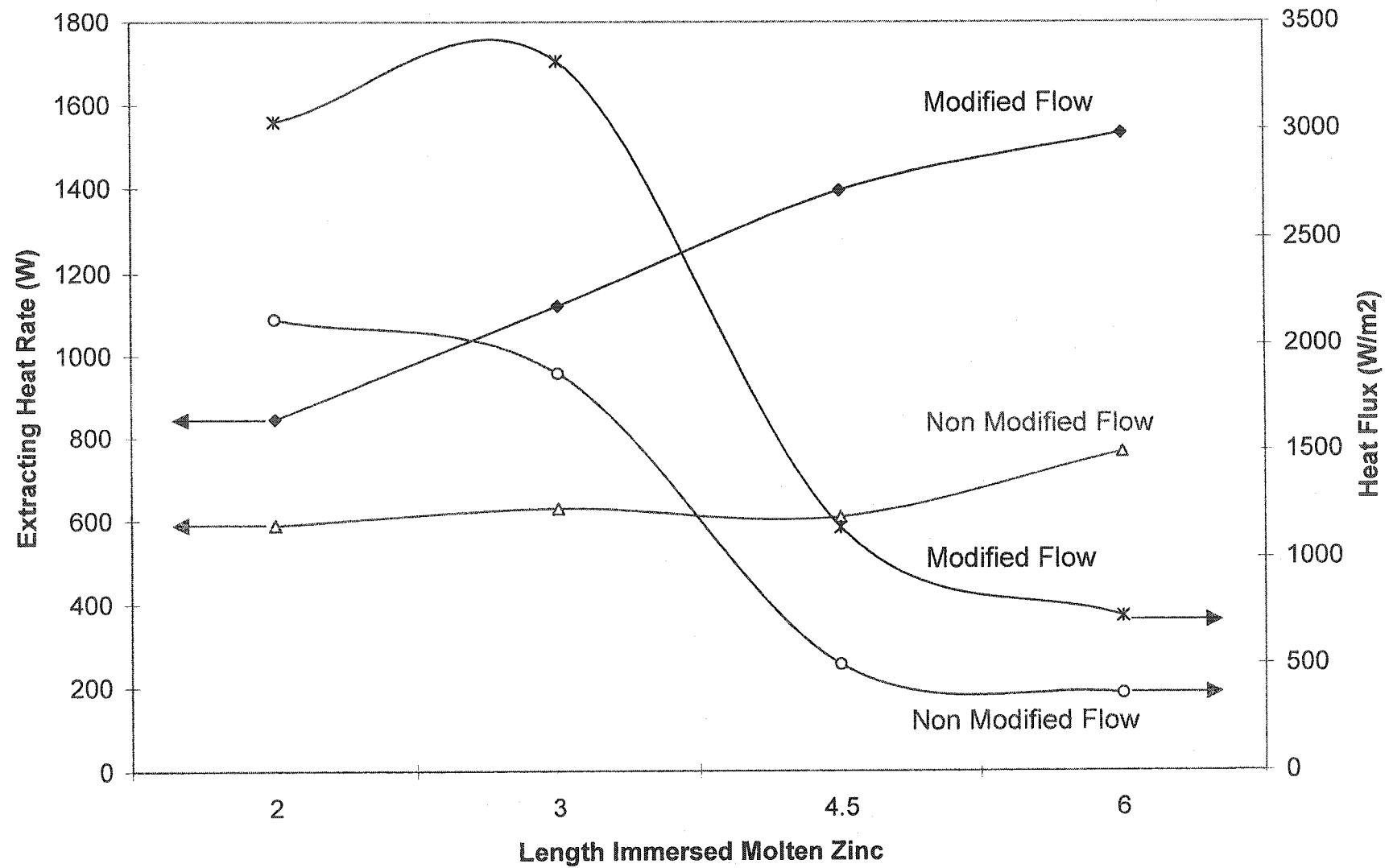
Figure 7-18. Extracting Heat and Heat Flux of Flow Modified Heat Pipe and Conventional Heat Pipe
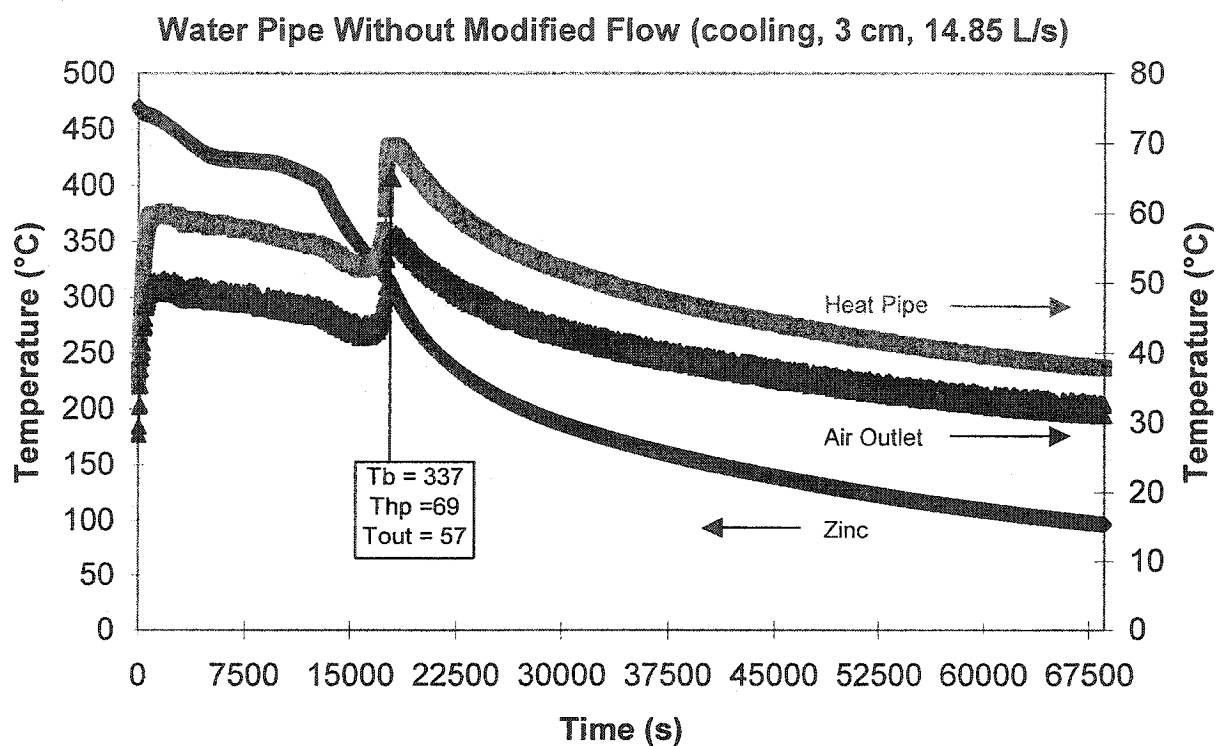
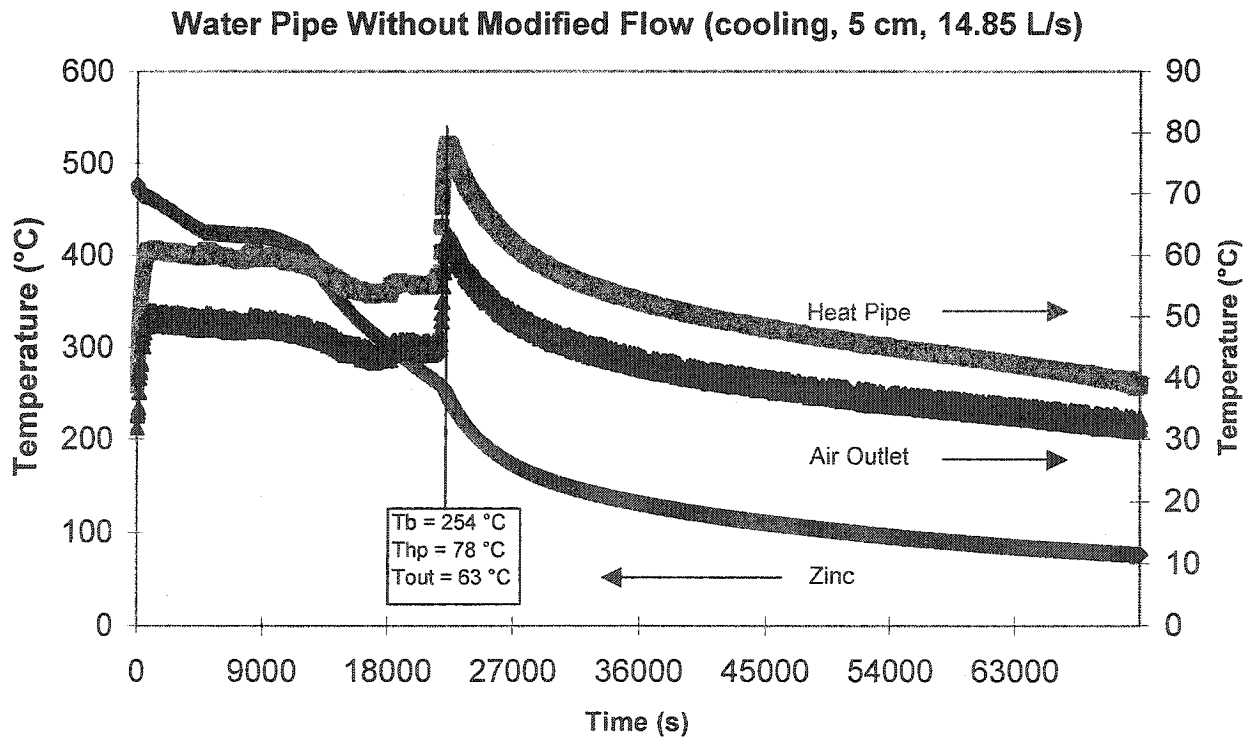Figure 7-19. Freezing of Conventional Heat Pipe (3 cm) in Zinc.

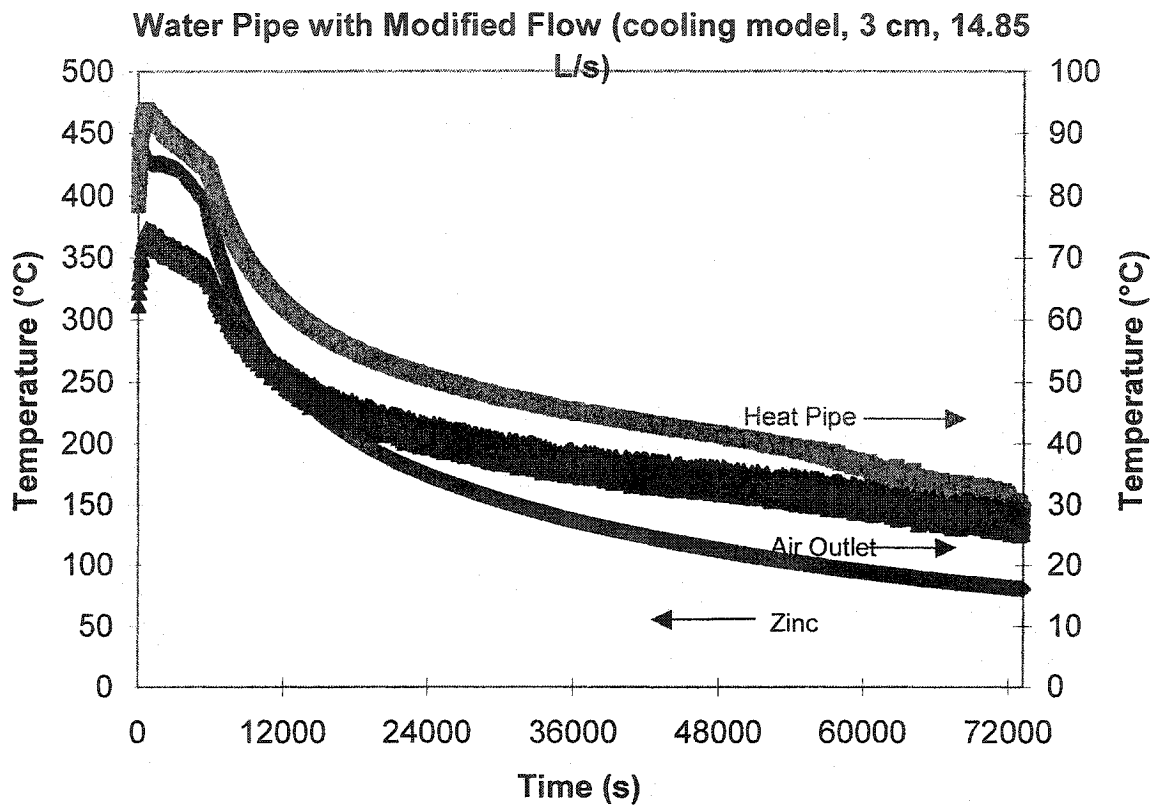Figure 7-20. Freezing of Conventional Heat Pipe (5 cm) in Zinc

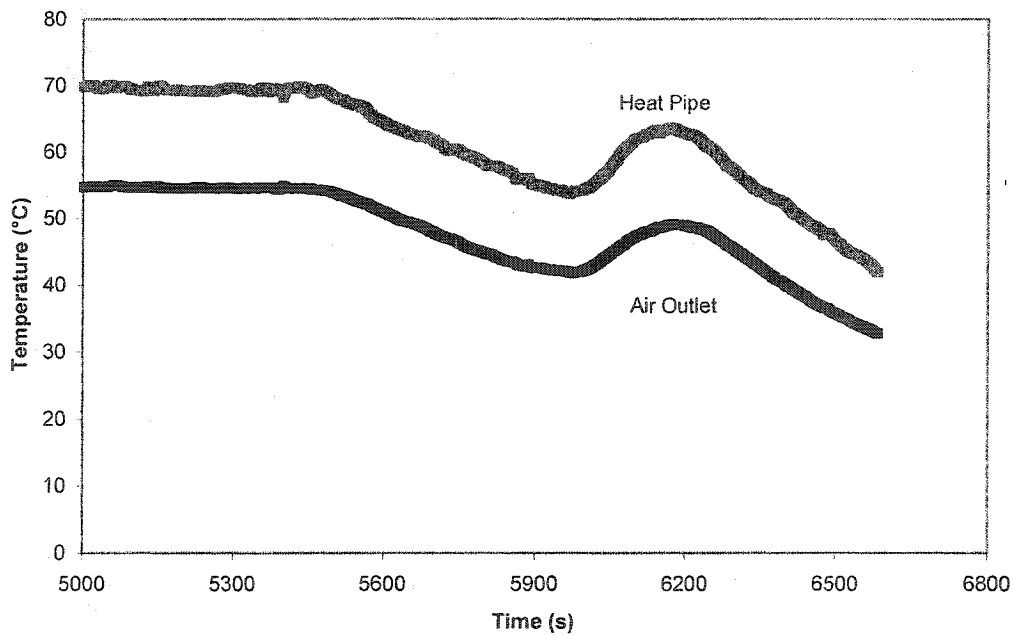Figure 7-21. Freezing of Modified Flow Heat Pipe (3 cm) in Zinc

Figure 7-22. Cooling of Conventional Heat Pipe in Air (Film Cutting)

201

The results from 3 immersion depths (3, 4 and 5 cm) are reported. All tests were carried out with a cooling air flow rate of 15.3 Nl/s. The results for a 4 cm immersion of the conventional heat pipe are shown in Figure 7-23. One can see from these results that as the zinc approached 440 °C, the heat pipe and cooling air temperatures showed sudden drops. At this point, the zinc was molten. These temperature drops were caused by the onset of film boiling. After the heat pipe is dominated by film boiling, the heat extraction capability of the heat pipe dramatically decreased (temperature of air outlet decreased from 75 to 55 °C). Therefore, the zinc temperature continuously increased.

Contrast this with the results for the heat pipe containing the flow modifier as shown in Figure 7-24. In this case there is only nucleate boiling. One can see that as the zinc melted and the interfacial resistance was reduced, the rate of heat extraction, as denoted by the cooling air temperature curve, increased to a new level (i.e. an increase of about 50%). At a certain point, the zinc temperature turned down because the power supplied by the furnace was lower than the rate of heat extraction of the heat pipe.

A comparison of the two heat pipes for an immersion of 4 cm is shown in Figure 7-25. One can see that up to a zinc temperature of about 320 °C (A-B in Figure 7-25), the 2 pipes were essentially identical in heat extraction capability. However, as the zinc melted, the abilities of the 2 pipes to extract heat started to diverge. The segment B-C in Figure 7-25 is mixed stage of nucleate boiling and film boiling. When the zinc temperature reached 420 °C, the zinc was completely molten in the bath and directly touched the evaporator of the heat pipe. At this point, the heat transferred from the liquid zinc to the heat pipe increased dramatically, such that film boiling was fully developed inside the heat pipe without the flow modification. Therefore, the heat extraction rate of the heat pipe reached a new low point, D in Figure 7-25.

Similar results were also observed when 3 cm was immersed in the zinc, as presented in Figure 7-26. Compared with the 4 cm immersion in the zinc, only difference is the turning points B and C are delayed to 400 °C and 470 °C, respectively, due to less evaporator area.
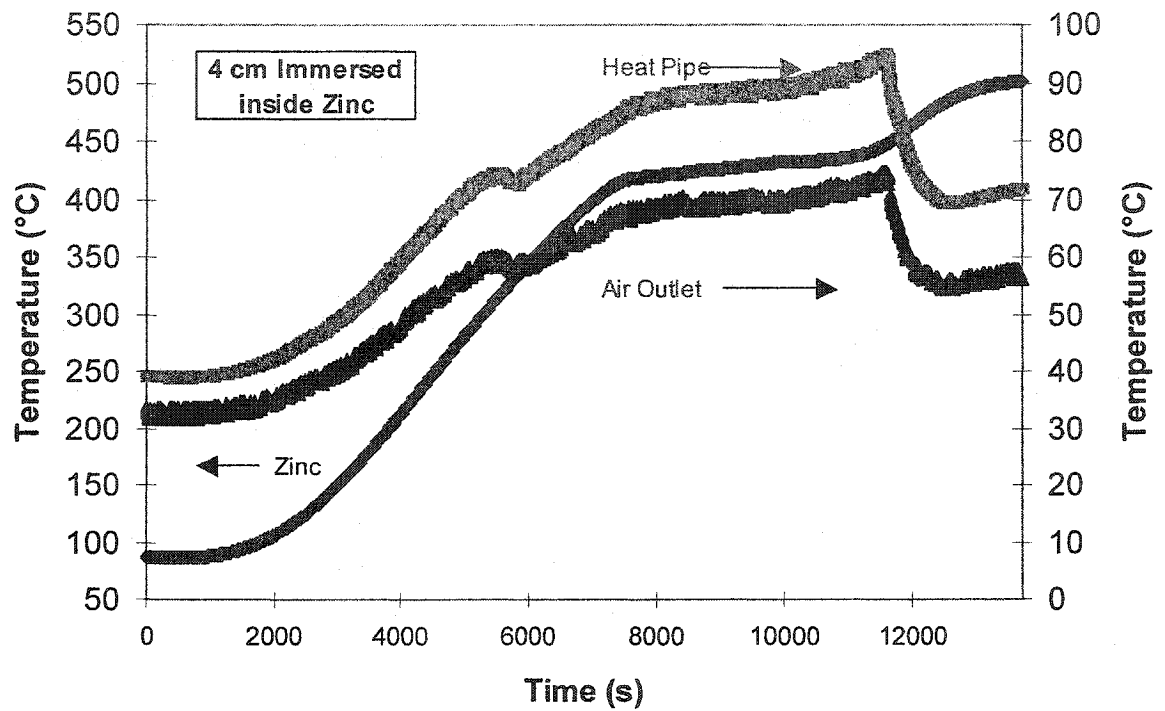
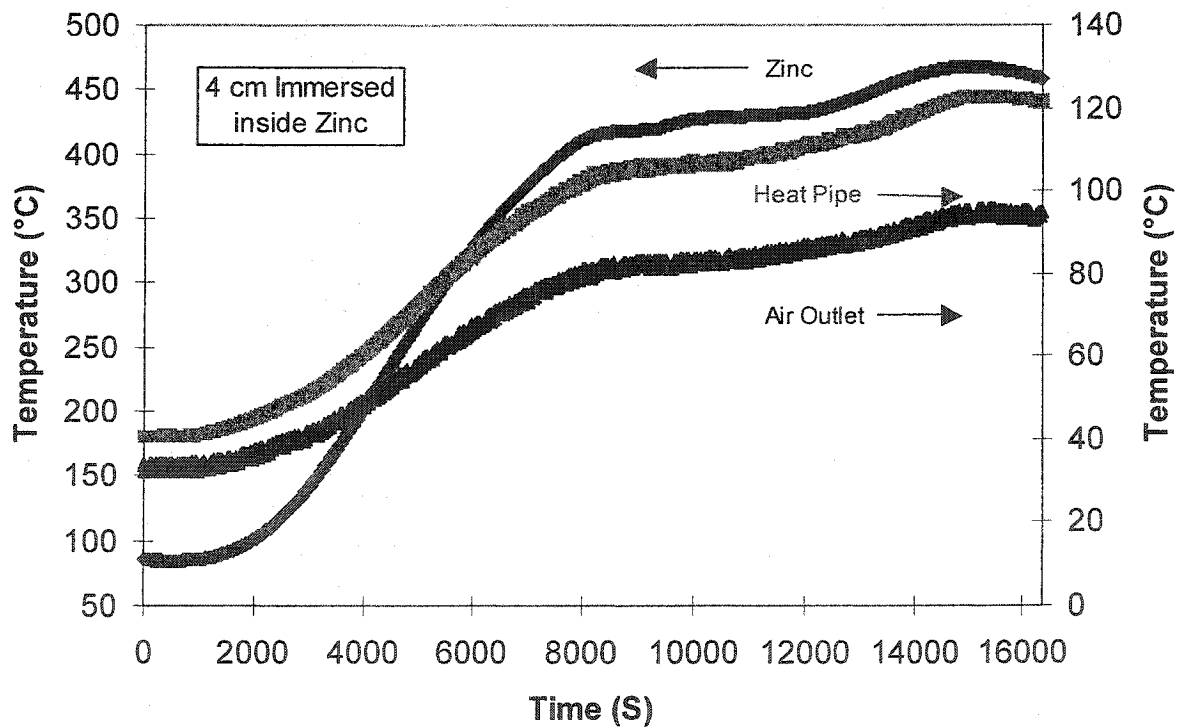Figure 7-23. Heating of Conventional Pipe (4 cm) in Zinc

Figure 7-24. Heating of Modified Heat Pipe (4 cm) in Zinc.

Similar tests for immersions of 5 cm were also performed. The results for the conventional pipe are shown in Figure 7-27. The effect of film boiling is clear. Moreover, one can see that even as the zinc melt temperature approached 500 °C (i.e. 80 °C of superheat), the heat pipe was only at about 65 °C. The heat extraction at this point was equivalent to that when the zinc was solid and at only about 250 °C. Film boiling was fully developed when all the zinc in the bath was completely melted (438 °C).

With the heat pipe containing the flow modifier, the results shown in Figure 7-28 were obtained. Clearly, there was no film boiling in this case. In fact, heat extraction was so intense that as the interfacial resistance between the frozen zinc and the outer heat pipe wall disappeared, it was not possible to supply enough heat to the melt to sustain an increasing melt temperature.

The results from these two tests are summarized in Figure 7-29. At low zinc temperatures (~250 °C) one can see the onset of partial film boiling as the 2 curves start diverging. However, as the zinc/pipe interfacial resistance is eliminated when the zinc melts, the divergence is dramatic. The beneficial effect of the flow modifier in enhancing the boiling limit of the heat pipe is obvious.

7.3.4 Analysis and Discussion of the Results

The effect of flow modification in a heat pipe was shown by the results of Figure 7-17. As more of the heat pipe was inserted, the rate of heat extraction increased. Also notable is the fact that because the melt temperature was decreasing during this period, the rate of heat extraction did not increase in proportion to the increase in area. This was expected as the temperature driving force for convection with the zinc was decreasing. Moreover, as the melt temperature decreased, a layer of zinc froze on the pipe. This created an interfacial resistance, which also caused the rate of heat extraction to slow down. The equivalent results for the un-modified heat pipe (or said conventional heat pipe) are presented in Figure 7-16. One can see that when the immersion was increased from 3 cm to 4.5 cm, the total heat extraction actually decreased. This was due to the production of a thicker, more stable vapor film.
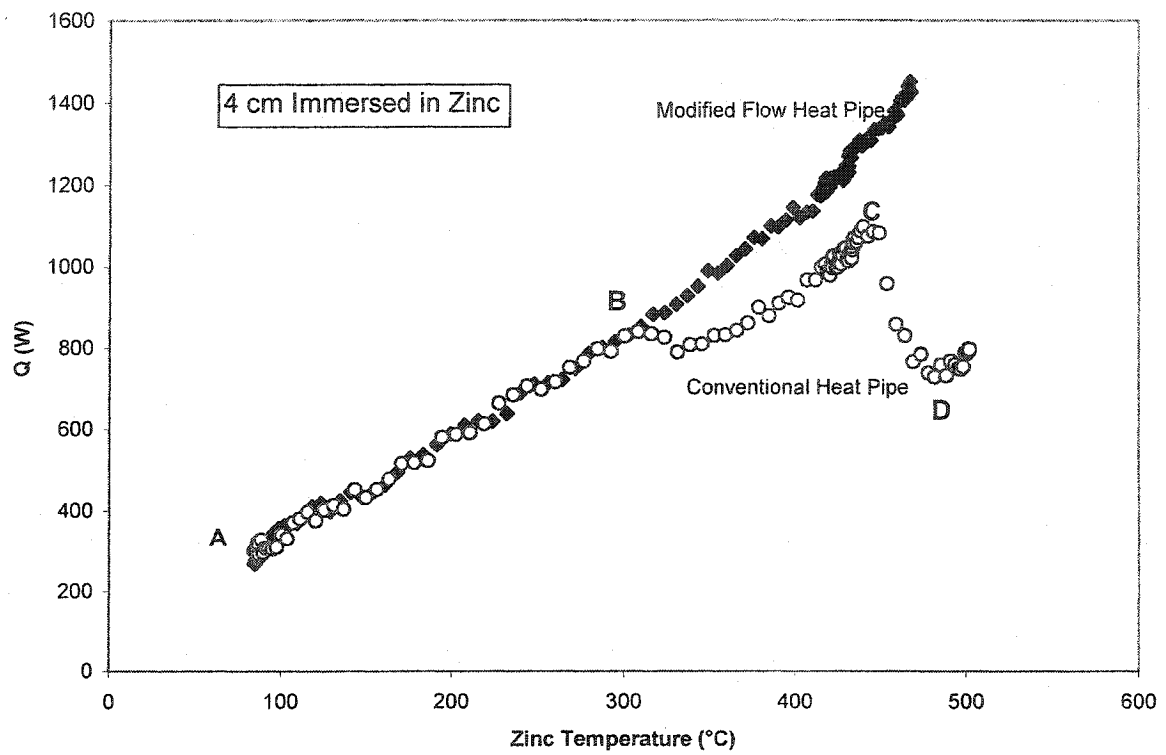
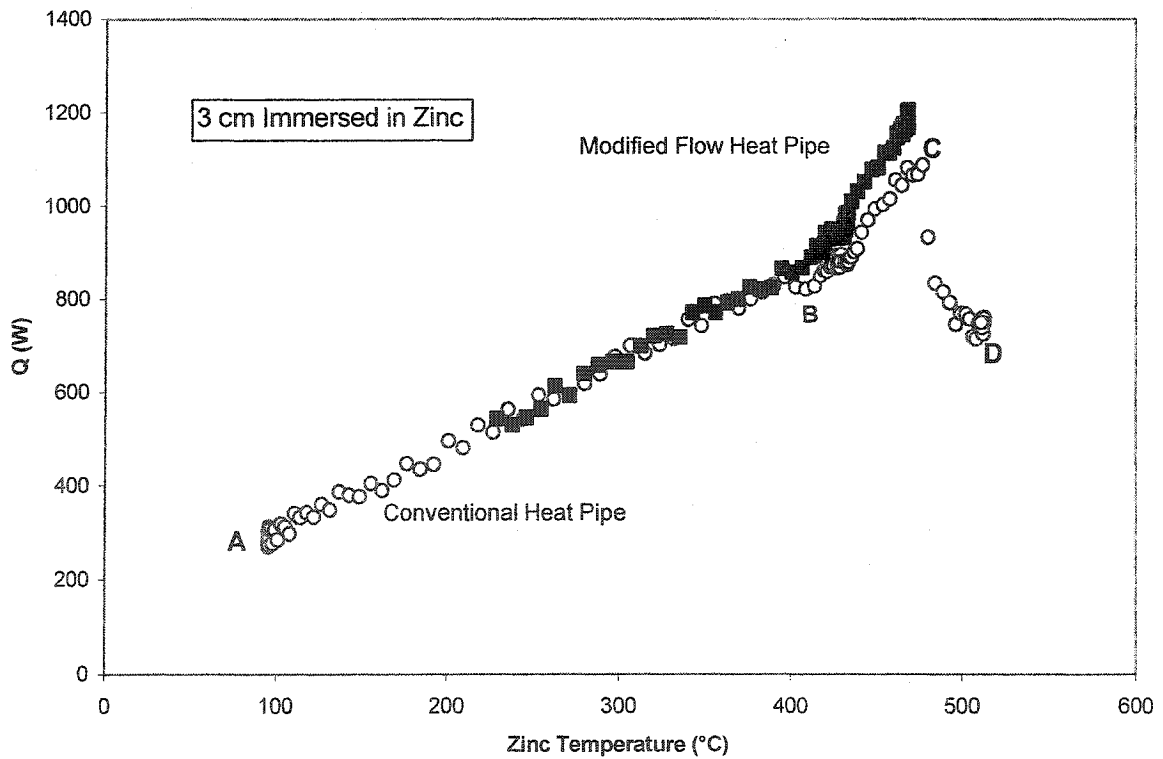Figure 7-25. Comparison of Heat Extraction for Both Heat Pipes (4 cm)

Figure 7-26. Comparison of Heat Extraction for Both Heat Pipes (3 cm).
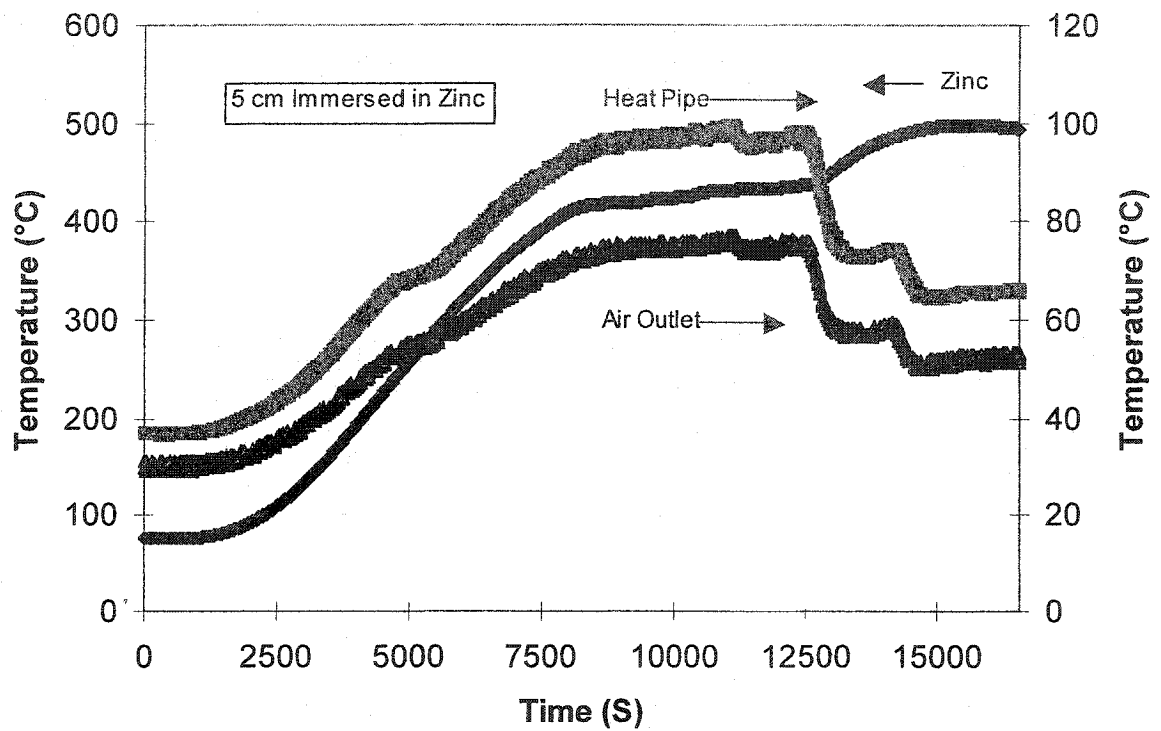
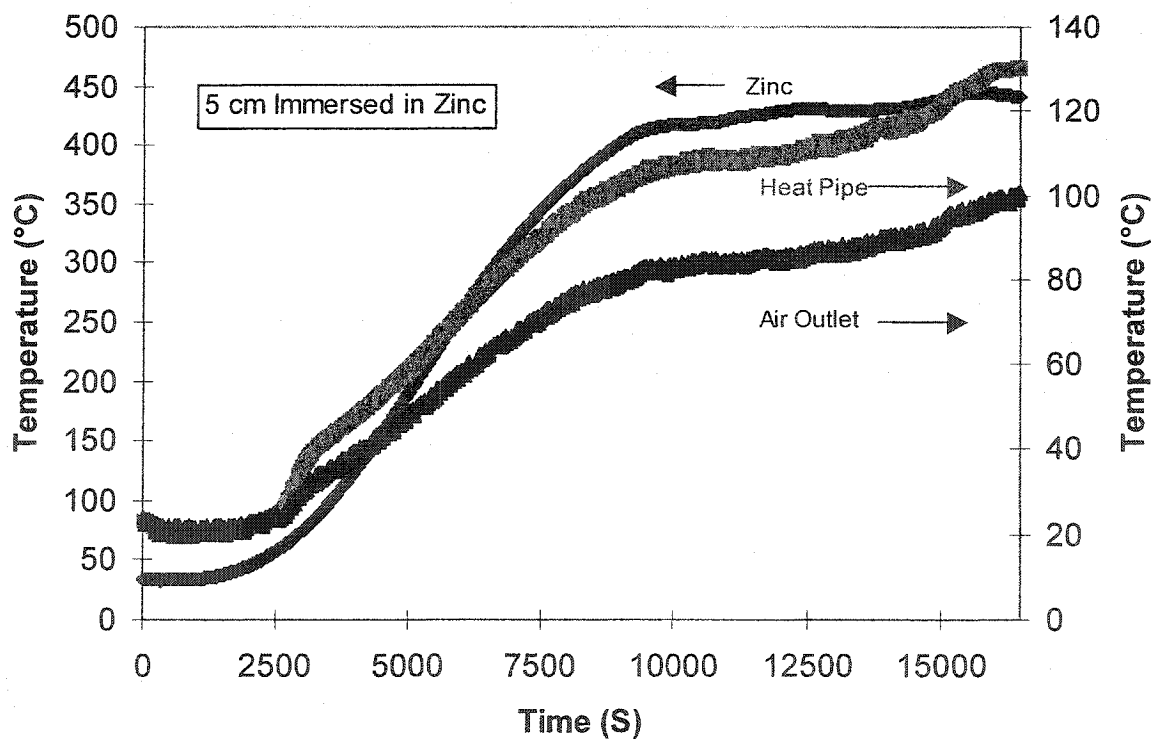Figure 7-27. Heating of Conventional Heat Pipe (5 cm) in Zinc

Figure 7-28. Heating of Modified Heat Pipe (5 cm) in Zinc
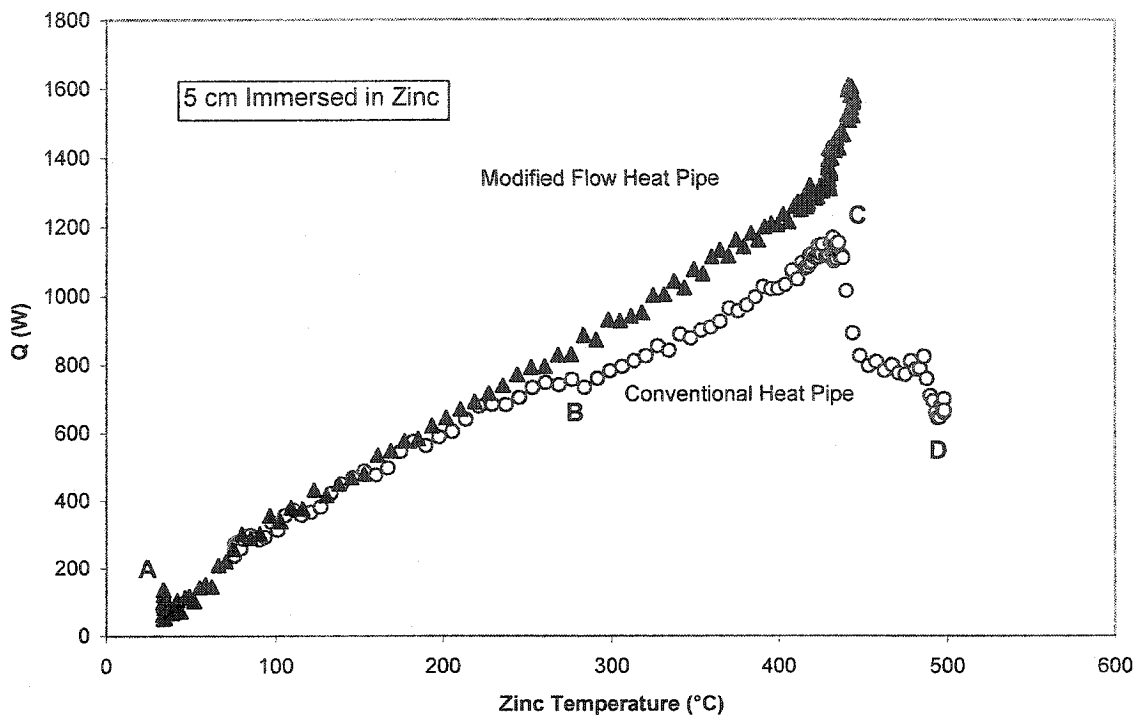
Figure 7-29. Comparison of Heat Extraction for Both Heat Pipes (5 cm)

The experiments dealing with the freezing of the heat pipes in the zinc (Figures 7-19 to Figure 7-21) are revealing and clearly illustrate whether a vapor film is present in a heat pipe unit. The greater the immersed length of pipe the greater is the temperature spike when the film collapses as can be seen from Figures 7-19 and 7-20. With the modified flow heat pipe this temperature spike does not occur as seen from Figure 7-21. This confirms that the heat pipe with flow modification did not experience film boiling.

Similar phenomena were observed when the heat pipes were first frozen in the zinc and then reheated. Figures 7-23 and 7-26 show the results for the conventional heat pipe for 4 and 5 cm immersions. As the zinc was heated, heat extraction proceeded smoothly until the zinc temperature range of 250-300 °C. The onset of film boiling was then noted as a slowing in the heating up of the heat pipe and the outlet air. Film boiling, however, intensified dramatically when the zinc was around the melting temperature. This is explained by the fact that the interfacial resistance at the zinc/pipe interface decreased at this point. As a result, the heat flux to the pipe increased sufficiently to promote a stable vapor film, which in turn caused the net heat flux to the pipe to decrease

substantially. The peak heat flux for the 5 cm immersion depicted in Figure 7-29 (Heating Model) was computed to be 736 kW/m^2. With the onset of film boiling, the heat flux dropped to about ½ this value and it did so in 2 stages.

Contrast these results to those shown in Figure 7-24 and 7-28, which were carried out under similar conditions. One will note from these results that there is no evidence of film boiling. The heat pipe and cooling air temperature curves track the zinc temperature in a smooth manner with no abrupt changes. The maximum heat flux for the 5 cm immersion was 1060 kW/m^2. This heat flux would have continued to increase with increasing melt temperature, however, the test was terminated because the zinc temperature could not be increased further. Other tests not reported here have also shown that heat fluxes in excess of 1 MW/m^2 are attainable.

The results from Figure 7-23 and 7-24 for an immersion of 4 cm are summarized in Figure 7-25. They are shown as the rate of heat extraction plotted as a function of the temperature of the zinc. It can be seen that up to a temperature of about 300 °C there is no noticeable difference between the two heat pipes. A divergence occurs at this point and persists until the melting of the zinc. As the zinc melts, the un-modified pipe shows a rapid drop in heat extraction. However, the flow modified pipe shows the opposite effect. The melting of the zinc causes an increase in the rate of heat extraction. Figure 7-26 gives a summary of the 3 cm immersion in zinc. Compared with Figure 7-25 and Figure 7-26, the curve shapes are very similar. However, the divergence happened at about 400 °C. It is almost 100 °C higher than the case of 4 cm.

Similar results for a 5 cm immersion are presented in Figure 7-29. Once again one can see the drop in heat extraction for the conventional heat pipe as the zinc melts. On the other hand, heat extraction increases dramatically for the modified heat pipe as the zinc melts. The rapid increase in heat extraction for the modified pipe illustrates how much of an interfacial resistance exists at the solid zinc/pipe interface. As the zinc is melted, this resistance is eliminated (or dramatically reduced) with the result that heat extraction increases greatly. Thus, it is evident that one can easily study interfacial resistances with this technique, which includes using a modified heat pipe.

The same results were classified and presented in Figure 7-30 and Figure 7-31. These illustrated the change that occurs as the length immersed in the zinc is changed.

If one measures the slopes of the flow modified heat pipe results shown in Figure 7.31, one finds that the rate of heat extraction is on average about 3 times (slopes ratio = 6.6/2.2) that before the elimination of the resistance for the 3 cm immersion. In the case of the 5 cm immersion, the slope after melting of the zinc is about 6.6 times that before melting (slopes ratio = 21/3.2). Clearly, these results show that the size of the resistance is appreciable and variable.

Film boiling in closed, water-cooled systems can greatly limit the rate of heat extraction. The critical heat flux (CHF) values for open systems are substantially larger than the CHF's for closed confined systems. Thus, one must be cautious when defining the boiling limit (i.e. CHF) for a conventional heat pipe. If a heat pipe system attains the critical heat flux while in transient mode (i.e. still heating up), the heat flux will start declining and the wall temperature will accelerate to higher values. This will continue until steady state is attained. Under such a condition, the heat pipe wall will run hot while the interior of the heat pipe will run cold and the rate of heat extraction will be relatively low.

The flow modified heat pipe, incorporating a twisted tape insert, overcomes the above deficiencies by stripping the vapor film from the walls of the heat pipe. In this way, the heat pipe can be viewed as operating in the forced convection domain. As a result, this pipe can be operated at heat fluxes that can be up to an order of magnitude greater than those typically associated with a water-based, conventional heat pipe.

These comparative tests in the laboratory have confirmed these findings. Flow modification in heat pipes has been shown to be viable and of practical importance. Heat pipe systems that are susceptible to film boiling can be readily modified to allow for the extraction of heat fluxes that are much greater than those attainable with conventional heat pipes. Moreover, flow modification in a heat pipe can provide an extra degree of security with respect to the integrity of the heat pipe when operated in harsh environments.
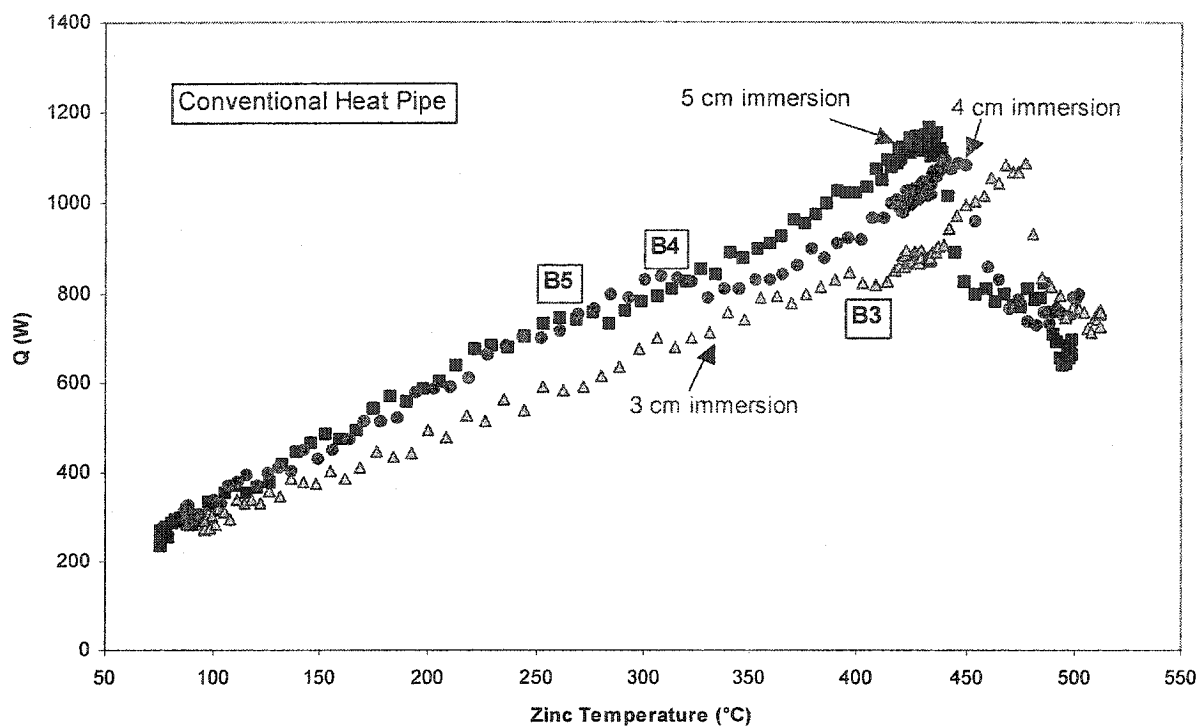
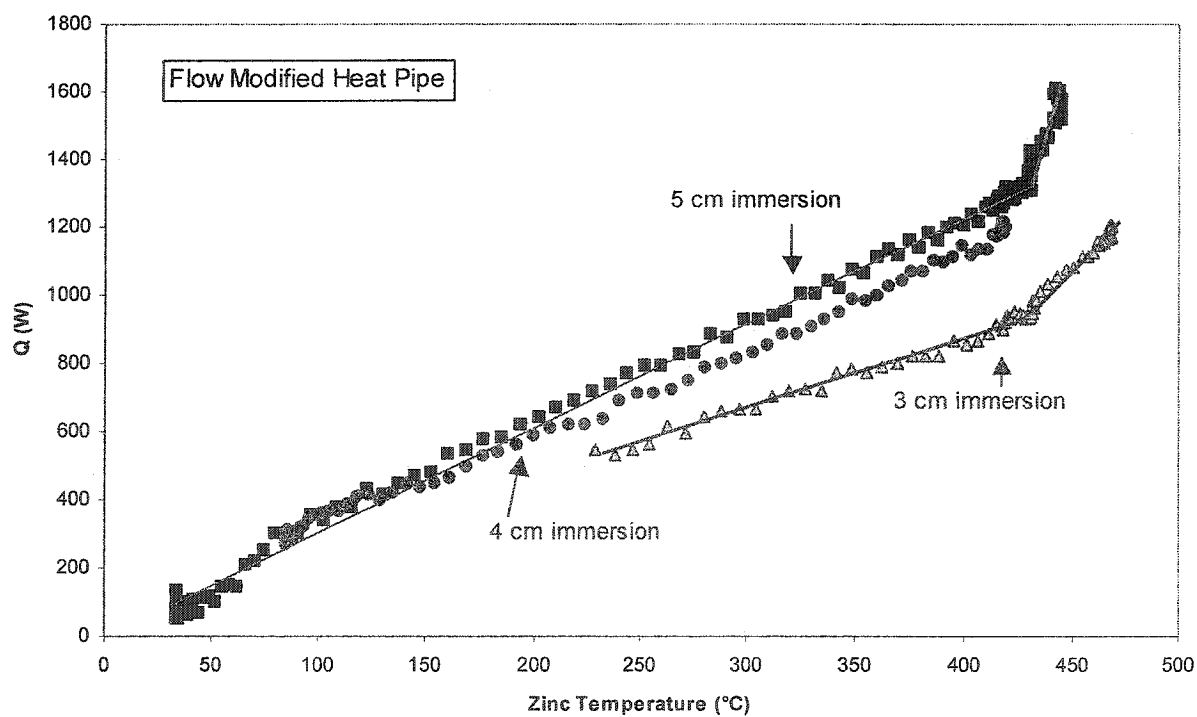Figure 7-30. The Comparison of Conventional Heat Pipe in Various Immersion

Figure 7-31. The Comparison of Flow Modified Heat Pipe in Various Immersion

7.4 Calculation of Heat Transfer Coefficient

The swirl flow caused by a twisted tape insert leads to a substantial increase in CHF. Many publications have reported experimental results for various conditions of heat and mass transfer [12-15].

Manglik and Bergles [6] proposed a Mean Nusselt Number for turbulent flow heat transfer with twisted-tape inserts. A strategy similar to that used for the friction factor was employed. This is consistent with the fundamental premise of the heat and momentum transfer analogy. Their data is for y = 2.5—6.0, and the hydraulic diameter Reynolds number Re_{dh} = 300—100,000. The average Nusselt number ratio for turbulent flow in this range is:

$$(Nu/Nu_{y=\infty}) = [1 + 0.769/y] \tag{7.1a}$$

Where,

- Twist ratio: $y = H/d$, H is the pitch for every 180° twist (see Figure 7-2), while d is twisted tape width (if it fully fixed in the tube, it is the tube inner diameter);

- Nusselt number for a straight tape insert ($y = \infty$):

$$Nu_{y=\infty} = 0.023\,Re^{0.8}\,Pr^{0.4}\left(\frac{\pi}{\pi - 4\delta/d}\right)^{0.8}\left(\frac{\pi + 2 - 2\delta/d}{\pi - 4\delta/d}\right)^{0.2}\Phi \tag{7.1b}$$

δ = thickness of twisted tape, m

$\Phi = (T_b/T_w)^m$ or $(\mu_b/\mu_w)^n$, n = 0.18 for liquid heating, 0.3 for liquid cooling.

m = 0.45 for gas heating and 0.15 for gas cooling.

μ_b = fluid dynamic viscosity at bulk fluid temperature, kg/m s

μ_w = fluid dynamic viscosity at tube wall, kg/m s

Combining 7.1a and 7.1b, we obtain:

$$Nu = 0.023\,Re^{0.8}\,Pr^{0.4}\left(\frac{\pi}{\pi - 4\delta/d}\right)^{0.8}\left(\frac{\pi + 2 - 2\delta/d}{\pi - 4\delta/d}\right)^{0.2}\left[1 + \frac{0.769}{y}\right]\Phi \tag{7.2}$$

The twisted tapes are generally classified as swirl flow devices and are a part of the general area of confined swirl flows [5]. The insertion of a twisted tape improves the

heat transfer characteristics of a heat tube. This heat-transfer enhancement can be attributed to the following four twisted-tape effects [12]:

(i) Reduction of the hydraulic diameter.

(ii) Blockage of the tube flow cross-sectional area resulting in increased flow velocity.

(iii) Helically swirling fluid motion has longer flow path, which increases flow velocity.

(iv) Secondary flow motions also increase flow path and thus increase flow velocity.

From hydrodynamic considerations, the flow field is significantly influenced by the tube blockage, increased flow path, and secondary fluid circulation. The tape insert increases the wetted perimeter, reduces the flow cross-sectional area, and, because the fluid has to follow a partitioned, twisting path, it increases the flow length. Furthermore, due to the helically rotating fluid flow, a centrifugal force is superimposed over the longitudinal flow, which produces secondary motion. The net effect is that higher pressure drops and heat transfer coefficients are obtained in comparison with those for equivalent smooth tube flows [5].

7.4.1 Reduction of Hydraulic Diameter

Insertion of the tape divides the circular flow path, which results in a hydraulic diameter d_h smaller than the tube inner diameter d.

$$d_h = d \frac{1-(4\delta/\pi d)}{1+(2/\pi)[1-(\delta/d)]} \qquad (7.3)$$

If this hydraulic diameter is used instead of the tube diameter as the characteristic length in dimensionless numbers of the Dittus and Boelter correlation [16], the following expression is obtained.

$$Nu = 0.023 \, \mathrm{Re}^{0.8} \, \mathrm{Pr}^{0.4} \left[\frac{1+\dfrac{2}{\pi}\left(1-\dfrac{\delta}{d}\right)}{1-(4\delta/\pi d)} \right]^{0.2} \qquad (7.4)$$

212

Where the tube diameter is used for the characteristic length in Nu and Re and the superficial velocity for an empty tube is used to calculate Re given in:

$$Re = Vd/v \qquad\qquad (7.5)$$

7.4.2 Velocity Increase due to Blockage

For a constant flow rate, when the heat pipe reaches a steady-state, the insertion of a tape decreases the flow cross-sectional area which increases the flow velocity. For a tube with a twisted-tape insert, the velocity V_{bl} is related to that for an empty tube by the following equation [12]:

$$V_{bl} = V_{emp}\left[\frac{1}{1-(4\delta/\pi d)}\right] \qquad\qquad (7.6)$$

Taking into consideration this increase in flow velocity due to blockage, equation (7.4) becomes:

$$Nu = 0.023\,Re^{0.8}\,Pr^{0.4}\left[\frac{1+\dfrac{2}{\pi}\left(1-\dfrac{\delta}{d}\right)}{1-(4\delta/\pi d)}\right]^{0.2}\left[\frac{1}{1-(4\delta/\pi d)}\right]^{0.8} \qquad\qquad (7.7)$$

7.4.3 Velocity Increase due to Helical Flow

Compared to an axially straight flow, a swirling flow passes through a longer flow path. This increase in flow path is proportional to the degree of twist, and a longer flow path leads to a higher relative flow velocity along the tube wall. Assuming the flow to be composed of stream lines parallel to the contact line Ls described by the edge of the tape in contact with the wall, the resultant vector diagram in Figure 7-32 is used to compute the following increase in flow velocity due to the helical flow.

$$V_s = V_{emp}\left[\frac{1}{1-(4\delta/\pi d)}\right]\left[1+\left(\frac{\pi}{2y}\right)^2\right]^{\frac{1}{2}} \qquad\qquad (7.8)$$
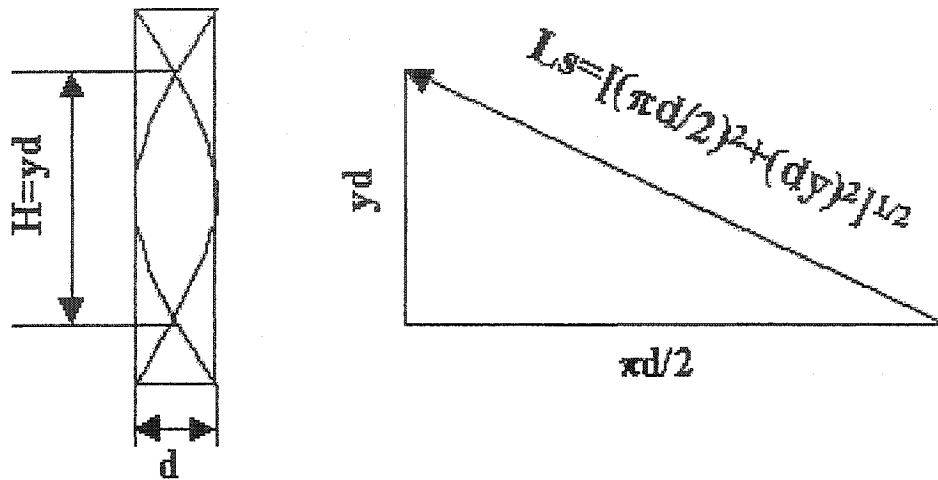
Figure 7-32. Increased Flow Length due to Helical Flow

Fujita and Lopez [12] cited and confirmed the above relationship. An increase in flow velocities leads to improved heat transfer. Modifying equation (7.7) to include the effects of the helical flow gives equation (7.9).

$$Nu = 0.023\,\mathrm{Re}^{0.8}\,\mathrm{Pr}^{0.4}\left[\frac{1+\dfrac{2}{\pi}\left[1-\dfrac{\delta}{d}\right]}{1-(4\delta/\pi d)}\right]^{0.2}\left[\frac{1}{1-(4\delta/\pi d)}\right]^{0.8}\left[1+\left(\frac{\pi}{2y}\right)^2\right]^{0.4} \qquad (7.9)$$

7.4.4 Velocity Increase due to Secondary Flow

From a numerical analysis of swirl flow, Fujita and Lopez [12] also predicted that, as twisted ratio becomes smaller, two vortices would form in each partition on either side of the tape insert, Manglik and Bergles [5] observed this secondary flow motion. Figure 7.33a and 7.33b show their findings that, as Re increases and r decreases, one vortex in a partition becomes two vortices. Similar phenomena were also observed by other researchers [12].

214

TAPE INDUCED SWIRL MOTION

BUOYANCY DRIVEN CIRCULATION

(a)   (b)   (c)
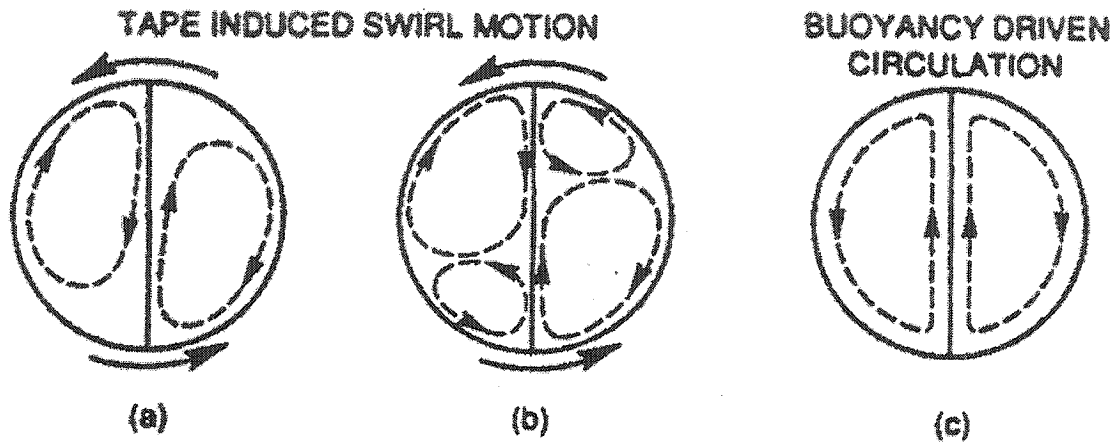
Figure 7-33. Secondary flow due to (a) tape twist at low Re or moderate twist ratios, (b) tape twist at high Re or small twist ratios, and (c) buoyancy driven free convection

The secondary circulation, which causes transverse fluid transport across the partitioned duct cross section, is qualitatively shown in Figure 7.33a for a low Reynolds number flow with a tape of moderate twist pitch. For a smaller, or a higher velocity, this circulation breaks up into two nonsymmetrical, counter-rotating vortices, shown in Figure 7.33b. However, at very low flow rates, swirl may not set in and the fluid simply follows a twisted path. In such situations, the flow resistance increases due to the tape thickness and longer flow path. In the limit when either m $\to$ 0, or $y \to \infty$, the duct geometry effectively becomes partitioned into two semi-circular segments and there is no secondary circulation, and undisturbed streamline fluid motion prevails.

Assuming that there are two vortices in a partition and the vortices divide the cross section equally, then one vortex imposes a velocity component along a quadrant of the tube as shown in Figure 7-34 [12]. If ones further assumes one complete circulation of a vortex for every 360° tape twist, that is, every two twist pitches, then the following expression for the secondary flow velocity is obtained.

$$V_{2s} = V_{emp} \left[\frac{1}{1 - (4\delta/\pi d)} \right] \left[1 + \left(\frac{\pi}{2y} \right)^2 + \frac{1}{4y^2} \left(\frac{\pi}{4} + 1 \right)^2 \right]^{\frac{1}{2}} \qquad (7.10)$$
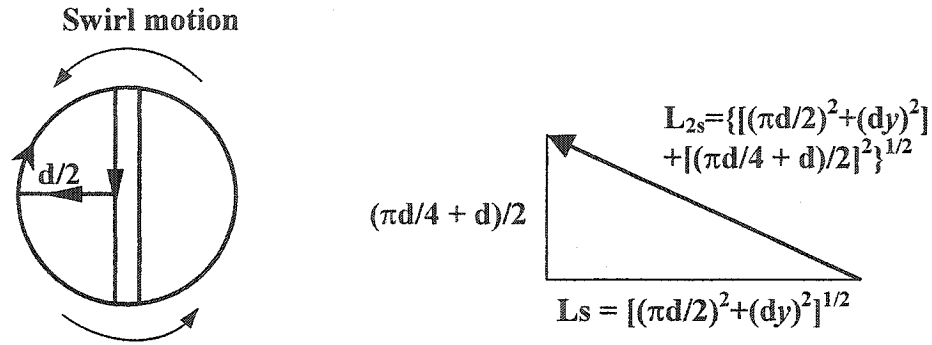
Figure 7-34. Increased Flow Length due to Secondary Flow

The increase in flow velocity due to secondary flow motion also results in higher heat transfer coefficients. Secondary flow motion effects are included in the following expression for heat transfer.

$$Nu = 0.023 \, \text{Re}^{0.8} \, \text{Pr}^{0.4} \left[\frac{1 + \frac{2}{\pi}\left(1 - \frac{\delta}{d}\right)}{1 - (4\delta/\pi d)} \right]^{0.2} \left[\frac{1}{1 - (4\delta/\pi d)} \right]^{0.8} \left[1 + \left(\frac{\pi}{2y}\right)^2 + \frac{1}{4y^2}\left(\frac{\pi}{4} + 1\right)^2 \right]^{0.4} \quad (7.11)$$

7.4.5 Overall Heat Transfer Enhancement

In our particular experimental case, the twisted tape had the following parameters:

H = 11 cm

d = 1.885 cm

δ = 0.2 cm

y = 11 cm / 1.885 = 5.83.

Table 7-1 gives some Pr number data for saturated water in the regime of heat pipe operation. For a particular temperature, equations (7.2), (7.4), (7.7), (7.9) and (7.11) can be simplified into:

$$Nu = a \, \text{Re}^{0.8} \quad (7.12)$$

Figure 7-35. Comparison of Constant--a of Various Equations for Liquid

Figure 7-36. Comparison of Constant--a of Various Equations for Vapor

217

Table 7-1. Pr Number of saturated Water [16]
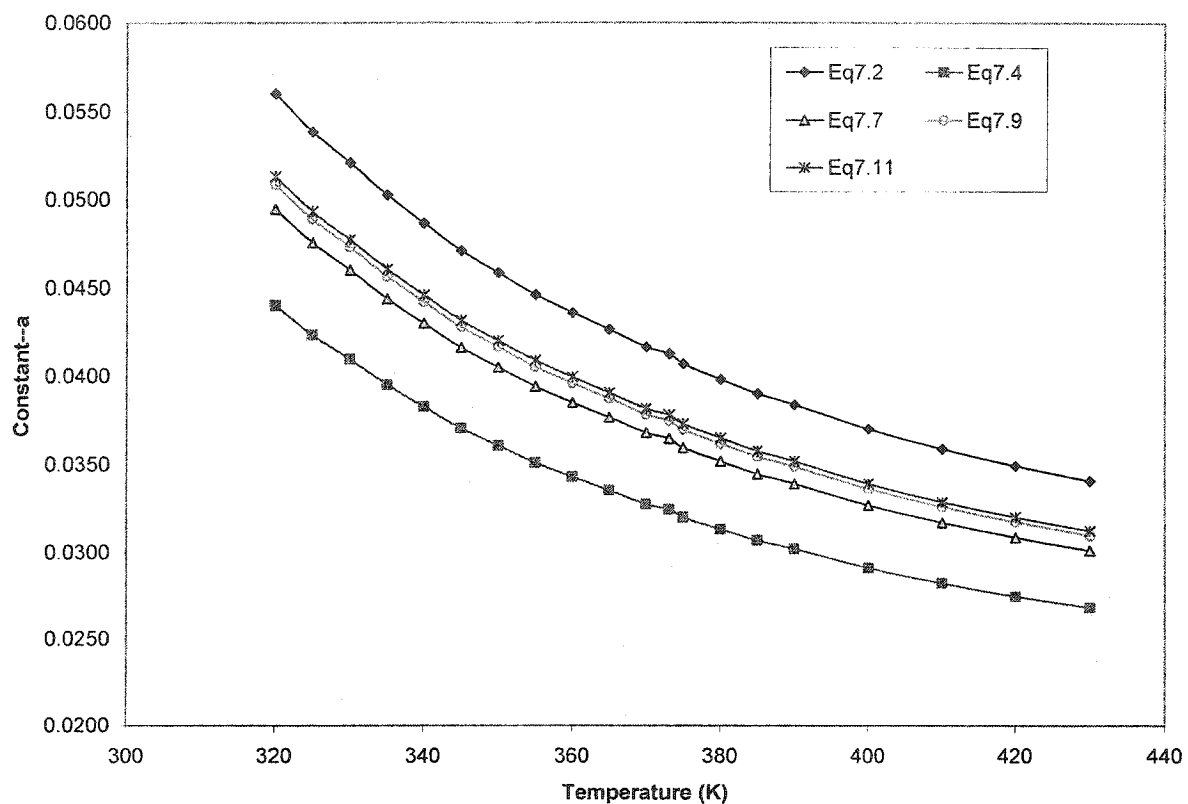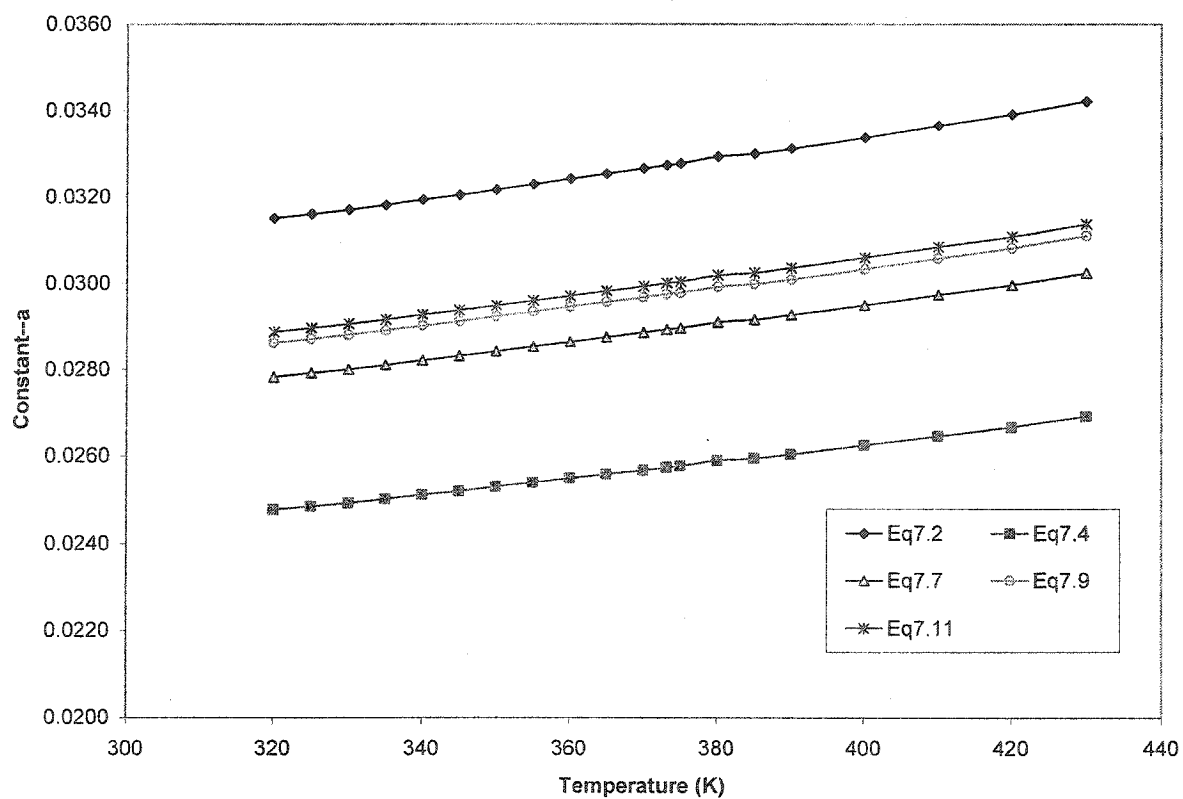
Temperature (K)	Pr Number (Liquid)	Pr Number (Vapour)	Temperature (K)	Pr Number (Liquid)	Pr Number (Vapour)
320	3.77	0.894	370	1.80	0.978
325	3.42	0.901	373.15	1.76	0.984
330	3.15	0.908	375	1.70	0.987
335	2.88	0.916	380	1.61	0.999
340	2.66	0.925	385	1.53	1.004
345	2.45	0.933	390	1.47	1.013
350	2.29	0.942	400	1.34	1.033
355	2.14	0.951	410	1.24	1.054
360	2.02	0.960	420	1.16	1.075
365	1.91	0.969	430	1.09	1.10

One will note that Φ in equation (7.2) wasn't considered in subsequent calculations. Thus, 'a' is a constant, which only relates to temperature. The constant-a for the related equations (7.2), (7.4), (7.7), (7.9) and (7.11) were calculated, and separated into two groups- liquid and vapour. The cumulative effects of the five heat transfer enhancement mechanisms of twisted tape inserts are shown in Figure 7-35 and Figure 7-36. Examination of Figure 7-35 and Figure 7-36 reveals that the empirical correlation of Manglik and Bergles (equation (7.2)) leads all other equations, in that it presents the highest level of heat transfer enhancement. The effects of flow velocity are increased by hydraulic diameter, blockage, helical flow and secondary flow. On the other hand, although the secondary flow motion contributes to heat transfer enhancement, this contribution is negligible since the curves of helical flow and secondary flow are very close.

Fujita and Lopez [12] observed that the decrease in hydraulic diameter given by equation (7.4) is the greatest contributing factor to the heat transfer enhancement shown in Figure 7-37. This effect and the effect of the increase in flow velocity due to blockage given by equation (7.7) are independent of twist ratio. On the other hand, although the contributions to heat transfer of helical flow and secondary flow motion as given by

equation (7.9) and (7.11) respectively increased with decreasing twist ratio, for $y \geq 10$, these contributions are negligible.
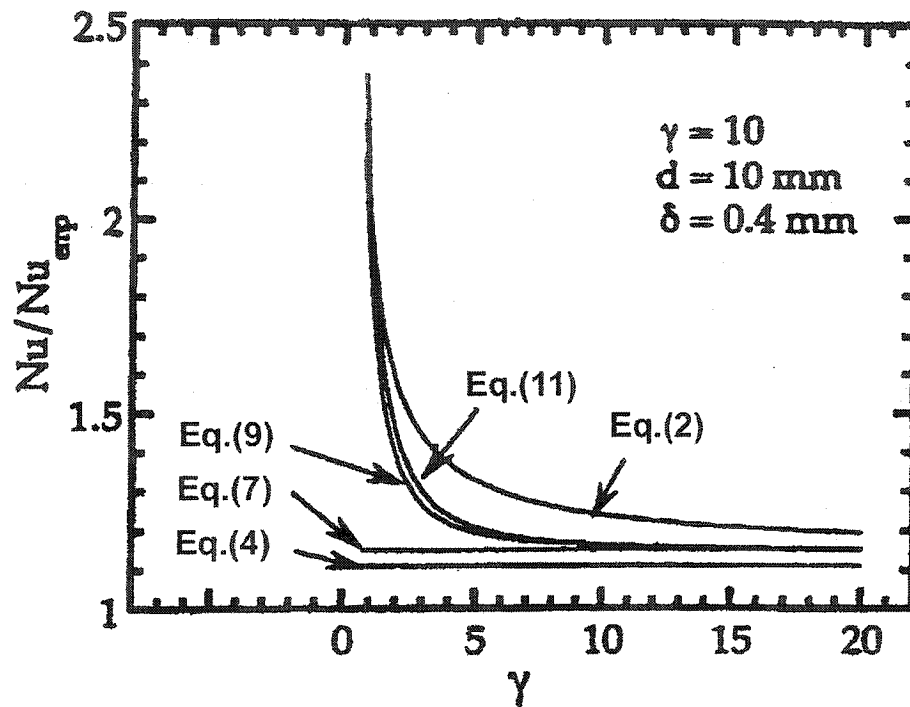
Figure 7-37. Predicted Heat Transfer Enhancement as a Function of Twist Ratio

7.4.6 The Mathematical Modeling of Heat Transfer Coefficient

As an approximation, the vapour temperature inside the heat pipe is the operating temperature of the heat pipe. First, let's revisit the heat extraction situation, as discussed in a previous section. For the various immersion lengths, Figure 7-38 illustrates the relations of different equations vs the heat pipe temperature. From this diagram, we can see the changes of the constant a are very small for each particular equation. Therefore, the average values are used to calculate equation (7.12). These average values are listed in Table 7-2.

Manglik and Bergles [5] presented a flow regime map for 4 regions (I to IV) of flow speed, as shown in Figure 7-39 [5] where, once again, the thermal behaviour is qualitatively illustrated for the four flow regimes. The phenomenological descriptions for each flow regime are as follows:

Table 7-2. The Average Values of Equations

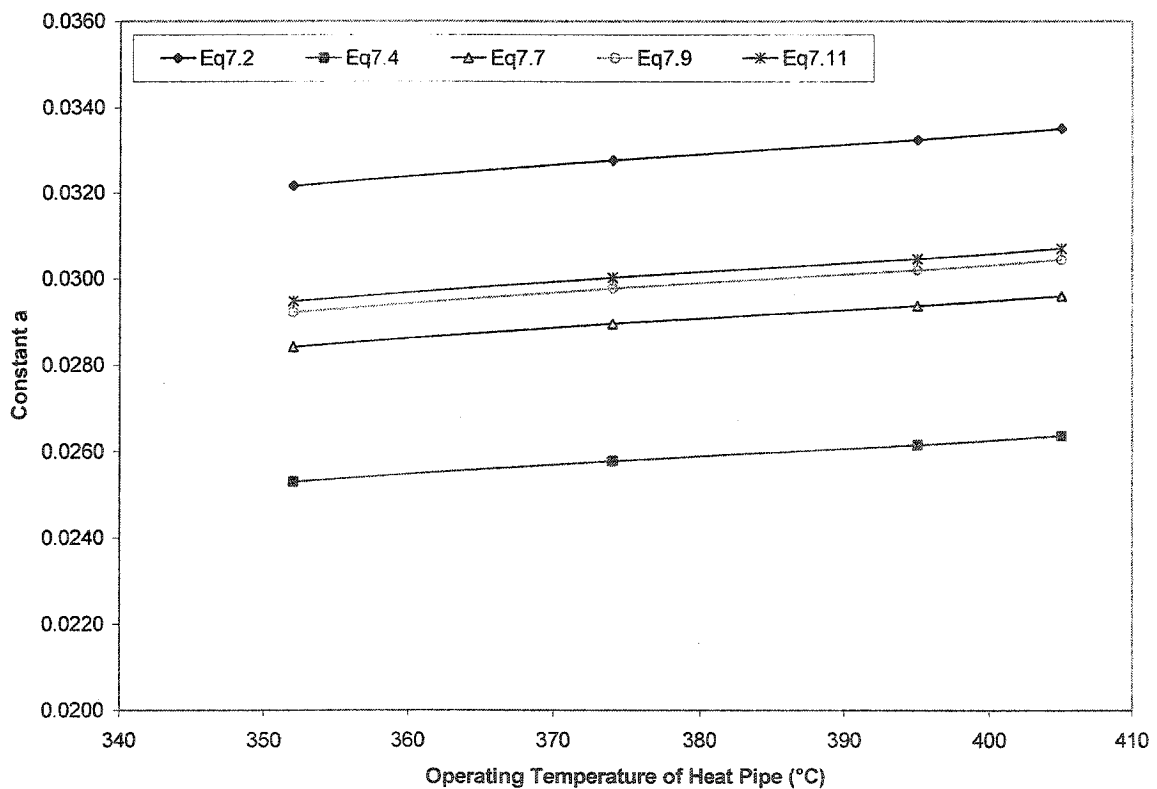| Immersion length	Temperature (K)	Eq7.2	Eq7.4	Eq7.7	Eq7.9	Eq7.11
2	352	0.0322	0.0253	0.0284	0.0292	0.0295
3	374	0.0328	0.0258	0.0290	0.0298	0.0300
4.5	395	0.0332	0.0261	0.0294	0.0302	0.0305
6	405	0.0335	0.0264	0.0296	0.0304	0.0307
Average constant		**0.0329**	**0.0259**	**0.0291**	**0.0299**	**0.0302**

Figure 7-38. The Relation of Constant a with Heat Pipe Operating Temperature

- Region I   Viscous flow; thermally developing boundary layer with superimposed buoyancy-driven secondary flows in the presence of large wall-to-bulk ΔT; tube flow blockage.

- Region II   thermally developed swirl flow; centrifugal forces due to the twisted tape wipe out free convection effects; tape induced secondary motion, longer flow path, and tube blockage.

- Region III   Swirl-turbulent transition; competing effects of centrifugal forces and turbulent pulsations, with the former tending to dampen the latter instability; diminishing swirl flow effects.

- Region IV   Fully developed turbulent swirl flow; increased flow velocity due to tube blockage and swirl mixing.
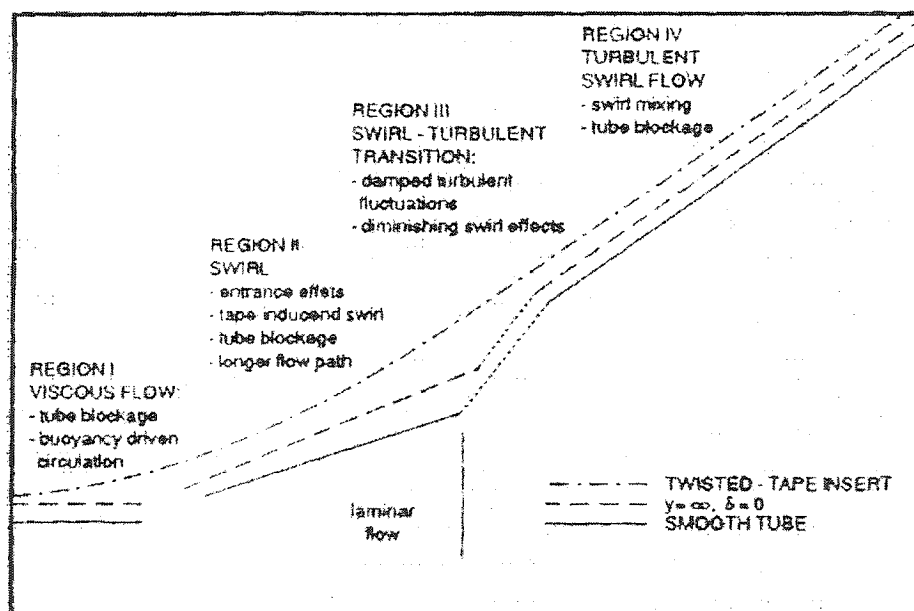
Figure 7-39. Flow Regime Map for Nusselt Number in the Flows with Twisted-Tape Insert

The calculation results using equation (7.12) are presented in Figure 7-40. Comparing Figure 7-40 with Figure 7-39, it is clearly indicated that the experimental results fall into Region III—swirl turbulent and the heat pipe temperatures are used to estimate the constant a.

In this continuous experiment shown in Figure 7-17, the liquid zinc temperature dropped from 480 to 430 when the heat pipe was immersed into the liquid zinc. The average temperatures of liquid zinc are 465.5 (2 cm), 448.5 (3 cm), 436 (4.5 cm), and 430 (6 cm), respectively. The average inner wall temperatures of the evaporator are about 358

°C (2 cm), 340 °C (3 cm), 338 (4.5 cm), and 344 °C (6 cm), respectively. The Nu number and Re numbers calculated by these results are shown in Figure 7-41.

We summarized the Re numbers in the changing regime for particular immersion lengths in Table 7-3. The biggest gap for the five equations is 3 cm while the smallest is for 6 cm.

Table 7-3. The Re Number Region In Various Immersion Lengths

Immersion length	Temperature (K)	Changing Region of Re Number
2	352	$30 \times 10^5 \sim 40 \times 10^5$
3	374	$37 \times 10^5 \sim 50 \times 10^5$
4.5	395	$9.9 \times 10^5 \sim 13 \times 10^5$
6	405	$5.6 \times 10^5 \sim 7.5 \times 10^5$
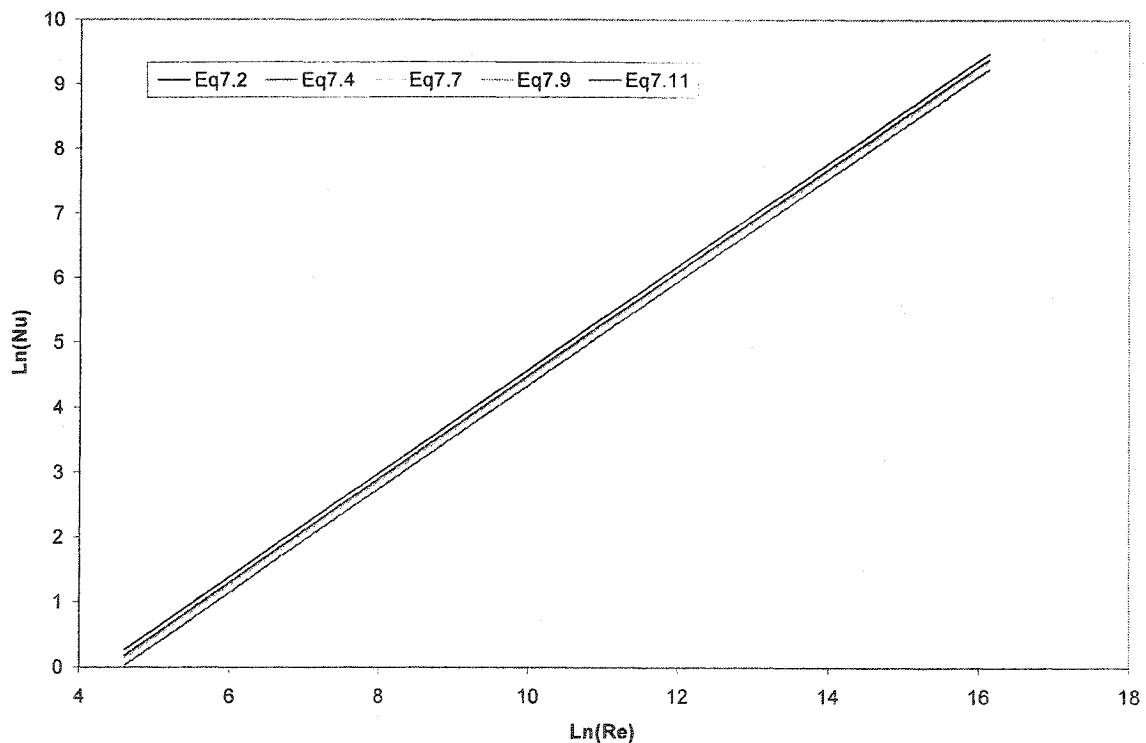
Figure 7-40. Flow Regime by Calculation Results

222

As mentioned, the heat pipe has a solid bar with 2.9 cm layer forming the bottom. The heat flux calculation only used inner bottom area of the evaporator, as shown in Figure 7-42a. As the immersion length was increased from 2 to 3 cm, the differences among five equations were big, as shown in Figure 7-41. One sees the Re number or the heat transfer benefits from swirl flow effects such as blockage, hydraulic diameter, helical flow and secondary fluid motion. When the immersion length was further increased from 4.5 to 6 cm, more heat extraction comes from the side area of the evaporator, as seen in Figure 7-42b. The swirl flow effects are smaller and smaller, as shown in Figure 7-41. It may be that those swirl flow effects have been cancelled out by the side flow generated by the side extracting heat. It was also indirectly proven in the experiment, dealing with heat pipe startup. When the immersion length of an operating heat pipe is increased suddenly from 2 cm to 8 cm, the heat transfer model switches from nucleate boiling to film boiling.

Figure 7-41. Calculated Re Number Based on Experimental Data

Experimental Re Number also can be calculated by 7.5. That is

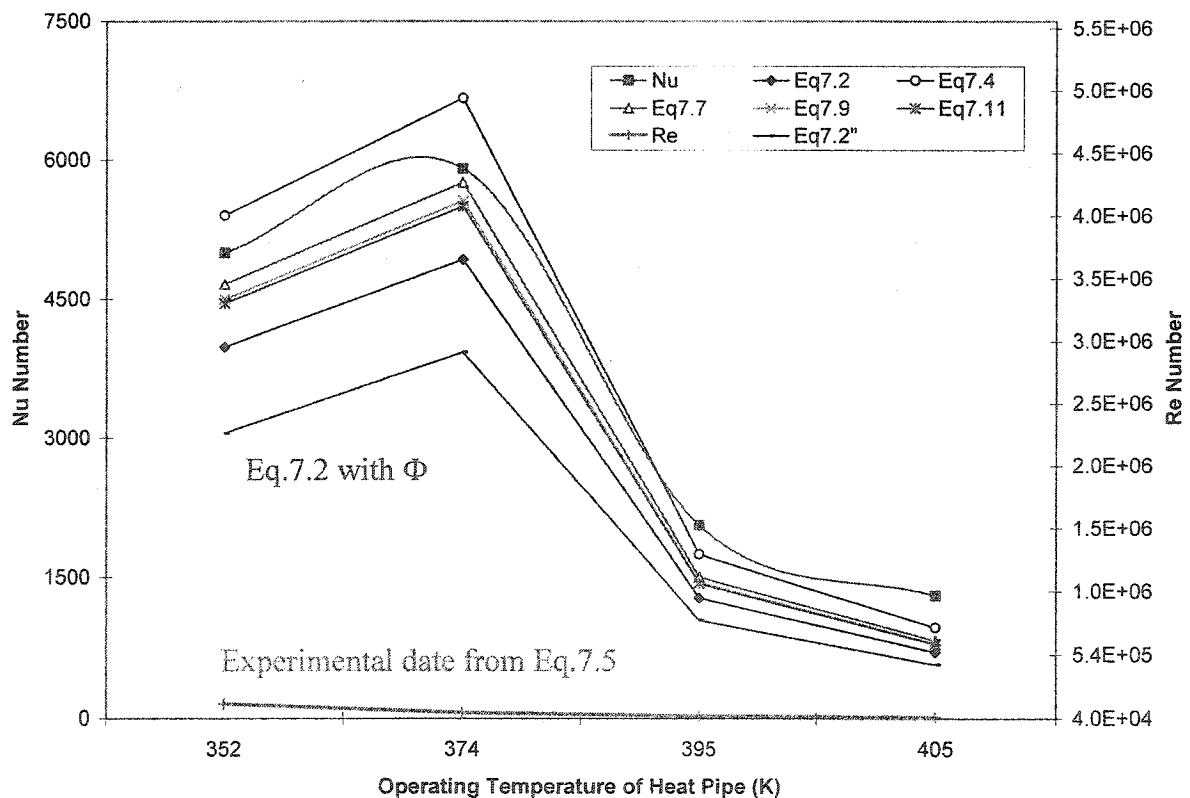$$Re = \frac{Vd}{v} = \frac{(\dot{m}/A\rho)d}{v} = \frac{4\dot{m}}{\pi d\rho v}$$

a. Only Bottom Area   b. Side and Bottom Area
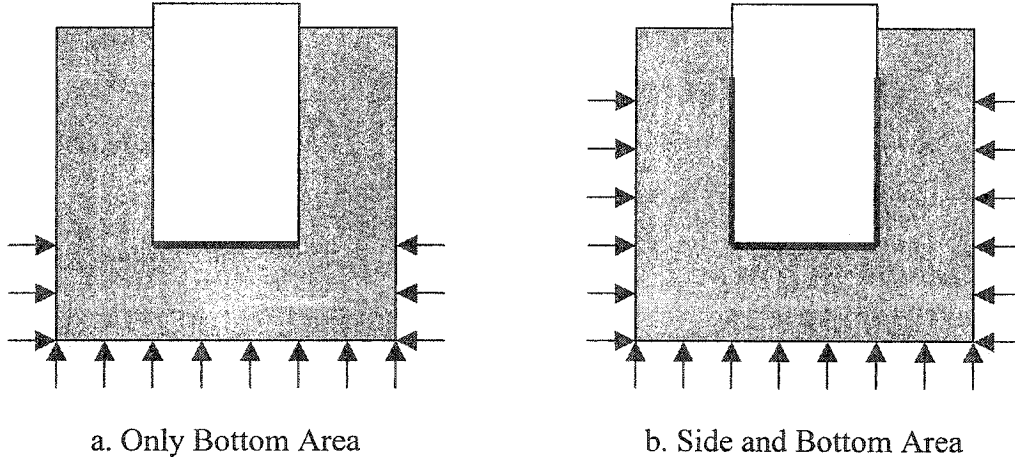
Figure 7-42. Heat Transfer Area in Evaporator

The mass flow rate m can be determined using:

$$Q_{exp} = \dot{m}C_{pl}\Delta T_l + \dot{m}\bar{h}_{special} + \dot{m}C_{pg}\Delta T_g$$

The operating temperature of the heat pipe is the bulk temperature of the heat pipe since the heat pipe temperature is uniform. The ΔT_l and ΔT_g are approximately equal to 0. The calculated results are displayed in Figure 7-41.

Now, it is necessary to add a correction factor Φ in equation (7.2). First find the viscosity ratio exponent because this correction factor normalizes heating and cooling effects rather well in the present study data. In the case of the temperature ratio of gas flows, the exponents have been chosen as the consensus value based on previous research [6]. The results of equation (7.2) with Φ were also presented in Figure 7-41.

Compared to all those equations in Figure 7-41, the experimental data using Equation (7.5) is the closest to results of equation (7.2) using the experimental data. However, it is still low about 10 times less than the smallest value obtained with equation (7.2) with $\Phi = (T_b/T_w)^{0.45}$. The predicted value is higher than the experimental value.

Equation (7.2) covers the swirl flow effects. Experimental data is lower than this value. There are two reasons that are responsible for this. Firstly, the swirl flow is cancelled by side heat transfer. Secondly, it may have bubbles in wick which influence the heat extraction from side-wall of the evaporator. Table 7-4 gives the heat extraction comparison of the heating up case of the heat pipe starting in frozen zinc to that of the heat pipe sliding into liquid zinc. It is clear that heat extraction for the heating up case is higher than that of the sliding-in case. Since the heat pipe was heated up as the zinc was heated, the swirl flow generated by the twisted tape has enough time to fully develop. No bubbles formed in the wick. However, the sliding-in case, the formed bubbles were cut by the swirl flow. However, some of bubbles, which were trapped in the wick, couldn't be removed due to capillary forces in the wick structure. The problem and solution method will be discussed in next chapter.
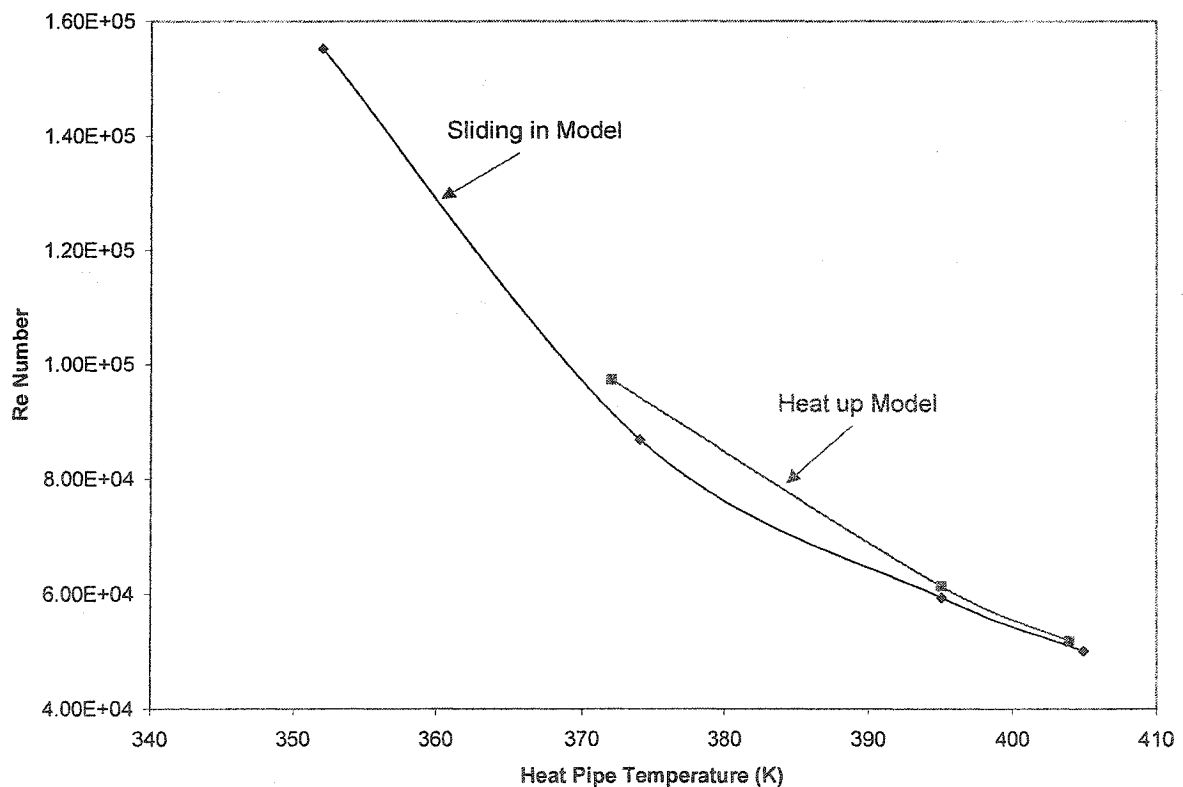
Figure 7-43. The Experimental Re Numbers in Heat up and Slide in Models

Figure 7-43 shows the Re numbers for both cases. The Re number for the heat up case is higher than that for the sliding-in case.

Therefore, It is necessary to add another correction factor α in equation (7.2). It is directly related to the effect of the side-wall of the evaporator. Here $\alpha = 2$ x ratio of inner wall area that is used to calculate heat flux to the area really touching the liquid zinc (outside area of the evaporator). Thus, equation (7.2) has been changed to:

$$Nu = 0.0329 \ Re^{0.8} Pr^{0.4} \Phi \ \alpha^{0.8} \qquad (7.13)$$

Table 7-4. The Heat Extracting Comparison of Heat up Model and Slide in Model

Heat up from frozen zinc		Slide in molten zinc	
Immersion length (cm)	Extracting heat (W)	Immersion length (cm)	Extracting heat (W)
3	1204	3	1144
4	1451	4.5	1405
5	1610	6	1560

Table 7-5 gives α values corresponding to the different immersion lengths. After substituting the α results into equation (7.13), the calculated results and experimental values were plotted in Figure 7-44. One sees the predicted values matched very well the experimental values except for the 2 cm of immersion. It is evident that equation (7.13) gives the more generalized correlation for heat transfer in turbulent swirl flow in the heat pipe. It satisfies calculation requirements.

Table 7-5. The Values of Correction Factor α

Immersion Length (cm)	2	3	4.5	6
Heat Pipe Temperature (K)	352	374	395	405
Ratio $=A_{inner}/A_{outer}$	16.3	17.7	6.65	5
α	32.6	35.4	13.3	10

With experimental data, Re number is 5.01 x 10^4 in 6 cm, where the heat pipe operating temperature is 132 °C. We have assumed the heat pipe temperature is uniform inside the whole pipe. Therefore, the working fluid temperature is also equal to 132 °C. According to equation (7.5), the mean axial velocity is:

V = vRe /d

Where V = mean axial velocity, m/s

v = kinematic viscosity, m^2/s (water = 1.13 x 10^{-6} m^2/s)

$d = d_h$ hydraulic diameter, m (=0.0104 m)

Substitution of the above values into the equation, yields:

V = 5.44 m/s

The mass flow rate of water at this velocity is calculated by:

$$\dot{m} = AV\rho = \frac{\pi d_h^2 V\rho}{4} = \frac{3.14 \times (0.0104)^2 \times 5.44 \times 1.67}{4} = 0.76 \quad g/s = 45.35 \quad g/min$$
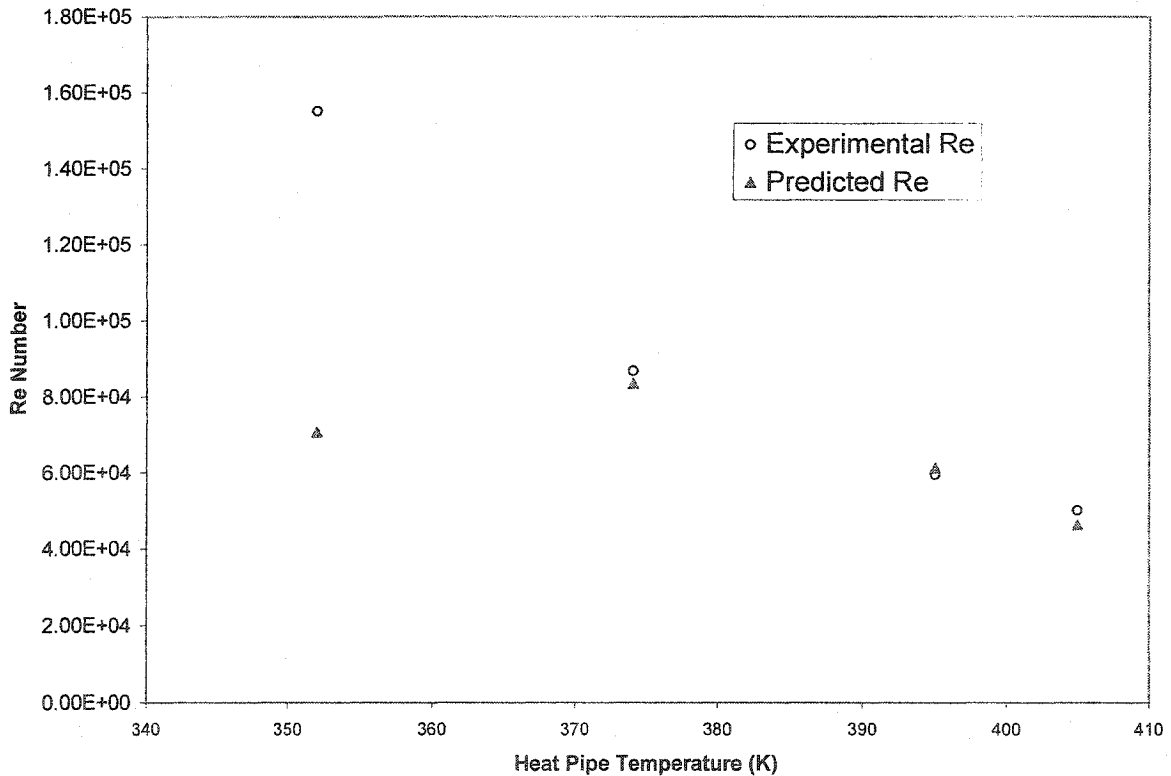
Figure 7-44. The Comparison of Experimental Values with Predicted Values

Thus, the charge of 40 g of water will completely vaporise at this high mass flow rate in 53 seconds if condensed liquid cannot be returned to the evaporator. This may lead to the dry out of the heat pipe especially in the bottom of the evaporator. In fact, it is hard to return liquid back to the bottom of the evaporator when the vapor and the condensed liquid are in the single pipe. Therefore, the new structure of the heat pipe—loop heat pipe is designed to resolve this problem and other, as mentioned in previous sections, such as start up, air bubbles trapped in the evaporator wick etc.

CHAPTER 8. CONCEPT LOOP HEAT PIPE AND TEST

8.1 Problem Review and Loop Heat Pipe Solution

The loop heat pipe has been described in detail in Chapter 3. Loop heat pipes (LHPs) are robust, self-starting, and passive two-phase thermal transport devices. LHPs are used to transport excess heat from a heat source to a low temperature heat sink, while maintaining the temperature within specified limits. A typical LHP consists of an evaporator, a reservoir (also called the compensation chamber or hydro-accumulator), vapor and liquid lines, a sub-cooler, and a condenser. The compensation chamber is thermally and hydro-dynamically connected to the evaporator. A conventional LHP uses wick capillary force or heat pump to circulate working fluid. Its transport line of condensed liquid is independent from the vapor transport line. Such advantages of LHPs compensate for the disadvantages of flow modified heat pipes, which have been discussed in the previous Chapter. Thus, LHPs were employed to overcome three main deficiencies of the Flow Modified Heat Pipe design.

- **Start up**. Since a LHP is self-starting and controllable, it is effective to eliminate the start up problem. In a flow modified heat pipe, start up is very hard since the swirl flow doesn't have enough time to develop and cut the formed film at the beginning. In controllable LHPs, the working fluid can be first held in the reservoir (compensation chamber), until the evaporator is heated up to a certain temperature, and then the liquid is added into the evaporator. Since there is no liquid in bottom of the evaporator in the beginning, the liquid flows into the evaporator and spreads all over the area of the bottom, and it quickly forms the vapor flow that is used to generate swirl flow. Therefore, it can efficiently overcome the startup problem. This applies for a working fluid with low operating temperature, such as water. In fact, since the vapor line and liquid line are independent of each other, fluid from the reservoir can flow directly into the bottom. It breaks the formed film. On the other hand, the vapor easily escapes from the liquid layer because there is little liquid in the vapor line and because the

pressure of the liquid is reduced in the open vapor line. This also makes the heat pipe startup easy and automatic.

- **Bubbles trapped in the wick structure.** This problem can be solved in three ways. First, with controllable LHPs, the heat pipe starts up with an empty evaporator (no liquid in the bottom at the beginning). Bubbles are not formed in the wick structure due to a lack of liquid. A strong and stable swirl flow does not allow bubbles to form during steady state operation. Last, it may be the simplest way, and that is to remove the wick structure. The swirl flow will take care of liquid redistribution, which is one of benefits of having a wick, because strong swirl flow continuously pushes the liquid droplets inside the flow against the heat pipe wall due to centrifugal force generated by swirl flow. Thus, the liquid droplets can be uniformly distributed on the evaporator wall and are vaporized to form vapor, which then joins the swirl flow. Thus, a wick may not be necessary.

- **Dry out due to the strong swirl flow.** As stated in the previous Chapter, the swirl flow is very strong and has very high speed (5.4 m/s). It can hang up liquid above the evaporator and cause the evaporator to dry out. The test of the sodium based heat pipe immersed in molten copper upon closer examination provides some evidence of this case. The subsequent analysis of the immersed tip of the pipe showed an irregular frozen shell unlike the frozen shell obtained in the Zn test. In Figure 8-1 are shown 2 photographs of the tip of the heat pipe after it was removed from the copper melt. We can see from these pictures that the frozen shell was not uniform. Actually, the leading end of the pipe including the bottom did not have a frozen shell. This was unexpected and can only be explained by the fact that the liquid was forced out the bottom by the helical swirler. Liquid return to the bottom was impeded by the swirler. This caused the heat pipe bottom to overheat. Because the thermocouple was located slightly above this region of the heat pipe, we were unable to measure the temperature changes. Nonetheless, the visual evidence strongly indicates that the liquid was unable to return into the bottom. With time the leading end of the heat pipe would be destroyed. Therefore, the hang up of liquid is not acceptable in some high temperature systems. It is necessary to return the liquid, which is hung up, back to the evaporator bottom.

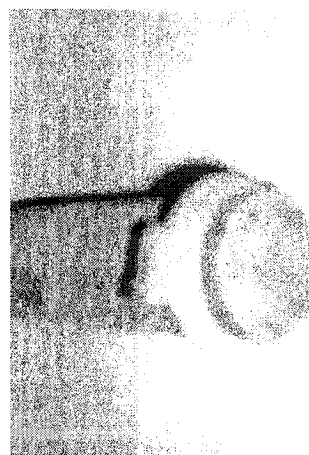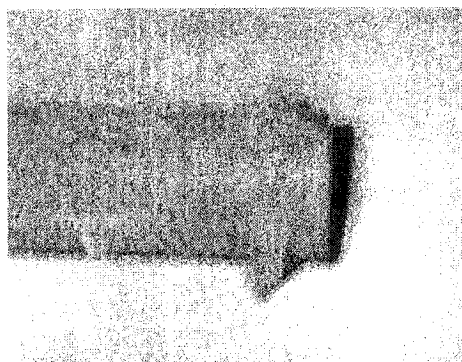LHPs can restore the fluid from the reservoir to the evaporator bottom via an independent liquid line.

Figure 8-1. Freeze Cu View in the End of the Heat Pipe

8.2 Design of the First Loop Heat Pipe

Chapter 3 has summarized several designs of loop heat pipes found in the literature. Compared with these LHPs, the loop heat pipe we have developed is based on the flow modified heat pipes that have been presented in the previous chapters. This novel technology has led to the development of a loop heat pipe of superior operating characteristics not available from current designs. Moreover, this improved technology, which includes swirlers such as twisted tapes that are fitted into conventional heat pipes, allows us to eliminate the porous wicking material as the means of returning liquid from the condenser to the evaporator.

Based on the principle of the flow modified heat pipe, in the loop heat pipe, the vapor that is generated in the evaporator forms the strong swirl flow, and it pumps liquid up the circular wall against gravity and distributes the liquid uniformly over the circumferential area of the wall of the pipe. The vapor continuously rises up via the vapor line, and condenses in the condenser section, and then the cooled liquid is collected in the reservoir (compensation chamber). The condenser liquid is returned to the evaporator by a liquid head static pressure, which is higher than the pressure in the evaporator, because

of the height of the compensation chamber of the condenser via the liquid line relative to the evaporator.

Based on this idea, the first loop heat pipe was designed and made. It is shown in Figure 8-2. In order to transport the vapor mixed with liquid, the twisted tapes were set in both the evaporator and the top vapor line. The working substance was 100 g of water. The loop heat pipe was tested in the furnace, as is described in Chapter 5 (see in Figure 5-22). The loop heat pipe is rectangular in shape and is shown in Figure 8-2. The loop heat pipe has 16 cm inside the furnace (starting at the outer brick surface). The thermocouple well is in the liquid return line (bottom pipe) and near the vertical pipe with the twisted tape. One set of experimental results is shown in Figure 8-3. From that, one can see the results have lost some regularity as was also shown for the conventional heat pipe and the flow modified heat pipe presented in previous chapters. That is, the heat extraction increases as the flow rate of cooling air increases. If we look at the heat pipe temperature shown in Figure 8-4, it is much higher than 100 °C, which not only exceeds the design specification, but is also much higher than the experimental value we obtained in others. It was also observed that the heat pipe temperature was very unstable, it was low when the thermocouple was moved out to the condenser side. This means that the location of the thermocouple is in an area which is partly dry since most of the return liquid was hung up in the liquid line and the reservoir. Therefore, the static pressure generated by liquid head is lower than required pressure that is required to offset the pressure in evaporator vapor.

Table 8-1. Comparison of Testing Results for Various Heat Pipes

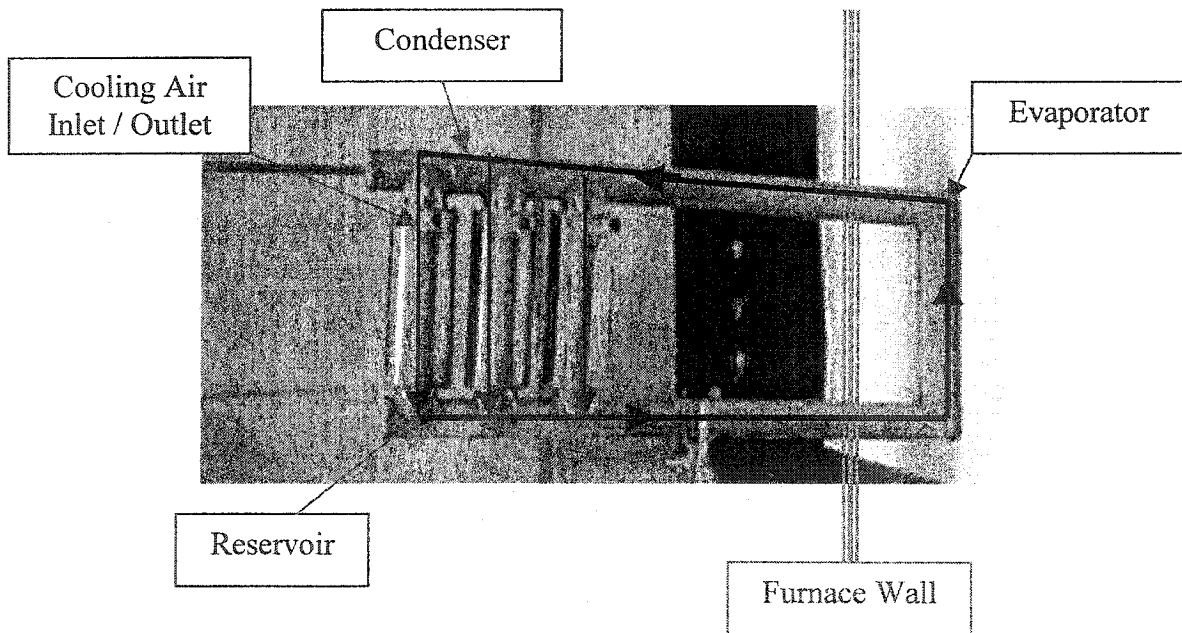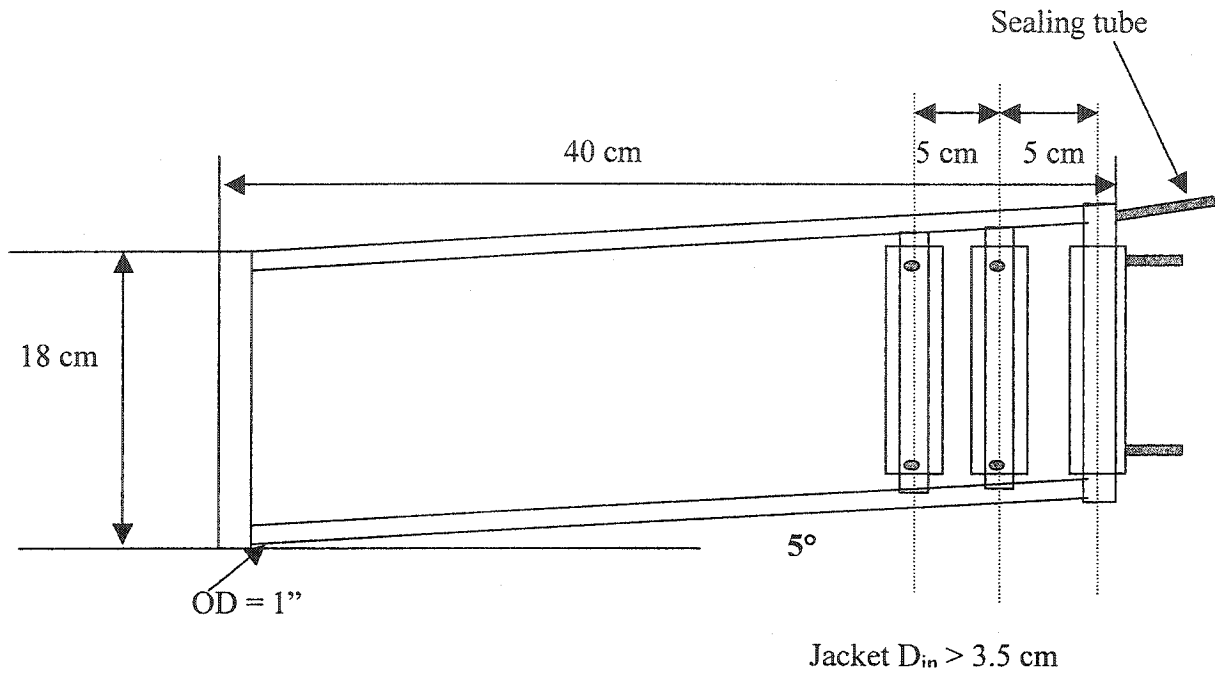| Cooling Panel Air Flow Rate = 4.41 Nl/s			Conventional Heat pipe Air Flow Rate = 5.04 Nl/s			Loop Heat Pipe Air Flow Rate 5.40 Nl/s		
$T_{furnace}$ (°C)	T_{out} (°C)	Q (W/m²)	$T_{furnace}$ (°C)	T_{out} (°C)	Q (W/m²)	$T_{furnace}$ (°C)	T_{out} (°C)	Q (W/m²)
850	110.45	65164	555	91.71	17557	950	163.38	14861
790	103.45	59494	506	80.35	14737	900	129.31	11011
730	94.76	52455	453	68.95	11906	850	105.20	8770
670	84.76	44355	404	59.03	9443	800	95.81	8210
610	73.95	35599	356	49.86	7166	750	88.85	7009

Figure 8-2. The First LHP Structure, Also Shown Are Vapor and Liquid Stream Lines
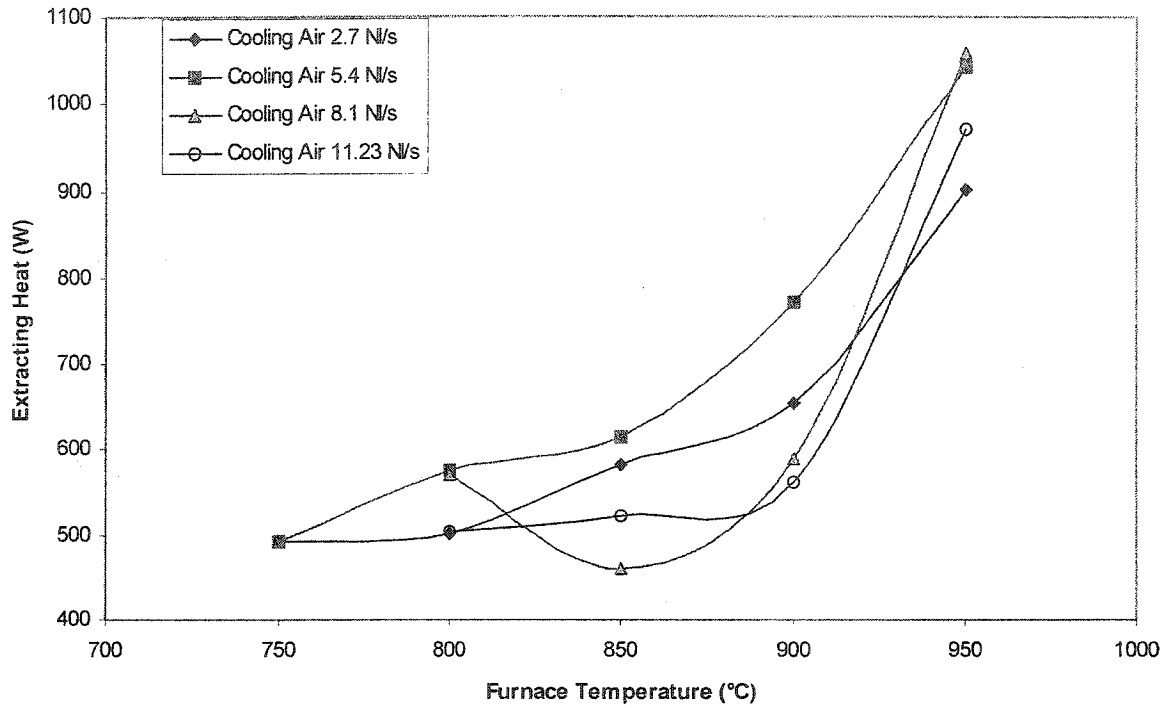
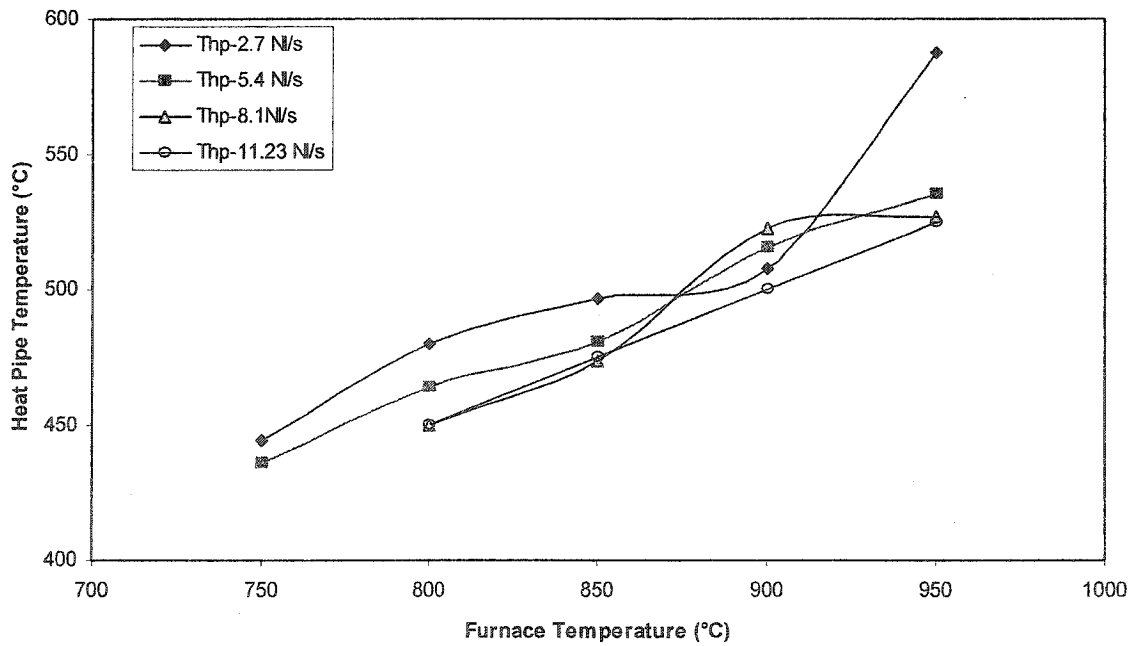Figure 8-3. The Extracting Heat of the First Loop Heat Pipe

Figure 8-4. The Loop Heat Pipe Temperature Vs Furnace
Temperature for the First LHP

Table 8-1 gives the comparison of testing results for three kinds of heat pipes. It is clear that the flux of heat extraction for the loop heat pipe is the lowest among these kinds of heat pipes that we have designed and tested.

As one can see, these results are much lower than those of the flow modified heat pipe, which have been presented in a previous chapter. Thus, these results are not what was expected. At that point it became clear that it would be necessary to redesign the loop heat pipe.

8.3 Pressure Drop for Twisted Tape Inserts in Turbulent Flow

As mentioned in Chapter 7, *Re* number of swirl flow inside the flow modified heat pipe with the twisted tape inserts is greater than 10^5. Since the flow rate for $Re \geq 10^4$ can be considered to be in the fully developed regime [1], then, the vapor flow inside the heat pipe is in turbulent flow. The following gives some main considerations for the pressure drop in the design of a flow modified heat pipe.

8.3.1 Isothermal Friction Factor

The influence of the twist rate, *y*, on turbulent flow friction factors is quite different from that in laminar, swirl flow situations, described by Manglik and Berglik [1]. They proposed the following equation for turbulent flow in a tube with twisted tape inserts.

$$\frac{f}{f_{y=\infty}} = \left[\frac{1 + \frac{2}{\pi}\left(1 - \frac{\delta}{d}\right)}{1 - (4\delta/\pi d)} \right]^{1.25} \times \left[\frac{1}{1 - (4\delta/\pi d)} \right]^{1.75} \left(1 + \frac{2.752}{y^{1.29}}\right) \qquad (8.1)$$

$$f_{y=\infty} = 0.079 \frac{1}{Re^{0.25}} \qquad (8.2)$$

Where: f friction factor.

$f_{y=\infty}$ friction factor of empty tube.

δ twisted tape thickness.

d inner diameter of heat pipe.

y twisted ratio $= H/d$, H pitch of twisted tape.

It is seen from Figure 8-5 that equation 8.1 describes within $\pm$ 5% most of the available data in the literature. Also given in this figure are the predictions from the correlations reported by a couple of researchers [1]. For the primary range of twist ratios employed by these investigators, equation 8.1 is in very good agreement with their predictions. Clearly, equation 8.1 is a more generalized correlation, which covers a broad database of available empirical data and as such, is recommended for design purposes.

Figure 8-6 shows the friction factor for tubes with twisted tape inserts normalized against that for an empty tube. The experimental data is also shown in the same figure.

8.3.2 Heat Transfer Enhancement and Increase in Pressure Drop

Enhancement of heat transfer usually entails a trade-off in the form of increased pressure loss. Thus the application of heat transfer enhancement strategies is subject to a given constraint condition. Let us consider the case of vapor flow in the tube of inner diameter, d. Under the condition that pumping power and the total rate of heat transfer over the length of the tube both remain constant, the benefits of a twisted tape insert can be evaluated by calculating the change in tube length. For example, given a tube of length L, mass flow rate m, heat transfer rate Q, pumping power P, Nusselt number Nu, and friction factor f, the ratio of power and heat transfer rates between tubes with twisted tape inserts and an empty tube are given by the following two equations [2].

$$\frac{\dot{m}}{\dot{m}_{emp}} = \left[\frac{1 - 4\delta/\pi d}{1 + \frac{2}{\pi}\left(1 - \frac{\delta}{d}\right)} \right]^{0.579} \left[1 - (4\delta/\pi d)\right]^{0.473} \left[\frac{1 + 0.769/y}{1 + 2.752/y^{1.29}} \right]^{0.526} \tag{8.3}$$

$$\frac{L}{L_{emp}} = \left[\frac{1 + \frac{2}{\pi}\left(1 - \frac{\delta}{d}\right)}{1 - (4\delta/\pi d)} \right]^{0.342} \left[1 - (4\delta/\pi d)\right]^{0.447} \frac{(1 + 2.752/y^{1.29})^{0.447}}{(1 + 0.769/y)^{1.447}} \tag{8.4}$$

Here 'emp' refers to the empty tube condition, and incorporating $P = P_{emp}$ and $Q = Q_{emp}$. The calculated results from equations 8.3 and 8.4 are shown in Figure 8-7. Although an insertion of a twisted tape results in lower mass flow rates to maintain the same pressure drop, shorter heated lengths become possible only for twist ratios less than 1.2.

With our particular Flow Modified heat pipe ($y = 5.83$), the friction factor, f, can be calculated by equation 8.1. The calculated results are shown in the Figure 8-8. The f increased as the length immersed in the zinc melt was increased.

Note that f, hence dp/dx, is a constant in the fully developed region. The friction factor is defined by the following equation [3]:

$$f \equiv \frac{-(dp/dx)d}{\rho u_m^2 / 2}$$
(8.5)

The pressure drop $\Delta p = p_1 - p_2$ associated with fully developed flow from the axial position x_1 to x_2 may then be expressed as

$$\Delta p_{vf} = -\int_{p_1}^{p_2} dp = f \frac{\rho u_m^2}{2d} \int_{x_1}^{x_2} dx = f \frac{\rho u_m^2}{2d} (x_2 - x_1)$$
(8.6)

C. C. Silverstein [4] gives a vapor pressure relationship for which the change in the pressure of the vapor in the heat pipe as it flows from the evaporator. The expression is obtained by applying the conservation of momentum principle in the same manner as it was employed for an incompressible fluid. However, the vapor density is now considered to be variable, and any force on the vapor due to gravity/acceleration is assumed to be negligible. The equation is then the following:

$$\Delta P_v = \Delta P_{vf} + \Delta P_{vm} = \Delta P_{vf} + \rho_{ve} u_{ve}$$
(8.7)

Where ΔP_{vf} denotes the frictional term, which was defined in equation 8.6. ΔP_{vm} denotes the momentum term, and the subscript e denotes conditions at $x = L_e + L_a$.

Substitution of equation 8.6 into equation 8.7 and letting FM be equal to the ratio of the frictional and momentum pressure drops $\Delta P_{vf}/\Delta P_{vm}$, Equation 8.7 can be written in the following form

$$\Delta P_v = P_{vi} - P_{ve} = (1 + FM)\rho_{ve}u_{ve} \qquad (8.8)$$
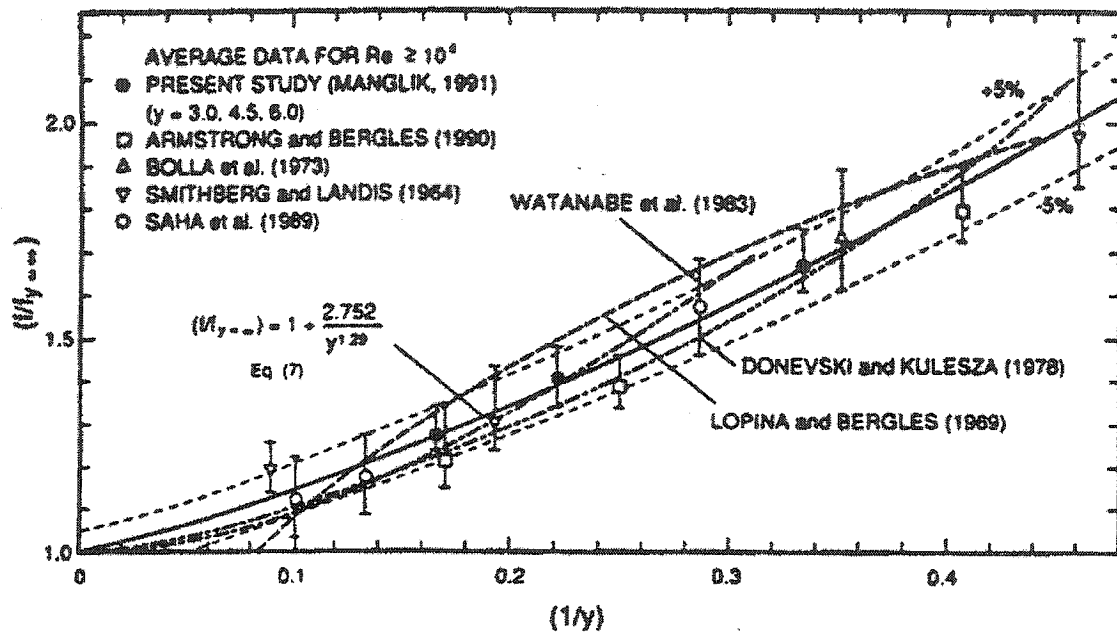

Figure 8-5. Correlation of Turbulent Flow Isothermal Friction factors in Tubes with Twisted-Tape Inserts
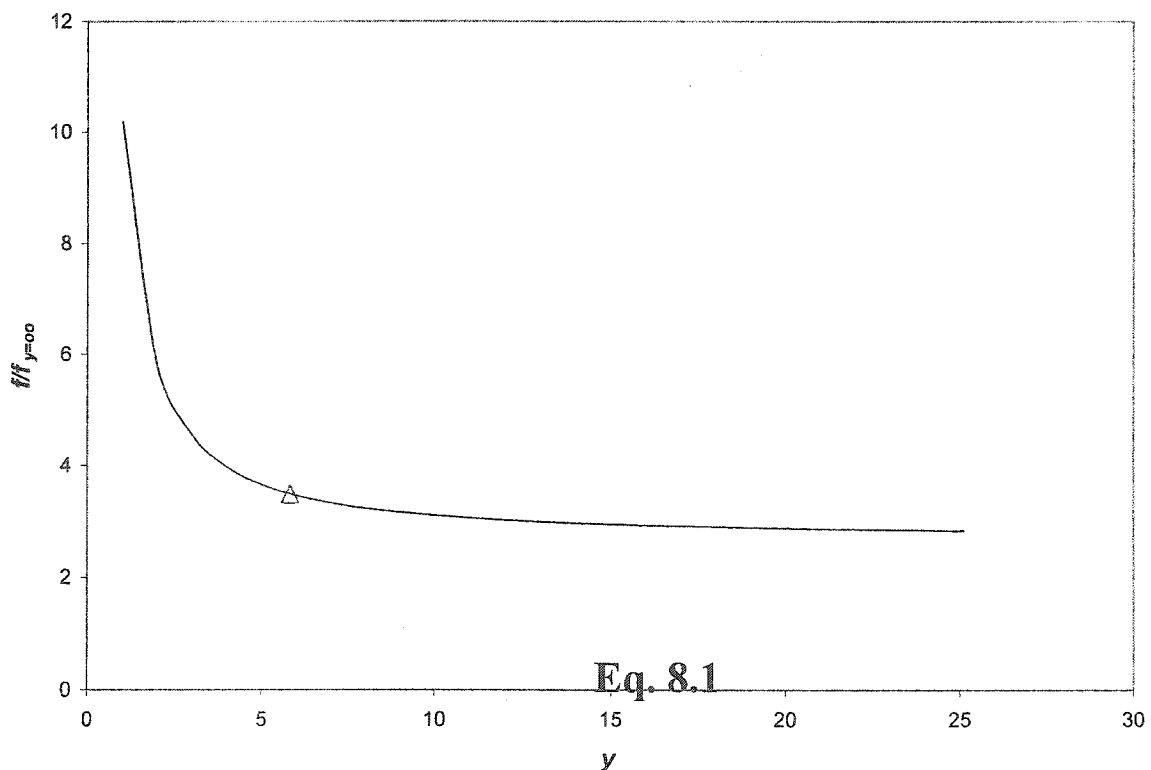

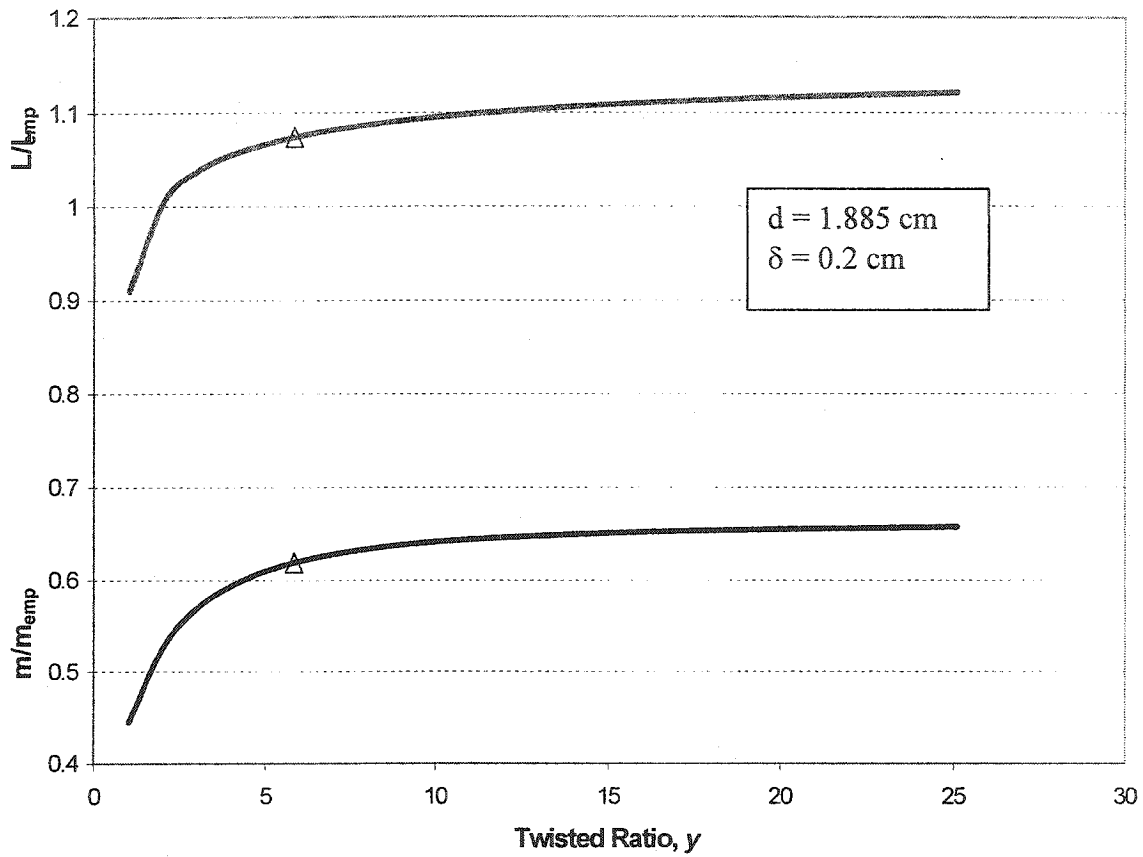Figure 8-6. Friction Factor as a Function of Twist Ratio

Figure 8-7. Change in Heated Length and Mass Flow Rate as a Function of Twist Ratio under the constant Pumping Power and Heat Transfer Rate
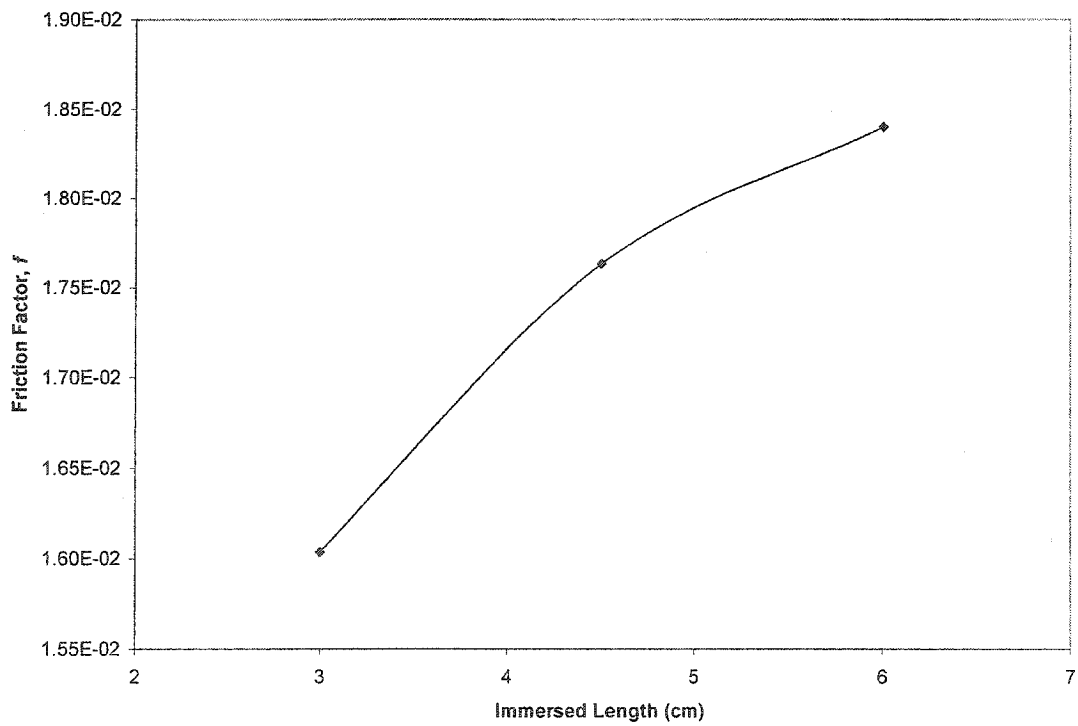

Figure 8-8. Friction Factors for a Flow Modified Heat Pipe

Where P_{vi} is the vapor pressure at x = 0 (the beginning of the evaporator).

The Mach number Ma is defined as

$$Ma = u_v/u_s \qquad (8.9)$$

Where u_s is the sonic velocity. Thus, the velocity u_{ve} can be expressed in terms of the sonic velocity u_{se} by the relation

$$u_{ve} = Ma_e u_{se} \qquad (8.10)$$

On the assumption that the vapor behaves as a perfect gas, the following equations apply:

$$\rho_{ve} = \frac{P_{ve}}{R_g T} \qquad (8.11)$$

$$u_{se} = \sqrt{k_s R_g T_{ve}} \qquad (8.12)$$

Where R_g is the gas constant and k_s is the ratio of specific heats at constant pressure and constant volume ($= c_p/(c_p - R_g)$). Upon substitution of equations 8.10, 8.11 and 8.12 into equation 8.8 and simplifying, we obtain the final results for the ratio of initial vapor pressure P_{vi} to exit pressure P_{ve}.

$$P_{vi}/P_{ve} = 1 + (1 + FM)Ma_e^2 k_s \qquad (8.13)$$

Since $Ma_e = 1$ at the sonic limit, then

$$P_{vi}/P_{vc} = 1 + (1 + FM)k_s \qquad (8.14)$$

Where P_{vc} is the exit pressure at the sonic limit. P_{vi}/P_{vc} is increased as the FM is increased. Therefore, the wick structure strongly raises the risk of reaching the sonic limit. Actually, the wick structure inside the wall of the heat pipe creates a major problem in that it increases the friction force due to the rough surface, and it make the top area pressure low. This pressure plus the head pressure generated by the differences between the evaporator bottom and end of the condenser are not enough to cancel the lose of

pressure created by the friction force. Thus, when the condensed liquid tried to flow back to the bottom of the evaporator, it was blocked by this back pressure. In the first loop heat pipe the problem of heat transfer was created because of the lack of liquid. In actual fact, the temperature at this point is unstable based on the liquid accumulated on the walls of the liquid return pipe that connects to the evaporator. When a certain quantity of the liquid is accumulated, the head pressure is high and more liquid flows into the evaporator. The lower temperatures were observed during this period. Conversely, the results were opposite.

8.4 Design of the Concept Loop Heat Pipe

To solve the problems observed during the test of the first loop heat pipe, there are two possibilities. First, one can remove the wick structure from the heat pipe. The wick structure not only creates a friction force, it also traps bubbles inside the wick network. Moreover, the breaking of these bubbles can be very difficult. It was shown and explained in Chapter 7. Actually, the wick structure was introduced to re-distribute the condenser liquid on the evaporator walls to avoid hot spots, as mentioned in Chapter 4. After the flow-modifier elements were introduced, liquid redistribution as provided by the wick structure was replaced by the modified flow generated by the swirlers. In addition, the wick capillary force, that delivers the condenser liquid into the evaporator, is not necessary because the vapor and the condensed liquid use separate lines in the loop heat pipe. Therefore, the wick structure can be removed from the novel heat pipe design.

The second solution is to increase the head pressure to obtain a bigger static force to push the condensed liquid from the condenser into the evaporator. It can be implemented by moving the condenser further above the top of the evaporator.

The concept of the novel loop heat pipe is displayed in Figure 8-9. In this heat pipe, the condenser is above the top of the evaporator. In it, a reservoir is incorporated to handle the condensing liquid and a small liquid return pipe leads the cooled liquid back to the evaporator. With low temperature working substances such as water, the liquid return line can be placed on the outside of the heat pipe. However, with high temperature working substances, the liquid return line should be assembled inside the heat pipe for safety reasons and to avoid the freezing of the working substance. With regards to this

novel structure of the loop heat pipe, it is radically different from the traditional loop heat pipe which was mentioned and reviewed in Chapter 3. A major difference is in the liquid return part. Thus, it was named as the semi-loop heat pipe by the researchers at McGill. This loop heat pipe was tested by the research group in liquid zinc. This pipe increased rate of the heat extraction by 15% since it eliminated the wick structure. Moreover, it can start by itself.

Since the reservoir is above the top of the evaporator, its design can be flexible both structure and shape. One can determine its structure and shape based on the application requirements. It may have a single cooling jacket or multiple cooling elements (pipes). It may also be round or rectangular in shape. The reservoir capacity is decided based on the quantity of the working substance in the heat pipe. With a low temperature working substance such as water, more space is required than when a high temperature working substance, such K and Na, is used. Also the reservoir is dependent on the actual application. Compared with the conventional heat pipe, the amount of working substance is more flexible in the novel heat pipe. One can use much more working substance in the novel heat pipe design since the reservoir will handle the excess the working substance. As mentioned in previous chapters, the coiled wire twisted tape and helical rabbit can be used as the flow modifier elements, depending on the application. Usually, the simplest twisted tapes with various twisted rates (pitch) are utilized. However, the twisted tapes restrict heat pipe temperature measurement since the thermocouple well can't be extended to the evaporator area (bottom) of the heat pipe. Therefore, in those cases where temperature measurement are required, the helical rabbits can be used to replace twisted tapes because the center bar (made by pipe) of the helical rabbit is used as the thermocouple well of the novel heat pipes. In some cases with very high heat momentum, the cheaper coiled wire is utilized to replace the twisted tapes. In those cases, there is more space inside the heat pipe chamber to place the thermocouple well and other elements such as the liquid return line, which requires assembling it inside the heat pipe.

The condenser of the novel heat pipe can be placed under the reservoir. But it can also be on the top of the reservoir. In this case, the condenser and the reservoir can be placed some distance away from the evaporator. They link together via a flexible pipe.
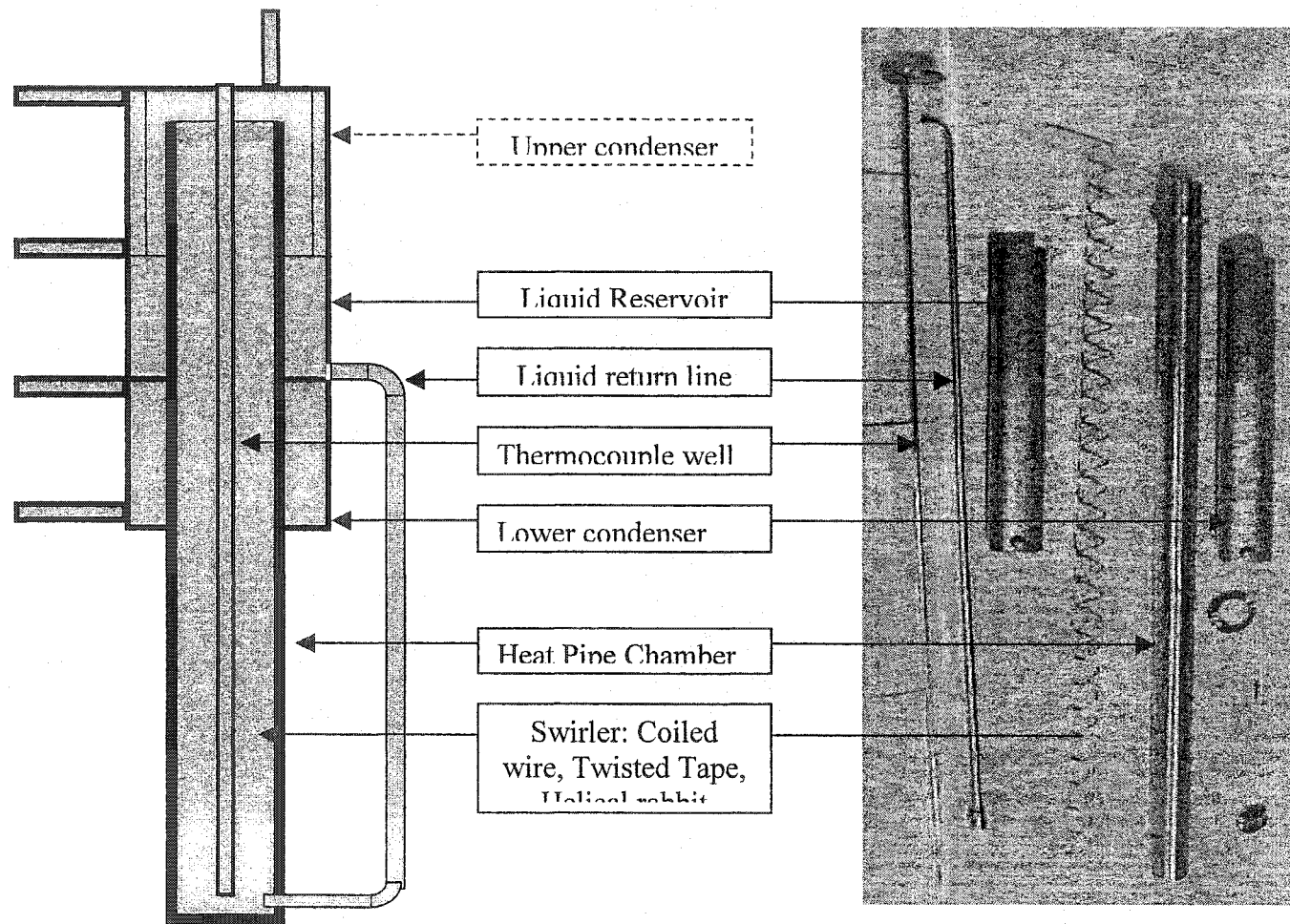
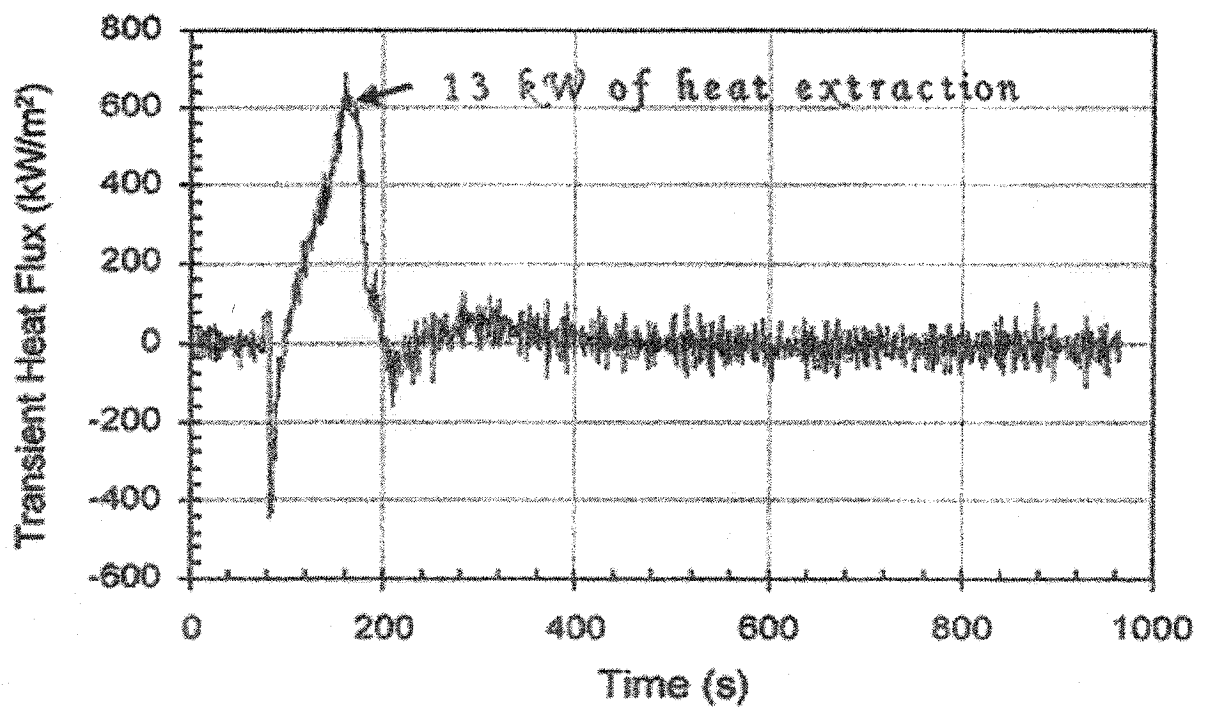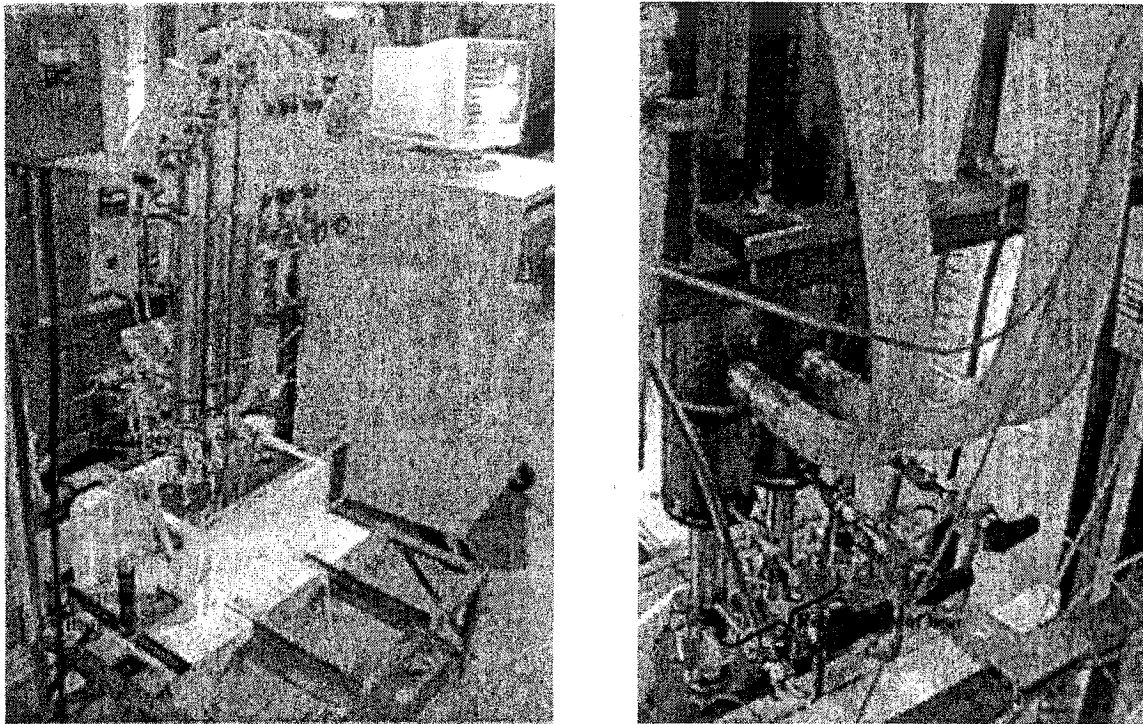Figure 8-9. The Structure and the Concept of the Novel Heat Pipe

Figure 8-11. Transient Heat Extraction by the Novel Heat Pipe
during the Casting of Aluminum

The liquid return line can also be flexible. In some cases, to strengthen the vapor cooling, the condenser can be separated and placed in both under and above the reservoir.

It is very clear that the design of the novel concept loop heat pipe efficiently overcomes the deficiencies of the first loop heat pipe and completely solves the disadvantages of the flow modified heat pipe when introducing the flow modified elements. Those disadvantages are listed in previous sections. Right now, we have the whole image of the novel heat pipe package. Therefore, this novel heat pipe has been fully developed.

The concept of the novel loop heat pipe has been successfully applied to the casting of aluminum [5] and in the oxygen lance that is used in steel making.

In the application, three different sizes of this kind of loop heat pipe were used. Each sat on top of the casting mold. The evaporator extended into the wall in the form of a hole. The heat pipe chamber was formed by welding the hole to the adiabatic and condenser which included the reservoir. The set up is shown in Figure 8-10 [5]. In this design, a valve was placed in the liquid return line, and was used to control the startup or stopping of the heat pipe. It is very important and a great idea in the temperature control of casting molds.

Its heat extraction capability (up to 1 MW/m^2, see Figure 8-11[5]) is substantially better than water-cooled passages. The heat pipe unit has been used successfully in the casting of aluminum to control a number of parameters (shrinkage, DAS, etc...).

CHAPTER 9. CONCLUSIONS AND ORIGINAL CONTRIBUTIONS TO KNOWLEDGE

9.1 Conclusions

In the present work, novel heat pipes were investigated by conducting both fundamental and experimental studies. Based on the results and discussions presented in Chapters 5 to 8, the following conclusions can be drawn.

1. The major performance action of the wick structure on a gravity-assisted heat pipe is to redistribute the condensing working fluid over the entire evaporator section via the capillary force of the wick. The wick can thus eliminate potential hot spots that may be generated by non-uniform return liquid flow on the evaporator surface under high temperature circumstances. The wick structure can ensure that the working fluid covers and protects the entire evaporator section.

2. The role of forced convection cooling as applied to the condenser section of the heat pipe was investigated. With a suitable cooling jacket in place it is possible to operate the heat pipe at a relatively low temperature for a given set of conditions. Moreover, when the coiled wires flow enhancement was introduced into the cooling jacket of the heat pipe, heat transfer to the cooling air improved greatly. The results relating to rate of heat extraction, heat transfer coefficient and heat pipe efficiency in the heat pipe with the coiled wire are much better than those for the heat pipe without the coiled wire, and especially for those cases where the cooling air entered from the bottom of the cooling jacket.

3. The cooling panel with internal condenser is better than the convectional cylindrical heat pipe as measured by heat pipe efficiency. However, because of the high manufacturing cost and following serious problems under high heat flux circumstances, the cooling panel was abandoned and emphasis shifted to develop a novel heat pipe.

4. Film boiling of the working fluid inside the heat pipe was created and investigated under high heat flux conditions. With the film boiling inside the heat pipe, there were cases when the heat pipe failed under high heat fluxes. In the

nucleate boiling regime such pipes worked well. However, the onset of film boiling could lead to catastrophic consequences. For working substances with low operating temperatures such as water, film boiling is very clear and impressive under high heat fluxes (liquid zinc melt). The experimental results strongly indicated the heat pipe was operated in the range of classical film boiling.

5. The flow modified heat pipe was invented and investigated systematically. In this kind of heat pipe, a flow-modifier element such as a twisted tape, helical rabbit or coiled wire was introduced into the heat pipe chamber to improve the heat transfer of the two-phase flow. The experimental data indicated that the flow modified heat pipe was dramatically better than a conventional heat pipe under a comparable high heat flux load. This novel heat pipe brings forth a new design concept for conventional heat pipes. This should then make it possible for conventional heat pipes to be applied in high heat flux circumstances such as are found in the metallurgical and energy industries.

6. The flow-modifier elements dramatically improved heat transfer inside the heat pipe chamber. The swirl flow generated by the flow-modifier elements successfully and efficiently removed the vapour films on the inner surface of the evaporator, under high heat flux operation when the swirl flow is a turbulent flow with Re number $\geq 10^4$, the rate of heat extraction of the novel heat pipes is up to or greater than 1 MW/m^2 in experiments when the heat pipe was immersed in liquid zinc.

7. A correlation for the heat transfer coefficient in the flow modified heat pipe was derived.

8. The first novel heat pipe to combine the concepts of flow modified heat pipe and loop heat pipe was designed and investigated. The experimental data showed that the wick structure could be removed from the novel heat pipe. Its function to redistribute condensing working fluid was replaced by the swirl flow and the ensuring centrifugal force generated by the flow-modifier elements inside the heat pipe.

9. The concept of a novel heat pipe—termed the semi-loop heat pipe was described. This kind of heat pipe overcomes all the disadvantages of the flow modified heat pipe and loop heat pipe after the wick was removed from the internal structure of the heat pipe. The main task of the wick was taken over by the swirl flow. This novel generation of heat pipe can be used in applications with high heat flux areas such as found in the metallurgical and energy industries.

9.2 Original Contributions to Knowledge

The results obtained in this work are of industrial as well as academic interest, and include the following original contributions to knowledge:

1. For the first time, a novel heat pipe that combines the flow modified heat pipe and the loop heat pipe has been proposed, described and designed successfully and has since been applied to aluminium casting and oxygen lancing.

2. For the first time, flow modified heat pipes were described and investigated systematically. A new generation of heat pipe has been proposed, designed, fabricated and tested successfully. It completely changes the design philosophy of heat pipes that are used in high heat flux operations.

3. It has been demonstrated experimentally that the film boiling phenomenon can be a serious problem when a conventional heat pipe is used under high heat flux conditions. Film boiling can make a conventional heat pipe lose its ability for sustained heat transfer with a small temperature gradient.

4. It has been demonstrated experimentally that the swirl flow generated by flow-modifier elements, which were introduced into the heat pipe in the design of the novel heat pipe, successfully and efficiently overcame film boiling by collapsing the formed films. It has been shown that the novel heat pipes are suitable for high heat flux and high temperature operation where a conventional heat pipe will not function.

5. Forced-convection cooling on the condenser provides the possibility of controlling the heat pipe operating temperature at any desired level. Air cooling on the condenser offers several advantages over a self-cooled system and a

water-cooled system. In addition, the coiled wires introduced into heat pipe cooling jackets improved the heat transfer coefficient for the condenser of the heat pipe and increased the utilization rate of cooling air. The current research showed how to apply this to the novel heat pipe.

6. The wick structure is not required in the design of the novel heat pipes since the action of redistributing working fluid on the evaporator surface is now replaced by the swirl flow from flow-modifier elements. The presence of a wick can, in fact, be detrimental as it can act to form a bubble trap and thus reduce heat transfer. This is an important original contribution of the current research.

7. Some components of the loop heat pipe such as the heat pump, or porous structure or heat switcher, which were used to restore condensing liquid to the evaporator, can be discarded if one incorporates an appropriate design for the reservoir and the flow-modifier elements.

REFERENCES

Chapter 1

1. Karen S. Yoshiki-Gravelsins, James M. Toguri, and Roland T. C. Choo, "Metals Production, Energy, and the Environment, Part I: Energy Consumption", JOM, 1993 May, pp15-20.

2. Vlandimir Stepanov and Sergey Stepanov, "Energy Use Efficiency of Metallurgical Process", Energy Convers. Mgmt, Vol. 39, No. 16-18, 1998, pp1803-1809.

3. Guohui Zheng and Janusz A. Kozinski, "Solid Waste Remediation in the Metallurgical Industry: Application and Environmental Impact", Environmental Progress, Vol. 15, No.4, Winter 1996, pp283-292

4. Ishwar P. Murarka "Solid Waste Disposal and Reuse in the United States", Volume I, 1987.

5. Cigan J. M., Mackey T. S., U'Keefe T. J. "Lead--Zinc--Tin '80", TMS--AIME World Symposium on Metallurgy and Environmental Control, 1980.

6. Karen S. Yoshiki-Gravelsins, James M. Toguri, and Roland T. C. Choo, "Metals Production, Energy, and the Environment, Part II: Environmental Impact", JOM, 1993 August, pp23-29.

Chapter 2

1. Silverstein, Calvin C., "Design and Technology of Heat Pipes For Cooling and Heat Exchange", Hemisphere Publishing Corporation, 1992

2. Web site: Los Alamos Heat Pipe Home Page
   fttp://www.ext.lanl.gov/orgs/epe/Heat_Pipe_Site/Ht_Pipe_top.html, July, 2000

3. A. Faghri, "Heat Pipe Science and Technology", Taylor & Francis, Washington D.C., 1995.

4. L. L. Uasilier, "State-of the-Art on Heat Pipe Technology in the Former Soviet Union", Applied Thermal Engineering, Vol. 18, No. 7, 1998, pp507.

5. G.P. Peterson, "An Introduction to Heat Pipes", John Wiley & Sons, 1994

6. G. M. Grover, T. P. Cotter, and G. F. Erickson, "Structures of Very High Thermal Conductance," J. Appl. Phys. Vol. 35, 1964, p1990.

7. T. P. Cotter, "Theory of Heat Pipe", Los Alamos Scientific Laboratory of the University of California, Los Alamos, 1965.

8. S. W. Yuan and A. B. Finkelstein, "Laminar Flow with Injection and Suction Through a Porous Wall," Heat Transfer and Fluid Mechanics Institute, Los Angeles, 1955.

9. B. W. Knight and B. B. McInteer, "Luninar Incompressible Flow in Channels with Porous Walls," LADC-5309.

10. W. E. Wageman and F. A. Guevsra, "Fluid Flow Through a Porous Channel," Phys. Fluids, No.3, 878 (1960).

11. C. A. Busse, "Theory of the Ultimate Heat Transfer Limit of Cylindrical Heat Pipe", J. Heat Mass Transfer, Vol. 16, 1973, pp169-186.

12. K. R. Chun, "Some Experiments on Screen Wick Dry-out Limits", ASME, J. Heat Transfer, Vol. 94, No. 1, p46, 1972.

13. S. Seshan and D. Vijayalaskshmi, "Heat Pipe – Concepts, Materials and Applications", Energy Convers. Mgmt, Vol. 26, No. 1, p1, 1986

14. A. A. Rohani and C. L. Tien, "Steady Two-Dimensional Heat Pipe and Mass Transfer in the Vapor-Gas Region of a Gas Loaded Heat Pipe", Journal of Heat Transfer, Vol. 95, p377, 1972.

15. K. Hijiakata, S. J. Chen and C. L. Tien, "Noncondensable Gas Effect on Condensation in a Two-phase Closed Thermo-syphon", International Journal of Heat Transfer, Vol. 27, p 1319, 1984.

16. R. P. Boboco, "Variable Conductance Heat Pipe Performance Analysis: Zero-to Full Load", Journal of Thermophysics, Vol. 3, No. 1, 1989.

17. V. H. Gray, ASME Paper No. 69-HT-19, 1969.

18. F. Polasek, Proceeding of the Forth International Heat Pipe Conference, 1973.

19. D. Khrustalev and A. Faghri, "Thermal Analysis of a Micro Heat Pipe", J. of Heat Transfer, Vol. 116, Feb., p189, 1994.

20. B. R. Babin, G. P. Peterson and D. Wu, "Steady-State Modeling and Testing of a Micro Heat Pipe", Journal of Heat Transfer, Vol. 112, August, p595, 1990.

21. J. F. Maidanik et al. United State Patent # 4515209, May 7, 1985.

22. T. Zapach et al, United States Patent #5842514, Dec 1, 1998.

23. H. Kuwahara et al, United States Patent #5925929, Jul. 20, 1999.

24. T. M. Vipalla et al, United States Patent #5910883, Jun. 8, 1999.

25. R. Bhatia, et al, United States Patent #5880929, Mar. 9, 1999

26. D. R. Adkins, "Design Condiderations for Heat-Pipe Solar Receivers", Journal of Solar energy Engineering, Vol. 112, August, p169, 1990.

27. X. Wu, P. Johnson, and A. Akbarzadeh, "Application of Heat Pipe Exchangers to Humidity Control in Air-Conditioning System", Applied Thermal Engineering, Vol. 17, No. 6, p561, 1997.

28. E. Mast, F. Mucciardi, M. Brown, Self-Cooling Lance or Tuyere, U.S. Patent 5,310,166, 1994.

29. F. Mucciardi and N. Jin, "Inclined Heat Pipe Lance or Tuyere with Controllable Heat Extraction", U.S. Patent Application filed Oct. 1997.

30. J. Kay and F. Mucciardi, "A Computational Investigation of a Heat Pipe Injection Lance", Steel Research, Vol. 66, No. 1, p8, 1995.

31. F. Mucciardi and N. Jin, "Top Blowing Oxygen Lance for Copper Smelting and Converting", Canadian Metallurgical Quarterly, Vol. 35, No. 5, p395, 1996.

32. F. Mucciardi, N. Jin and E. Palumbs, "Modeling a Novel, Air-cooled Caster, Twin Roll Caster", Computer Application Symposium, Calgary, Canada, August 15-20, 1998.

33. Kearney et al, United State Patent #5391337, Feb. 21, 1995.

34. M. Mahfoud, F. Mucciardi and J. E. Gruzleski, "On-Line Control of Heat Extraction during Thermal Analysis of Aluminum Alloys", Int. J. Cast Metals Res., No. 10, p191, 1998.

35. K. S. Gam, "A Stable Microcomputer-Controlled Heat Pipe Furnace and Test of New Noble Metal Thermocouples", Measurement, Vol. 18, No. 2, p101, 1996.

36. J. T. Richardson, S. A. Paripatyadar, and J. C. Shen, "Dynamics of a Sodium Heat Pipe Reforming Reactor", AIChE Journal, Vol. 34, No. 5, p743, 1988.

Chapter 3

1. Y. F. Maidanik et al, "Heat Transfer Apparatus", US Patent No. 4515209, May 7, 1985.

2. P. J. Wirsch and S. K. Thomas, "An Experimental Investigation of a Stainless Steel/Ammonia Loop Heat Pipe", AIChE Symposium series, Vol. 91, No. 306, p337, 1995.

3. F. J. Stenger, "Experimental Feasibility Study of Water-Filled Capillary Pumped Heat Transfer Loops", NASA X-1310, NASA LeRC, 1966.

4. Y. Maidanik, G. Fershrater, and K. A. Goncharrov, "Capillary-Pump Loop for the System og Thermal Regulation of Spacecraft", Proceedings of the 4th European Symposium on Space Environmental and Control System, European Space Agency, ESA Paper SP-324, 1991.

5. Y. Maidanik et al, "Theoretical Basis and Classification of Loop Heat Pipes and Capillary Pumped Loops", 10th International Heat Pipe Conference, Stuttgart, Germany, 1997.

6. Kiseev et al, "Heat Transporting Device", US patent, No. 4467861, August 18, 1984.

7. A. Basiulis, "Separate Liquid Flow Heat Pipe System", US patent, No. 4627487, December 9, 1986.

8. Akachi et al, "Structure of a Heat Pipe", US patent, No. 4921041, May 1, 1990.

9. Cornog et al, "Mechnically Pumped Heat Pipe", US patent, No. 5911272, June 15, 1999.

10. Cullimore and Ring Technologies Inc., "Loop Heat Pipe Prebuilt Model", User Documentation, Rev. 2, May 18, 1998.

Chapter 4

1. C. A. Busse, "Theory of the Ultimate Heat Transfer Limit of Cylindrical Heat Pipe", Int. J. Heat Mass Transfer, Vol. 16, p169, 1973.

2. V. G. Rajesh and K. P. Ravindran, "Optimum Heat Pipe Design: A Nonlinear Programming Approach", Int. Comm. Heat Mass Transfer, Vol. 24, No. 3, 1997, P371.

3. A. Faghri, "Heat Pipe Science and Technology", Taylor & Francis, 1995.

4. C. C. Silverstein, "Design and Technology of Heat Pipes For Cooling and Heat Exchange", Sphere Publishing Corporation, 1992.

5. G. P. Peterson, "An Introduction to Heat Pipes", John Wiley & Sons, 1994.

6. S. W. Chi, "Heat Pipe Theory & Practice", McGraw Hill, New York, 1976.

Chapter 5

1. N. Jin, "Heat Pipe Cooled Injection Lances - Experimental Investigation and Mathematical Modelling, Ph.D. Thesis, McGill University, 1997.

2. F. Mucciardi, "Report of an Invention on: Loop Heat Pipe", Internal Report, 2000

3. A. Faghri, "Heat Pipe Science and Technology", Taylor & Francis, 1995.

4. C. C. Silverstein, "Design and Technology of Heat Pipes For Cooling and Heat Exchange", Sphere Publishing Corporation, 1992.

5. G.P. Peterson, "An Introduction to Heat Pipes", John Wiley & Sons, 1994.

6. F. Mucciardi, "Advanced Extraction Metallurgical Process", Class Notes, Department of Mining & Metallurgical Engineering, Sept. 1998.

7. F. Bozet and S Morales, "Study of the Performance of a heat Extraction Box", Project Report, Department of Mechanical Engineering, McGill University, April, 1997.

Chapter 6

1. G.P. Peterson, "An Introduction to Heat Pipes", John Wiley & Sons, 1994.

2. F. Mucciardi and G. Zheng, "Heat Transfer in the Boiling Regime", Ottawa, 1999.

3. L.A. Bromley, "Heat Transfer in Stable Film Boiling ", *Chem Engr. Progress, Vol 46*, 1950, P 221.

4. N. Zuber, "On the Stability of Boiling Heat Transfer", Trans ASME, *Vol 80*, 1958, P711.

5. F. P. Incropera and D. P. D$_E$Witt, "Fundamentals of Heat and Mass Transfer", Third Edition, John Wiley & Sons, New York, 1990.

Chapter 7

1. M. Yilmaz, O. Comakli and S. Yapici, "Enhancement of Heat Transfer by Turbulent Decaying Swirl Flow", Energy Conversion & Management Vol. 40, 1999, P1365.

2. S. V. Alekseenko, at al, " Helical Vortices in swirl flow", J. Fluid Mech., Vol. 382, 1999, P195.

3. S. Yapici, M. A. Patrick, and A. A. Wragg, "Hydrodynamics and Mass Transfer in Decaying Annular Swirl Flow", Int. Comm. Heat Mass Transfer, Vol. 21, 1994, P41.

4. M. A. Kedzierski and M. S. Kim, "Convective Boiling and Condensation Heat Transfer with a Twisted-Tape Insert for R12, R22, R152a, R134a, R32/R134a, R32/R152a, R290/R134a, R134a/R600a", Thermal Science & Engineering, Vol. 6, No. 1, 1998, P113.

5. R. M. Manglik and A. E. Bergles, "Heat Transfer and pressure Drop Correlations for Twisted-Tape Inserts in Isothermal Tubes: Part I—Laminar Flow", Journal of Heat Transfer, Vol. 115, November 1993, P881.

6. R. M. Manglik and A. E. Bergles, "Heat Transfer and pressure Drop Correlations for Twisted-Tape Inserts in Isothermal Tubes: Part II— Transition and Turbulent Flows", Journal of Heat Transfer, Vol. 115, November 1993, P890.

7. F. Mucciardi, G. Zheng, and N. Jin, "Extending Lance Life in Top Blowing", Copper '99, TMS, 1999.

8. A. Faghri, "Heat Pipe Science and Technology", Taylor & Francis, 1995.

9. J. M. Toutnier and M. S. EI-Genk, "Modeling of the Startup of a Water Heat Pipe from Frozen State", ALChE Symposium Series, P323.

10. J. M. Toutnier and M. S. EI-Genk, "Transient Analysis of the Start-up of a Water Heat Pipe from Frozen State", Numerical Heat Transfer, Part A, Vol. 28, 1995, P461.

11. F. Mucciardi and G. Zheng, "Heat Transfer in the Boiling Regime", Ottawa, 1999.

12. Y. Fujita and A. M. Lopez, "Heat-Transfer Enhancement of Twisted-Tape Inserts in Turbulent Pipe Flows", Heat Transfer--Japanese Research, 24(4) 1995, P378.

13. J. Weisman, J. Y. Yang, and S. Usman, "A Phenomenological Model for Boiling Heat Transfer and the Critical Heat Flux in Tubes Containing Twisted Tapes", Int. J. Heat Mass Transfer, Vol. 37, No.1 1994, P69.

14. M. Yimaz, O. Comakli and S. Yapici, "Enhancement of Heat Transfer by Turbulent Decaying Swirl Flow ", Energy Conversion & Management, Vol. 40, 1999, P1365.

15. A. Klaczak, "Heat Transfer by Laminar Flow in a vertical Pipe with Twisted Tape Inserts", Heat and Mass Transfer, Vol. 36, 2000, P195.

16. F. P. Incropera and D. P. D_EWitt, "Fundamentals of Heat and Mass Transfer", Third Edition, John Wiley & Sons, New York, 1990.

Chapter 8

1. R. M. Manglik and A. E. Bergles, "Heat Transfer and pressure Drop Correlations for Twisted-Tape Inserts in Isothermal Tubes: Part II— Transition and Turbulent Flows", Journal of Heat Transfer, Vol. 115, November 1993, P890.

2. Y. Fujita and A. M. Lopez, "Heat-Transfer Enhancement of Twisted-Tape Inserts in Turbulent Pipe Flows", Heat Transfer--Japanese Research, 24(4) 1995, P378.

3. F. P. Incropera and D. P. D_EWitt, "Fundamentals of Heat and Mass Transfer", Third Edition, John Wiley & Sons, New York, 1990.

4. C. C. Silverstein, "Design and Technology of Heat Pipes for Cooling and Heat Exchange", Hemisphere Publishing Corporation, Washington, 1992.

5. F. Mucciardi, J. E. Gruzleski, C. Zhang, and K. Elalem, "Use of Heat Pipes for Cooling Permanent Molds", MMPC Annual Meeting, McGill University, Montreal, Canada, Dec. 7, 2001.